Design, Synthesis and Biological Evaluation of Synthetic and Nanocarrier Delivery System for Targeted Cancer Therapy

Thesis Submitted to Academy of Scientific and Innovative Research (AcSIR)
for the Award of the Degree of
DOCTOR OF PHILOSOPHY
in Chemical Sciences

By

S. Maniganda

Registration No: 10CC12A39004

Under the guidance of

Dr. KAUSTABH KUMAR MAITI

CSIR-NATIONAL INSTITUTE FOR INTERDISCIPLINARY SCIENCE AND TECHNOLOGY (CSIR-NIIST)
THIRUVANANTHAPURAM-695019, KERALA, INDIA

June, 2019

Dedicated to

my family, teachers

and friends

Declaration

I hereby declare that the matter embodied in the thesis entitled: " **Design, Synthesis and Biological Evaluation of Synthetic and Nanocarrier Delivery System for Targeted Cancer Therapy**" is the result of the investigations carried out by me at the Organic chemistry section, Chemical Sciences and Technology Division, CSIR-National Institute for Interdisciplinary Science and Technology (CSIR-NIIST), Trivandrum, under the supervision of Dr. Kaustabh Kumar Maiti and the same has not been submitted elsewhere for any other degree.

In keeping with the general practice of reporting scientific observations, due acknowledgement has been made wherever the work described is based on the findings of other investigators.

S. Maniganda

National Institute for Interdisciplinary Science and Technology (NIIST)
Council of Scientific and Industrial Research (CSIR)
Industrial estate P.O., Thiruvananthapuram- 695019
Kerala, India

Dr. Kaustabh Kumar Maiti
Senior Scientist
Chemical Sciences and Technology Division

Tel: 0471-2515475
Mob: +91-8547761544
e-mail: kkmaiti@niist.res.in
kkmaiti29@gmail.com

June, 2019

Certificate

This is to certify that the work embodied in this Ph.D. thesis entitled "**Design, Synthesis and Biological Evaluation of Synthetic and Nanocarrier Delivery System for Targeted Cancer Therapy**" submitted by **Mr. S. Maniganda** to Academy of Scientific and Innovative Research (AcSIR), in partial fulfilment of the requirements for the award of the **Degree of Doctor of Philosophy in Chemical Sciences**, has been carried out under my supervision and guidance at the Organic chemistry Section, Chemical Sciences and Technology Division of the CSIR-National Institute for Interdisciplinary Science and Technology (CSIR-NIIST), Thiruvananthapuram. I further certify that this work has not been submitted to any other University or Institution in part or full for the award of any degree or diploma.

Dr. Kaustabh Kumar Maiti
(Thesis Supervisor)

Acknowledgements

It is with great pleasure that I extend my deep sense of gratitude to Dr. Kaustabh Kumar Maiti, my thesis supervisor, for suggesting the research problem, for his valuable guidance, support, encouragement and scientific freedom of thought and action, leading to the successful completion of this work.

I thank Dr. A. Ajayaghosh, Dr. Gangan Prathap, and Dr. Suresh Das, present and former Directors of CSIR- NIIST, Trivandrum, for providing me the necessary facilities for carrying out this work.

I express my deep sense of gratitude to our collaborator Dr. K.G. Raghu from CSIR-NIIST- Trivandrum and Dr. T.T. Sreelekha for biological studies and valuable suggestions.

I owe my deepest gratitude to:

- *Dr. Mangalam S. Nair and Dr. R. Luxmi Varma, Dr. Suresh C.H. former and present AcSIR coordinators.*
- *Dr. Sujatha Devi P. Dr. K. R. Gopidas, Dr. D. Ramaiah Former Head, Chemical Sciences and Technology Division for their support*
- *Dr. K.V. Radhakrishnan, Dr. Binod Parameswaran. and Dr. R. Luxmi Varma my DAC members*
- *Dr. G. Vijay Nair and Prof. M. V. George, for their inspiring presence*
- *Dr. L. Ravi Sankar, Dr. B. S. Sasidhar, Dr.A. Kumaran, Dr.Shridevi. D and Dr.Sunil Varughese Scientists of Organic Chemistry Section, for their help and support extended to me*
- *Dr. Raghu K. G for providing initial cell culture facilities.*
- *Dr. Jubi John and Dr. Ganesh Chandra Nandi for their valuable suggestions and support*
- *Sincere thanks to Dr. Manu M. Joseph, Dr. Vandana shankar, Ms. Varsha Karunakaran and Dr. Vishnupriya M. for teaching and helping biological experiments.*
- *Special thanks to Dr. Dhanya SR, Dr. Sajin Francis Dr. Parvathy Rathnam, Mr. Shanmuga Sundharam, Dr. R.Ramakrishnan, Dr. Shameel T. Dr. G.Jaggaiah Naidu, Dr.*

Baku Nagendra, Dr. C.H.Chandra Sekhar, Dr. Vineeth Vijayan, and Dr. Susan Alex for their timely help and support.

- *Mrs. M. Saumini Mr. P. Saran Mr. R. Gokul and Mr. Syam for NMR, Mrs. S. Viji, Ms. Athira for mass spectral analyses and Mr. Kiran M. and Mr. Robert Philip for TEM analysis*
- *Dr. Balachandra, Mr. Arun, Mr. Praveen, Mr. Mohan, Mr. Prasanna my friends and roommates.*
- *Sincere thanks to my group members Dr. Nisha N., Dr. Jyothi B Nair., Ms. Ramya A.N., Mr. Sujai P.T., Ms. Saranya Giridharan, Ms. Bincy, Ms. Arya J.S., Mr. Shamjith S., Ms. Deepika S., Mr. Madhukrishnan M., Mr. Shihas, Ms. Anjitha, and Mr. Jerin for their love, friendship and support.*
- *Special thanks to Dr. Sudharshan and Mr. Rambabu my teacher for the inspiration.*
- *All my beloved teachers at every stages of my academic career.*
- *All students of organic chemistry section.*
- *All my friends at NIIST.*
- *CSIR & UGC for the financial assistance.*

I am deeply and forever indebted to my parents, my brother, my sisters and my friends for their constant source of love, inspiration and support.

I would like to thank my teachers and friends starting from my school days to those at NIIST, who motivated and blessed me.

S.Maniganda

CONTENTS

List of Schemes

List of Figures

List of Abbreviations

3T3-L1	Fibro blast cell lines
A375	Human melanoma cell lines
A549	Adenocarcinomic human alveolar basal epithelial cells
AcOH	Acetic acid
atm	Atmosphere
ADT	Anethole dithiolethione
$AlCl_3$	Aluminium chloride
AMLS	Etholedithiolethione loaded magnetic nanoliposome
APOP	Apoptosis
ATMP	Azido trimannose6-phospharamidite
Arg	Arginine
BBB	Blood brain barrier
BBr3	Boron tribromide
BC	Before Christ
BHQ	Black Hole Quencher
Boc	Butoxycarbonyl
BCE	Before Common Era
BTB	Blood–testis barrier
CathB	Cathepsin B
^{13}C-NMR	Carbon-13 nuclear magnetic resonance
$CDCl_3$	Deuterated chloroform
CD-MPR	Cationic -dependent mannose6-phophate receptor

$CHCl_3$	Chloroform
CH_3CN	Acetonitrile
CI-MPR	Cationic- independent mannose6-phophate receptor
cm	Centimeter
CMC	Critical micellization concentration
CO_2	Carbondioxide
CPPs	Cell-penetrating peptides
CS	Chitosan
CT	Computed tomography
$CuSO_4$	Copper(II) sulfate
d	Doublet
dd	Double doublet
DAPI	4′,6-Diamidino-2-phenylindole
DCM	Dichloromethane
DDS	Drug delivery system
DHFR	Dihydrofolate reductase
DIC	N,N'-Diisopropylcarbodiimide
DIPEA	N,N-Diisopropylethylamine
DLS	Dynamic light scattering
DMEM	Dulbecco's modified eagle's medium
DMF	Dimethyl formamide
DMSO	Dimethyl sulfoxide
DNA	Deoxyribonucleic acid

Dox	Doxorubicin
DPPH	2,2-Diphenyl-1-picrylhydrazyl
ε	Molar extinction coefficient
ECM	extracellular matrix
EDC	3-(dimethylamino)-propyl)-N′-ethylcarbodiimide
EGF	Epidermal growth factor
EGFR	Epidermal growth factor receptor
EPR	Enhanced permeability and retention
EDTA	Ethylene di amine tetra acetic acid
eq.	Equivalent
EtOAc	Ethyl acetate
FBS	Fetal bovine serum
FDA	Food and Drug Administration
$FeCl_3$	Ferric chloride
FITC	Fluorescein isothiocyanate
Fl	Fluorescein
FR	Folate receptor
FRAP	Ferric reducing ability of plasma
FRET	Fluorescence resonance energy transfer
G8	Dendron based octa-guanidinium
GFP	Green fluorescent protein
Gly	Glycine
GSH	Glutathione

GSSG	Glutathione disulfide
H_2O	Water
H_2S	Hydrogen sulphide
HATU	1-[Bis(dimethylamino)methylene]-1H-1,2,3-triazolo[4,5-b]pyridinium 3-oxide hexafluorophosphate
HBTU	(2-(1H-benzotriazol-1-yl)-1,1,3,3-tetramethyluronium hexafluorophosphate, Hexafluorophosphate Benzotriazole Tetramethyl Uronium)
HBr	Hydrobromic acid
HCl	Hydrochloric acid
HeLa	Cervical Cancer cell line
HER2	Human epidermal growth factor receptor2
HEPES	(4-(2-hydroxyethyl)-1-piperazineethanesulfonic acid)
HIV	Human immunodeficiency virus
HMPA	Hexamethylphosphoramide
HPLC	High performance liquid chromatogrphy
HRMS	High resolution mass spectrometry
HR-TEM	High-resolution transmission electron microscopy
Hz	Hertz
J	Coupling constant
λ	Wavelength
LDH	Lactate Dehydrogenase
Leu	Leucine
λ_{ε}	Excitation wavelength

Ln	Lanthanide
KBr	Potassium bromide
K_2CO_3	Potassium carbonate
KDR	kinase insert domain receptor
m	Multiplet
M^+	Molecular ion
M6P	Mannose6-phosphate
MALDI-TOF	Matrix-assisted laser desorption ionization-time of flight
mAbs	Monoclonal antibody
max	Maximum
MCF-7	Human breast cancer cell line
MDA-MD-231	Epithelial, human breast cancer cell line
MDR	Multiple drug resistance
mg	Milligram
$MgSO_4$	Magnesium sulfate
MHz	Mega hertz
min	Minutes
mL	Millilitre
mm	Millimeter
mM	Millimolar
mmol	Milli mole
MMP	Matrix metalloproteinases

Mol	Mole
MPLC	Medium pressure liquid chromatography
MRI	Magnetic resonance imaging
MSNPs	Mesoporous silica nanoparticles
MTT	3-(4,5-dimethylthiazol-2-yl)-2,5-diphenyltetrazolium bromide
MW	Molecular weight
m/z	Mass-to-charge ratio
N_2	Nitrogen gas
NA	Numerical aperture
NADPH	Nicotinamide adenine dinucleotide phosphate
$NaHCO_3$	Sodiumbicarbonate
$NaNO_2$	Sodium nitrite
NaOAc	Sodium acetate
Na_2SO_4	Sodium sulfate
NaCl	Sodium chloride
NaOH	Sodium hydroxide
NC's	Nanocubes
ng	Nanogram
NGF	Neural growth factor
NH_4Cl	Ammonium chloride
NHS	N-hydroxysuccinimide
NIR	Near-infrared
nm	Nanometer

nM	Nanomolar
NMR	Nuclear Magnetic resonance
NO	Nitric oxide
NPs	Nanoparticles
NSCLC	Non-small cell lung carcinoma
^{31}P-NMR	phosphorus 31p nuclear magnetic resonance
PABC	P-aminobenzyloxycarbonyl
PAI	Photoacoustic imaging
PBS	Phosphate buffered saline
PCB	Poly carboxybetaine methacrylate
PD	Pharmacodynamic
$Pd(OAc)_2$	Palladium acetate
PDPA	Poly (2-(diisopropylamino)ethyl methacrylate)
PDT	Photodynamic therapy
PEG	Poly(ethylene glycol)
PET	Positron Emission Tomography
Pgp	Plasma glyco protein
PGs	Prostaglandins
pH	Hydrogen ion concentration at logarithmic scale
Phe	Phenyl alanine
PI	Propedium iodide
PK	Pharmacokinetic
ppm	Parts per million

PPh_3	Triphenyl phosphine
PS	Photo sensitizer
PSA	Prostate specific antigen
PTT	Photothermal therapy
Ptxl	Paclitaxel
QDs	Quantum dots
QE	Quercetin equivalents
RES	Reticulo-endothelial system
RGD	Arg-Gly-Asp sequence
RNA	Ribonucleic acid
ROS	Reactive oxygen species
rpm	Revolutions per minute
RT	Room temperature
$	Dollar sign
s	Seconds
SERS	Surface-enhanced Raman scattering
siRNA	Small interfering Ribonucleic Acid
SKOV3	Ovarian Canccer cell line
SPR	Surface plasmon resonance
SPPS	Solid phase peptide synthesis
SPION	Superparamagnetic iron-oxide nanoparticles
T	Temperature
t	Triplet

TAT	transactivator of transcription
TDDS	Targeted drug delivery system
TEA	Triethylamine
THF	Tetrahydrofuran
TMS	Tetramethylsilane
US	United States
US	Ultra Sound
UV	Ultraviolet
µg	Microgram
µm	Micrometer
µM	Micromolar
$\boldsymbol{\nu}_{\mathbf{em}}$	Frequency of emission
$\boldsymbol{\nu}_{\mathbf{ex}}$	Frequency of excitation
WI-38	a diploid human cell strain composed of fibroblasts derived from lung tissue of a 3-months gestation female fetus

PREFACE

Cancer is one among the burning issues in human health that needs collective effort to successful combat and cure. Chemotherapy is the largely exploited treatment modality among others like surgery, radiation therapy and targeted molecular therapy etc., to treat cancer which off-course come-up with undesirable side-effects. Ongoing research interest on understanding the targeted drug delivery systems resulted an impressive array of molecularly targeted therapies that could be an efficient treatment against cancer. Chapter-1, covers the identification of appropriate cancer targets based on a detailed understanding of the molecular changes, possible mutations underlying with the overexpression of target proteins. This approach contrasts with the conventional, more empirical approach used to develop cytotoxic chemotherapeutics-the mainstay of cancer drug development in past decades. Mostly, the current progress in targeted therapy, and detailed focusing on the potential targets that are emerging. New design for drug delivery vehicles such as synthetic molecules and nano-carriers, which have so far proved to be a promising class to target the cancer cells or tissues leading to better treatment mortality. Therefore, the present challenges associated with these areas and opportunities to address long-standing problems and improve the future prospective also discuss in this chapter.

Delivery systems typically employ vehicles to carry therapeutics in order to improve the drug solubility, reduce toxicity, prolong circulating time, defined bio-distribution, achieve specific targeting, control drug release, and diminish immunogenicity. Chapter 2, encompasses the design and synthesis of lysosome targeted drug delivery system utilizing sorbitol scaffold linked to octa-guanidine to a peptide substrate of lysosomal cysteine cathepsin B. The major objective is to deliver the potential anti-cancer drug, doxorubicin (Dox) to the target sites efficiently, thereby minimizing dose-limiting toxicity. The targeted sorbitol carrier approach is promising, since it has advantage over free Dox which possesses dose-limiting toxicity, posing risk of injury to normal tissues.

For the third chapter which addresses, with anti-cancer evaluation of an active biomolecule Hydnocarpin (Hy) showed promoted moderate cytotoxicity in cancer cells. Consequently, the modified synthetic construct of Hy-dendron executed superior cytotoxicity preferentially on cancer cells followed apoptosis by caspases 3 mediated pathways with an anti-metastatic effect. While the intrinsic complexity of natural product based drug delivery

requires interdisciplinary approaches the transition of naturally occurring molecules to a drug candidate could be accomplished prior to legitimate engineering of potential leads.

Targeting with nano-carrier delivery system facilitate improved circulation with enhanced EPR effect which intern reach the target site and definitely show great promise in clinical development. Chapter-4 describes with the divergent effort of carbohydrate analogue of mannose-6-phosphate receptor targeted nano-carrier system with high drug loaded and multi-drug delivery properties towards breast cancer cells. This nanoparticles delivery system co-loaded with Dox and Resveratrol (Res) exerted maximum therapeutic effect. The anti-tumor activity of combined Dox and Res-loaded nano-carrier chemotherapeutic strategy is made in order to overcome the drawbacks of single Dox delivery systems.

In summary, a comprehensive understanding of the challenges and opportunities related to targeted delivery systems were presented. Chemotherapy in combination with other therapeutic modality including immunotherapy and alternative medicines (CAM) derived from certain natural products and / or semi-synthetic active analogues , and nano-encapsulated targeted delivery system have been discussed. One of the main focus has been explored towards the convergence of designed synthetic molecular entity with nano-carrier platform for the successful development of nanomedicine aiming to clinical potential for cancer therapy.

References

[1].**Maniganda, S.**;Sankar, V.; Nair, J. B.; Raghu, K. G.;Maiti, K. K. A lysosome-targeted drug delivery system based on sorbitol backbone towards efficient cancer therapy, *Org. Biomol. Chem*,2014, 12, 6564.

[2].Mathai, B. M.; Joseph, M.M.; **Maniganda, S.**; Nair, J. B.; Arya, J.S, Karunakaran, V.; Radhakrishnan, K. V.; K. Maiti, K.K. Guanidinium Rich Dendron- Appended Hydnocarpin Executes Superior Anti-Neoplastic Effects Through Caspase Mediated Apoptosis, *RSC Adv*, 2016,6, 52772.

[3]. **Maniganda, S.**; Vishnupriya,M.;Maiti, K. K. Investigation of Multifunctional Targeted Nano-carrier for Stimuli-responsive Co-delivery of Doxorubicin and Resveratol in Breast Cancer cells,2019, Manuscript under preparation.

Chapter -1

Current Trends in Targeted Drug Delivery Systems for Cancer Management

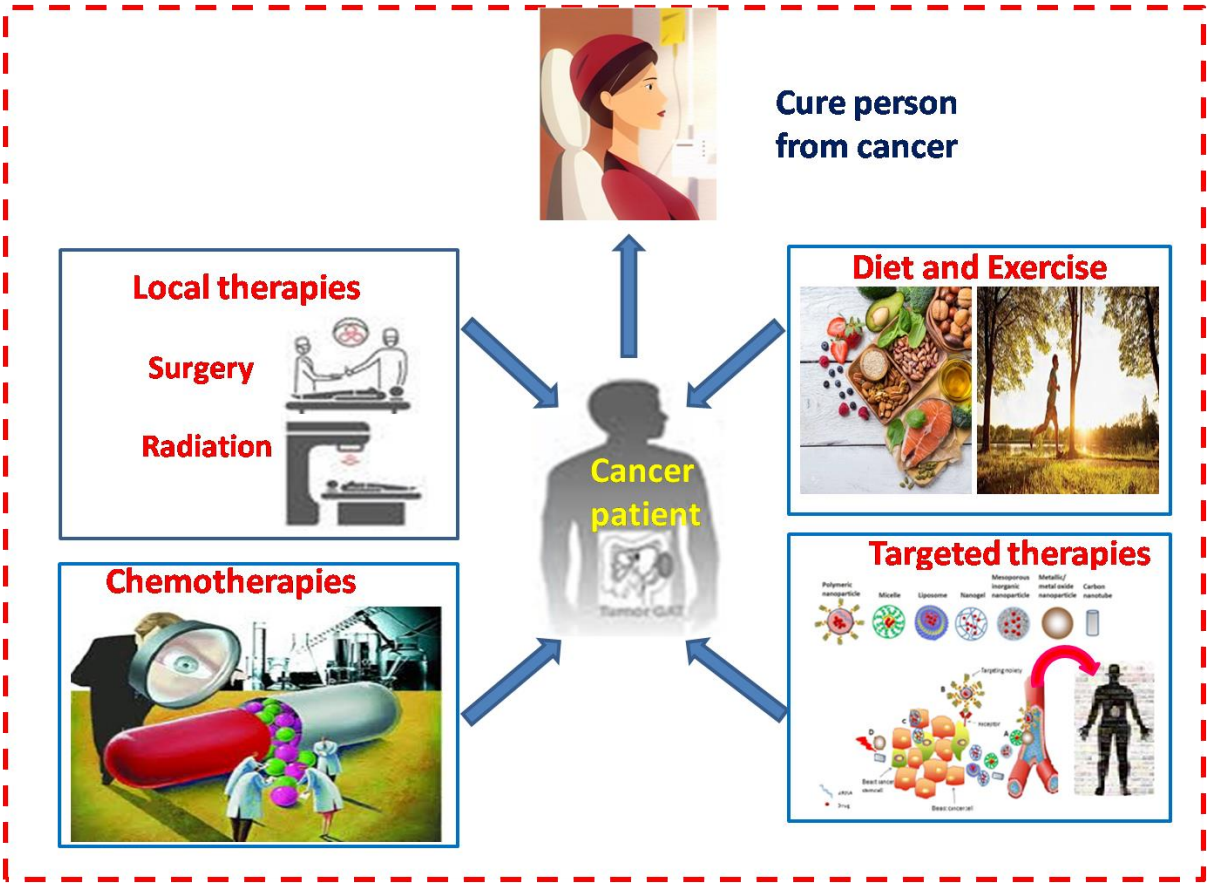

1.1. Abstract: The limitations exist to the conventional chemotherapy mainly due to its poor bioavailability, high-dose requirements, low therapeutic indices, development of multiple drug resistance, and non-specific targeting. Targeted drug delivery systems (TDDS) hold greater promise in terms of efficacy and safety for the delivery of a proven therapeutic agent with a negligible effect in healthy cells and high affinity to tumor cells. This chapter highlights the recent achievements with appropriately designed drug delivery vehicles such as synthetic molecular carrier and nanocarrier in targeted cancer therapy. Specifically, the major breakthroughs in theranostics where combined therapeutic effects monitored by diagnostic modalities step forward towards potential use in personalized medicine including cancer chemotherapy. Despite promising development of TDDS witnessed in the field of nanomedicine having multiple targeting motifs especially in forms of peptide, protein and

monoclonal antibodies conjugated to synthetic/nanocarriers. Therefore, the scope of this chapter unfolds numerous drug delivery carriers including nanocarriers towards cancer therapy and also extended further to targeted strategies with combination of targeting motifs. It is also anticipated to multi-component therapeutic modality and their accurate delivery towards target site which will be an emerging next-generation platform for anti-cancer drug delivery.

1.2. Progress with drug developments in cancer therapy

In a historical report written by Edwin Smith Papyrus, an ancient Egyptian, described about the earliest exposition of breast cancer approximately 3000 B.C. Another evidence of human bone cancer was found in mummies in ancient Egypt and in ancient manuscripts dated about 1600 B.C.[1] Origin of the word cancer dates back from a Greek word karkinos to describe carcinoma tumors by a physician Hippocrates (460–370 B.C.E.). The world's oldest recorded case of breast cancer hails from ancient Egypt in 1500 B.C. and it was recorded that there was no treatment for cancer except palliative care.[2]

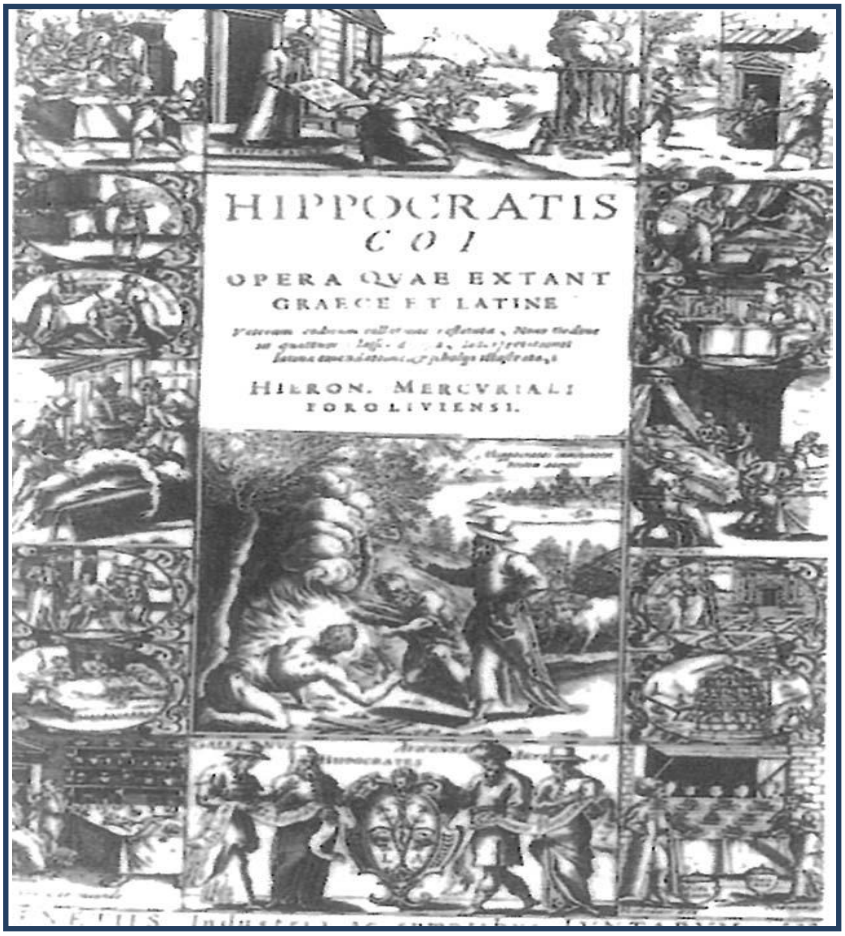

Figure 1.1. Diagram showing one of the historical evidence writings of Hippocrates printed in Venice in 1588.

Eventually, the first studies between tumors and their microenvironment was performed in 1863 by Rudolph Virchow, who observed that leukocyte infiltration was characterization of solid tumors.[3] Consequently, Pagetis recognized the tumor microenvironment concept.[4] Till 1980's cancer research was dominated by a tumor-centric perspective suggesting that mutations in oncogenes and tumor suppressor genes were sufficient to determine carcinogenesis and actively influences progression in cancer.[5] Accordingly, cancer is one among the most life-threatening diseases in the world and responsible for one in eight deaths worldwide. It encompasses more than 100 distinct diseases with diverse risk factors and epidemiology which originate from most of the cell types and organs of the human body and are characterized by relatively unrestrained proliferation of cells that can invade beyond normal tissue boundaries and metastasize to distant organs.[6] Numerous advances have been made in developing new technologies for cancer diagnosis and therapy which has contributed to the continuous decline in the cancer death rate over several decades.[7] However, the limits of the current "one-size-fits-all" diagnostic and therapeutic strategies for treatment of this deadly disease has heralded the need for "personalized medicine" approaches.[8] One of the advance to this goal is to verify the patient's geneticin formation and then conduct treatment with minimal delay after diagnosis.[9] While genotyping technologies such as polymerase chain reaction can be employed to identify genetic information and select treatment methods for individual patients, theranostics-based strategies, which combine diagnosis and targeted therapy, can be utilized to treat the diseases and diagnose continuous changes in the patient's disease state simultaneously. Therefore, theranostics is expected to promote the personalized medicine that enables to improve the pharmacokinetics, reduce the side effects and react immediately to the progress of diseases and conditions of patients by monitoring the therapeutic responses in real-time.[10] Now the entire processes for discovery and development of a potential drug is an expensive, demanding task and candidate to its delivery into the human body takes an average of 10-15 years and cost around US$1.6 - 2.0 billion per drug.[11,12] The general processes of involving drug discovery has a long and strenuous process from the initial stage of laboratory bench to clinical trials and eventually to the entry of drugs into the market launching. This drug delivery activity contains the drug's chemical formulation, medical devices or drug-device combination products. The concept of drug delivery is deeply blended with dosage form and route of administration. Medications can be taken through multiple routes such as non-invasive oral (through the mouth), topical (skin), transmucosal (nasal, buccal/sublingual, vaginal, ocular and rectal), carrier-based, inhalation or intravenous injection routes. The drug

delivery systems are engineered technologies for site-targeted delivery and/or controlled discharge of therapeutic agents.[13,14] Present-day efforts in the area of drug delivery include (1) the growth of site-targeted delivery, in which the drug is only active in the specific target area of the body and (2) constant release formulations, in which the drug is discharged over a period of time in a controlled manner from a formulation. Different kinds of constant release formulations exist that include liposomes, proliposomes, microspheres, gels, prodrugs, cyclodextrins, drug-loaded biodegradable microspheres (nanoparticles) and drug-polymer conjugates.[15] Therefore, the discovery of novel anticancer drugs is critical for pharmaceutical research and development, and patient treatment of anticancer drugs, which may contribute to the systematic discovery of new anticancer drugs. Around, 150 anticancer drugs have been approved by FDA from 1949 to 2014 (**Table1.1**) which is known to hold important roles in successful cancer treatment and novel anticancer drug development. These drugs can be broadly classified into two basic categories, cytotoxic and targeted agents based on their mechanisms of action. Most of the cytotoxic drugs are alkylating agents, anti-microtubule agents, topoisomerase inhibitors while most of the targeted drugs belong to signal transduction inhibitors, gene expression modulators, apoptosis inducers, hormone therapies, and monoclonal antibodies.[16,17]

Table 1.1. Summary of some FDA-approved anticancer drugs

Anticancer Drug	Approval year	Therapeutic class	Targeting gene	Delivery type
Mechlorethamine	1949	Lung cancer; Leukemia; Lymphoma	DNA synthesis	Single
Methotrexate	1953	Leukemia; Breast cancer; Head and neck cancer; Lung cancer; Lymphoma; Bone cancer; Gestational trophoblastic disease	DHFR Both	Single
Chlorambucil	1957	Leukemia; Lymphoma	DNA synthesis	Single
Vinblastinesulfate	1965	Lymphoma; Testicular cancer; Choriocarcinoma; Breast cancer	TUBA1A; TUBB; TUBD1; TUBE1; TUBG1	Combination
Doxorubicin hydrochloride	1974	Leukemia; Breast cancer; Stomach cancer; Lymphoma; Ovarian cancer; Lung cancer; Sarcoma; Thyroid cancer; Bladder cancer; Kidney cancer	TOP2A; DNA synthesis	Single
Cisplatin	1978	Testicular cancer;Ovarian cancer; Bladder cancer	DNA synthesis	Both
Etoposide	1983	Testicular cancer;Lung cancer;	TOP2A; TOP2B	Combination

Carboplatin	1989	Ovarian cancer	DNA synthesis	Both
Paclitaxel	1992	Breast cancer; Lung cancer; Pancreatic cancer; Ovarian cancer; Sarcoma	TUBA4A; TUBB1	Both
Docetaxel	1996	Prostate cancer; Breast cancer; Head and neck cancer; Stomach cancer; Lung cancer; Brain cancer	TUBA4A; TUBB1	Both
Imatinib mesylate	2001	Leukemia; Stomach cancer	BCR-ABL	Single
Mitomycin	2002	Stomach cancer; Pancreatic cancer	DNA synthesis	Both
Hydroxyurea	2010	Melanoma; Leukemia; Ovarian cancer; Head and neck cancer	RRM1	Single
Cabozantinib	2012	Thyroid cancer	KDR; MET; RET	Single
Nivolumab	2014	Melanoma	PDCD1	Single

1.3. Conventional and targeted delivery for treatment of cancer

The present cancer treatment option includes surgical intervention, chemotherapy, and radiation therapy or a combination of these options. Conventional chemotherapeutic agents works primarily by interfering with DNA synthesis and mitosis, leading to the death of rapidly growing and dividing cancer cells. However, these practices are non-selective and can also damage healthy normal tissues, causing severe unintended and undesirable side effects like loss of appetite, nausea, vomiting, diarrhoea, abdominal cramps and constipation, anemia, fatigue, hyperthermia, loss of hair etc. Additionally, as the bio-accessibility of these drugs to tumor tissues is relatively poor, higher doses are required, leading to elevated toxicity in normal cells and an increased incidence of multiple drug resistance. Current treatment options are highly inadequate in addressing this problem and to overcome some limitations of conventional non-targeted approaches. There are generally two types of drug targeting motifs to deliver therapeutic cargos with improved therapeutic efficacy.[18] The passive targeting is based on enhanced permeability and retention (EPR) effect caused by leaky vasculature and poor lymphatic drainage. The EPR effect is a unique phenomenon, by which macromolecules and nanoparticles escape from the blood flow and preferentially accumulate more in tumors rather than in normal tissues. It occurs frequently in solid tumors,

in which blood vessels commonly have defects. Additionally, defective lymphatic drainage leads to the loss of the ability to clear infiltrating substances. These distinguishing anatomical and pathophysiological characteristics of solid tumors have been generally utilized in tumor targeting.

On the other hand, active targeting is based on targeting moieties such as ligands and antibodies. These targeting methods are different from mechanistic or direct targeting strategies that employ monoclonal antibodies (mAbs) or small-molecule compounds to bind to surface proteins or to interfere in biochemical pathways that are up regulated in cancer.[19,20] Unfortunately, many mechanistically targeted chemotherapeutic agents have limitations such as toxicities to the heart, skin, and gastrointestinal tract,[21] low accumulation in tumor lesion,[22] and resistance in cancer cells.[23]Active targeting of anticancer therapeutics may increase their affinities and endocytic internalization in tumors.[24,25] These linked targeting moieties may selectively bind to surface molecules (proteins, sugars, or lipids), perturbing tumor accumulation and residence time.[26–28] Indeed, many of the small molecules in mechanistic and direct targeting have been used either as delivery agents (e.g., probestin for CD13) or cargos in active targeting. Despite tremendous efforts made towards discovering novel materials and biomolecule markers for TDDS, very few of them are truly specific after intravenous injection and the targeting still remains chance-dependent. Both active and passive targeting approaches require exogenous drug vehicles to disperse and voyage in circulation for a long time to passthrough the leaky vasculature or detect the surface markers. However, the circulating environment, in which many drug vehicles cannot have a long enough circulating time to achieve targeted binding, is extremely complicated.[29,30] In addition, the human body has an innate defence mechanism for invasion. For example, the reticuloendothelial system (RES) rapidly recognizes foreign bodies and destroys them via a series of biological processes. The RES, also called the mononuclear phagocyte system, comprises primarily of bone marrow progenitors, blood monocytes, and tissue macrophages.[31] Furthermore, the EPR effect is somehow heterogeneous in the tumor microenvironment and varies among patients. For example, hypoxic regions of solid tumor generally do not even exhibit EPR effects because of poor angiogenesis.[32,33] Considering the complexity and sophistication of *in vivo* conditions, conventional passive and active targeting strategies still remain inadequate. Hence, developing novel TDDS with truly specific targeting is a formidable challenge for modern medicine and nanotechnology (**fig 1.2**).

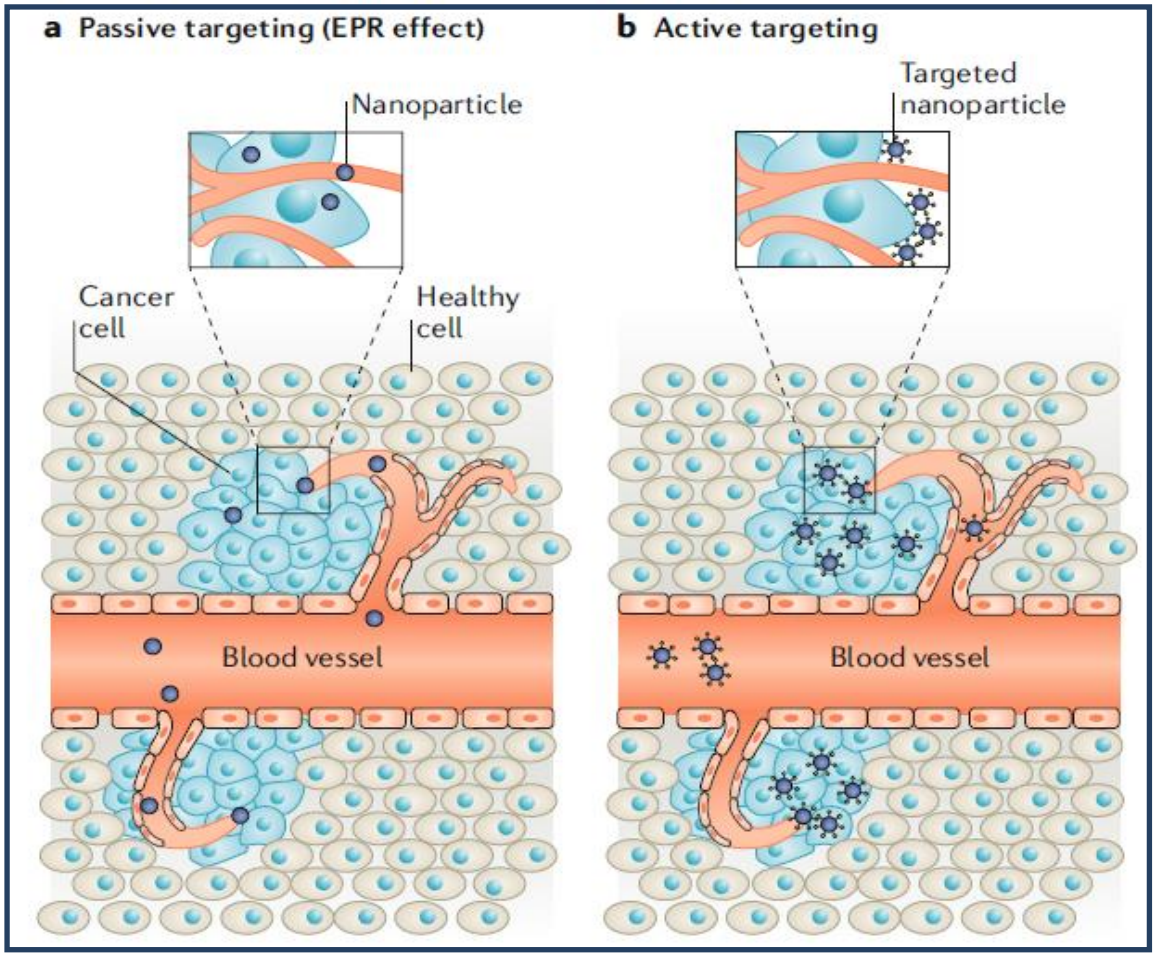

Figure 1.2. Targeted drug delivery to tumors. a) Passive targeting of nanomedicines is accomplished by virtue of their ability to extravasate out of the leaky tumor vasculature in combination with ineffective lymphatic drainage, also known as the enhanced permeability and retention (EPR) effect. b) Active targeting is realized by functionalizing nanomedicines with targeting ligands that recognize tumor cell markers to increase cell specificity and uptake.

1.4. Targeted delivery: Stimuli responsive pathway of drug release

Stimuli responsive target-specific delivery of therapeutic agents are based on either endogenous (pH, redox, enzyme) or exogenous stimuli (temperature, acoustic, light) as shown in **fig 1.3**. The major development of stimuli responsive drug delivery systems is to minimize systemic toxicities, unfavourable drug-plasma interactions and appropriate dose to treat disease more efficiently.

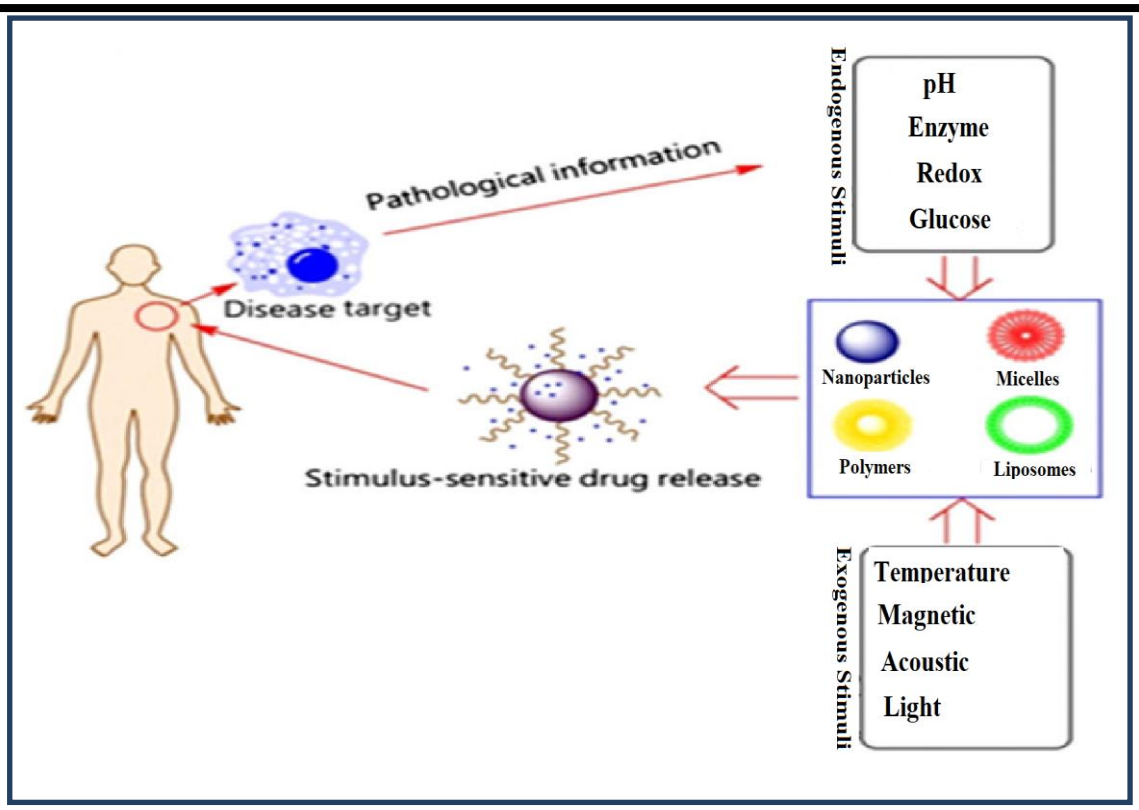

Figure 1.3. Schematic illustration of stimuli-responsive DDS

1.4.1. Drug release through endogenous triggering

To enhance the physicochemical properties of polymeric nanoparticles (NPs) and to incorporate targeting therapeutic agents into their design has allowed new generations of controlled-release polymeric NPs to navigate the complex and chemically rich *in vivo* environment. With improvements in the understanding of biological processes in diseased states, the design of controlled-release polymeric NP drug delivery systems has evolved from classical release mechanisms to the utilization of local biochemical changes in various disease states to trigger and activate drug release. In diseases such as cancer, an inevitable shift in homeostatic chemical equilibrium occurs, such as amplified or triggered enzymatic activity, a change toward acidic pH, reductive or oxidative states, or an increase in reactive oxygen species.[34] These differential biochemical signatures can be exploited for the development of more precise therapies and offer substantial opportunity for polymer design, rendering further control over the site-specificity and kinetics of drug release.

1.4.1.1. pH-Responsive drug release

Tumor exists in an acidic environment and endosomes can be harnessed in the design of stimuli-sensitive targeted DDS.[35,36] An example, all cell penetrating peptides (CPPs) contain

lysine residues; their primary amines are the main cause of the nonspecific interactions, but they also play a key role in their membrane transduction and nuclear localization functions. Some β-carboxylic amides are stable at neutral pH but quickly hydrolyze at acidic pH to regenerate the corresponding amines. Once in the acidic tumor interstitial stimuli (pH < 7) or cell endo/lysosomes (pH 4-5), the acid-labile amides would be hydrolysed, activating the CPPs and exposing their functions. This strategy would enable CPPs to be used in various *in vivo* applications particularly in delivery systems.[37]

The stimulus sensitivity of PEG coatings can enable the preparation of nanoparticle drug delivery systems (NDDSs) with functions that are unveiled and activated only after the PEG molecules are detached. The use of ester and hydrazone moieties between the PEG moieties and NDDSs (which are stable at a neutral pH, such as in the blood, but hydrolyse at a pH of 6 or below) eliminates the protective effect of PEG during internalization by the target cell but also enables prolonged circulation in the blood. PEG is removed once the NDDS is inside the acidified targets. PEG was detached from pH sensitive PEG–hydrazone-phosphatidylethanolamine-based micelles and liposomes at lower pH values, resulting in a cellular uptake that is similar to that of PEG-free NDDSs (**fig 1.4**).[38,39]

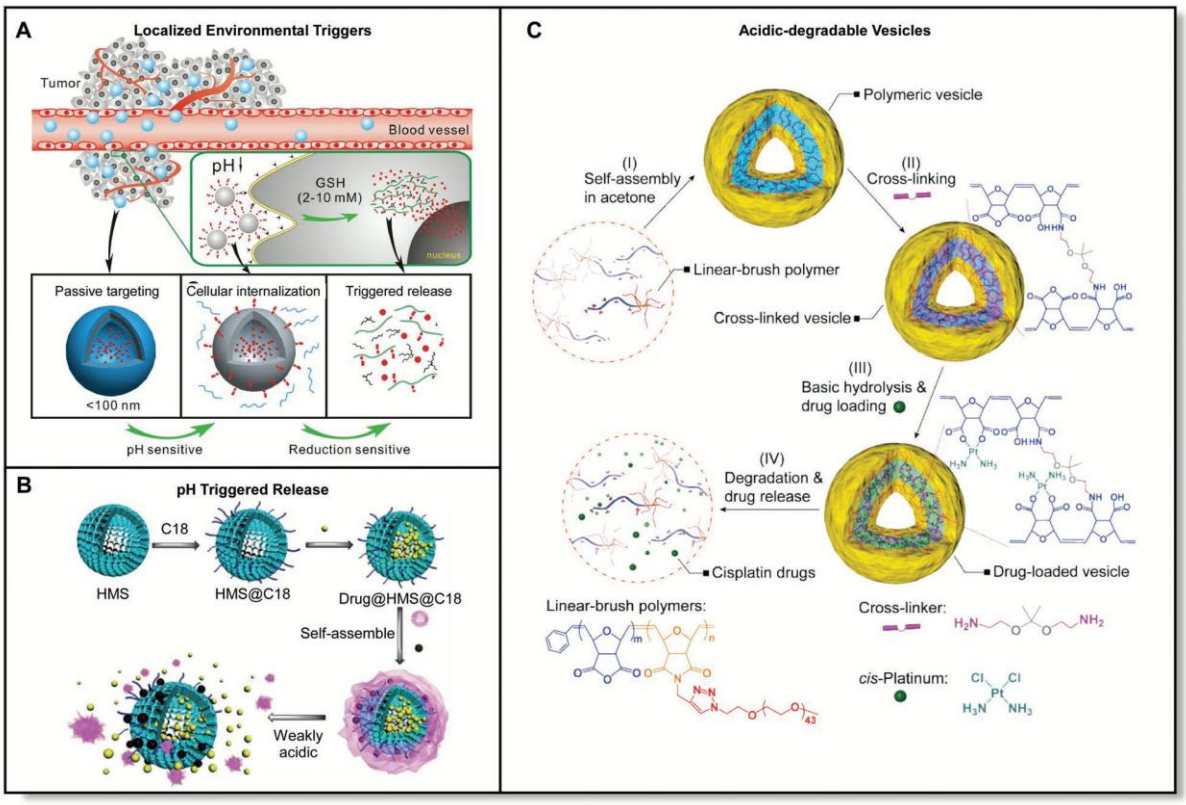

Figure 1.4. Schematic representation of pH responsive DDS. A) Localized regions throughout diseased tissue can be exploited for selective uptake of polymer vesicles and triggers for drug delivery. B) Controlled release of anticancer therapeutics from nanoparticles due to localized weakly acidic pH conditions. C) Acid-degradable polymers for the release of anticancer drugs.

1.4.1.2. Enzyme-responsive drug release

Enzymes play critical roles in the progression and spread of cancer, as they are involved in the processes of cancer cell growth, angiogenesis, and metastasis among others. This importance makes them suitable targets for therapeutic and diagnostic purposes.[40,41] There are many unique aspects of tumor physiology and pathology that can be utilized for targeting and treatment. Enzyme-catalyzed drug release has many advantages, owing to their high efficiency, selectivity, and specificity, which can be achieved under mild physiological conditions. A wide variety of enzyme classes are overexpressed in tumor microenvironments, such as proteases, lipases, oxidoreductases and phosphatises which serve as potential targets for using cancer therapy and imaging enzymes like cathepsins, matrix metalloproteinases (MMP), caspases and urokinases are extensively employed.[42,43] With a specific protease in mind, responsive drugs and imaging probes can be designed for that target to increase selectivity and efficacy. It is interesting to note that currently most of the existing examples involve responsive elements to one specific enzyme type, while, future developments definitely explore with the incorporation of multi-enzyme-based cascade reactions that can target the release of drugs in a more controlled manner (**fig 1.5**).

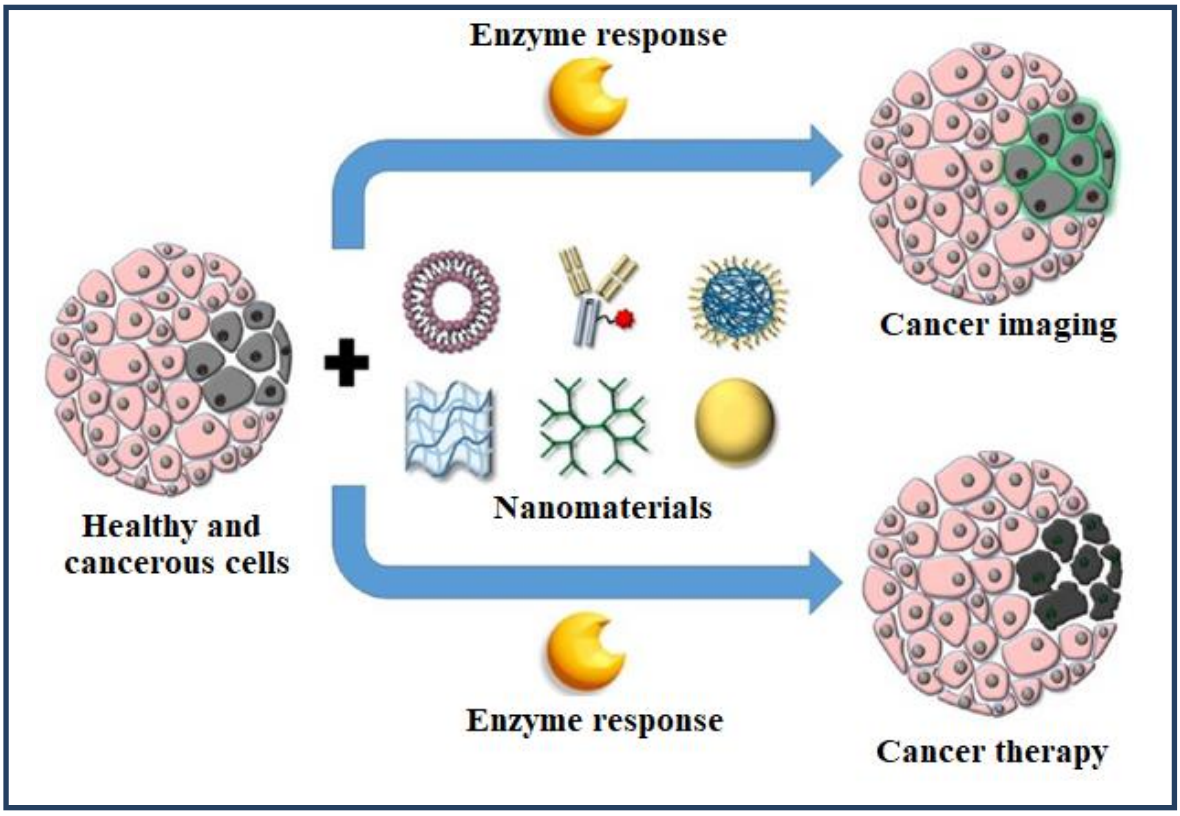

Figure 1.5. Illustration of tissues containing healthy (pink) and tumor (gray) cells can be treated with various nanomaterials, such as (from left to right) liposomes, protein-conjugates, polymeric nanoparticles, hydrogels, dendrimers, and inorganic metal nanoparticles, to deliver imaging agents or anticancer drugs with improved selectivity to tumor cells by incorporation of protease-responsiveness into the design of nanomaterials.

The MMP-2 cleavable peptide sequence GPLGVRG is placed between poly (ethylene glycol) and diethylenetriamine-modified poly-(aspartamide) to produce the di-block copolymer PEG227-GPLGVRG-PAsp(DET) (**fig 1.6**). This polymer is complexed with DNA to form polyplexmicelles. Upon MMP-2 cleavage in tumors, the PEG shell layer was shed, which revealed a positive surface for interaction and uptake into cancer cells, respectively. Another recent example of a cathepsin-responsive nanomaterial system is developed by Cui and co-workers, comprising of molecular probes that self-assembles into a supramolecular structure called nanobeacons. Their nanobeacons are comprised of hydrophobic and hydrophilic domains, where the amphiphilic nature helps to induce the self-assembly of the probes into core-shell micelles in aqueous environments. The hydrophobic domain consists of a fluorescent green dye, 5-carboxyfluorescein (5-FAM) and a black hole quencher, BHQ-1, whereas the hydrophilic domain consists of an HIV-1 derived cell-penetrating peptide sequence, Tat48−60, where the charged residues allow the nanobeacons to be responsive to changes in pH. The fluorophore and quencher are held in close proximity for fluorescence

resonance energy transfer (FRET) by a cathepsin B (CatB) cleavable linker (GFLG sequence). The imaging modality is contained within the nanobeacon after spontaneous assembly into micelles and thus protected from CatB cleavage, until the nanobeacons are converted back to their monomeric form by pH or dilution to below its critical micellization concentration (CMC). Then anobeacons proved effective after incubation with MCF-7 human breast cancer cells *in vitro*, where confocal imaging and flow cytometry showed localization of the fluorescence signal in lysosomes and an increasing signal over time.[44]

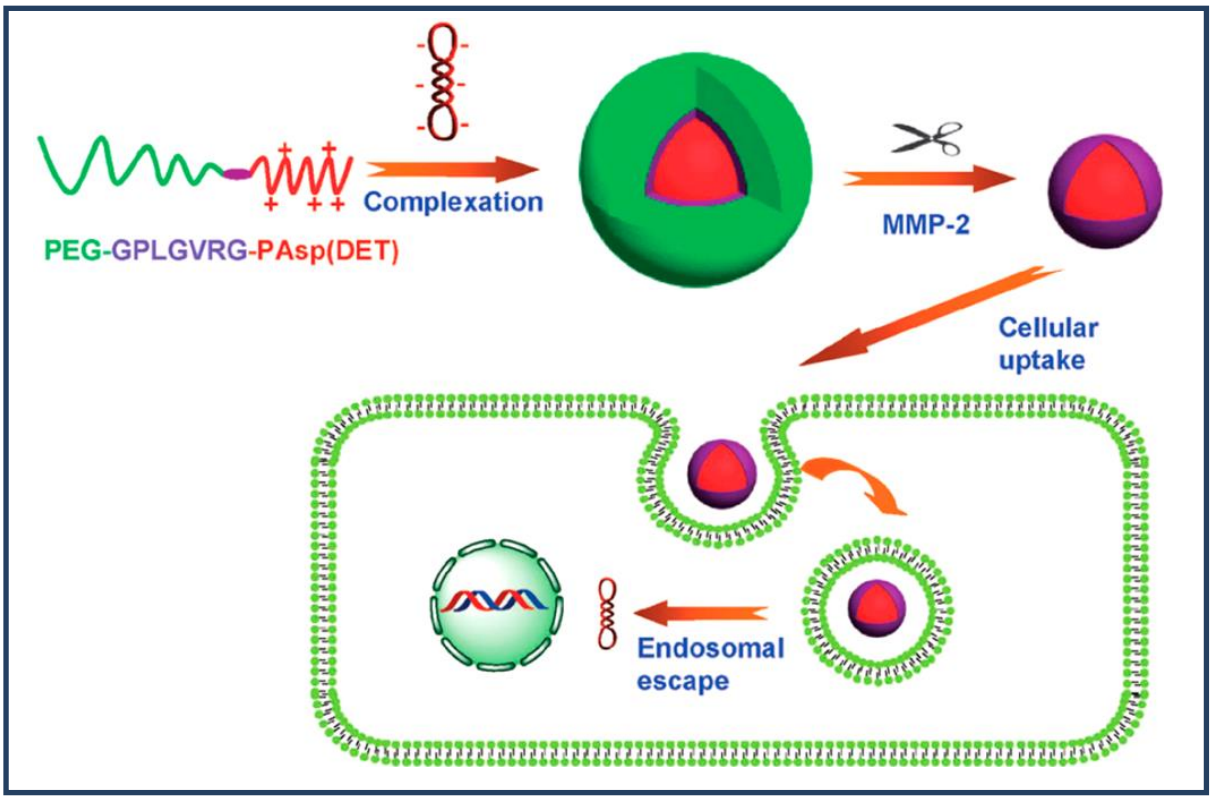

Figure 1.6.PEG-sheddable micelle polyplexes responsive to MMP-2 leading to enhanced cellular uptake and endosomal escape for gene therapy.

1.4.1.3. Redox-responsive drug release

Glutathione tripeptide (γ-glutamyl-cysteinyl-glycine, GSH) is a common biological reducing agent and controls a variety of cellular processes including cell differentiation, metabolism, antioxidant defence and balancing carcinogenicity. Moreover, GSH plays a critical role in maintaining detoxification and anti-oxidation equilibria of many cellular functions through which neutralization of ROSs in conjunction with its conversion from a reduced to oxidized form (glutathione disulfide, GSSG). GSSG is readily reduced by the enzyme GSH reductase. However, GSH deficiency or overexpression causes dysfunction of related cellular processes, which results in a high level of oxidative stress. In body fluids like blood and extracellular

matrices as well as on the cell surface, proteins are rich to stabilize disulfides as a result of a relatively high redox potential due to low concentrations of GSH (ca. 2−20 μM). In contrast, GSH inside cells is about 2−10 mM based on reduction by nicotinamide adenine dinucleotide phosphate (NADPH) and GSH reductase, maintaining a highly reductive environment. Moreover, the amount of GSH is at least 4 times higher in tumor tissues than in normal tissues owing to the proliferation of tumor cells, leading to the more reductive environment of tumors compared to the normal tissues. Li et al. synthesized hyaluronic acid−deoxycholic acid (HA-ss-DOCA) conjugates for redox-sensitive release of paclitaxol (Ptxl), and micelles formed from this conjugate were shown to disassemble in the presence of 20 mM glutathione (**fig 1.7**). Both in vitro toxicity studies with MDA-MB-231cells and *in vivo* xenograft tumor experiments confirmed differential and enhanced therapeutic efficacy.[45]

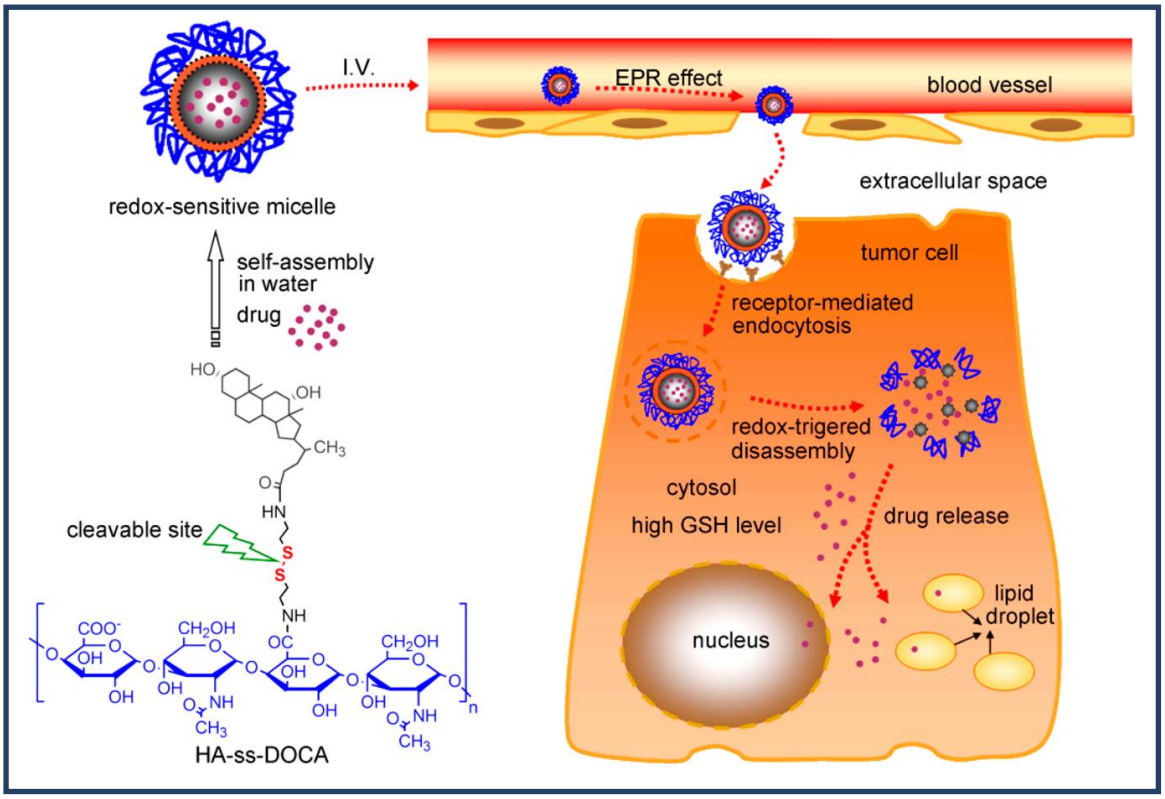

Figure 1.7. Illustration of self-assembly of reduction-responsive drug-loaded HA-ss-DOCA into redox-sensitive micelles, their intracellular trafficking pathway, and drug release. The cleavage of the disulfide bond in the intracellular reducing environment results in disconnection of pendant DOCA groups and disassembly of HA-ss-DOCA micelles, releasing the drug in the cytoplasm.

1.4.2. Drug release through exogenous triggering

The drug-delivery systems can take advantage of externally applied stimuli, including temperature changes, magnetic fields, ultrasounds, light and electric fields (**fig 1.8**). Therefore, controlled activation or release of prodrugs can be achieved using exogenous

stimuli, which have high potential for clinical applications with reduced systemic toxicity and side effects.

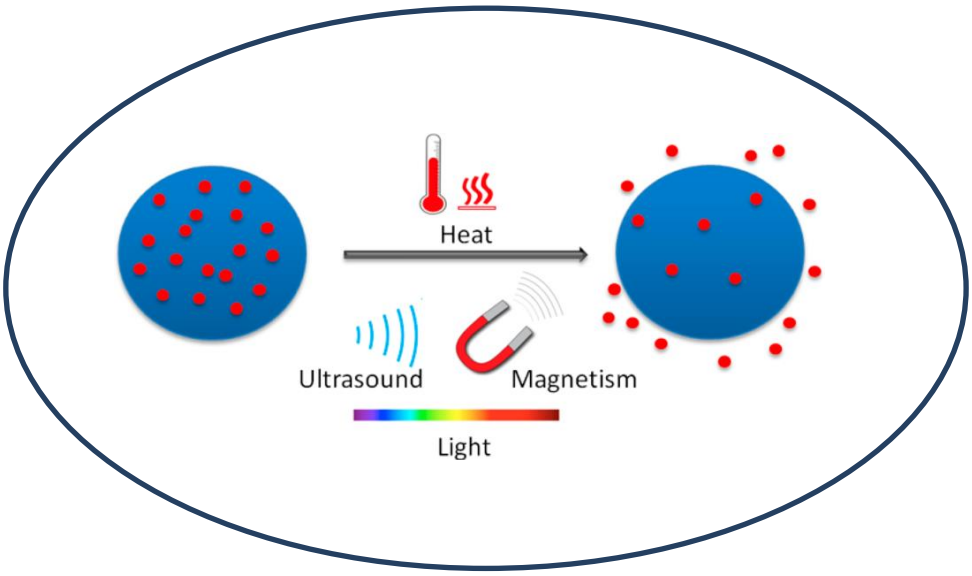

Figure 1.8. Illustration of exogenously triggered drug release by stimuli such as heat, ultrasound, magnetic energy and light.[46]

1.4.2.1. Thermoresponsive drug release

In the late 1970s attempts have been made in using thermosensitive liposomes for smart DDS based on a temperature-responsive mechanism. Thermoresponsiveness is usually governed by a nonlinear sharp change in the properties of at least one component of the nanocarrier material with temperature. Such a sharp response triggers the release of the drug following a variation in the surrounding temperature. Ideally, thermosensitive nanocarriers should retain their load at body temperature (~37°C), and rapidly deliver the drug within a locally heated tumor (~40–42°C) to counteract rapid blood-passage time and washout from the tumor. Temperature differences between normal and tumor tissue have also been used to diagnose early-stage tumors and malignancy.[47-49] Besides these intrinsic temperature variations, larger temperature changes can be induced artificially at specific locations by applying heat from an external source. This formed the basis for hyperthermia treatment, which exploits the higher sensitivity of tumor tissues to high temperatures as compared to normal tissues.[50] According to the National Cancer Institute of the NIH, "hyperthermia is a type of cancer treatment in which body tissue is exposed to high temperatures (up to 45°C) to damage and kill cancer cells".[51] Both intrinsic tumor temperature variations and externally induced hyperthermic temperature changes offer attractive stimuli for the site-specific delivery of chemotherapeutic agents. Thermoresponsive systems are generally liposomes, or polymer micelles or

nanoparticles (usually poly (*N*-isopropyl acrylamide), PNIPAM) that exhibit a lower critical solution temperature. For liposomes, thermoresponsiveness usually arises from a phase transition of the constituent lipids and the associated conformational variations in the lipid bilayers. *In vivo*, heat is generally applied by using temperature-controlled water sacks, radiofrequency oscillators or miniature annular-phased array microwave applicators.

1.4.2.2. Magnetic field responsive drug release

The privilege of using a magnetic field relies on the different nature of the magnetic response which is advantageous in the drug delivery pathway. Furthermore, there is a possibility of performing magnetic resonance imaging to associate with diagnosis and therapy within a single system (the so-called theranostic approach). For example, super paramagnetic ironoxide nanoparticles (SPIONs) can be loaded into nanocarriers such as liposomes, micelles or solid nanoparticles together with drugs and can increase drug localization in tumors under exposure to a magnetic field. Another example demonstrated the application of liposomes co-loaded with methotrexate and SPION localized to tumors in mice. NDDSs containing SPIONs and a taxane drug could be additionally modified with PEG for longevity or with antibodies for tumor targeting.[52,53]

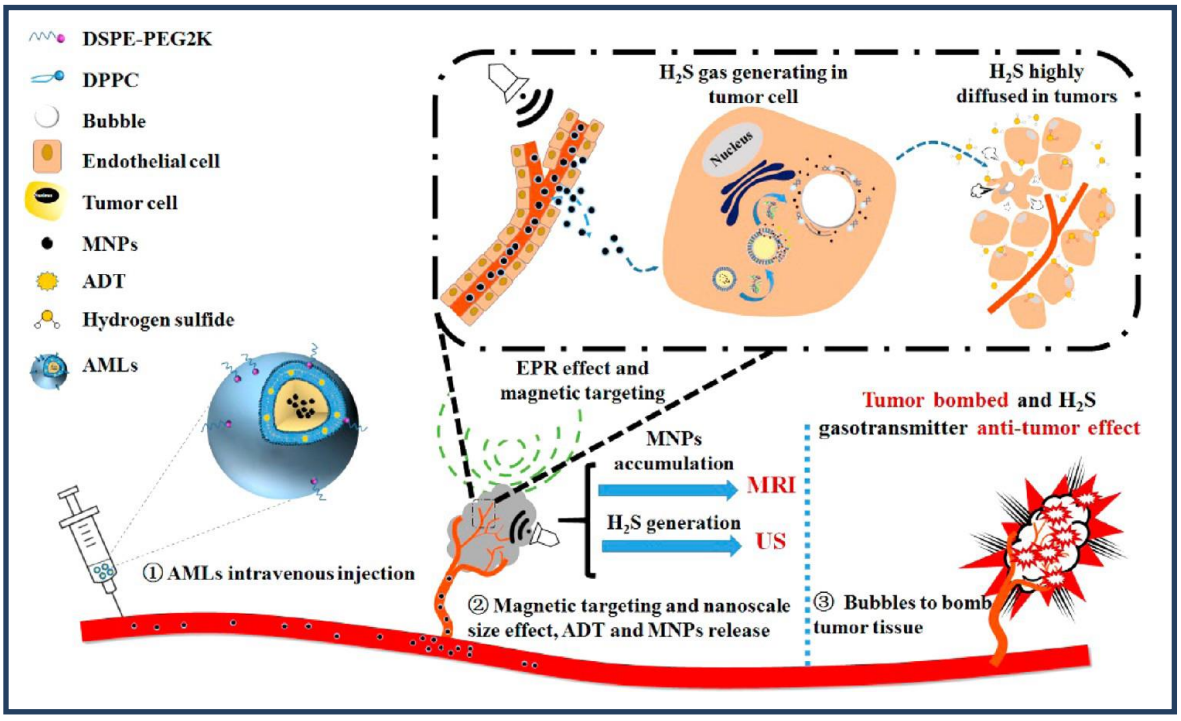

Figure 1.9. Concepts and schematics of AMLs and their nano to micro conversion for US/MR dual modal imaging and the spatiotemporal bombed combination tumor therapy.

As shown in **fig 1.9**, such a nano to micro size change enables an anethole dithiolethione (ADT) loaded magnetic nanoliposome (AMLs) to be localized within the tumor microenvironment, preventing their washout. Simultaneously, real-time ultrasound (US) imaging can be used to determine the dynamic H_2S microbubble production process. Moreover, guided by microbubble- enhanced US imaging, the H_2S microbubbles acting like an intratumoral bomber could explode to ablate the local tumor tissue when applying a higher acoustic intensity for bubble cavitation. The burst of microbubbles and the diffusion of intratumoral high concentration of H_2S molecules in the deep tumor region may synergistically enhance the antitumor effect.[54] Therefore, the unique feature of *in situ* microbubble generation ensures that AMLs could provide significant contrast enhancement in magnetic resonance and US dual modal imaging. As a synergistic "Trojan Horse" like bomber, H_2S gasotransmitter antitumor agents further strengthen tumor ablation efficiency.

1.4.2.3. Light-responsive drug release

The advantage of nanocarriers undergoing physical or chemical changes in response to light irradiation are attractive for designing safe treatment regimens that offer spatiotemporal control over the release of encapsulated therapeutic payloads. Generally, two main strategies are used to design light-responsive metallodrugs: (i) direct photo activation of prodrugs through photo induced structural changes to form bioactive species, either metal complexes or free ligands; (ii) generation of toxic ROS through irradiation of photosensitizers to induce cell death. The second strategy is known as photodynamic therapy (PDT) and is currently used in the clinic for cancer treatment.[55] However, PDT is effective only in the presence of oxygen for current clinical sensitizers, which may limit the biological utilization since the cancer cells are usually deficient in oxygen. The light-responsiveness can be regulated by optimizing the light wavelength, intensity, or exposure time. Although all of the light in ultraviolet, visible, and near-infrared (NIR) regions can serve as triggers for metallodrugs, only NIR light possesses excellent tissue penetration and is thus more suitable for use *in vivo*.[56,57] Photolabile caging groups have been exploited for the light-activated assembly of proteins. Lipid vesicles loaded with caged DNA and with the reacting and enzymatic components needed for transcription and translation enabled, upon local ultraviolet irradiation-mediated DNA uncaging, the activation of green fluorescent protein and the synthesis of enzymatically active luciferase (**fig 1.10a**). Light-to-heat transduction mediated by NIR irradiation of gold nanorods caused a rapid rise in the local temperature, which was exploited to induce dehybridization of DNA helices conjugated at the gold surface, allowing

the release of doxorubicin molecules bound to consecutive cytosine–guanine base pairs (**fig 1.10b**).[58]

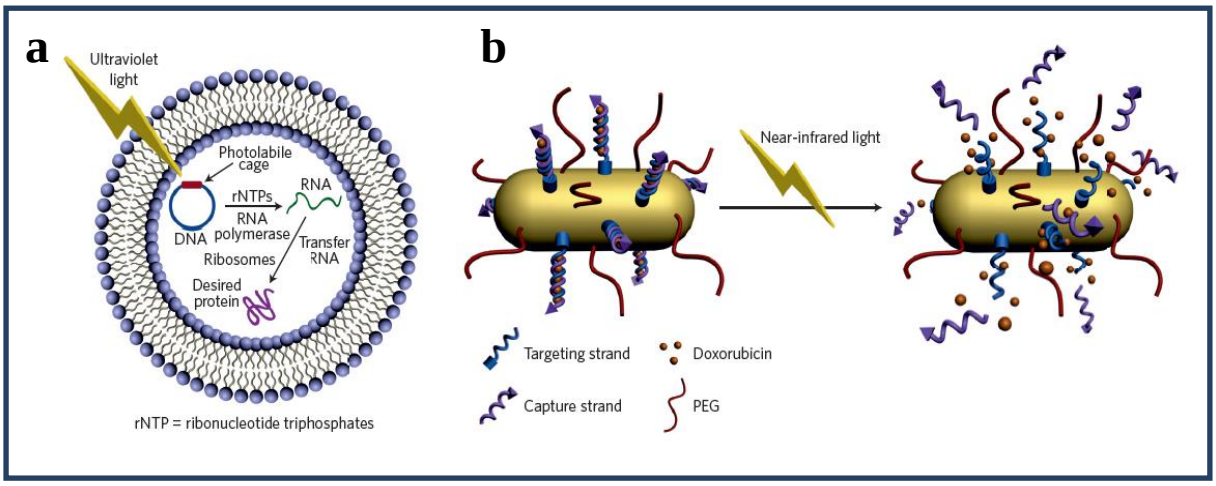

Figure 1.10. Illustration of light-triggered drug delivery; a) Schematic representation of an encapsulated *in vitro* transcription–translation liposomal system triggered by irradiating caged DNA with light; b) Delivery of doxorubicin through the near-infrared-triggered induction of dehybridization of the DNA conjugated at the surface of gold nanorods.

1.5. Approaches towards divergent scaffold based drug delivery systems

An important strategy of drug-related research has long been the synthesis and discovery of potent, pharmacologically active agents to manage, treat, or cure disease. The mode of delivery affects numerous factors that contribute to therapeutic efficacy, including pharmacokinetics, distribution, cellular uptake and metabolism, excretion and clearance, as well as toxicity. Moreover, drugs can lose their pharmacological activity due to changes in environmental factors such as moisture, temperature, and pH, which can occur in the body or during storage. As the biotechnology industry continues to develop new classes of biopharmaceuticals, improved fundamental understanding of how drug delivery affects safety and efficacy, along with new delivery technologies, are needed.[59] However, drug delivery remains a prominent challenge which includes the limited understanding of biological barriers and its internalization mechanisms. These unmet needs and limitations have given rise to considerable research efforts focused on the design, implementation, and translation of synthetic small molecules, sugar molecules and nanomaterials (eg., liposomes, NP's, micelles, hydrogels, fibers and films) for drug delivery. The advantage of personalized drug delivery system (DDS) is to maximize therapeutic efficacy while minimizing side effects. Several considerations need to be addressed prior to designing nano and micromaterials decorated with targeting ligands or molecules, such as peptides, antibodies, aptamers, and

proteins, that are specific to the receptors expressed or overexpressed on aberrant cells and their surrounding microenvironments in targeted drug delivery systems.[60] Unfortunately, very few of these nanomedicines have shown clinical efficacy due to significant challenges associated with the trafficking and targeting *in vivo* (**fig 1.11**).

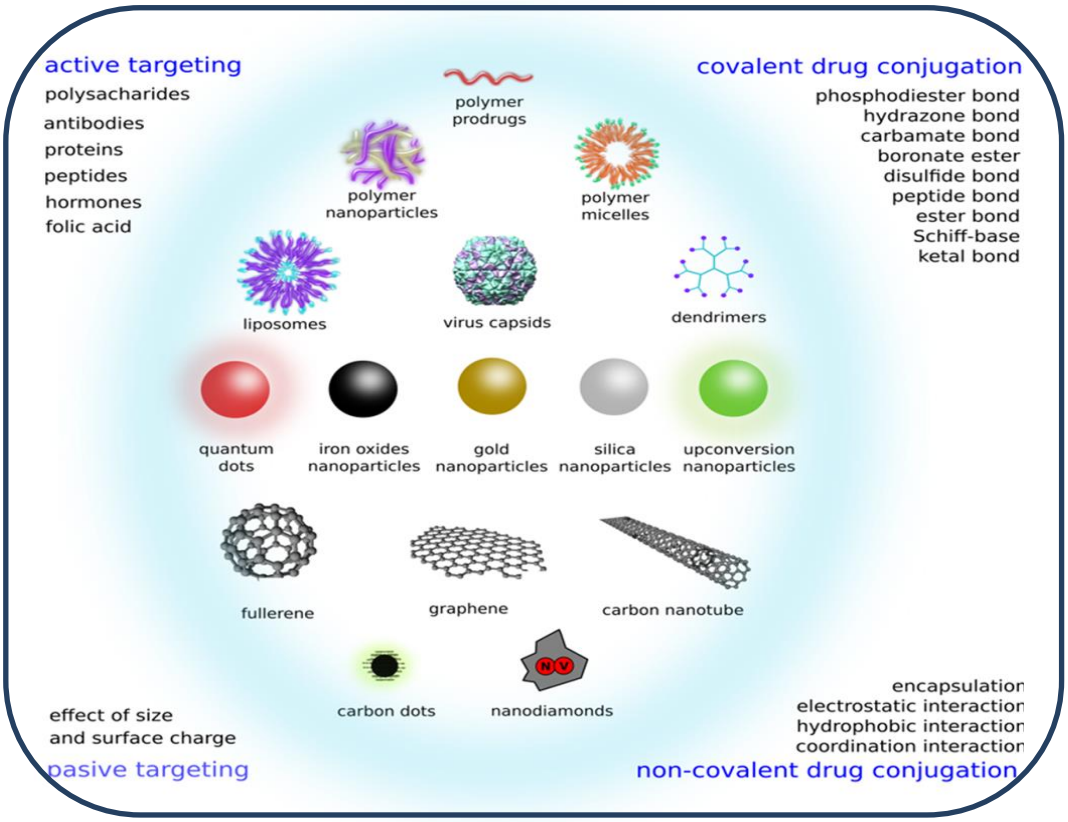

Figure 1.11. Diagram explaining outline of polymer, nanoparticle, and other drug delivery systems with various possibilities of drug targeting and its attachment.

1.5.1. Carbohydrates in drug delivery

In recent years, carbohydrates have been widely explored for the synthesis, characterization, and biological evaluation of carbohydrate-based biomedical copolymers for targeted delivery of anticancer drugs into solid tumors. Carbohydrates play important roles in key recognition events with a variety of receptor proteins such as hormones, enzymes, toxins, lectins, antibodies, viruses, and bacteria. They are also involved in numerous biological processes such as cell growth, recognition and differentiation, cancer metastasis, inflammation, bacterial and viral infection. These specific interactions occur through glycoproteins, glycolipids, and polysaccharide on cell surfaces through proteins with carbohydrate-binding domains, known as “endogenous lectins”. The potential of carbohydrate-based drug delivery

systems for drug targeting, also termed "glycotargeting" has been the subject of fairly intensive exploration since the 1990s.[61,62] Most of the glycotargeting strategies have exploited the lectin-mediated endocytotic uptake of carbohydrate-containing drug delivery systems. Upon internalization, the drug may be released from the carrier to target a selective subcellular organelle and promote biological activity (**fig 1.12**).[63] Carbohydrate containing liposomes, NP's, and polymers have been investigated for their ability to deliver drugs to specific cells and tissues.

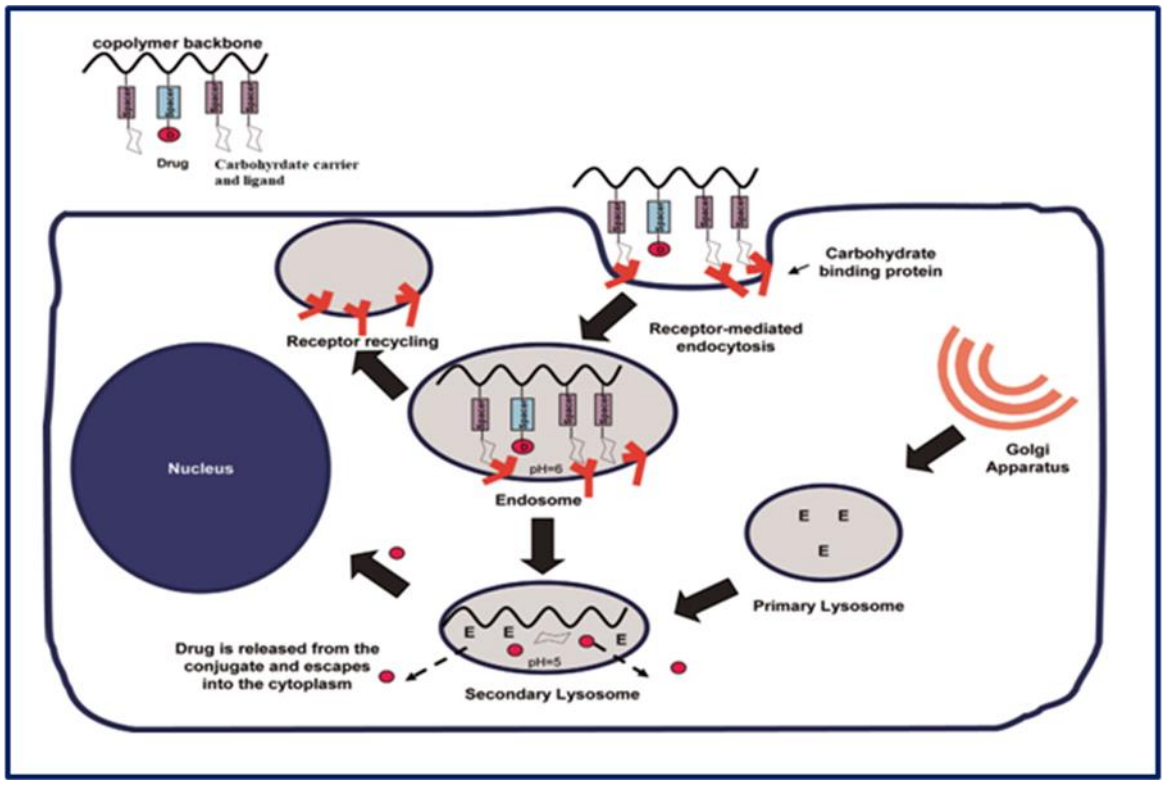

Figure 1.12. Binding of the carbohydrate ligands to their target carbohydrate receptors promotes receptor-mediated internalization, followed by endocytic uptake of the polymer conjugate from the tumor interstitium. As the early endosome matures and finally fuses with the digestive lysosome to form the secondary lysosome, there is a gradual drop in the pH from ~6 to 5. Further, the lysosome is a reservoir for a large number of digestive enzymes such as the thiol proteinases. Depending on the linkers used, the drug will usually be released intracellularly on exposure to lysosomal enzymes (for example, Gly-Phe-Leu-Gly sequence is cleaved by cathepsin B) or lower pH (for example, a hydrazone linker degrades in endosomes and lysosomes (pH 6.5<4.0) to exert cytotoxic activity. E represents enzymatic activity.

1.5.2. Molecular transporters based on guanidinium scaffold in drug delivery

Molecular transporters are a class of agents that enable or enhance the passage of drugs or probes across biological barriers. In 2000 a new terminology molecular transporters was introduced for molecules such as cell penetrating peptides (CPPs). This terminology framed

the more general expectation and demonstrated finding that many non-peptidic systems could function in a fashion similar or superior to CPPs. Actually, Wender, Rothbard, and co-workers first reported that the uptake of the CPPs, $Tat_{49–57}$ (RKKRRQRRR), showed a function of its arginine residues and not its peptide backbone and proposed the uptake efficiency is related to the number and spatial array of its guanidinium groups.[64,65] Multiple mechanisms have been advanced to explain the paradoxical behaviour of an oligo-cation which is highly water-soluble and polar agent crossing the nonpolar cell membrane to enter cells. Both adaptive translocation and endocytotic mechanisms have been proposed and indicated that some proposed mechanisms work simultaneously. Robust uptake is generally observed for a variety of cell types, although there are differences in rates and mechanisms of uptake depending on cell line, cargo, and transporter variations. Mechanistically, the guanidinium groups are proposed to form bifurcated hydrogen bonds with cell surface anions (e.g., carboxylates, sulfates, and phosphates), and the resultant, charge-neutralized complexes are driven inward by the polarization of the membrane or by encapsulation in an endosome (**fig 1.13**). Guanidinium-rich molecular transporters thus function as "polarity chameleons", being highly water-soluble in the extracellular milieu but becoming nonpolar upon complexation with membrane components, allowing for rapid cellular uptake. Guanidinium-rich molecules and cell-penetrating peptides can to enter in to living cells through a non-endocytic energy-independent manner and transport a wide range of cargos, including drugs and biomarkers. This challenges the fundamental concept that charged molecules cannot spontaneously diffuse across the cell membrane. The mechanism behind this puzzling effect follows three essential steps: (a) peptide binding to plasma membrane components; (b) spontaneous peptide absorption across the hydrophobic barrier imposed by the plasma membrane; and (c) breakage of the strong ionic bonding between the peptide and the membrane when the peptide reaches the cytosol. A variety of guanidinylated transporter scaffolds, including peptides, peptoids, oligocarbamates, oligocarbonates, and carbohydrates have been used to deliver cargos such as small molecules, DNA, siRNA, imaging agents, peptides, and metals. In addition to uptake in cell membranes, guanidinium-rich molecular transporters have also been shown to cross skin, ocular, buccal, and blood−brain barriers, and have been advanced into clinical trials.[66, 67]

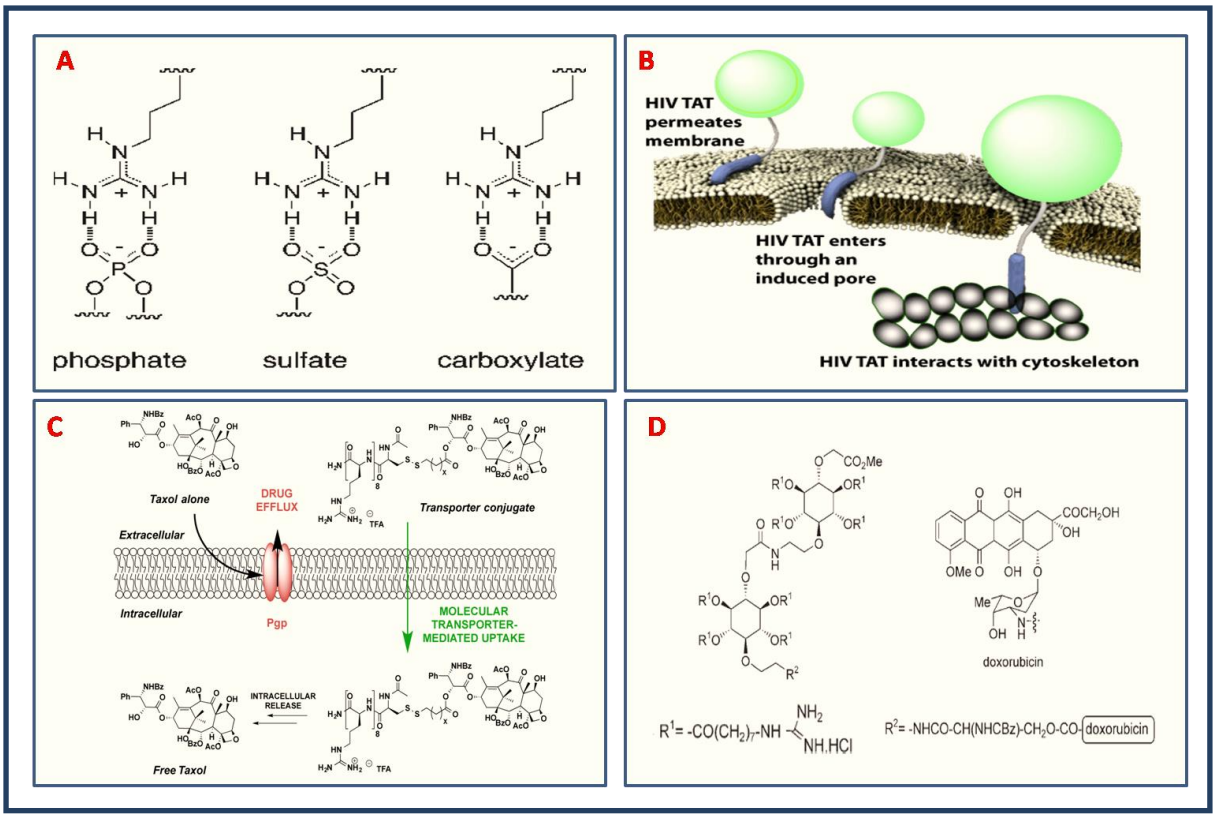

Figure 1.13. A)Schematic diagram showing the mechanism of H-bond formation of guanidinium groups with cell surface anions (e.g., carboxylates, sulfates, and phosphates, B) Cartoon representation of HIV permeating the membrane, C) Lipophilic drugs that are substrates for Pgp export, upon conjugation to molecular transporters, afford drug-transporter conjugates that are highly water-soluble, which are not recognized by Pgp pumps, and rapidly enter cells., D) Guanidinium molecular transporter of inositol conjugated doxorubicin therapeutic molecules.

1.5.3. Dendrimers in drug delivery

During the last few decades, medical science has witnessed the exploration of several delivery devices. Among them a multitalented versatile star named as "dendrimers" is now an established entity majorly in biomolecules and materials fabrication. Dendrimers represent a unique class of macromolecules with a highly branched, three-dimensional architecture, whose shape and size can be precisely controlled. Their unique properties, such as their well-defined, ordered molecular architecture, combined with the high reactivity of the functional groups within the cascade structure or on the periphery (**fig 1.14**), as well as their possible aqueous solubility, are credited for the applicability of dendrimers in nanomedicine.[68] The ability of these characteristic structure allows them to interact effectively and specifically with cell components (plasma membranes, cell organelles such as endo-lysosomes, mitochondria, nucleus, enzymes, etc.), and can easily cross various biological barriers (endothelial, epithelial, blood–brain barriers, etc.).[69] This makes them suitable for

administration via many routes, including intravenous, intraperitoneal, oral, trans-dermal diffusion, trans-nasal diffusion and ocular delivery.[70] Hence, dendrimers are effectively designed for the delivery of genes, drugs, for example, anti-cancer and anti-inflammatory drugs, and imaging agents. Both drug encapsulated dendrimers and drug-conjugated dendrimers have been developed. Some of them strongly improve the *in vitro* and *in vivo* efficiency as well as reducing the side effects of the drug.

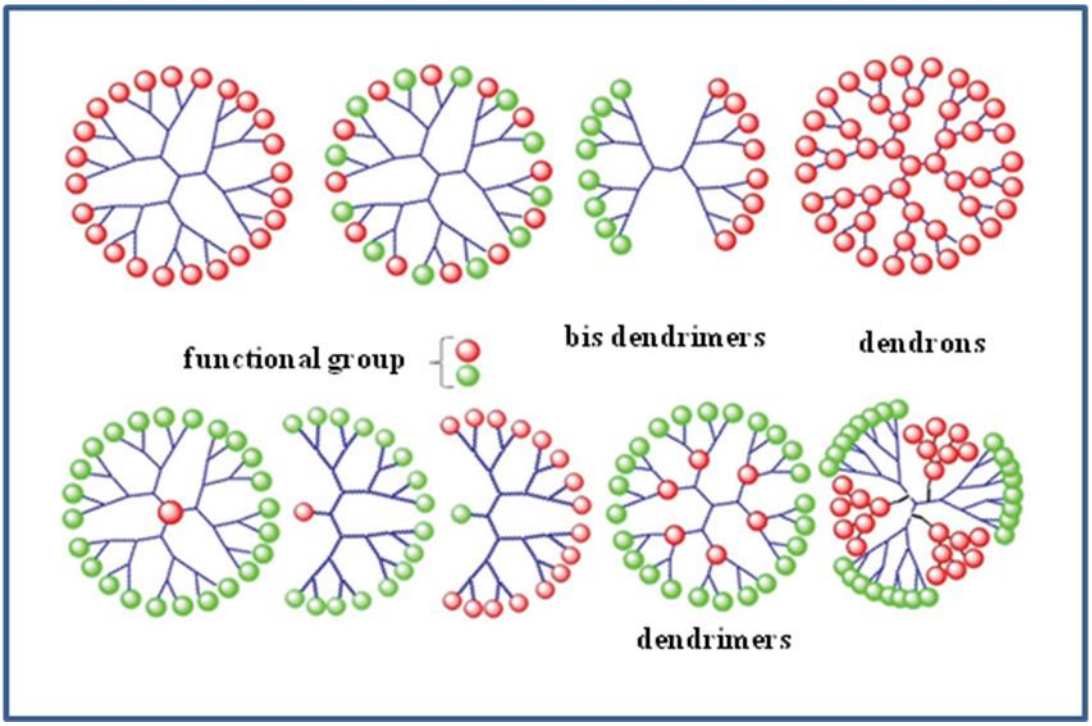

Figure 1.14. Schematic diagram explaining the chemical diversity and functionalization of dendrons, bis-dendrons, and dendrimers

1.5.4. Nanomaterialsfor therapeutic carriers

The hunt for an effective, divergent nanocarriers (NCs) for the targeted delivery of therapeutic compounds have the potential to radically improve disease outcomes and to increase drug solubility and stability, prolong drug half-lives in plasma, minimize off target effects, and concentrate drugs at a target site. Nanotechnology is traditionally defined as submicron sized molecular devices or NP's predominantly ranging from 5 to 500 nm in at least one dimension.[71] Therefore, NCs used as diagnostic/therapeutic tools encompass a wide range of substances, both organic (e.g., liposomes, natural and synthetic polymers including dendrimers, and carbon nanotubes) and inorganic materials (e.g., quantum dots (QDs), metallic nanostructures, and metal oxides (particularly magnetic iron oxides, up-converting nanophosphors, and zeolites)) (**fig 1.15**). Decorated with special functionalities, NCs allow

the application of different molecular imaging techniques, such as computed tomography (CT), magnetic resonance imaging (MRI), single-photon emission tomography (SPECT), positron emission tomography (PET), ultrasound imaging, and optical imaging methods.[72] Their fascinating and unique properties are also exploitable across a range of therapies, including chemotherapy, photodynamic therapy, neutron capture therapy, thermal therapy, and magneto-therapy. NCs may be engineered in such a fashion to permit a combination of these therapies to be used, leading to synergetic medical effectiveness.

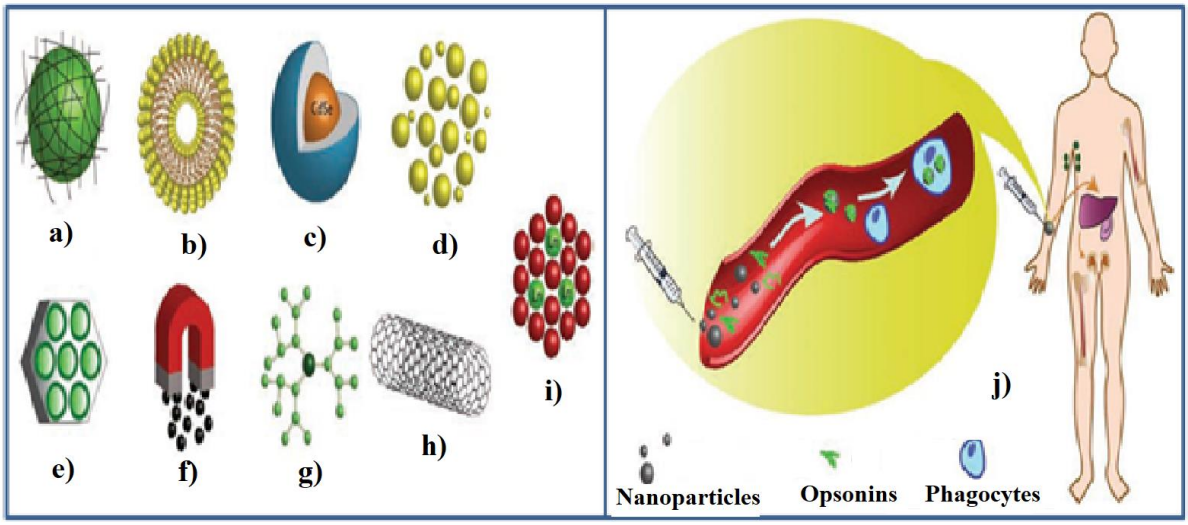

Figure 1.15. Scheme of diagram explaining the various kinds of nanoparticles used for cancer treatment and diagnosis. a) polymeric nanoparticles, b) liposomes, c) QDs, which usually posses a CdSe core, d) gold NPs, e) zeolite L, f) magnetic NPs, traditionally iron oxide, g) dendrimers, h) nanotubes, i) upconverting nanophosphors, j) Clearance of NPs by the reticuloendothelial system (RES). When larger NPs are injected into the blood stream, a group of proteins called opsonins cover their surface (opsonization), enabling phagocytic cells in the blood stream to recognize the NPs and remove them by degradation, renal excretion or accumulation in one of the RES organs (liver, spleen, etc.)

1.5.5. Biomolecular carrier for targeting therapy

Biomolecules including erythrocytes, leukocytes, platelets, and stem cells can serve as ideal drug delivery carriers for a number of reasons. They are highly mobile and able to travel through blood flow without immunogenicity. Circulating cells are involved in various disease processes, including infection, inflammation, and cancer development, so they have provided multiple advantages for disease targeting. For instance, leukocytes have the innate ability to cross the blood brain barrier (BBB) to access tumor cells in the brain. Inflammatory responses and wound healing of many diseases involve cell homing processes that spontaneously attract circulating cells to disease sites. Furthermore, using circulating cells as

delivery vehicles is advantageous as it significantly reduces immune clearance and prolongs the biological half-life time for drug delivery.

Exosomes vehicles (EV) have showed a cutting-edge in targeted therapeutic applications and these are small membrane vesicles heterogeneous in size (20 nm to 2 μm) bounded by a phospholipid bilayer and released by all cell types in various biological fluids and extracellular space. The progressive evidence indicates that exosomes from cancer cells transfer oncogenic proteins and nucleic acids that modulate the activity of recipient cells and play decisive roles in tumorigenesis, cell proliferation, progression, metastasis, and drug resistance (**fig 1.16**). This would be particularly beneficial when multiple pathways are targeted, as is the case in Alzheimer's disease (miR-29) and cancer (e.g., tumor suppressor miR-7 and miR-128 replacement therapy in glioblastoma). Hence, the exosome siRNA delivery technology could be a wide spread application for diseases in which manipulation of gene expression is desired.[73]

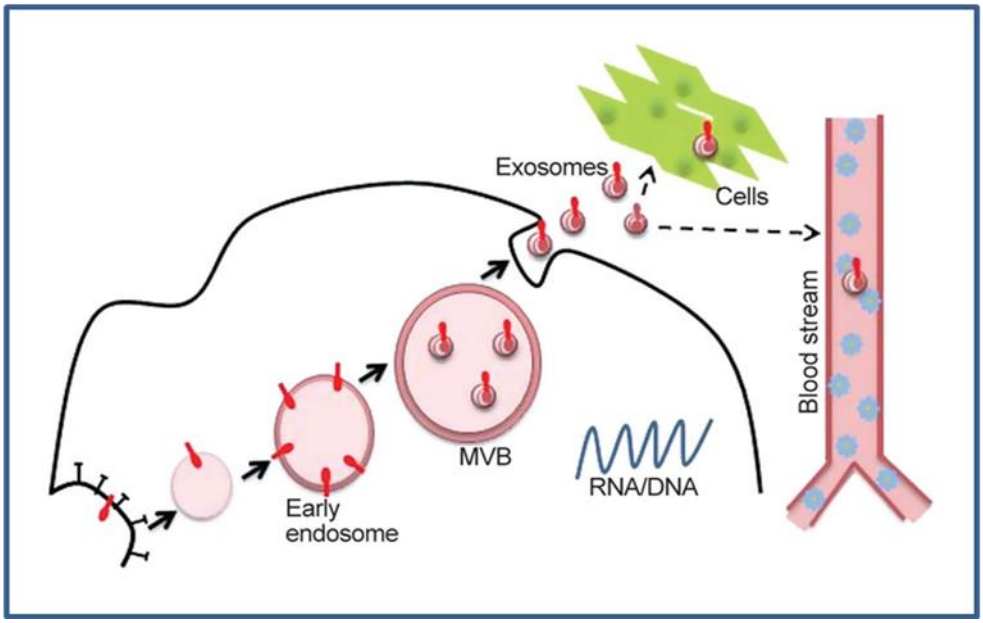

Figure1.16. Illustration of biogenesis and release of extracellular vesicles: represented diagram depicts a typical extracellular vesicle biogenesis and release.

1.6. Natural product and their semi-synthetic analogues in therapeutic applications

Historically, the plants played a dominant role in the development of new drugs for the treatment of a wide spectrum of ailments. Progressive milestones of Egyptian medicine dates back to 2900 BC, and another the best known record is the "Ebers Papyrus" which dates from 1500BC and documents over 700 drugs, mostly of plant origin. Records documenting the

uses of approximately 1000 plant derived substances in Mesopotamia date from around 2600BC, and many are still used today for the treatment of ailments ranging from coughs and colds to parasitic infections and inflammation. Similarly, documentation of the Indian Ayurvedic system dates from 1000 B.C. (Charaka; Sushruta and Samhitas with 341 and 516 drugs respectively). In addition, the ancient Greeks and Romans made substantial contributions to the rational development of the use of herbal drugs, with Dioscorides, a Greek physician (100 B.C.), accurately recording the collection, storage, and use of medicinal herbs during his travel with Roman armies throughout the then "known world", and Galen (130-200 B.C.E.), a practitioner and teacher of pharmacy and medicine in Rome, being well-known for his complex prescriptions and formulas used in compounding drugs.

A long history and discovery of several effective anti-cancer agents from plants may be attributed, directly or indirectly, to the relevant plants in traditional medicine. During the 20^{th} century, medicine is radically transformed. But until the 19^{th} century that scientists isolated active components from various medicinal plants, for example, morphine from *Papaver somniferum,* penicillin from *Penicillium notatum,* atropine from *Atropa belladonna* and Taxols from the bark of the Pacific yew tree. Therefore, natural products and analogues played a dominant role in maintaining human health as therapeutic agents against cancer, microbial infection, inflammation and other diseases.[74] Newman and Cragg published the third in their series of analyses of the sources of drugs in year 2007 and it's covering the period from 1981 to the middle of 2006 and showing the sources. The investigation revealed that the continuing and valuable contributions of Nature as a source not only provided potential chemotherapeutic agents but also gave lead compounds that have provided the basis and inspiration for the semi-synthesis or total synthesis of effective new drugs. Possibly the simplest approach to optimizing such a lead is to modify the natural product by simple functional group transformations. This can be achieved by chemical or enzymatic methods. A large number of analogues can be rapidly generated by such semi-synthetic approaches and which have more potential advantages than that of existing parent compounds. For example, the marketing of lovastatin was soon followed by the introduction of simvastatin (Zocor), a closely related analogue produced via synthetic modifications. It is noteworthy that the difference between lovastatin and simvastatin is a single methyl group, arguably the most lucrative methyl group in pharmaceutical history. Similarly, commercialization of the tubulin inhibitor paclitaxel (Taxol) was soon followed by docetaxel (Taxotere), prepared semi-synthetically from 10-deacetyl baccatin III. However, many desired transformations cannot

be accomplished due to incompatibilities with pre-existing functional groups or the lack of a feasible reaction.

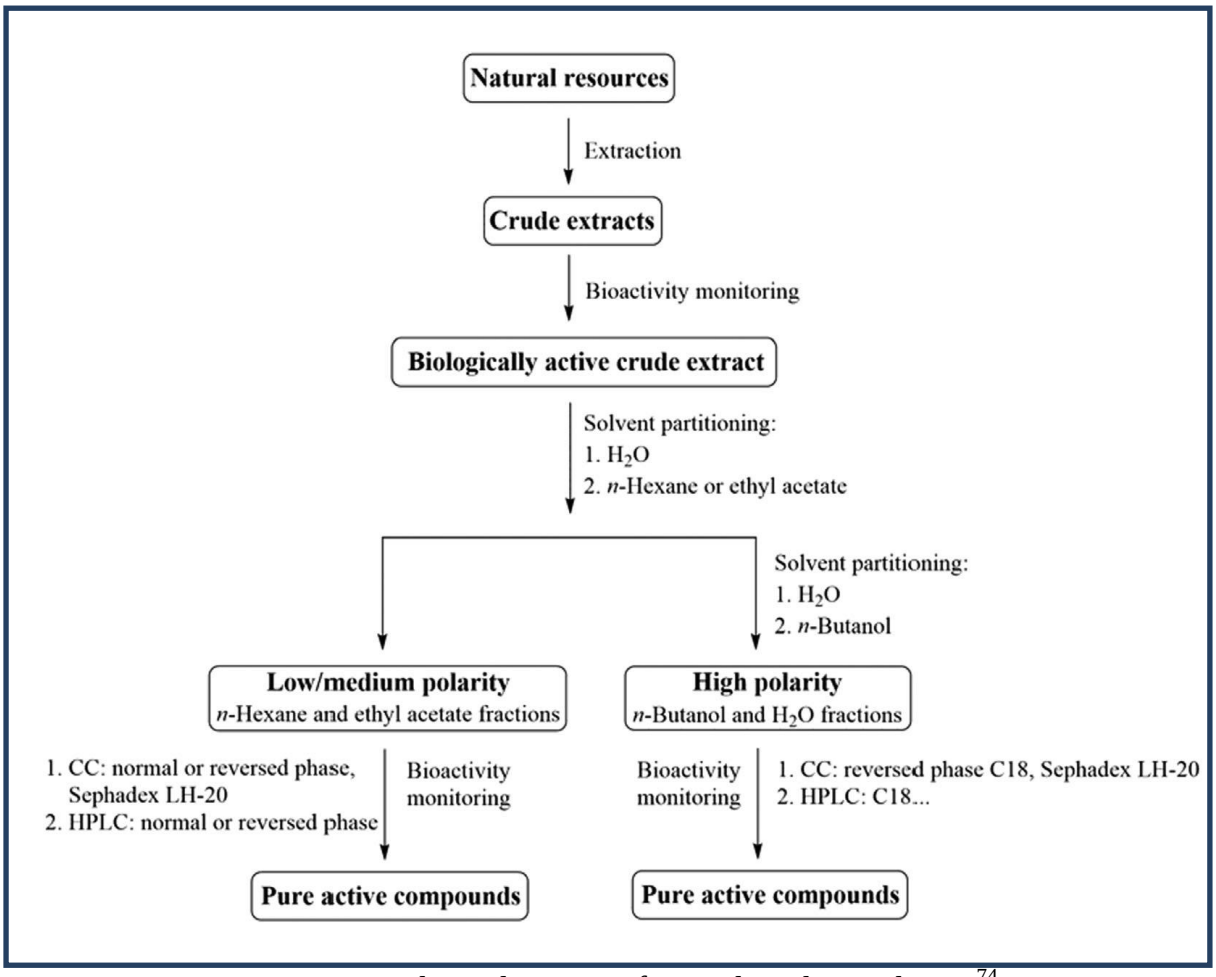

Figure 1.17. Traditional process of natural product isolation.[74]

1.7. Combination therapy

The expeditious progress with the new therapeutic molecules is not that effective as expected. Tumor microenvironment (TME) plays a critical role in tumor initiation, progression, invasion, and metastasis. Consequently, the long-term repeated treatment of cancer with a single therapy can promote cancer cell resistance to the applied treatment. Multi-drug resistance (MDR) is the main reason for the failure of successful chemotherapy and P-glycoprotein (P-gp) mediated drug efflux is one of the best characterized MDR mechanisms. Therefore, treatment of cancer with a P-gp inhibiting drug and a normal chemotherapeutic drug is an important strategy for overcoming MDR. In the recent years, researchers reveal that using DDS for therapeutic application has shifted away from monotherapy towards combined therapy (**fig 1.18**).[75] For example, Idriset al. demonstrated Lanthanide (Ln)-doped upconversion nanoparticles-mediated PDT through simultaneous activation of two

photosensitizers and found the use of two photosensitizers in unison is more effective than using a single one.

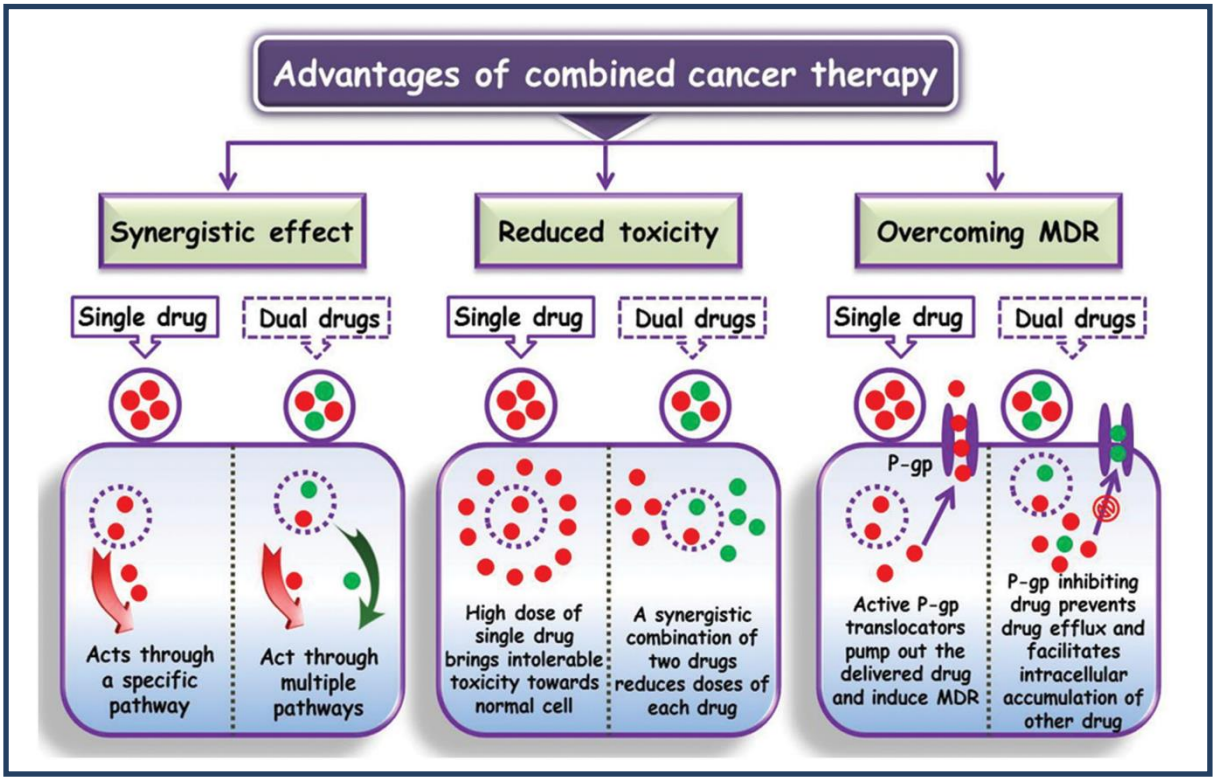

Figure 1.18. Schematic representation depicting the superior advantages between single and combination cancer therapy.

Combination of immunotherapeutic agents and chemotherapy is predicted to reinforce and synergistically increase the anti-tumour effects of either therapy, as shown in recent clinical trials. As chemotherapies remain the first-line treatment for many cancers, a thorough characterization of their immuno-modulatory effects will be required to rationalize their optimal combination with immunotherapy. The optimal scheduling of these agents also need to be analysed. Interestingly, results of a phase II clinical trial have suggested an improved efficacy of ipilimumab in patients with previously untreated non-small-cell lung carcinoma when combined with paclitaxel and carboplatin as a phased, but not concurrent regimen.

1.8. Biological barriers in therapeutic intervention

Effective delivery of therapeutics, whether systemic or targeted, is limited by various physiological barriers, including the capillary endothelial barrier, intestinal barrier, cerebral spinal fluid barrier, blood-brain barrier, and many others defend against foreign substances and restrict the passage of certain molecules. Important approaches have been developed to easily understand the functional properties of these barriers and developing novel means to

overcome them through the use of nanomaterials or drug nanocarriers to be effective at the diseased site. Depending on the mode of exposure and route of administration, external and internal biological barriers can be differentiated. The primary structural barriers are skin and mucosa that protects the hosts from the external environment. Hence external barriers include the epithelia of the skin, the nasal tract, the respiratory system, the retina, and the gastrointestinal tract. The stratum corneum comprises the physical barrier of the skin, whereas the other barriers are covered with a mucosal layer that has to be overcome by a nanomaterial via the aforementioned exposure routes in order to reach the blood circulation and/or the targeted tissue.

Secondary or internal biological barriers such as the endothelium of the blood vessels, the BBB, the blood–testis barrier (BTB), the placental barrier, the interstitial space and extracellular matrix (ECM), and reticuloendothelial system. Usually blood endothelial tissue is tight and does not allow nanomaterials to translocate. However, cancerous tissue, as well as inflammatory reactions causing activation and secretion of proinflammatory cytokines (tumor necrosis factor (TNF), interleukin (IL)-1, IL-6, vascular endothelial growth factor (VEGF)), shows induction of endothelial fenestration, i.e., a loss of cellular integrity inducing a gap between the endothelial cells. This feature can enable the nanomaterials to extravasate from the blood system into the cancerous and/or inflamed tissue. Another possibility is the clearance of the nanomaterials via the lymph system. Diseases such as cancer and liver fibrosis reveal an altered ECM and an increased number of fibroblasts, which affect the penetration of nanomaterials through the tissue.[76, 77]

1.9. Future perspective of targeting drug delivery system (TDDS)

The growing interest in applying nanotechnology to cancer treatment is largely attributable to its unique appealing features for drug delivery, diagnosis and imaging. The existing common cancer treatments comprises of surgery (49%), radiotherapy (40%) and chemotherapy (11%).[78] Therefore, emergence to research opportunities and challenges with the team of chemists, biologists and clinicians aims to develop new targets, therapeutic modalities for efficient cancer management. More recently, the developed drug delivery devices are practiced to *in vivo* drug sensitivity and biomarker analysis in patient tumours. One such device that can be implanted directly into tumors via biopsy needle is shown **fig 1.19a**. It can be used to administer and subsequently evaluate the effects of up to 16 different drugs simultaneously via drug-releasing microwells. Three drugs released from microwells are

depicted here for simplicity. The drugs diffuse from the microwells into confined regions of the tumor. The tumor tissue is then biopsied using a second coring needle that retrieves the device itself and a small column of tissue adjacent to the device. This tissue contains regions exposed to the drugs and is used to evaluate drug effects, such as apoptosis or growth arrest (**fig 1.19a**).[79] In addition, exosomes can be efficiently captured from blood by using a nanoplasmonic exosome sensor. This chip technique has been recognized for concentration of targeting protein as well as extract RNA from exosomes (**fig 1.19b**).

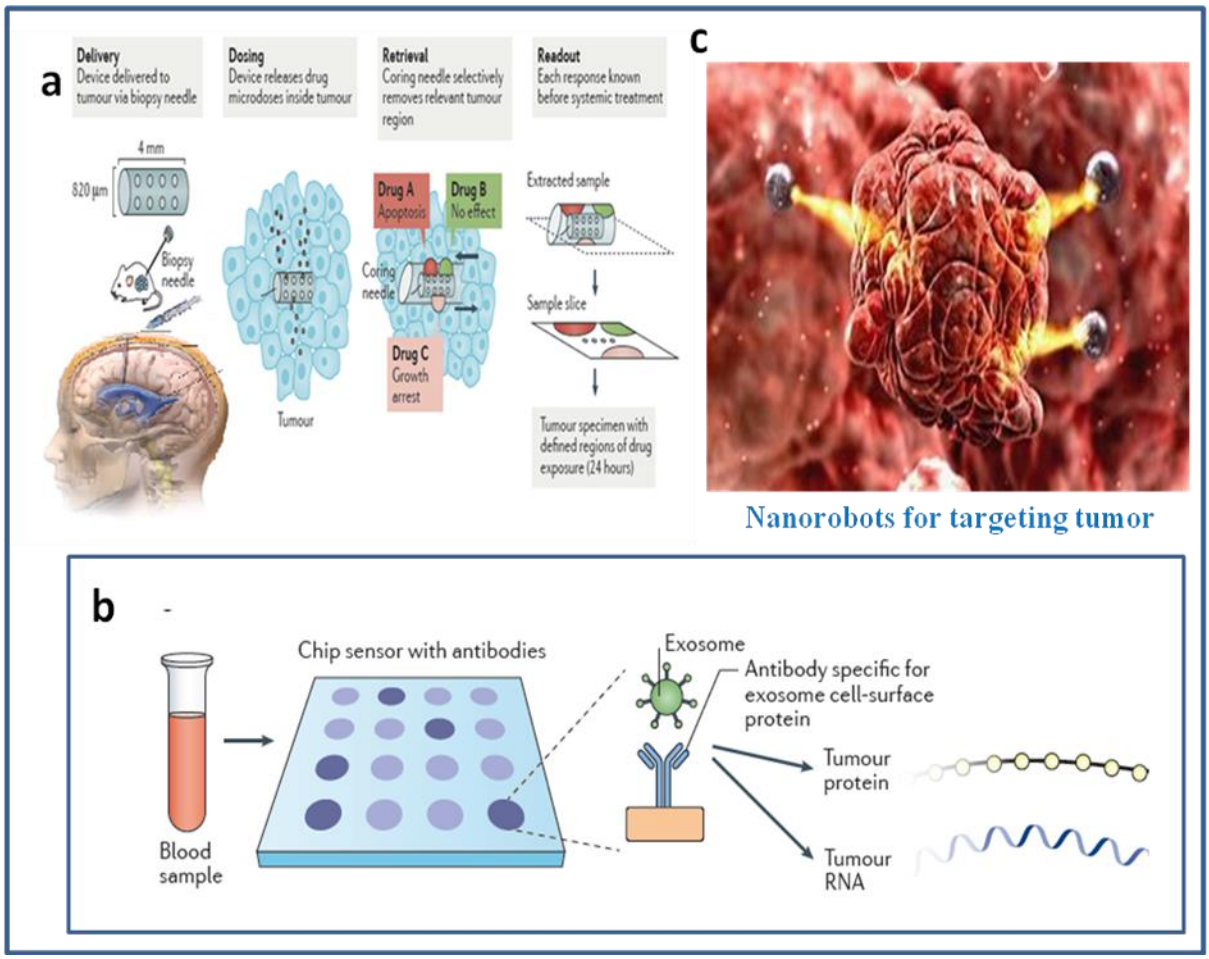

Figure 1.19. Diagram depicting, a) an implantable microdevice to perform high-through put *in vivo* drug sensitivity testing, b) Exosome display technology for early cancer detection and c) Nanorobots for targeting in tumors.

In divergent exploration of nanotechnology, nanorobotics is considered as a useful model of cancer therapy in the future. Nanorobots could carry and deliver large amounts of anti-cancer drugs into cancerous cells without harming healthy cells, thereby reducing the side effects related to conventional chemotherapy. In addition, the clinical use of nanorobots for diagnosis, therapeutic and surgical purposes should be done with intravenous injection.

Therefore, nanorobots can be delivered directly into the patient's bloodstream. After nanorobots cross cellular membranes to the target site, drug retention in the tumor will determine the therapeutic efficiency (**fig 1.19c**). The chemotherapy is influenced by drug transfer processes from plasma to tissue in achieving more effective tumor chemotherapy based on its composition.[80] Thus, the major advantage of nanorobots for cancer drug delivery is to minimize the side effects.

1.10. Conclusion

Although the field of targeted cancer therapy is advancing rapidly, the design and development of ideal delivery technologies still require more steps to go. Novel delivery systems could improve cancer therapy because of the engineered properties of the platforms themselves, including those for targeted and/or localized delivery, controlled release, increased stability and vaccination. Apart from the delivery platforms described in this chapter, more rooms are available to improve the delivery of chemotherapeutic agents to overcome the innate heterogeneity of cancer which anticipate with new inventions in the coming years. For example, many systems, including nanoparticles, scaffolds, hydrogels and cells, can be loaded with multiple therapeutic agents that are chosen on the basis of targets identified in patient biopsy samples. The personalized therapeutic approach would enable more comprehensive and potentially curative approaches to TDDS in cancer. Thus, the way forward to drug delivery research at both the fundamental and applied levels will pave new innovation towards targeted therapies such as cancer.

1.11. References

[1]. Breasted, J, H. The Edwin Smith Surgical Papyrus. Chicago, University of Chicago Press,**1930**.

[2]. Steven, I.; Hajdu, M, D.*Cancer*, **2011**, 117, 1097.

[3]. Schmidt, A.; Weber, O. F. *Contrib.Microbiol,* **2006,** 13, 1.

[4]. Paget, S. *Cancer Metastasis Rev,***1989,**8, 98.

[5]. Maman, S.; Witz, I.P.*Nat. Rev. Cancer,* **2018,**18, 359.

[6]. Michael, R. S.; Peter, J. C.; Andrew, F.P.*Nat Rev Cancer,***2009,**458, 719.

[7]. Xingshu, L.;Jihoon, K.;Juyoung, Y.;Xiaoyuan, C. *Adv. Mater,***2017**, 29, 1606857.

[8]. Ryu, J. H.; Lee, S.; Son, S.; Kim, S. H.; Leary, J. F.; Choi, K.;Kwon,I. C. *J. Control. Release*, **2014**, 190, 477.

[9]. Kojima, R.;Aubel, D.;Fussenegger, M. *Cur. Opin. Chem. Bio.* **2015**,28, 29.

[10]. Kumar, R.; Shin, W. S. K.;Sunwoo, W. Y.; Kim, K.S.;Bhuniya,S.; Kim, J. S. *Chem. Soc. Rev.* **2015**, 44, 6670.

[11]. DiMasi, J.A.; Hansen, R.W.; Grabowski, H.G. *J Health Econ,***2003,**22, 151.

[12]. Adams,C.P.;Brantner, V.V. *Health Econ,***2010,** 19, 130.

[13]. Rask-Andersen, M.; Almen, M.S.; Schioth, H.B. *Nat Rev Drug Discov*, **2011,** 10, 579.

[14]. Blake, R.A. *Methods MolBiol,***2007,** 356, 367.

[15]. Agrawal, P. *J Drug Discov Develop and Deliv,***2014,**1, 2.

[16]. Paul,S.M.;Mytelka, D.S.;Dunwiddie, C.T.;Persinger, C.C.;Munos, B.H.;Lindborg, S.R.; Schacht, A.L. *Nat Rev Drug Discov,***2010,** 9, 203.

[17]. Sun, J.;Wei, Q.;Zhou, Y.;Wang, J.;Liu, Q.;Xu, H. *BMC. Syst. Biol,* **2017,** 11, 87.

[18].Torchilin, V.P. In:MonikaSch¨afer-Korting, Ed. Handbook of Experimental Pharmacology, Springer Berlin Heidelberg: Berlin,**2010,** 197, 3.

[19]. Aggarwal,S. *Nat Rev Drug Discov,***2010,** 9, 427.

[20]. Huang, M.; Shen, A.; Ding, J.;Geng, M. *Trends PharmacolSci*, **2014,** 35, 41.

[21]. Widakowich, C.; de Castro, G.; Azambuja, E.;Dinh, P.; Awada, A. *Oncologist,***2007,**12, 1443.

[22]. Tannock,I.F.; Lee, C.M.; Tunggal, J.K.; Cowan, D.S.;Egorin, M.J. *Clin. Cancer. Res,***2002,** 8, 878.

[23]. Brown, R.; Links, M. *Exp Rev Mol Med,***1999,**1,1.

[24]. Byrne, J.D.; Betancourt, T.; Brannon, P. L. *Adv Drug Deliv Rev,***2008,** 60, 1615.

[25]. Alexis, F.;Pridgen, E.; Molnar, L.K.;Farokhzad, O.C. *Mol. Pharm,***2008,** 5, 505.

[26]. Cheng, Z.; Al Zaki, A.; Hui, J.Z.;Muzykantov, V.R.;Tsourkas, A. *Cost Science,***2012,** 338, 903.

[27]. DesRieux, A.;Pourcelle, V.;Cani, P.D.;Marchand, B.J.;Preat, V. *AdvDrugDeliv Rev,***2013,** 65, 833.

[28]. Muller, P.Y.; Milton, M.N. *Nat Rev Drug Discov,***2012,** 11, 751.

[29]. Torchilin, V. P.; Trubetskoy, V. S. Adv. *Drug Delivery Rev,***1995,** 16, 141.

[30]. Greenwald, R. B.; Choe, Y. H.; McGuire, J.; Conover, C. D.Adv. *Drug Delivery Rev,* **2003,** 55, 217.

[31]. Alexis, F.; Pridgen, E.; Molnar, L. K.; Farokhzad, O. C. *Mol. Pharmaceutics,***2008,** 5, 505.

[32]. Fang, J.; Nakamura, H.; Maeda, H. *Adv. Drug Delivery Rev,* **2011,** 63, 136.

[33]. Tatum, J. L. *Int. J. Radiat. Biol,***2006,** 82, 699.

[34]. Mura, S.; Nicolas, J.; Couvreur, P. *Nat. Mater,***2013,** 12, 991.

[35]. Helmlinger, G.; Sckell, A.; Dellian, M.; Forbes, N. S.; Jain, R. K. *Clin. Cancer Res.* **2002,**8, 1284.

[36]. Wojtkowiak, J. W.; Verduzco, D.; Schramm, K. J.; Gillies, R. J.;*Mol. Pharm.* **2011,**8, 2032.

[37]. Morris, M. C.; Chaloin, L.; Heitz, F.; Divita, G.*CRC Press: Boca Raton,***2002,** 93.

[38]. (a) Xu, P. S.; Van, K.E. A.; Zhan, Y. H.; Murdoch, W. J.; Radosz,M.; Shen, Y. Q. *Angew Chem., Int. Ed,* **2007,** 46, 4999. (b) Lee, Y.;Fukushima, S.; Bae, Y.; Hiki, S.; Ishii, T.; Kataoka, K. *J. Am. Chem. Soc,***2007,** 129, 5362. (c) Du, J.Z.; Sun, T.M.; Song, W.J.; Wu, J.; Wang, J.*Angew. Chem., Int. Ed,***2010,** 49, 3621.

[39]. Helmlinger, G.; Yuan, F.; Dellian, M.; Jain, R. K. *Nat. Med,***1997,**3, 177.

[40]. Torchilin, V. P. *Nat Rev Drug Discov,***2014,** 13, 813.

[41]. Nejadnik, H.; Ye, D.; Lenkov, O. D.; Donig, J. S.; Martin, J. E.;Castillo, R.; Derugin, N.; Sennino, B.; Rao, J.; Daldrup-Link, H.*ACS Nano,***2015,** 9,1150.

[42]. Gialeli, C.; Theocharis, A. D.; Karamanos, N. K. *FEBS* ,**2011,** 278, 16.

[43]. Vartak, D. G.; Gemeinhart, R. A. *J. Drug Target,***2007,** 15, 1.

[44]. Lopez-Otin, C.; Matrisian, L. M. *Nat. Rev. Cancer,***2007,** 7, 800.

[45]. Ding, Y.; Kang, Y.; Zhang, X. *Chem. Commun*, **2015,** 51, 996.

[46]. Kamaly, N.; Yameen, B.; Wu, J.; Farokhzad, O.C. *Chem. Rev*, 116, **2016,** 2602.

[47].Yatvin, M.; Weinstein, J.; Dennis, W.; Blumenthal, R. *Science,***1978,** 202, 1290.

[48]. Kelson, I.; Keisari, Y.; Gannot, I. *J. Biomed. Opt,***2013,** 18, 111410.

[49]. Stefanadis, C.; Markou, D.; Petraki, K.; Panagiotakos, D. B.;Fasoulakis, C.; Kyriakidis, A.; Papadimitriou, C.; Toutouzas, P. K.*J. Clin. Onco,*.**2001,** 19, 676.

[50]. Issels, R. D.*Eur. J. Cancer*,**2008,** 44, 2546.

[51]. Hyperthermia in Cancer Treatment.http://www.cancer.gov/ about cancer/treatment/types/surgery/hyperthermia-fact-sheet.

[52]. Yang, H.W.;Hua, M.Y.; Liu, H.L.; Huang, C.Y.; Tsai, R.Y.; Lu, Y.J.; Chen, J.Y.; Tang, H.J.; Hsien, H.Y.; Chang, Y.S.; Yen, T.C.; Chen, P.Y.; Wei, K.C. .*Biomaterials*, **2011,**32,6523.

[53]. Xie, J.; Liu, G.; Eden, H. S.; Ai, H.; Chen, X. *Acc. Chem. Res*,**2011,**44, 883.

[54]. Liu, Y.; Yang, F.; Yuan, C.; Li, M.; Wang, T.; Chen, B. *ACS Nano*, **2017,**11, 1509.

[55]. Dolmans, D. E. J. G. J.; Fukumura, D.; Jain, R. K.*Nat. Rev. Cancer,***2003,** 3, 380.

[56]. Staderini, M.; Martín, M. A.; Bolognesi, M. L.; Menendez, J.C. *Chem. Soc. Rev*,**2015,** 44, 1807.

[57]. Rai, P.; Mallidi, S.; Zheng, X.; Rahmanzadeh, R.; Mir, Y.;Elrington, S.; Khurshid, A.; Hasan, T. *Adv. Drug Delivery Rev*,**2010,**62, 1094.

[58]. A) Narayanan, N.; Karunakaran, V.; Paul, W.; Venugopal, K.; Sujathan, K.; Kumar, M. K. *BiosensBioelectron,* **2015**,70, 145. B) Duarte, S.;Faneca, H.;Lima, M. C. *Int. J. Pharm,* **2012,** 423, 365.

[59]. Mitragotri, S.; Burke, P. A.;Langer, R. *Nat. Rev. Drug Discovery,* **2014**,*13*, 655.

[60]. Torchilin, V. P. *Adv. Drug Delivery Rev,***2012,** 64, 302.

[61]. Paillard,F. *Hum. Gene Ther*,**1999,** 10, 337.

[62]. Monsigny, M. Midoux, P.; Mayer, R.; Roche, A. C.*Biosci. Rep,***1999,** 19, 125.

[63].Maniganda, S.;Sankar, V.; Nair, J. B.; Raghu, K. G.;Maiti, K. K. *Org. Biomol. Chem,***2014,** 12, 6564.

[64]. Maiti, K.K.; Jeon, O.Y.; Lee, W.S.; Kim,D.C.;Kim, K.T.; Takeuchi, T.; Futaki, S.; Chung, S.K.*Angew. Chem., Int.Ed*, **2006,** 45, 2907.

[65]. Maiti, K.K.; Lee, W.S.; Takeuchi,T.;Watkins, C.; Fretz, M.; Kim, D.C.; Futaki, S.; Jones, A.; Kim, K.T.; Chung, S.K.*Angew. Chem., Int. Ed,***2007,** 46, 5880.

[66].MacEwan,S. R.; Chilkoti, A. *Wiley Interdiscip. Rev.: Nanomed. Nanobiotechnol*,**2013,**5, 31.

[67]. Herce,H. D.; Deng, W.; Helma, J.; Leonhardt, H.; Cardoso, M. C. *Nat. Commun,***2013,**4, 2660.

[68]. (a) Nair,J.B.; Mohapatra, S.; Ghosh, S.; Maiti, K. K. *Chem. Commun,***2015,** 51, 2403;(b) Wu,L.P.;Ficker,M.;Christensen,J.B.;Trohopoulos,P.N.;Moghimi,S.M. *BioconjugateChem,***2015,** 26, 1198.

[69]. (a) Bosmann,A. W.; Jansen, H. M.; Meijer, E. W. *Chem. Rev,***1999,** 99,1665; (b) Medina S. H.; M. El-Sayed, E. H. *Chem. Rev*,**2009,** 109, 3141; (c) Mann, J. *Nat. Rev. Cancer,* **2002,** 2, 143; (d) Cragg, G. M.;Grothaus P. G.; Newman, D. *J. Chem. Rev*,**2009,** 109, 3012.

[70]. Mignani, S.;Kazzouli, S. El.;Bousmina M.;Majoral,J. P. *Adv. Drug Delivery Rev,***2013,** 65, 1316.

[71].Joseph,M.M.; Narayanan, N.; Nair, J. B.; Karunakaran, V.; Adukkadan, N. R.; Palasseri T.S.; Giridharan, S.; Jayadev , S. A.; Vineeth M. V.; Maiti, K. K.*Biomaterials,***2018,** 140, 181.

[72]. Cheon , J. J.; Lee , H. *Acc. Chem. Res,***2008 ,** 41 , 1630 .

[73]. Qin, J.; Yang, X.; Zhang, R. X.; Luo, Y. X.; Li, J. L.; Hou, J.; Zhang, C.; Li, Y. J.; Shi, J.; Lu, L.; Wang, J. X.; Zhu, W. L. *Nanomedicine,***2014,** 11, 391.

[74]. Priyadarshini,K.;Aparajitha,U. K. *Med. Chem*,**2012,** 2, 139.

[75]. Shen , J.; Yin , Q.; Chen , L.; Zhang , Z.; Li , Y. *Biomaterials*,**2012 ,** 33 , 8613 .

[76]. Lynch, T.J.;Bondarenko, I.;Luft, A.;Serwatowski, P.;Barlesi, F.; Chacko, R.; Sebastian, M.; Neal, J.; Lu, H.;Cuillerot, J.M.;Reck, M.*J. Clin. Oncol*, **2012,** 30, 2046.

[77]. Netti, P. A.; Berk, D. A.;Swartz,M. A.;Grodzinsky, A. J.;Jain,R. K.

*Cancer Res,***2000,** 60, 2497.

[78]. Jemal, A. The Cancer Atlas. Second edition ed, **2014**.

[79]. Mitchell, M.J.; Jain, R.K.; Langer, R. *Nat Rev Cancer*,**2017,**17, 659.

[80]. Artemov, D.; Solaiyappan, M.;Bhujwalla, Z. M.*Cancer Research,***2001,** 61, 3039.

Chapter -2

Cathepsin B Driven Lysosome Targeted Drug Delivery System Based on Sorbitol Scaffold towards Efficient Cancer Therapy

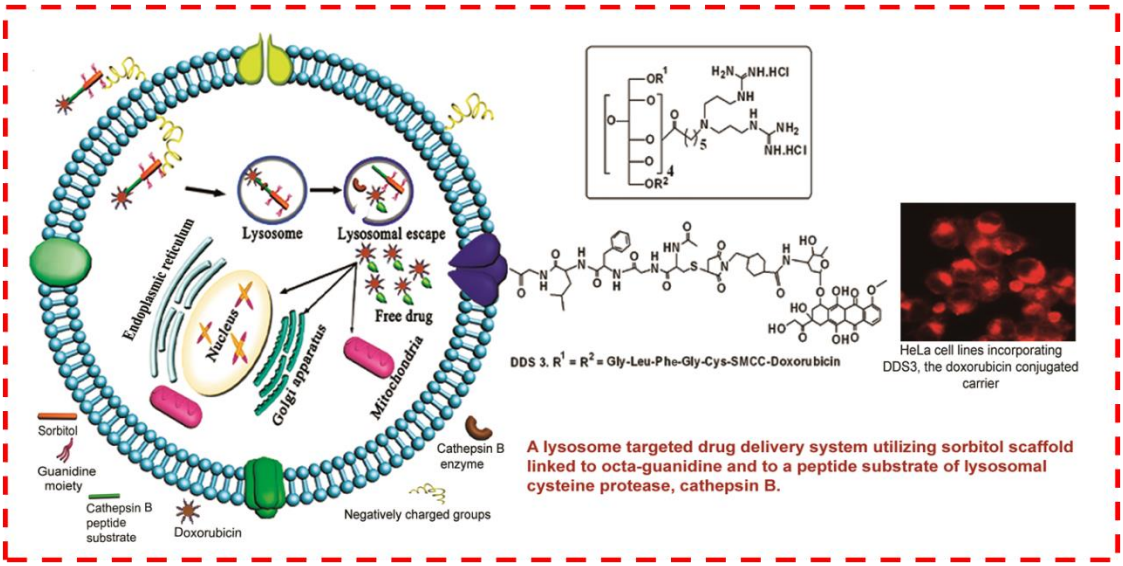

2.1. Abstract: Expression levels of the lysosomal cysteine proteases cathepsin B (Cat B) correlated with tumor progression and metastasis. However, its role in the hallmark processes of malignant growth remain poorly defined. In this study, a straightforward synthetic approach has been adopted for the construction of a lysosome targeted drug delivery system (TDDS) using sorbitol scaffold (Sor) linked to octa-guanidine and tetrapeptide GLPG, a peptide substrate specific to lysosomal cysteine protease, Cat B. The major objective is to deliver the potential anti-cancer drug, doxorubicin to the target sites efficiently, thereby minimizing dose-limiting toxicity. Three TDDS vectors have been synthesized viz. **DDS1: Sor-GLPG-Fl, DDS2: Sor-Fl** (control) and **DDS3: Sor-GLPGC-SMCC-Dox.** Dox release from **DDS3** in the presence of Cat B enzyme was studied by kinetics measurement based on the fluorescent property of Dox. Cellular internalization and co localization studies of all the three synthetic construct have been carried out by flow cytometry and confocal microscopy utilizing Cat B - expressing HeLa cells. **DDS1** and **DDS3** revealed significant localization within the lysosomes, in contrast to **DDS2** (control). The doxorubicin conjugated carrier, **DDS3** demonstrated

significant cytotoxic effect when compared to free Dox by MTT assay and also by flow cytometric analysis. The targeted approach with **DDS3** is expected to be promising, since it is indicated to be advantageous over free Dox which possesses dose-limiting toxicity, posing risk of injury to normal tissues.

2.2. Introduction

Targeted drug delivery systems (TDDS) have been extensively studied during the past several decades as a powerful tool to achieve improved therapeutic efficacy and diagnostic effects by remarkably improving the pharmacokinetics and pharmacodynamics. TDDS development is one among the challenging areas in pharmaceutical research that requires the growing need of multidisciplinary approach for the delivery of therapeutics to the site of action, without affecting healthy tissue or organ.[1,2] Delivery systems typically employ vehicles to carry therapeutics in order to improve the drug solubility, reduce toxicity, prolong circulating time, defined bio distribution, achieve specific targeting, control drug release, and diminish immunogenicity.[3-6] Ideal drug delivery vehicles should be biocompatible, biodegradable, easy to constructed by utilizing target specific groups mainly small molecules like peptide substrates, heterocyclics, oligonucleotides and monoclonal antibodies have been demonstrated widely by many research groups.[7-12] Focusing on cancer therapy, monoclonal antibodies against tumor-specific antigens have occasionally been successful in targeting tumors, but their irreducible bulk, hinders the penetration of solid tumors and excretion of unbound reagent.[13,14] In recent years, drug delivery systems based on mesoporous silica nanoparticles (MSNPs) and polymeric carriers e.g. N-(2-hydroxypropyl)methacrylamide (HMPA) have been well studied.[15-18] These carriers are known for passive targeting that takes the benefit of EPR effect (enhanced permeation and retention effect) of the tumor tissue. Such systems are simply distributed by blood circulation and are hardly selective. Hence majority of administered nanoparticles are known to accumulate in other organs, in particular, the liver, spleen and lungs. Keeping these in mind, researchers have attempted to construct drug delivery systems considering various cellular proteases as target sites.[19, 20] It has been reported that lysosomal delivery is one of the potential targets for cancer treatment.[13, 21] Likewise, lysosomal cysteine proteases (Clan CA; C1 papain family), the cysteine cathepsins, have recently attracted attention as tumour-promoting enzymes.[22,23] Eleven human cysteine cathepsin genes are present in the human genome: cathepsins B, C (dipeptidyl peptidase I), F, H, K, L, O, S,

V (L2), W (lymphopain) and X (Z).[24] Despite their general lysosomal localization, active cathepsins have been found in the extracellular matrix and in cellular compartments other than endosomes and lysosomes and are involved functionally in a variety of physiological and pathological processes.[25,26] There is increasing evidence suggesting that cysteine proteases, mostly cathepsins B and L and, to a lesser extent, cathepsins X, H, S and K, contribute to the proteolytic events during tumour progression.[27] Proteases of the cathepsin family are among the best studied lysosomal hydrolases.[28,29] Among these proteases, cathepsin B (Cat B), a lysosomal cysteine protease, is highly up regulated in malignant tumors and premalignant lesions at the mRNA and protein levels.[30] Overexpression of Cat B has been associated with oesophageal adenocarcinoma, breast cancer and other tumors.[31-33] Since Cat B expression is closely related to the invasive behaviour of tumors, it could be a promising target for novel drug delivery systems designed against invading tumor cells.

Cat B cleaves various Cat B specific peptide substrates viz., Leu, Arg-Arg, Ala-Leu, Phe-Arg, Phe-Lys, Ala-Phe-Lys, Gly-Leu-Phe-Gly, Gly-Phe-Leu-Gly and Ala-Leu-Ala-Leu, out of which tetrapeptide, Gly-Leu-Phe-Gly (GLPG), has been proven to be the most effective with respect to both plasma stability and rapid hydrolysis in the presence of Cat B.[34] Targeting Cat B enzyme in Cat B - enriched tumor cells, enhances efficacy of the anti-cancer drug, whilst minimizing toxicity to normal tissues. Having considered the above mentioned factors, we developed a synthetic strategy of a TDDS using Cat B peptide sequence GLPG, in conjugation with sorbitol core linked to multiple guanidine groups targeting to lysosomes of tumor cells and tissues. Transporters constructed on a sorbitol scaffold linked to guanidine residues by a methylene spacer, mimicking the Arg-8-mer or Tat (residues 49-57), showed significant translocation across the cell membrane, mitochondria and blood brain barrier efficiently.[35,36] The major advantage of a carbohydrate scaffold like sorbitol as the delivery carrier is that it possesses the highest density of functionality among organic compounds in terms of multiple hydroxyl groups. These groups are intended for divergent synthetic strategies facilitating transport of disparate cargos (molecular drugs, proteins, nucleic acids). Additionally, sorbitol occurs naturally in plants especially in apples, pears, cherries and largely devoid of any toxicity. It is also postulated that positively charged guanidine groups shows association with cell - surface negatively charged phospholipids and other negatively charged residues by electrostatic interaction via hydrogen bond formation,

facilitating cellular entry through the lipid bilayer.[37] Our key interest is to deliver Dox, a potential anti-cancer drug, utilizing this synthetic delivery system. The clinical applications of this drug have long been limited due to its severe dose- limiting toxicity. Taking advantage of the cleavable Cat B peptide sequence, a higher Dox concentration will be attained in tumor tissue when compared to normal tissue. The proposed mechanism of drug delivery has been illustrated in **scheme 2.1.**

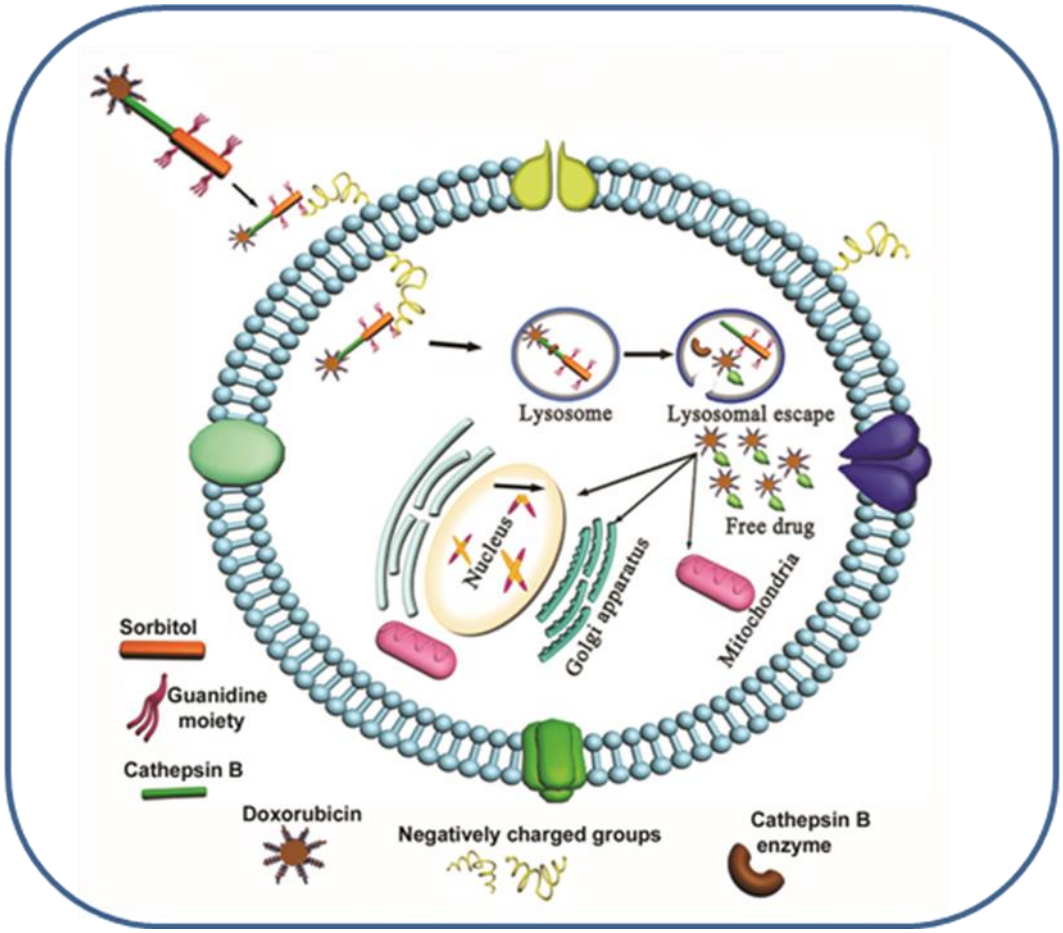

Scheme 2.1. Schematic representation of the proposed mechanism of drug delivery by the TDDS based on sorbitol scaffold. The TDDS is internalized through the lipid bilayer by electrostatic interaction between the guanidine moieties and negatively charged groups such as phospholipids / sulphates on the cell surface. The TDDS then enters into lysosomes, where doxorubicin is released by lysosomal cysteine protease, cathepsin B.

2.3. Results and Discussion

2.3.1. Synthesis of sorbitol based octa-guanidine carriers DDS1, DDS2 and DDS3

The TDDS synthesized on sorbitol scaffolds are represented as : **Sor-GLPG-Fl (DDS1), Sor-Fl (DDS2)** and **Sor-GLPGC-SMCC-Dox (DDS3)** (**Scheme 2.1**). **DDS1** is the targeted delivery carrier where the two terminal primary hydroxyl groups of sorbitol

have been utilized for conjugation of 1) Cat B- specific tetrapeptide i.e. N-acyl protected tetrapeptide, Ac-Gly-Leu-Phe-Gly-OH denoted as GLPG and 2) a fluorophore i.e fluorescein (**Fl**). **DDS2** has been used as the control where both the primary hydroxyl groups of sorbitol have been attached to **Fl** molecules by ester bond. In **DDS3**, both the primary hydroxyl groups of sorbitol are conjugated with **GLPGC** which are further linked to **Dox** via succinimidyl-4-(N-maleimidomethyl) cylohexane-1-carboxylate (SMCC).

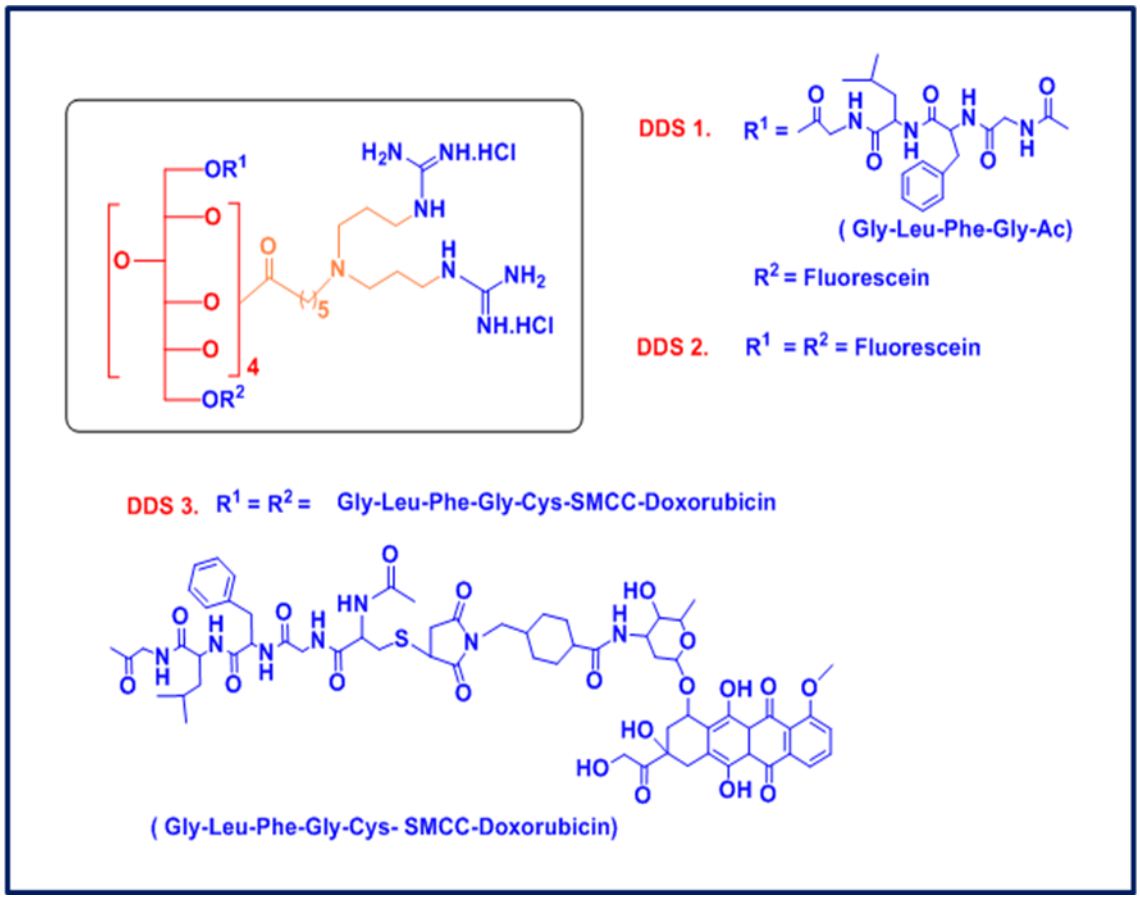

Scheme 2.2. Synthetic construct of sorbitol based octa-guanidine carriers **DDS1**, **DDS2** and **DDS3**

At one end of SMCC, **Dox** is coupled by amide bond, while at the other end, cysteine residue of **GLPGC** is linked to the maleimide group of SMCC. In this synthetic construct, **Dox** has been covalently conjugated to the carrier and the ratio of loading of drug to carrier is 2: 1. Cat B peptide sequence has been synthesized by solid phase synthesis using manual coupling of HMPB-MBHA resin. All the three DDS constructs have been purified by reversed-phase (C18) column chromatography after Boc-group deprotection from guanidine moiety. The key intermediates and target products, **DDS1**,

2 and **3** were characterized by HPLC, NMR spectroscopy and MALDI-TOF mass spectrometry.

2.3.2. Drug release profile for DDS3

To investigate the drug release of Dox conjugated carrier, **DDS3**, we incubated **DDS3** (60µg/100 µL, in 50mM NaOAc and 1mM EDTA, pH=5.1) with cathepsin B enzyme (62ng/1µL) at a ratio of 9:1 respectively. Taking advantage of the intrinsic fluorescent property of Dox, its release from **DDS3** was assessed by fluorescence measurement at 590 nm. Fluorescence was measured at different time intervals using *BioTec Synergy 4* spectrophotometer at 590nm , which has been reflected as % drug release (plotted in Y-axis) as shown in **fig. 2.1A & B**. Dox release generally occurred in the presence of lysosomal cysteine protease, Cat B in acidic pH. The protease cleaves the specific peptide substrate, subsequently releasing **Dox**.[38] As shown in **fig 2.1A**, above 50 % of **Dox** release occurred in the presence of enzyme at 20 hrs. **Dox** release from **DDS3** was measured after incubation of cathepsin B protease enzyme at 37°C. 10µL (concentration= 62ng/µL) of enzymatically active cathepsin B substrate was added to 90 µL of 0.1mM **DDS3** compound in buffer (50mM of sodium acetate and 1mM of EDTA , in the ratio 9:1) . A blank was carried out without cathepsin B enzyme, using 100µL of **DDS3** buffer solution. All measurements were carried out at different pH conditions (5.1, 7, 7.4 and 9) at specific time intervals from 0 to 24 hrs.[39] Moreover, stability of the Cat B peptide substrate[40] in **DDS3** has been evaluated at different pH conditions, which confirmed no significant drug release even at physiological pH (**Fig. 2.1B**).

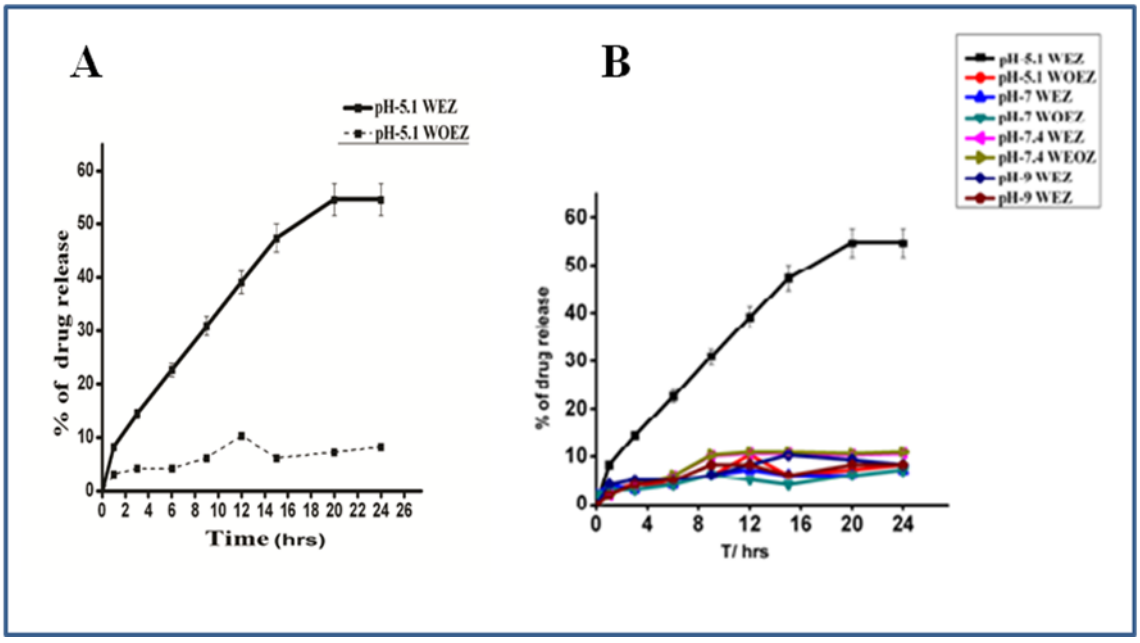

Figure 2.1. A) Line graph showing the release of doxorubicin from **DDS3** in the presence of cathepsin B enzyme at pH 5.1. B) Release of doxorubicin from **DDS3** in the presence of cathepsin B enzyme at pH 5.1, 7, 7.4 and 9. WEZ stands for with enzyme and WOEZ for without enzyme. T stands for time. The analysis was based on the percentage increase in the intrinsic fluorescence of doxorubicin caused due to its release. Data represented as mean ± standard deviation (SD), n=3.

2.3.3. MTT assay of DDS1 and DDS2

Fig.2.2A shows the results of MTT assay carried out after incubation of HeLa cells with different concentrations of **DDS1** for 24h. We next investigated the cellular internalization of **DDS1** and **DDS2** by flow cytometry. Both **DDS1** and **DDS2** were internalized by the cells demonstrated by the mean cell fluorescence levels in the FITC-A histograms (**fig. 2.2B**). **DDS1** uptake is evident by a shift in the fluorescence peak towards the right with regard to untreated control. A further shift in the peak with regard to **DDS1** uptake reveals **DDS2** cellular internalization.

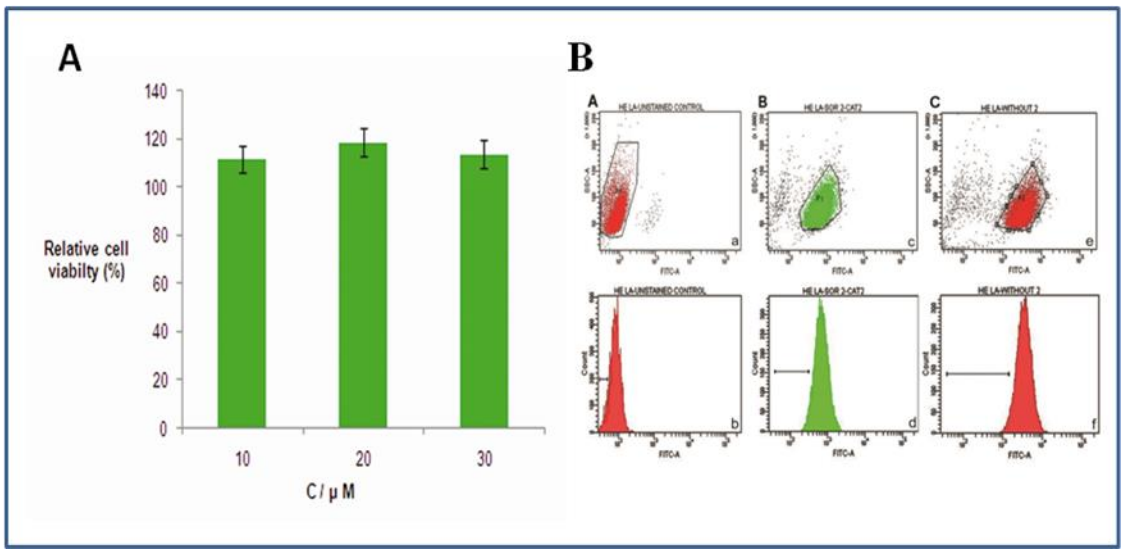

Figure 2.2. A) MTT assay demonstrating relative viability of HeLa cells on incubation with different concentrations of **DDS1** for 24h. C stands for concentration. B) Mean fluorescence (530nm emission) levels measured by flow cytometry demonstrating cellular uptake of **DDS1** and **DDS2** compared to untreated control cells. Dot plots and corresponding histograms: A (a & b) denote untreated control (shown in red), B (c & d) denote **DDS1** (shown in green), C (e & f) denote **DDS2** (shown in red).

2.3.4. Cellular uptake studies of DDS1, DDS2 and DDS3 by fluorescence imaging

Cellular uptake studies of **DDS1**, **2** and **3** were executed by fluorescence imaging of adherent cells. The cells were seeded at a density of 5x 10^3 cells/ well of 96 well black plates *(BD Biosciences, USA)* for the purpose. The cells were incubated with **DDS1**, **DDS2** and **DDS3** in HBSS individually for 1 h; at a concentration of 30µM. Images of

the cells were collected by high-content spinning disk facility *(*BD Pathway 855; BD Biosciences*)* using AttoVision 1.5.3 software. For imaging **DDS1** and **DDS2**, A488/10nm excitation filter and 515nm LP emission filter was used. For **DDS3**, B548/20nm excitation filter and 570 nm LP emission filter was used. **Fig 2.3.** represents fluorescent microscopic images revealing cellular uptake of **DDS1**, **2** and **3**

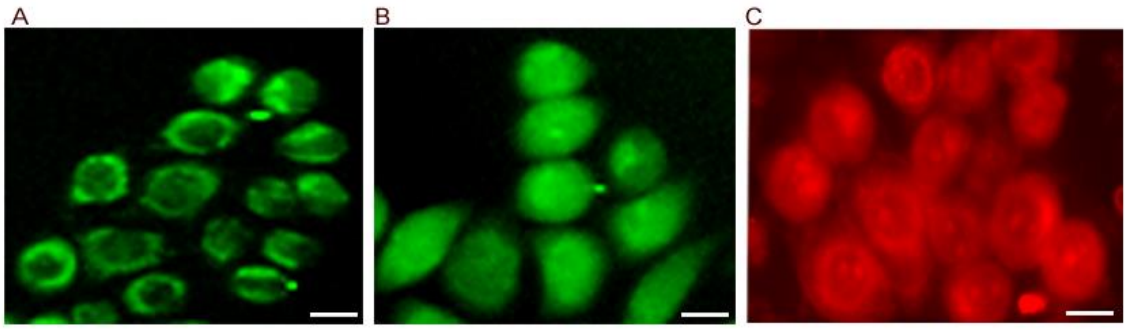

Figure 2.3. Cellular uptake of A. **DDS1** B. **DDS2** and C. **DDS3** demonstrated by fluorescence imaging. Scale bar: 25µm

2.3.5. Permeabilization of DDS1 and DDS3 in intracellular organelles

Further support for cellular uptake came from fluorescent imaging **DDS1** was found to localize in definite regions of the cytosol, as observed from its fluorescence pattern, whereas **DDS2** was found to accumulate in the entire region of the cell as the fluorescence was found to be diffused, rather than localized. As the fluorescence of **DDS1** was found to be localized in definite regions of the cell, we examined specific localization of **DDS1** in intracellular organelles by selective permeabilization of the plasma membrane using digitonin. Specific localization of **DDS1**, **2** and **3** in intracellular organelles was determined by selective permeabilization of plasma membrane by digitonin. Digitonin is a cholesterol-solubilizing agent; low concentrations of digitonin permeabilize cholesterol-rich membranes, such as the plasma membrane, but not cholesterol-poor lysosomal or mitochondrial membranes. Digitonin (Sigma) used at a concentration of 40µM selectively permeabilizes the plasma membrane, releasing the cytosolic dye, calcein AM (1µM) (Invitrogen) from the cells without altering the lysosomes. The localization of **DDS1/2/3** in the lysosomes has been validated by this approach.[41] There were 2 groups of treatments: one group of cells were incubated with **DDS1/2/3** individually for 1 hour, followed by incubation with the cytoplasmic probe, calcein (1µM) for 30 min at 37^{o}C. Cells immediately after incubation with **DDS1/2/3** as well as after incubating with calcein were washed with HBSS to remove unbound

DDS1/2/3 and calcein respectively. Another group of cells were incubated only with calcein and not **DDS1/2/3**, which is used as control. Both the groups were then treated with digitonin. Cell images were collected prior to and post- digitonin treatment. **Fig. 2.4A** represents selective permeabilization of cells incubated with **DDS2 / DDS3** along with calcein. Prior to digitonin treatment, we could observe uniform green cytoplasmic fluorescence corresponding to the cytosolic probe, calcein, in all the cells. But calcein fluorescence was completely lost within 10min of digitonin treatment demonstrating selective permeabilization of the plasma membrane (**fig. 2.4B**). On the contrary, a punctiform pattern of green fluorescence was observed in the cells even after 2 hrs of digitonin treatment. This punctiform fluorescence that remained intact indicates unambiguous localization of **DDS1** in intracellular organelles (**fig. 2.4C**). This punctiform fluorescence was absent for **DDS2** demonstrating that **DDS2** was localized only in the cytosol. But a red punctiform fluorescence was retained for **DDS3** showing its localization in intracellular organelles similar to **DDS1**. These organelles were presumed to be the lysosomes, which were further confirmed by co localization studies using confocal microscopy.

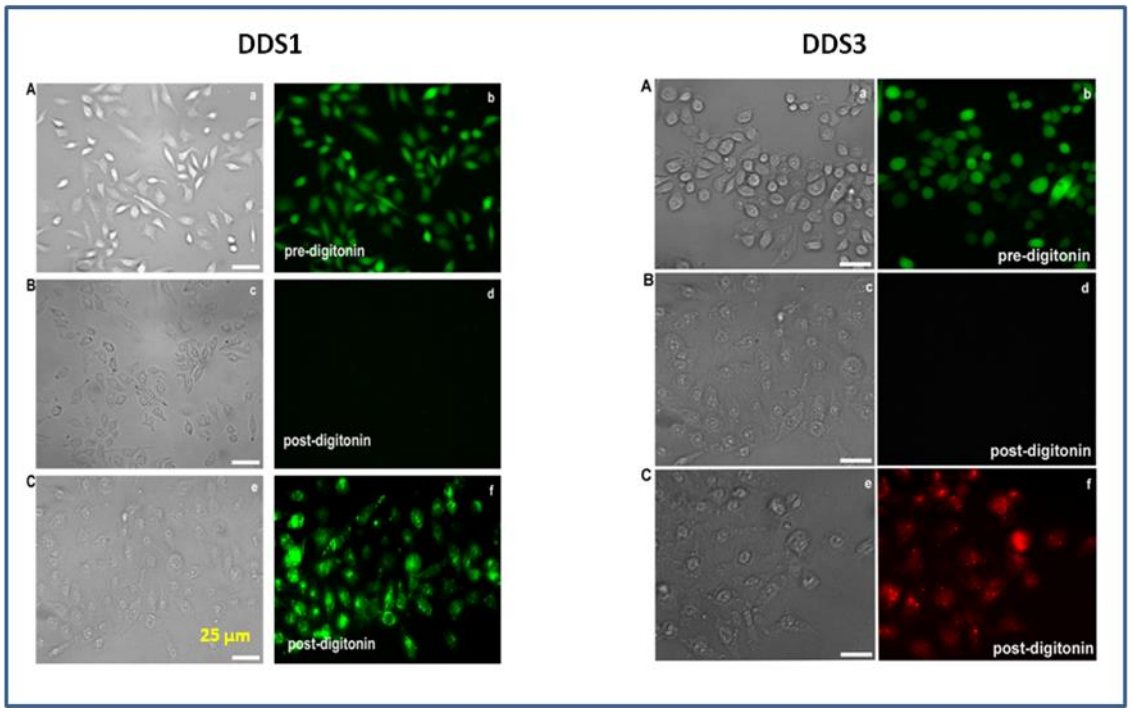

Figure 2.4. Specific localization of **DDS1** in intracellular organelles: transmitted light and corresponding fluorescence images. A-b denotes calcein (515 nm emission) incorporated cells prior to permeabilization by digitonin. B-d denotes loss of calcein fluorescence within 10min of digitonin treatment in cells loaded only with calcein, demonstrating permeabilization of plasma membrane. C-f denotes punctiform green fluorescence of **DDS1** (530nm emission) retained even after 2 hrs of digitonin treatment in cells loaded with both **DDS1** and calcein. A-a, B-c and C-e

show the transmitted light images of A-b, B-d and C-f respectively. Selective permeabilization of plasma membrane reveals no localization of **DDS2** in intracellular organelles, but specific localization of **DDS3** in the organelles. A-b denotes **DDS2** and calcein (515 nm emission) incorporated cells, prior to permeabilization by digitonin. B-d denotes loss of fluorescence within 10min of digitonin treatment in cells loaded with **DDS2** and calcein. No punctiform green fluorescence similar to **DDS1** was retained, demonstrating that **DDS2** was confined to the cytosol alone and had escaped along with calcein after permeabilization of the plasma membrane. A-a and B-c show the transmitted light images of A-b and B-d respectively. C-f shows the punctiform red fluorescence of **DDS3** (570nm emission) retained even after digitonin treatment in cells loaded with both **DDS3** and calcein. Calcein escaped from the cells on digitonin treatment. C-e shows the transmitted light image of C-f. Scale bar: 25µm

2.3.6. Co-localization studies of DDS1, DDS2 and DDS3

Fig.2.5A represents co-localization studies of **DDS1** and **3** individually with Hoechst. **DDS1** was found to localize significantly in the lysosomes as evident from the merged/ overlayed image of lysotracker red and **DDS1** (**fig. 2.5A**). **DDS3** was also found to localize within the lysosomes as evident from the merged image of lysosome GFP and **DDS3**. Neither **DDS1** nor **DDS3** was found to concentrate in the nucleus (**fig. 2.B**) **DDS2** did not show any specific organellar localization (data not shown). Overall, our results provide information that **DDS1** and **DDS3** confined to the lysosomes. Furthermore, the intrinsic fluorescent property of Dox has been exploited here to visualize the subcellular localization of **DDS3**.[42]

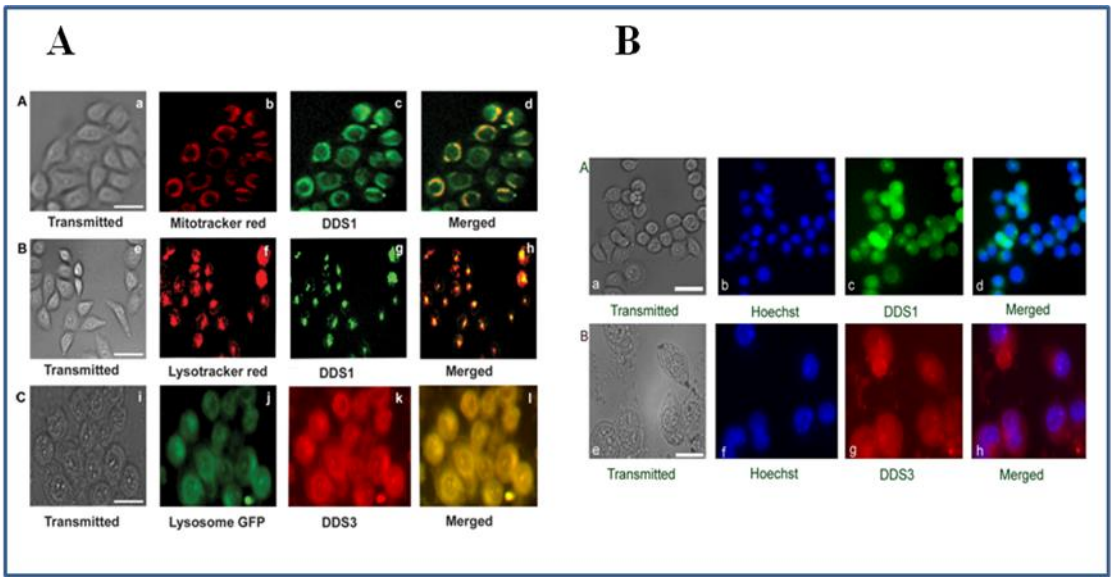

Figure. 2.5. (2.5A) Co localization studies by confocal microscopy: A. A little, but insignificant co localization of **DDS1** (30µM) observed within the mitochondria, indicated by the merged image [A-d] of mitotracker red (100nM) [A-b] & **DDS1** [A-c]. B. Significant co localization of **DDS1** within the lysosomes, indicated by the merged image [B-h] of lysotracker red (50nM) [B-

f] & **DDS1** [B-g]. C. Significant co-localization of **DDS3** (30µM) within the lysosomes, indicated by the merged image [C-l] of lysosome GFP [C-j] & **DDS3** [C-k]. A-a, B-e and C-i denote the corresponding transmitted light images. **(2.5B)** No significant localization of **DDS1** and **DDS3** in the nucleus. Merged image (A-d) of Hoechst (A-b) & **DDS1** (A-c) and the merged image (B-h) of Hoechst (B-f) & **DDS3** (B-g) demonstrates the fact. A-a and B-e represent corresponding transmitted light images. Scale bar: 25µm.

2.3.7. Flow cytometry for demonstration of cellular uptake of DDS1, DDS2 and DDS3

The flow cytometric data for **DDS1** and **DDS2** was recorded in the green channel (530nm emission), whereas data for **DDS3** was recorded in the red channel (570nm emission). Flow cytometric analysis of **DDS3** indicated its cellular uptake by the mean fluorescence levels in the PE-A histograms (**fig. 2.6**). The therapeutic efficiency of **DDS3** has also been disclosed by the concentration dependent increase in cell death that it provoked. At 30µM, **DDS3** induced 62.5± 6.3 % cell death. The percentage of cells showing the intrinsic red fluorescence of **DDS3** was found to decrease with increasing concentrations (5µM: 58%, 10µM: 49.9%, 20µM: 38.5%, 30µM: 23.4%) suggesting increase in cell death (**fig. 2.6**).

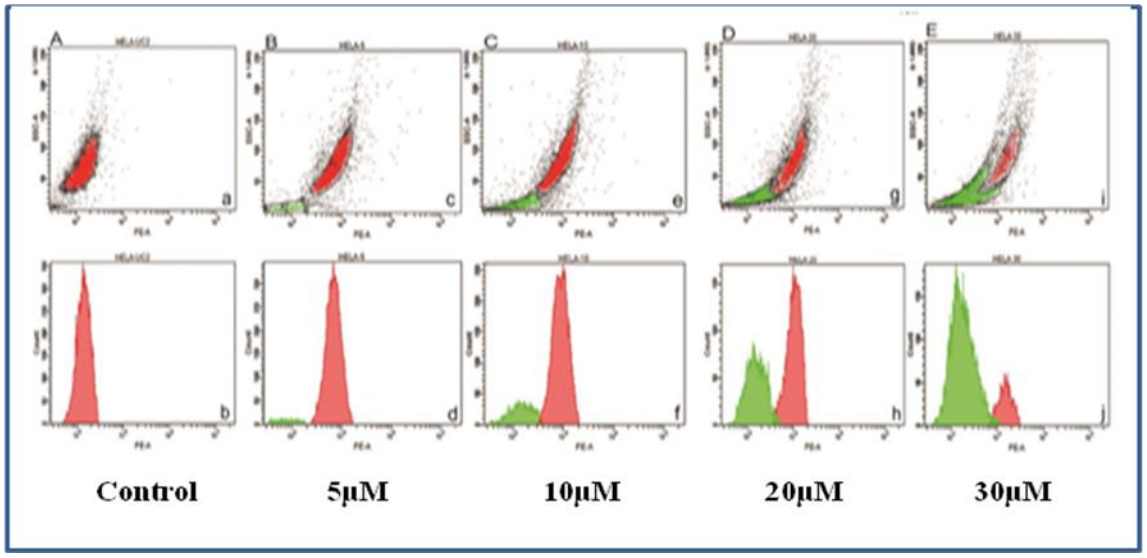

Figure 2.6. Flow cytometric data showing cellular uptake as well as cytotoxicity induced by different concentrations of **DDS3**. Cellular uptake has been demonstrated by the mean fluorescence levels in the PE-A histograms (red peaks; 570nm emission). Dot plots and corresponding histograms of A(a&b)-untreated control cells, B(c&d) - 5µM, C (e&f) 10µM, D (g&h) 20µM and E (i & j) 30µM. A concentration dependent increase in dead cell population has been shown by the green peaks in the histograms. The dead cell population in the dot plots has been gated and is shown as population P2 (green).

2.3.8. Cytotoxic evaluation of DDS1, Free Dox and DDS3 by MTT assay

We next investigated the beneficial effect of **DDS3** in comparison to free Dox by MTT assay. The results summarized in **fig 2.7** demonstrate that **DDS3** stimulated significant cytotoxicity when compared to free Dox which establishes the improved efficiency of targeted Dox-conjugated carrier over free Dox. This result is consistent with a previous study using chitosan/Dox/TAT where the conjugate was more effective than free Dox in killing CT-26 cells. In contrast, the free carrier, **DDS1** did not reveal any cytotoxicity under the same conditions (**fig. 2.7**).

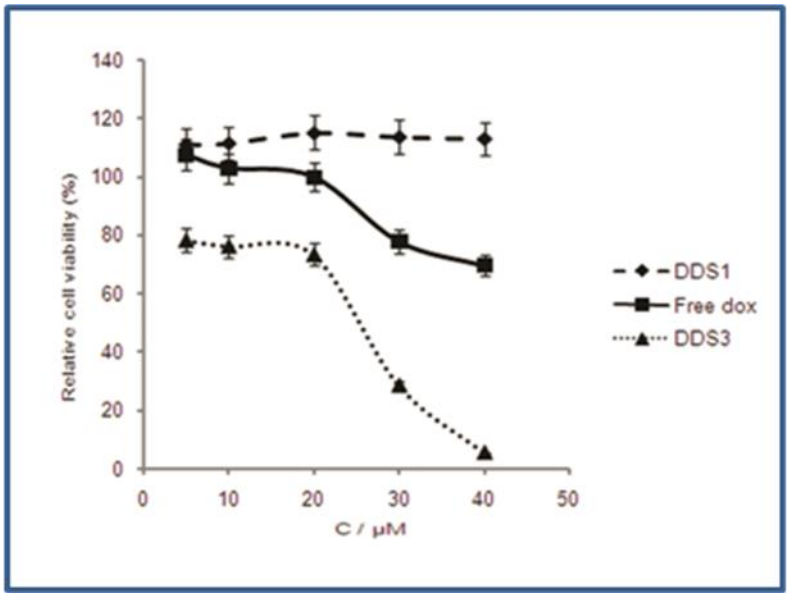

Figure. 2.7. MTT assay showing relative viability of HeLa cells on incubation with **DDS1**, free Dox and **DDS3** individually. The line graphs show that **DDS1**, the free carrier, does not induce any cytotoxicity, whereas the cytotoxicity stimulated by **DDS3**, the conjugated DOX, is higher than that of free Dox. *C* stands for concentration. Data expressed as mean±SD, n=6.

2.4. Summary of work

In summary, we have demonstrated a lysosome targeted drug delivery system that has been constructed using a sorbitol backbone with an octa-guanidine unit responsible for efficient cellular internalization. For lysosomal targeting, we have introduced Cat B tetrapeptide sequence into the sorbitol carrier. The release of Dox from the drug conjugate, **DDS3**, in the presence of cathepsin B enzyme, has been monitored by time dependent fluorescent measurement. Cellular internalization and targeting efficiency have been examined in HeLa cells that overexpress cathepsin B. The targeting efficiency of **DDS1** to intracellular organelles has been made obvious by selective permeabilization of the plasma membrane, whereas the specific lysosomal targeting efficacy revealed by co-localization with lysotracker dye. Similarly, **DDS3**, the **Dox**-carrier conjugate,

showed significant lysosomal localization. Therefore, we observed enhanced cytotoxicity for **DDS3** when compared to free **Dox** which definitely a promising candidate for further in vitro mechanistic studies and possible pre-clinical evaluation.

2.5. Conclusion

Hence the synthetic targeted carrier conjugated with **Dox** has been suggested to have the following applied advantages: 1) efficient targeted delivery of the anti-cancer drug as a result of its intracellular release, probably by enzymatic cleavage of Cat B peptide 2) enhanced cytotoxicity via **Dox** attached carrier in the tumor tissues and reduced undesirable side effects in normal cells and tissues; this may reduce dose-limiting toxicity as in chemotherapy. Supportive to this, a previous study demonstrated that a cathepsin-B cleavable doxorubicin prodrug (**Ac-Phe-Lys-PABC-Dox**) had increased anti-metastatic effects and reduced side effects, especially cardiotoxicity in a hepatocellular carcinoma model system.[43] Nonetheless, we believe that *in vitro* studies are not just adequate and the results obtained with the current investigation provide a firm foundation for future investigations of pharmacokinetic profile using *in vivo* / xenograft model.

2.6. Materials and Methods

2.6.1. Chemical Synthesis

Unless otherwise noted, all non-hydrolytic reactions were carried out in oven-dried glassware under an inert atmosphere of dry argon or nitrogen. All commercial chemicals were used as received, except for solvents, which were purified and dried by standard methods, prior to use. Analytical TLC was performed on a Merck 60 F254 silica gel plate (0.25mm thickness), and visualization was done with UV light (254nm and 365nm), or by spraying with a 5% solution of phosphomolybdic acid or ninhydrine solution, followed by charring with a heat gun. Column chromatography was performed on Merck 60 silica gel (60-120 or 100-200 mesh), and HPLC was performed on supeclean LC-C18-reversed phase silica gel. NMR spectra were recorded on Bruker AMX 300 (^{1}H-NMR at 300MHz;^{13}C-NMR at 75 MHz) and Bruker AMX 500 (^{1}H-NMR at 500MHz;^{13}C-NMR at 125MHz) spectrometers. Tetramethysilane was used as reference for ^{1}H-NMR, and the chemical shifts were reported in ppm and the coupling constant in Hz. Analytical and preparative HPLC were performed using Shimadzu

HPLC system consisting of SCL-10Avp system controller, two LC-8A solvent delivery units , SPD-M20A UV-vis photo diode array (PDA) detector, equipped with Multi PDA-LC solution (software) on a 250 mm x 4.6 mm i.d, 5µm, YMC-Pack R&D ODS analytical column (9YMC Co., Ltd. Japan). High resolution mass spectra were determined on a HR- EMI analysis of Thermo Scientific Exactive system, and MALDI-TOF mass spectra on a Shimadzu Biotech, AXIMA-CFR PLUS system. The standard extractive work-up procedure consist of pouring into a large amount of water, extracting with organic solvent indicated, washing the combined extracts successively with water and brine, drying the extract over anhydrous Na_2SO_4 or $MgSO_4$, and evaporating the solvent.

2.6.1.1. Synthesis of Cathepsin B peptide sequence (GLPG & GLPGC)

Preparation of GLPG and GLPGC was initiated with Fmoc- Gly-OH (337.6mg, 0.028 mmol) which was taken in dry dichloromethane (10mL) and DIC (0.218mL, 0.071mmol) was added. This was stirred at 0-5°C for 1hr under N_2 atmosphere. The Fmoc- Gly-OH activated DIC complex was concentrated and then dissolved in DMF along with 2-3 drops of DIPEA and charged into the resin bed of HMPB-MBHA resin (200mg, 0.0142mmol) which was swelled up in dry dichloromethane (6mL) for 30 min. The reaction was continued for 8 hrs with shaking. The progress of the reaction was monitored by the Kaiser test. After completion of the coupling, the resin was washed with DMF (3 x 3 mL), and the Fmoc protection group was removed by treatment with piperidine in DMF (20%, 3 x 2 mL, 3 x 15 min). The reaction cycle was continued in a similar manner with Fmoc- Phe-OH (165mg, 0.028mmol), Fmoc-Gly-OH (337.6mg, 0.028 mmol) and Fmoc -Cys-OH (249mg, 0.042mmol) amino acids charged to the resin. The resulting resin-bound tetrapeptide was washed with DMF (3 x 5 mL), dichloromethane (7 x 3 mL) and methanol (3 x 3 mL), dried *in vacuo* (10 hrs), re-swelled in dichloromethane (5 mL), and filtered. Finally desired peptide sequence was released from the resin by treatment with 2% trifluoroacetic acid in dichloromethane (10 x 2 mL). The resin washing was combined and concentrated under reduced pressure, and the residue co-evaporated with toluene. The residue was precipated with cold ether (3 mL) and filtered the residue peptide that afforded of white solid (74 mg, 89%). ^{1}H-NMR (500Mz, $CDCl_3$) : δ 1.84 (t, 2H), 2.16 (s, 3H),7.28-7.38 (m, 5H), 8.56 ppm (s, 5H) ; MALDI-TOF-MS: m/z calcd for $C_{24}H_{35}N_5O_7SNa$: 559.1452, found 559.1481 $[M+Na]^+$.

2.6.1.2. Synthesis of DDS1

Compound 1 has been synthesized as per our previously reported synthetic route

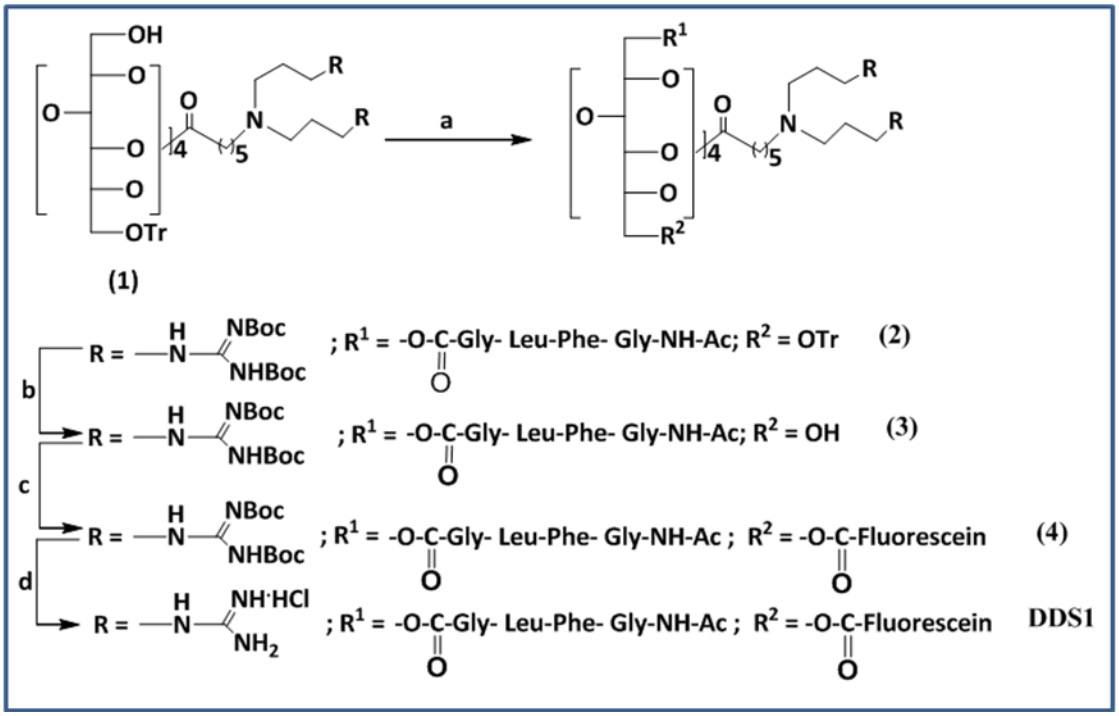

Scheme 2.3. Synthesis of **DDS1**., Reagent and conditions: a) **HO_2C-Gly-Leu-Phe-Gly-NH-Ac** (Cathepsin- B peptide sequence), EDC, DMAP, DIPEA, CH_2Cl_2, RT,16hrs, 62%; b) 2%TFA in CH_2Cl_2,RT,4hrs,76%; c) Fluorescein, EDC, DMAP,TEA,RT, dark,12hrs, 64%; d) HCl (gas), EtOAc, RT, 4hrs, 65%.

2.6.1.2.1. Synthesis of compound 2

Cathepsin B peptide sequence (**HO_2C-Gly-Leu-Phe-Gly-NH-Ac**, 11.15mg, 0.025mmol), EDC (5.7mg, 0.029mmol), N, N'- dimethyl amino pyridine (1.3mg, 0.011mmol), and DIPEA (1.8mL, 0.010mmol) were added to a solution of **1** (70mg, 0.021mmol) in dry CH_2Cl_2 (3mL). The mixture was stirred at RT for 16hrs under N_2 atmosphere. The crude product was purified using column chromatography on silica gel to afford the product **2** as a white foamy solid (49.87 mg, 62%). ^{1}H-NMR (500Mz, $CDCl_3$) : δ 0.83-0.97 (m, 6H), 1.48-1.67 (m, 186H), 2.01-2.36 (m, 19H), 3.58-3.71 (m, 5H), 3.92-3.94 (m, 5H), 4.13-4.22 (m, 4H), 7.23-7.24 (m, 4H), 7.28-7.44 (m, 20H), 8.49 (br s, 8H), 11.42 ppm (br s, 8H); MALDI-TOF-MS: m/z calcd for $C_{183}H_{296}N_{32}O_{51}Na$: 3781.1452, found 3781.3145 $[M+Na]^+$.

2.6.1.2.2. Synthesis of compound 3

Trifluoroacetic acid (0.15mL, 0.002mmol) was added to a solution of **2** (40mg, 0.011mmol) in dry CH_2Cl_2 (2mL), and the solution was stirred at RT for 4hrs. The result mixture was concentrated to give the crude product. This was purified using column chromatography on silica gel to afford the product **3** as a white foamy solid (27.85mg, 76%). ^{1}H-NMR (500Mz, $CDCl_3$): δ 0.73-0.82 (m, 6H), 1.18-1.50 (m, 184H), 2.96-3.57 (m, 32H), 4.09-4.14 (m, 4H), 4.33-4.35 (m, 5H), 7.18-7.26 (m, 5H), 7.21 ppm (s, 4H); MALDI-TOF-MS: m/z calcd for $C_{163}H_{286}N_{32}O_{47}Na$: 3467.0873, found 3467.4160 $[M+Na]^+$.

2.6.1.2.3. Synthesis of compound 4

Fluorescein (2.3mg, 0.0070mmol), EDC (1.7mg, 0.0088mmol), TEA (0.4117mL, 0.0029mmol) and DMAP (0.21mg, 0.0017mmol) were added into the solution of **3** (20mg, 0.0058mmol) in dry CH_2Cl_2. The reaction mixture was stirred in dark conditions at RT for 12hrs. The resultant mixture was concentrated to given the crude product and was purified using column chromatography on silica gel to afford the coupled product **4** as an orange colored foamy solid (18.4 mg, 64%). ^{1}H-NMR (500Mz, $CDCl_3$) δ 0.75-0.84 (m, 3H), 1.07-1.51 (m, 186H), 1.89-1.92 (m, 3H), 2.15-2.25 (m, 32H), 3.35-3.64 (m, 4H), 3.98-4.02 (m, 4H), 6.85-6.90 (m, 4H), 7.12-7.62 (m,10H), 7.84 (s, 4H); MALDI-TOF-MS: m/z calcd for $C_{183}H_{296}N_{32}O_{51}Na$: 3781.1452, found 3781.2492 $[M+Na]^+$.

2.6.1.2. Synthesis of compound DDS1

Ethyl acetate (4mL) saturated with gaseous HCl was added to a solution of **4** (12mg, 0.0032mmol) in ethyl acetate (1mL). The reaction mixture was stirred for 4hrs. Then the solution was concentrated and the residue was washed with dichloromethane to remove less polar impurities. The residue was dried and purified using MPLC on supelclean LC-18 reverse phase silica gel (CH_3CN / H_2O 9: 1 to 4: 1). The purified product was dissolved in de-ionized water, filtered through a PTGE syringe filter, and lyophilized to given **DDS1** as a light-greenish-yellow foamy solid (HCl salt, 6.0mg, 65%). ^{1}H-NMR (500Mz, $CDCl_3$) δ 0.75-0.81 (m, 3H), 1.12-1.28 (m, 42H), 1.92 (s, 3H), 2.15-2.25 (m, 32H), 3.98-4.02 (m,4H), 6.73-6.8 (m, 4H), 7.10-7.84 (m, 15H), 7.62 (br,s.; 4H); MALDI-TOF-MS: m/z calcd for $C_{103}H_{176}N_{32}O_{19}Na$: 2188.3690, found 2188.5821 $[M+Na]^+$; Analytical HPLC (Shimadzu-ODS): R_t = 4.24 min (Flow rate = 1mL / min, UV 480nm, CH_3CN: H_2O = 90:10).

2.6.1.3. Synthesis of DDS2

(Compound **5** has been synthesized as per our previous reported synthetic route**)**

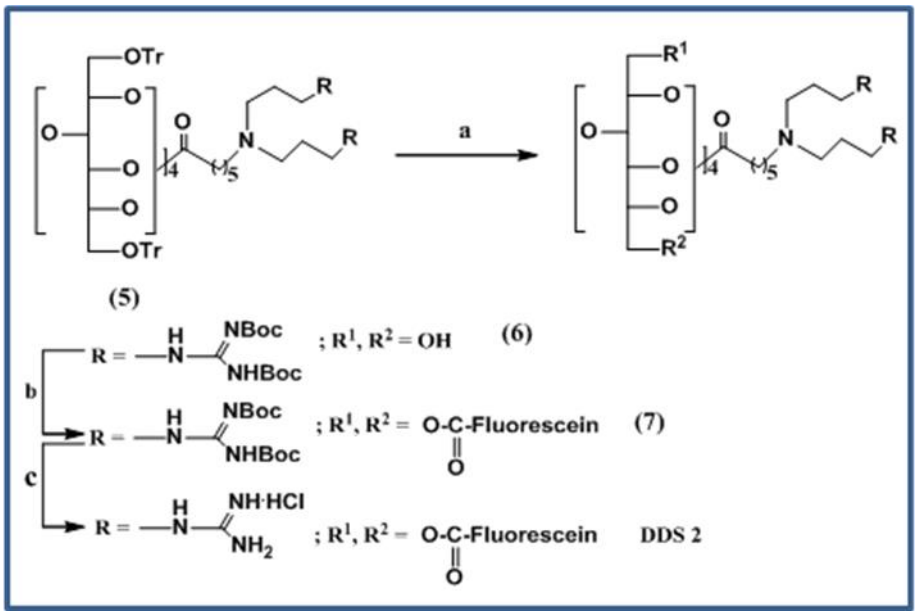

Scheme 2.4. Synthesis of **DDS2**., Reagent and conditions: a) 2%TFA in CH_2Cl_2, RT,4hrs,76%; b) Fluorescein, EDC, DMAP, TEA, CH_2Cl_2, RT,dark,72%; c) HCl (g), EtOAc, RT, 4hrs, 62%.

2.6.1.3.1. Synthesis of compound 6

Trifluoroacetic acid (0.89mL, 0.011mmol) was added to a solution of **5** (100mg, 0.029mmol), in dry CH_2Cl_2 and stirred at RT for 4hrs under nitrogen atmosphere. The resultant mixture was concentrated to given the crude product, which was purified by column chromatography on silica gel to afford the product **6** (65.2mg, 76%) as a white foamy solid. ^{1}H-NMR (500Mz, $CDCl_3$): δ 1.18-1.96 (m, 184H), 2.03-2.46 (m, 16H), 3.04-3.21 (m, 32H), 3.97-4.23 (m, 4H), 8.52-8.72 (m, 8H), 11.71 (br,s.; 8H); MALDI-TOF-MS: m/z calcd for $C_{142}H_{258}N_{28}O_{42}Na$: 3050.8813, found 3050.8472 $[M+Na]^+$.

2.6.1.3.2. Synthesis of compound 7

Fluorescein (7.9mg, 0.002mmol) was added to a solution of **6** (60mg, 0.020mmol), EDC (9.5mg, 0.050mmol), TEA (1.11mL, 0.008mmol) and DMAP (1.2mg, 0.010mmol) in dry CH_2Cl_2. This was stirred at RT for 12hrs. The reaction mixture was concentrated to give the crude product and which was purified by column chromatography on silica gel to afford the compound **7** as an orange colored foamy solid (52.4 mg, 72%). ^{1}H-NMR (500Mz, $CDCl_3$) δ 1.26-1.68 (m, 184H), 2.04-2.34 (m, 32H), 3.10-3.35 (m, 16H), 4.04-4.31 (m, 4H), 8.19-8.44 ppm (m, 12H); MALDI-TOF -MS: m/z calcd $C_{182}H_{278}N_{28}O_{50}Na$: 3679.9921, found: 3679.2496$[M+Na]^+$.

2.6.1.3. Synthesis of compound DDS2

Ethyl acetate (5mL) saturated with gaseous HCl was added to a solution of **7** (30mg, 0.008mmol) in ethyl acetate (1mL) at RT. After 4hrs of stirring, the solution was concentrated and the residue was washed with dichloromethane to remove less polar impurities. The residue was dried and purified using MPLC on supelclean LC-18 reverse phase silica gel (CH_3CN / H_2O 9: 1 to 3: 1). The purified product was dissolved in deionized water, filtered through a PTGE syringe filter, and lyophilized to give **DDS2** (HCl salt, 10 mg, 62%) as a light yellow foamy solid. ^{1}H-NMR (500Mz, $CDCl_3$) δ 0.90-1.45 (m, 40H), 2.07-2.34 (m, 16H), 4.12-4.36 (m, 4H), 5.36-5.51 (m, 6H), 6.85 (br,s.; 8H), 7.00-7.53ppm (m, 14H); MALDI-TOF-MS: m/z calcd for $C_{102}H_{158}N_{28}O_{18}Na$: 2086.2209, found: 2086.1063$[M+Na]^+$; Analytical HPLC (Shimadzu-ODS): R_t = 3.50 min (Flow rate = 1mL / min, UV 480nm, CH_3CN: H_2O = 90:10).

2.6.1.4. Synthesis of DDS3

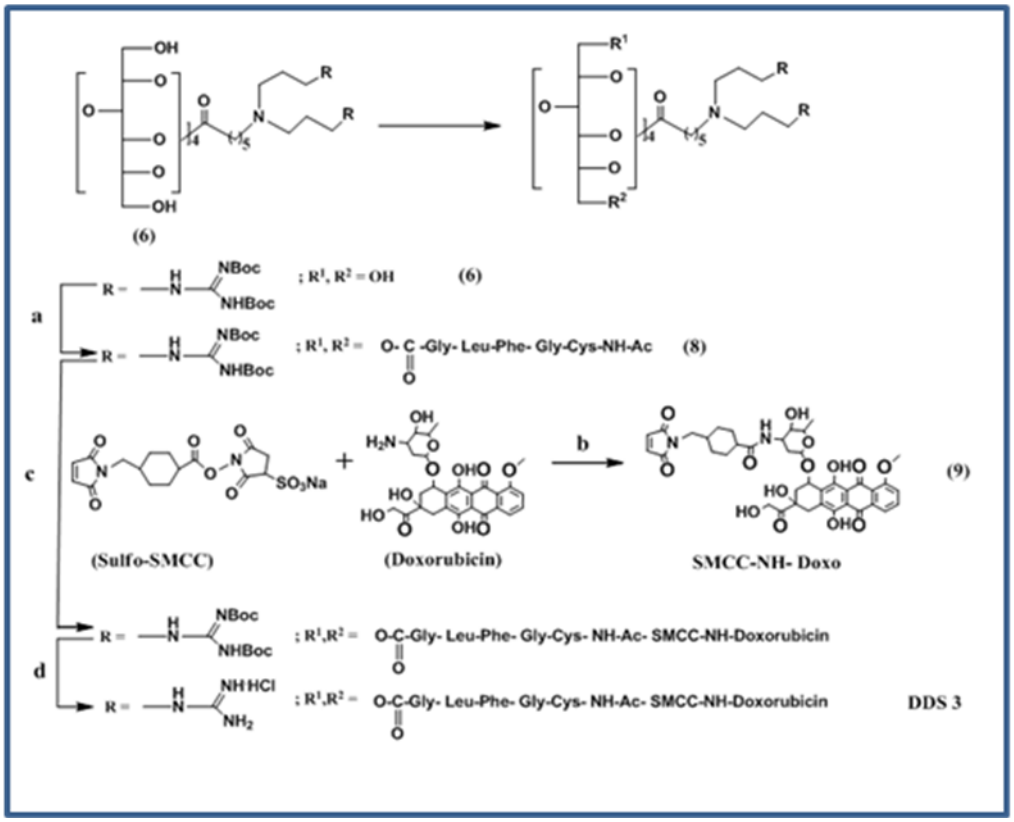

Scheme 2.5. Synthesis of **DDS3**., Reagent and conditions: a) **HO_2C-Gly-Leu-Phe-Gly-Cys-NH-Ac** (Cathepsin- B peptide sequence), EDC, DMAP, TEA, CH_2Cl_2, 12hrs, 94%; b) Sulfo-SMCC, Doxorubicin, TEA, DMSO, RT, dark, 12hrs, 90%; c) **8**, **SMCC-Doxo**, RT, DMSO, 15hrs, d) HCl(g) l(g), EtOAc,RT,4hrs,65%.

2.6.1.4.1. Synthesis of compound 8

Cathepsin-B peptide sequence (**HO_2C-Gly-Leu-Phe-Gly-Cys-NH-Ac**) (31.93mg, 0.041mmol) was added to a solution of sorbitol carrier **6** (56mg, 0.019mmol), EDC (8.9mg, 0.046mmol), triethylamine (1.06mL, 0.007mmol) and DMAP (1.16mg, 0.009mmol) in dry CH_2Cl_2. This was stirred at RT for 12hrs under N_2 atmosphere. The reaction mixture was concentrated to give the crude product and was purified by column chromatography on silica gel to afford the compound **8** as a white foamy solid (71.2 mg, 84%). ^{1}H-NMR (500Mz, $CDCl_3$) δ 0.79-0.87 (m, 12H), 1.31-1.59 (m, 188H), 3.07-3.17 (m, 32H), 4.70 (br, s; 14H), 6.70-7.35 (m, 10H), 7.89-7.79 (br,s,10H), 11.75 (br, s, 8H); MALDI-TOF-MS: m/z calcd for $C_{190}H_{324}N_{38}O_{56}Na$: 4121.3015, found: 4121.5228 $[M+Na]^+$.

2.6.1.4. Synthesis of DDS3

Doxorubicin (2.0mg, 0.003mmol) was taken in DMSO (2mL) and stirred with triethylamine (200 µL) for 10 min followed by addition of Sulfo-SMCC (2.6mg, 0.006mmol) to the stirred solution and continued stirring at room temperature for 12 hrs under N_2 atmosphere. The resultant mixture was concentrated under reduced pressure and the crude red colour sticky solid **9** (**SMCC-NH-Dox**) was added to a solution of **8** (10mg, 0.002mmol) in DMSO (4 mL) at RT under N_2 atmosphere. After 15 hrs of stirring, the reaction mixture was concentrated again under reduced pressure and dried thoroughly using high vacuum pump. The crude Dox- conjugated compound 10 (6. 2 mg) was taken in EtOAc (1mL), and ethyl acetate (4mL) saturated with gaseous HCl was added gently into it. After 4hrs of stirring at RT, the solution was concentrated and the residue was washed thoroughly with dichloromethane to remove less polar impurities. The residue was dried and purified using MPLC on supelclean LC-18 reverse phase silica gel (CH_3CN / H_2O 9: 1 to 5: 1). The purified product was dissolved in de-ionized water, filtered through a PTGE syringe filter, and lyophilized to afford DDS3 as a light red foamy solid (HCl salt, 4.2mg, 45%). ^{1}H-NMR ($CDCl_3$) δ 1.17-1.35 (m, 58H), 2.02-2.04 (m, 3H), 3.21-3.32 (m, 18H), 4.09-4.13 (m, 14H), 4.25-4.61 (m, 4H), 6.82 (m, 8H), 7.23-7.43 (m, 16H), 8.13ppm (br s, 10H); MALDI-TOF-MS: m/z calcd for $C_{188}H_{288}N_{42}O_{52}S_2Na$: 4053.0524, found: 4053.3603 $[M+Na]^+$; Analytical HPLC (Shimadzu-ODS): R_t = 4.37 min (Flow rate = 1mL / min, UV 480nm, CH_3CN: H_2O = 90:10).

2.6.2. HPLC purification of DDS1, DDS2 and DDS3

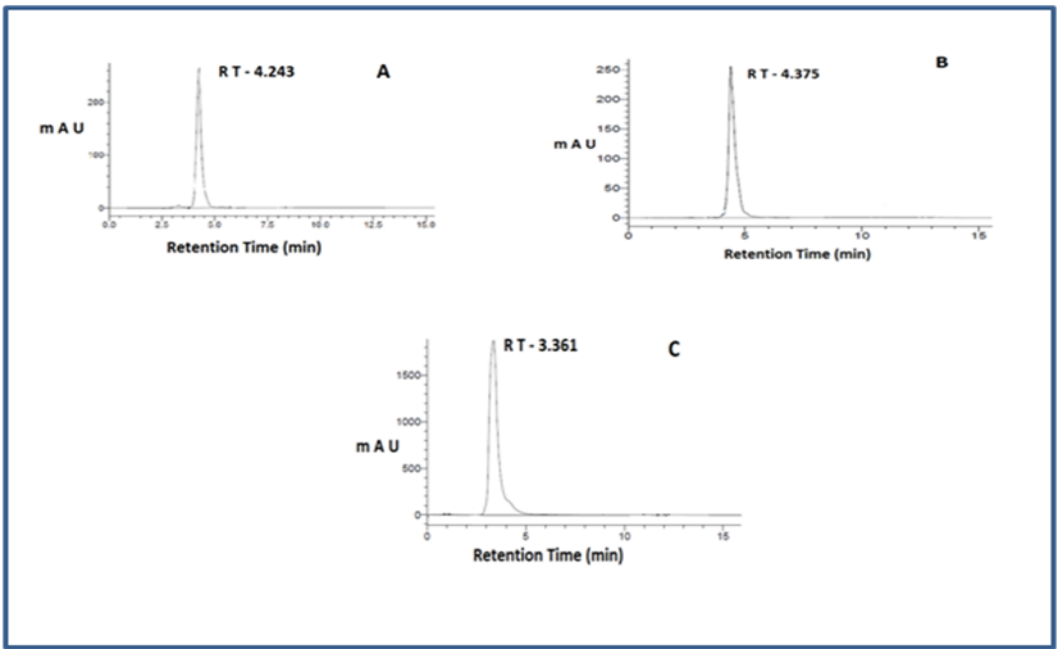

Figure 2.8. The compounds **DDS1** (A), **DDS2** (B) and **DDS3**(C) analyzed by HPLC.

The HPLC analysis was conducted using Shimadzu RP- HPLC ODS column with mobile phase consisting of 0.1% TFA in acetonitrile (A) and 0.1% TFA in water (B) The gradient was linearly increased from 0% to 80% B for 15 minutes at the flow rate of 1mL/min at ambient temperature. UV-VIS detection was monitored simultaneously at 254nm and 480nm wavelengths. The synthesized **DDS1**, **DDS2** and **DDS3** compounds were dissolved in 50mM Tris HCl buffer (pH 7.4) at 2mg/mL concentration and were purified by analytical HPLC.[44] The purity of compounds **DDS1**, **DDS2** and DDS3 is as shown in **fig 2.8**.

2.6.3. Cell culture studies

HeLa cells were obtained from National Centre for Cell Science, Pune, India. For the maintenance of cell lines, Dulbeccos Modified Eagle's Medium (DMEM) *(Sigma)* containing 10% fetal bovine serum (FBS) *(Gibco)*, antibiotics (100U/mL Penicillin and 100µg/mL streptomycin) and amphotericin (0.25µg/mL) *(HiMedia)* was employed. The cells were maintained in CO_2 incubators at 37^{o}C with 5% CO_2 in air and 99% humidity. Passaging of cells were done using 0.25% trypsin and 0.02% EDTA *(HiMedia)* in phosphate buffered saline (PBS). Experiments were carried out after 36 hrs of seeding the cells at appropriate density in suitable well plates.

2.6.4. Flow cytometric analysis of cellular uptake and kinetics

Cellular uptake of **DDS1**, **2** and **3** was evaluated by flow cytometric analysis using *BD FACS Aria II flow cytometer (BD Biosciences).* Acquisition and analysis of flow cytometric data were carried out using *BD FACS Diva software*. The cells were seeded at a density of 5 x 10^4 cells per well of 24-well plates. Subsequent to incubation of the cells with **DDS1**, **DDS2** and **DDS3** individually for 1 hr in HBSS, trypsinization was done to detach the cells from the well plate. Trypsin was inactivated with 10% FBS containing medium, followed by centrifugation at 2300 rpm for 1 minute. The pellets were resuspended in HBSS. They were again pelleted at 400g for 5 min at 4^{o}C, which were further resuspended in cold HBSS without calcium and magnesium for flow cytometric analysis. The whole procedure was executed under dark conditions.

2.6.5. MTT assay

In vitro cell- based assays have been carried out in HeLa cells expressing cathepsin B [45] that examined the uptake and targeting efficiency of the carriers. **DDS1** was first tested for its toxicity in HeLa cells by MTT assay. Cell viability after incubating the cells with different concentrations of **DDS1** was determined by methyl thiazolyl tetrazolium (MTT) assay. It is a colorimetric assay based on the ability of live, but not dead cells to reduce MTT (yellow) to a purple formazan product. The cells were spread in 96-well plates at 5x10^3 cells/well. After incubating with DDS1 for 24 h, the cells were exposed to MTT at a concentration of 50µg/well for 2.5 to 3 hrs at 37^{o}C in CO_2 incubator. The working solution of MTT was prepared in Hanks balanced salt solution (HBSS). After viewing formazan crystals under the microscope, the crystals were solubilised by treating the cells with DMSO: isopropanol at a ratio of 1:1 for 20 min at 37^{o}C. Plate was read at an absorbance of 570nm. The relative cell viability in percent was calculated as: Absorbance of treated /Absorbance of control x100. Cells without DDS1 used as control.

2.6.6. Confocal analysis of cellular localization of DDS1, DDS2 and DDS3

Co-localization studies were carried out to gather information on the subcellular localization of **DDS1**, **2** and **3**. Commercially available Mitotracker deep red *(Invitrogen),* Lysotracker deep red *(Invitrogen)* and Hoechst *(Invitrogen)* were used for the experiments. The cells were seeded at a density of 5x 10^3 cells/ well of 96 well black plates for the purpose. They were incubated with Mitotracker and lysotracker in HBSS individually for 30 min at 37^{o}C. This was followed by washing the cells twice with

HBSS to remove unbound dye. The cells were then exposed to **DDS1**, **2** and **3** in HBSS individually for 1 hr. Subsequent to washing with HBSS, nuclear staining was carried out with Hoechst for 20 min at room temperature. Images of the cells were collected using high-content spinning disk facility as described earlier.

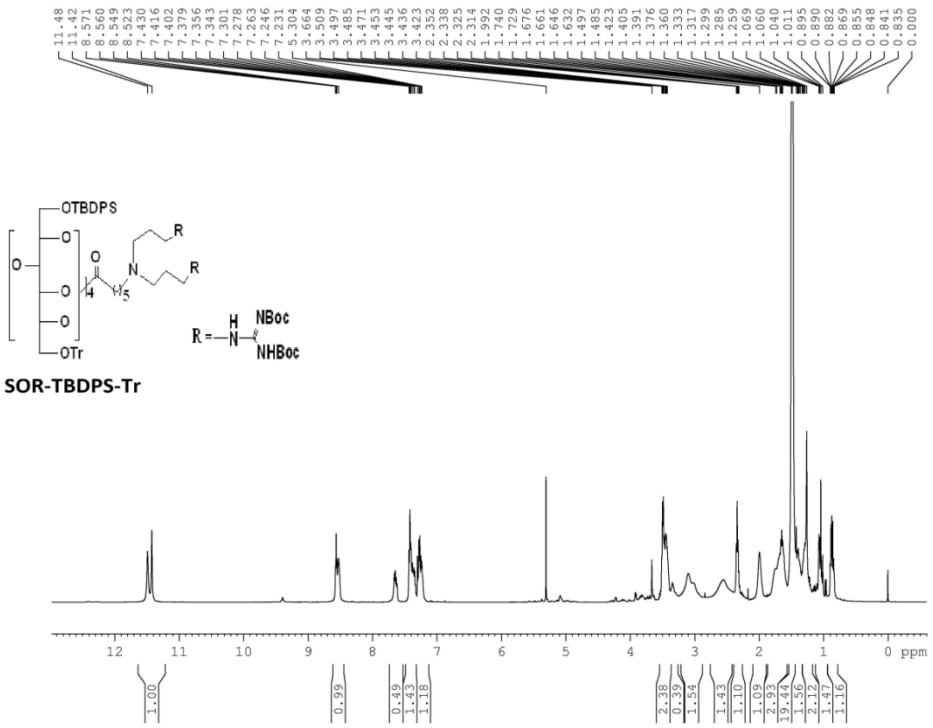

Figure 2.9. ^{1}H-NMR spectra of compound **Sor-TBDPS-Tr**

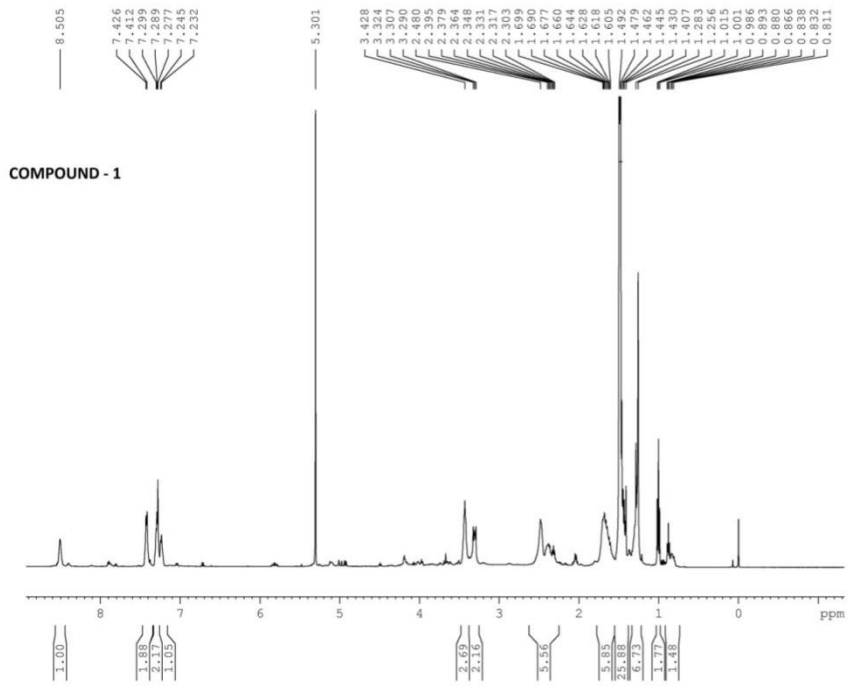

Figure 2.10. ^{1}H- NMR spectrum of compound-1 (500MHz, $CDCl_3$)

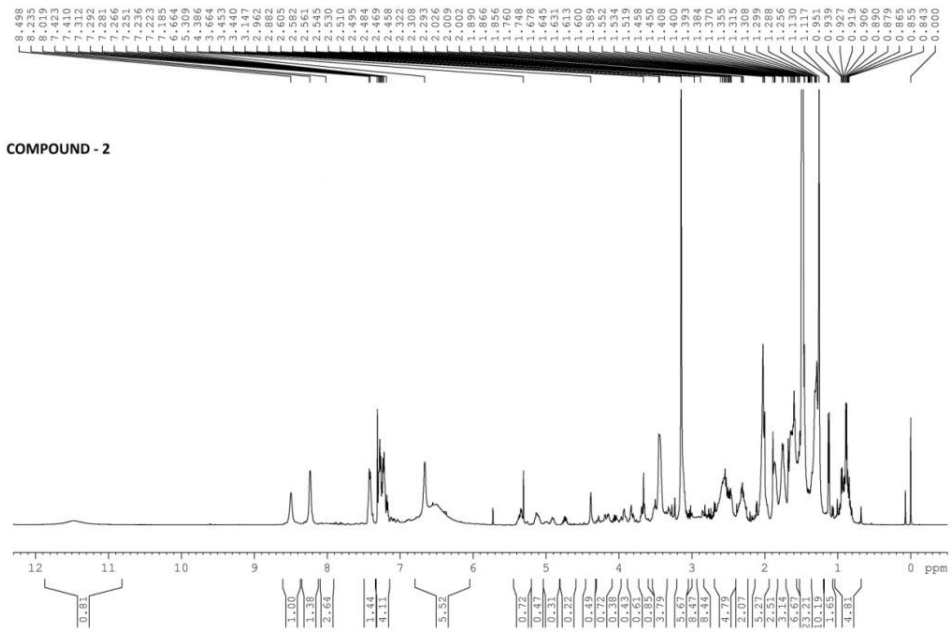

Figure 2.11. ^{1}H- NMR spectrum of compound-2 (500MHz, $CDCl_3$)

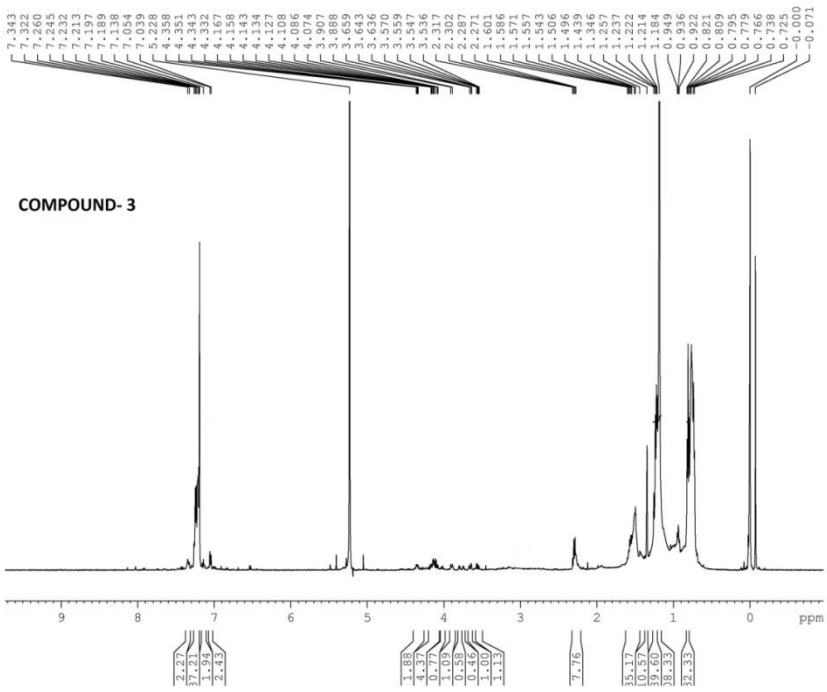

Figure 2.12. ^{1}H- NMR spectrum of Compound-3 (500MHz, $CDCl_3$)

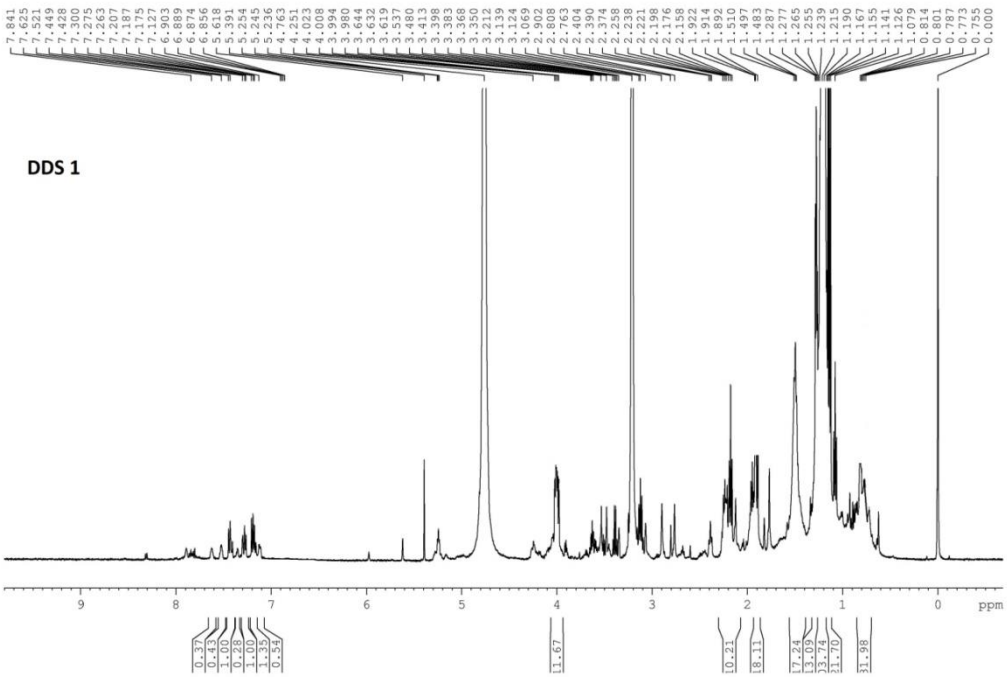

Figure 2.13. ^{1}H- NMR spectrum of **DDS1** (500MHz, CD_3OD)

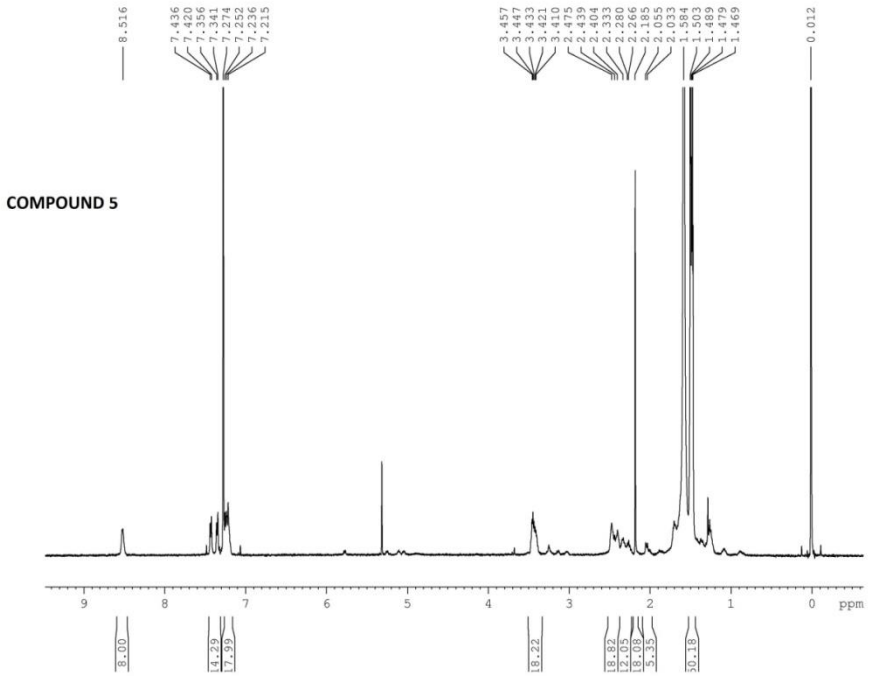

Figure 2.14. ^{1}H- NMR spectrum of compound-5 (500MHz, $CDCl_3$)

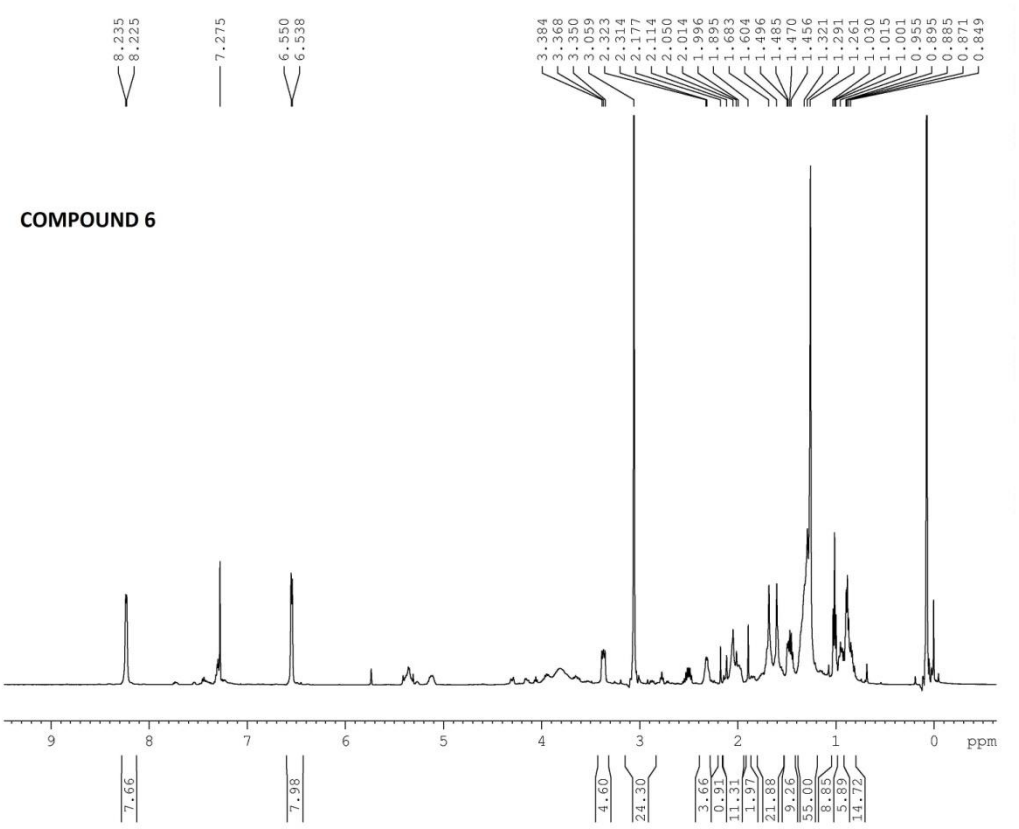

Figure 2.15. ^{1}H- NMR spectrum of compound-6 (500MHz, $CDCl_3$)

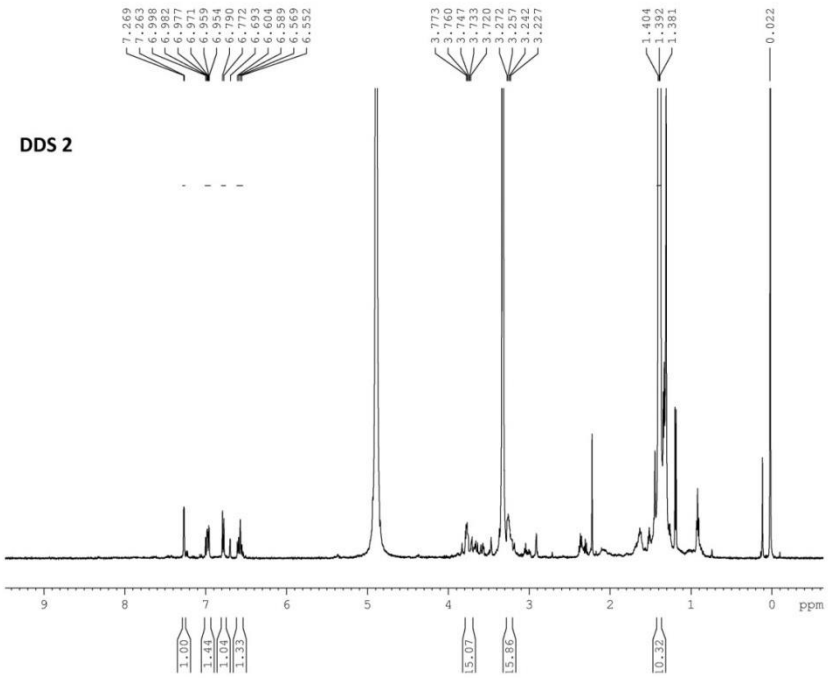

Figure 2.16. ^{1}H- NMR spectrum of **DDS2** (500MHz, CD_3OD)

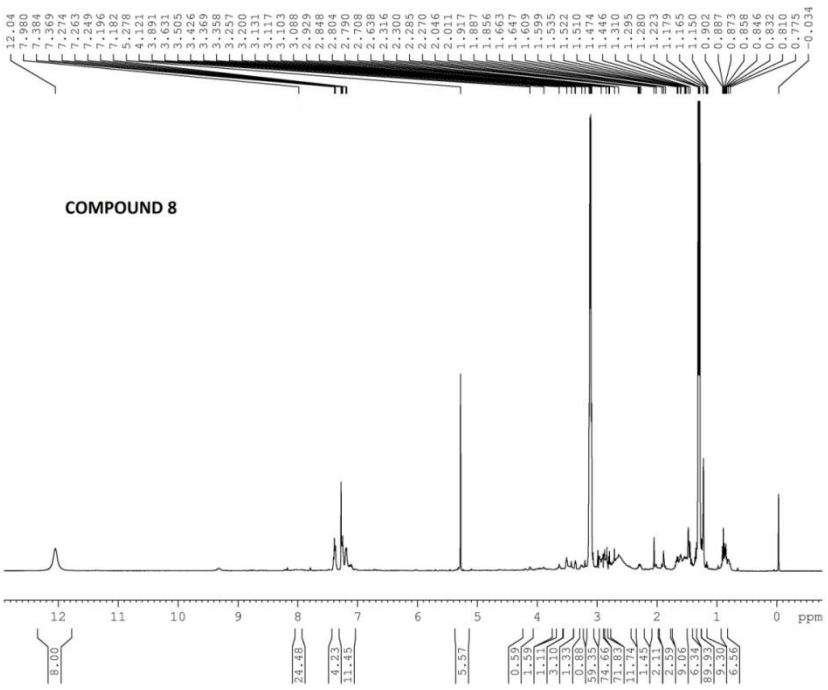

Figure 2.17. ^{1}H- NMR spectrum of compound-8 (500MHz, $CDCl_3$)

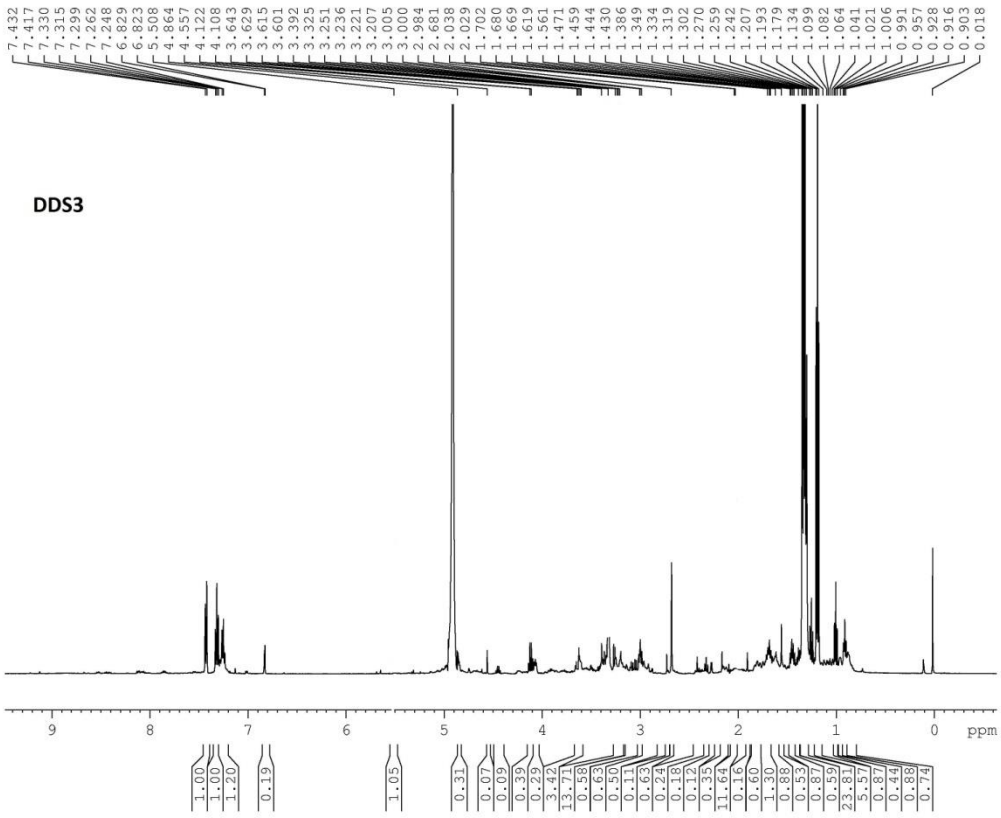

Figure 2.18. ^{1}H- NMR spectrum of **DDS3** (500MHz, CD_3OD)

2.7. References

[1]. Keefe, A. D.; Pai, S.; Ellington, A. *Nat Rev Drug Discov,* **2010,** 9, 537.

[2]. Torchilin, V. P. *Adv. Drug Deliv. Rev,* **2012,** 64, 302.

[3]. Copolovici, D.M.; Langel, K.; Eriste, E.; Langel, U. *ACS Nano,* **2014,** 8, 1972.

[4]. Senapati, S.; Mahanta, A.K.; Kumar, S.; Maiti, P. *Signal Transduct Target Ther,* **2018,** 3, 7.

[5]. Baillie, T.A. *Chem. Res. Toxicol.* **2008,** 21, 129

[6]. Shao,L.L.; Yaoyi,W.; Jingfang, Z. Wei, W.; Hua, L. *J. Mater.Chem. B,* **2017,** 5, 9546.

[7]. Wadia, J. S.; Stan, R. V.; Dowdy, S. F. *Nat. Med,* **2004,** 10, 310.

[8]. Nakase, I.; Niwa,; M, Takeuchi, T.; Sonomura, K.; Kawabata, N.; Koike, Y.; Takehashi M.; Tanaka, S.; Ueda, K.; Simpson, JC.; Jones, A.T.; Sugiura, Y.; Futaki, S. *Mol. Ther,* **2004,** 10, 1011.

[9]. Pipkorn, R.; Waldeck, W.; Spring, H.; Jenne, J. W.; Braun, K. *Biochim. Biophys. Acta,* **2006,** 606, 1758.

[10]. Chugh,A.; Eudes, F.; Shim,Y. S.; *IUBMB Life,* **2010,** 62, 183.

[11]. Munyendo, W.L.; Lv, H.; Benza-Ingoula, H.; Baraza, L.D.; Zhou, J. *Biomolecules,* **2012,** 2, 187.

[12]. Nasrollahi, S.A.; Taghibiglou, C.; Azizi, E.; Farboud, E.S. *Chem. Biol. Drug Des,* **2012,** 80, 639.

[13]. Jiang, T.; Olson, E.S.; Nguyen, Q.T.; Roy, M.; Jennings, P.A.; Tsien, R.Y. *Proc. Natl. Acad. Sci. U. S. A,* **2004,** 101,17867.

[14]. Scott, A.M.; Wolchok, J.D.; Old, L.J. *Nat. Rev. Cancer,* **2012,** 12, 278.

[15]. Wender, P.A.; Rothbard, J.B.; Jessop, T.C.; Kreider, E.L.; Wylie, B.L. *J. Am. Chem. Soc,* **2002,** 124, 13382.

[16]. Umezawa, N.; Gelman, M.A.; Haigis, M.C.; Raines, R.T.; Gellman, S.H. *J. Am.Chem. Soc,* **2001,** 124, 368.

[17]. Yu, D.H.; Lu, Q.; Xie, J.; Fang, C.; Chen, H.Z. *Biomaterials,* **2010,** 31, 2278.

[18]. Zhong, Y.J.; Shao, L.H.; Li, Y. *Int. J. Oncol,* **2013,** 42, 373.

[19]. Cudic, M.; Fields, G.B. *Curr. Protein Pept. Sci,* **2009,** 10, 297.

[20]. Torchilin, V. P. *Annu. Rev. Biomed. Eng,* **2006,** 8, 343.

[21]. Zhang, H.; Zhong, C.; Shi, L.; Guo, Y.; Fan. Z. *J. Immunol,* **2009,** 182, 6993.

[22]. Mohamed, M.M.; Sloane, B.F. *Nat Rev Cancer,* **2006,** 6, 764.

[23]. Gocheva, V.; Joyce, J.A. *Cell Cycle,* **2007,** 6, 60.

[24]. Rossi, A.; Deveraux, Q.; Turk, B.; Sali, A. *Biol Chem,* **2004,** 385, 363.

[25]. Turk, B.; Turk, .; Turk, V. *Biochim Biophys Acta,* **2000,** 1477, 98.

[26]. Vasiljeva, O.; Reinheckel, T.; Peters, C.; Turk, D.; Turk, V.; Turk, B. *Curr Pharm Des,* **2007,** 13, 385.

[27]. Jedeszko, C.; Sloane, B.F. *Biol Chem,* **2004,** 385, 1017.

[28]. Roshy, S.; Sloane, B. F.; Moin, K. *Cancer Metastasis Rev,* **2003,** 22, 271.

[29]. Fehrenbacher, N.; Jaattela,M.; *Cancer Res,* **2005,** 65, 2993.

[30]. Berquin, I. M.; Sloane, B. F. *Plenum Press, New York, NY,* **1996,** 281.

[31]. Bervar, A.; Zajc,I.; Katunuma, N. N.; Sloane, B. F.; Lah, T. T. *Biol. Chem,* **2003,** 384, 447.

[32]. Mullins, S.R.; Sameni, M.; Blum, G.; Bogyo, M.; Sloane, B.F.; Moin, K. *Biol. Chem,* **2012,** 393, 1405.

[33]. Reinheckel, T.; Peters, C.; Kruger, A.; Turk, B.; Vasiljeva, O.*Front. Pharmacol,* **2012,** 3, 133.

[34]. Maiti, K.K.; Jeon, O.Y.; Lee, W.S.; Kim, D.C.;Kim, K.T.; Takeuchi, T.; Futaki, S.; Chung, S.K. *Angew. Chem., Int.Ed,* **2006,** 45, 2907.

[35]. Maiti, K.K.; Lee, W.S.; Takeuchi, T.;Watkins, C.; Fretz, M.; Kim, D.C.; Futaki, S.; Jones, A.; Kim, K.T.; Chung, S.K. *Angew. Chem., Int. Ed,* **2007,** 46, 5880.

[36]. Dyba, M.;Tarasova, N.I.; Michejda, C.J. *Curr. Pharm. Des*., **2004,** 10, 2311.

[37]. Wender, P.A.; Galliher, W.C.; Goun, E.A.; Jones, L.R.; Pillow, T.H. *Adv Drug Deliv Rev,* **2008,** 60, 452.

[38]. Baeza, A.; Colilla, M.; Vallet-Regi, M. *Expert Opin Drug Deliv,* **2015,** 12, 319.

[39]. Z. Zhao, H. Meng, N. Wang, M. J. Donovan, T. Fu, M. You, Z. Chen, X. Zhang, W.Tan., Angew. Chem. Int. Ed., 2013, 52, 7487.

[40]. Dubowchik, G.M.; Firestone, R..;, Padilla, L.;Willner, D.; Hofstead, S.J.; Mosure, K.; Knipe, J.O.; Lasch, S.J.; Trail, P.A. *Bioconjugate Chem,* **2002,** 13, 855.

[41]. Werneburg, N.W.; Guicciardi, M.E.; Bronk, S.F.;, Kaufmann, S.H.; Gores, G.J. *Am J. Physiol Gastrointest Liver Physiol,* **2002,** 283, 947.

[42]. Lee, J.Y.; Choi, Y.S.; Suh, J.S.; Kwon, Y.M.; Yang, V.C.; Lee, S.J.; Chung, C.P.; Park, Y.J. *Int. J. Cancer,* **2011,** 128, 2470.

[43]. Wang, Q.; Zhong, Y.J.; Yuan, J.P.; Shao, L.H.; Zhang, J.; Tang, L.; Liu, S.P.; Hong, Y.P.; Firestone, R.A.; Li, Y. *J. Transl. Med,* **2013,** 11, 192.

[44]. Wang, T.; Ng, D. Y. W.; Wu, Y.; Thomas, J.; Tran, T. T.; Weil, T. *Chem. Commun,* **2014,** 50, 1116.

[45]. Wu, D.; Wang, H.; Li, Z.;Wang, L.; Zheng, F.; Jiang, J.; Gao, Y.; Zhong, H.; Huang, Y.; Suo, Z. *Histol. Histopathol,* **2012,** 27, 79.

Chapter -3

Evolution of Guanidinium Rich Dendron-Appended Hydnocarpin towards Anti-Neoplastic Effects through Caspase Mediated Apoptosis

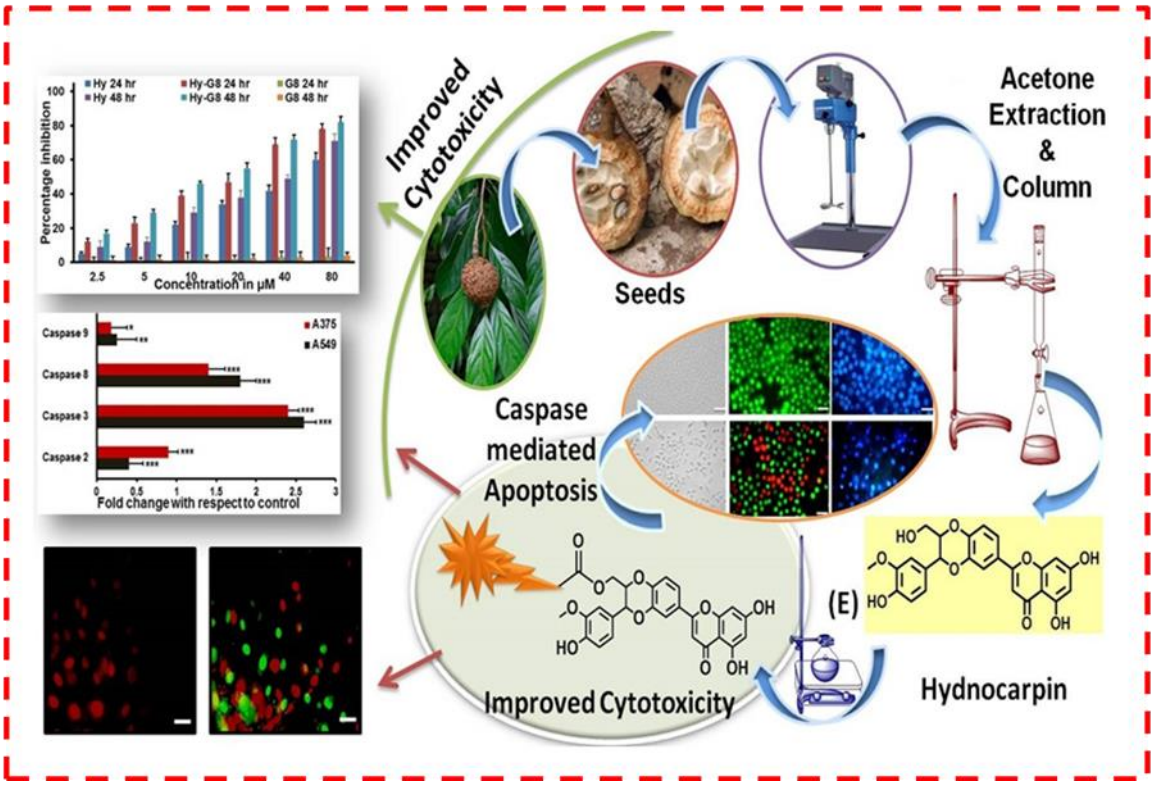

3.1. Abstract: Pharmacologically active chemical substances derived from animals, plants and microbes have been used to treat human disease since ancient times.Medicinal plants have truly demonstrated their potential as a repository of active biomolecules with promising therapeutic potential and represent an important pool for the identification of novel drug leads. *Hydnocarpus Wightiana Blume* is a popularly known medicinal plant and its acetone extract of the seed demonstrated superior free radical scavenging property with a high total phenolic and flavonoid content. Hydnocarpin (**Hy**), which has been isolated and purified from the acetone extract, promotes moderate cytotoxicity on cancer cells. In an attempt to increase the efficiency of **Hy** as an anticancer agent, chemical coupling with a highly efficient, non-toxic cell penetrating guanidinium rich poly-(propylene imine) dendron (**G8**) was attempted.

The resultant modified construct (**Hy-G8**) executes superior cytotoxicity preferentially on cancer cells through the induction of apoptosis mediated by caspases. The hybrid construct was also found to be a promising anti-metastatic agent. While the intrinsic complexity of natural product based drug delivery requires interdisciplinary approaches the transition of naturally occurring from a screening hit to a drug lead and finally a drug candidate could be accomplished prior to legitimate engineering of potential leads.

3.2. Introduction

The importance of natural products on the treatment of a broad range of diseases has been documented extensively.[1–7] Plant derived natural products in particular have been used for centuries to treat a wide variety of ailments.[8–11] A copious of natural resources for restorative uses exist around the world, of which numerous have not yet been successfully tapped for the development of conceivable drug candidates. [12] Although extensive research on compounds of natural origin to produce new drug substances occurs, research, specifically aimed at naturally derived medicines to optimize dosages for the intended route of administration and to design the most effective dosage forms, has become greater challenge. Many of the traditional medicines have real, beneficial effects and extracts of these crude combinations lead to the discovery of their active ingredients and eventually to the development of modern chemically pure drugs. While natural products continue to have a profound impact on human health, chemists have succeeded in generating semi-synthetic analogues that sometimes overshadow the original natural product in terms of clinical significance. Synthetic efforts based on natural products have primarily focused on improving their drug-like features while targeting utility in the same biological space. A less documented phenomenon is that natural products can serve as powerful starting materials to generate drug substances with novel therapeutic utility that is unrelated to the biological space of the natural product starting material.[13] In general phytochemicals identified from traditional medicinal plants are presenting exhilarating opportunities for the development of new drug candidates. Several studies revealed that chemically modified natural compounds, especially from medicinal plants[14] generated better response as candidate lead molecule in the field of cancer therapy. Cancer continues to be one of the major causes of death worldwide with only modest progress being made in reducing the morbidity and mortality of the disease. Phytochemicals from extracts of roots, bulbs, barks, leaves, stems and others parts of plants have shown promising potential as anti-cancer drugs, or for serving as lead compounds in the synthesis of new drugs. They are often utilized as traditional medicines in the form of home-made tinctures, teas, or

crude extracts but accompanied with drawbacks including batch to batch variation in preparation methods and hence the chemical composition. *Hydnocarpus Wightiana Blume*[15-18] (Flacourtiaceae), is widely cultivated in Southeast Asia mainly in China, Taiwan, Indonesia, Malaysia, and Thailand. Four species occur in India, which grows up to 50 feet and is commonly known as Chaulmoogra with globose fruits containing 15-20 seeds. Chaulmoogra oil, extracted from seeds is traditionally being effectively used in the treatment of leprosy, chronic skin disease, ophthalmia, and for dressing of wounds and ulcers. The plant has also been listed with anti-obesity activity and the seed[19] oil also used in traditional applications in rheumatism, sprains and bruise, sciatica and chest infections. The seeds possess high medicinal value because they are reported to contain array of therapeutically major classes of phytochemicals such as triterpenoids, flavones, aglycones, glycosides and a range of fatty acids and esters. Seed extracts yield compounds structurally related to the flavanolignans[20] namely hydnowightin, hydnocarpin, neohydnocarpin and luteolin. Even though all the five flavanolignans demonstrated anti diabetic, antioxidant activities and moderate cytotoxicity against few cancer cell lines[21, 22] hydnocarpin proved to be the most promising agent[16, 23] with significant cytotoxicity against cancer cells of various origins.

Given their phenomenal concoction assorted qualities and novel modes of action, natural products keep on working as lead compounds in many drug discovery programs. However, to keep up with the on-growing demand for new therapeutic agents, new strategies for enhancing their therapeutic potential are needed. Semi-synthetic modifications of natural products aimed at enhancing their biological properties or the total synthesis of analogues serve as great starting points for generating molecules with greater bio-availability, bio-distribution and rapid bio-response. Molecular transporters containing octa-guanidine residues enhanced the cell penetrating ability most effectively, and delivered a variety of cargos.[24] As of date our group developed a new guanidinium rich poly-(propylene imine) dendron based molecular transporter[25], which was observed to be non-toxic with higher cellular uptake efficiency contrasted with Arg-8-mer in various cancer cells. The high cell penetrating ability of the **G8**-dendron encourages us to develop a new hydnocarpin appended guanidium rich dendron (**Hy-G8**). The new synthetic derivative demonstrated excellent water solubility and improved cytotoxicity via caspase mediated apoptosis in cancer cells. The systematic approach adopted in the current study was illustrated in **Scheme 3.1.**

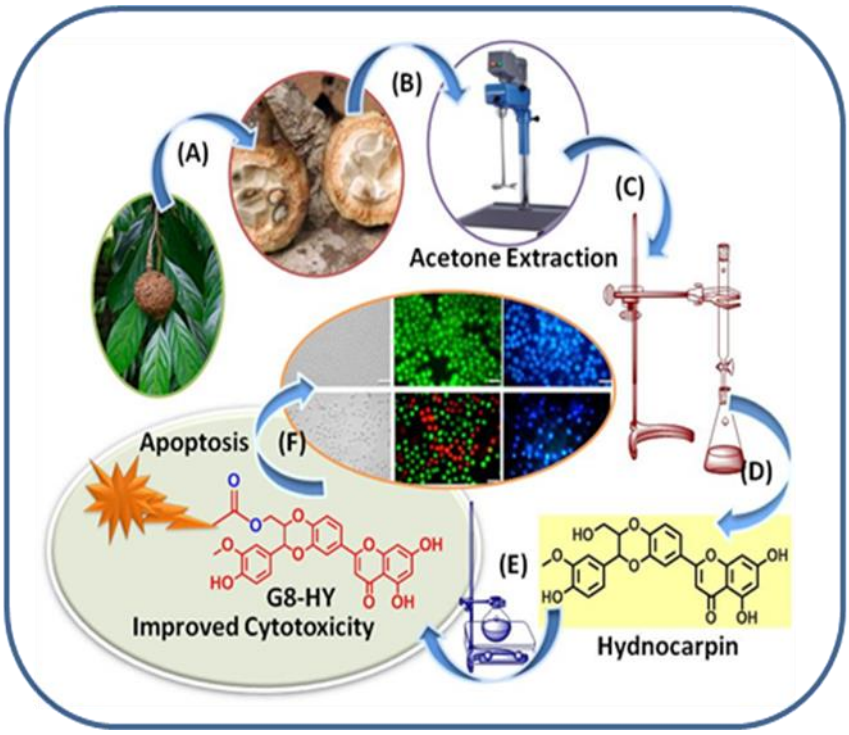

Scheme 3.1. Thematic representation of **Hy-G8** derivative synthesis. (A) Separation of seeds from *Hypnocarpus Wightiana Blume*, (B) Acetone extraction of seed, (C) Column choromatographic separation, (D) Isolation and purification of Hydnocarpin, (E) Synthetic transformation with **G8-PPI Dendron** and (F) Biological evaluation of **Hy-G8**.

3.3. Results and discussion

3.3.1. Isolation of crude extracts from *Hydnocarpous Wightiana Blume* seeds

The seeds were subjected to extraction using hexane and acetone. The acetone extract was selected to screen for antioxidant activity and further fractionalization. Thin layer chromatography of the acetone extract was carried out using solvents of polarity starting from 100 % chloroform to 10 % methanol in chloroform, after analysing TLC the extract was subjected to column chromatography. From the acetone extracts 574 fraction pools were collected and further sub column of 374-407 yielded the isolation of hydnocarpin in good yield (**fig 3.1**).

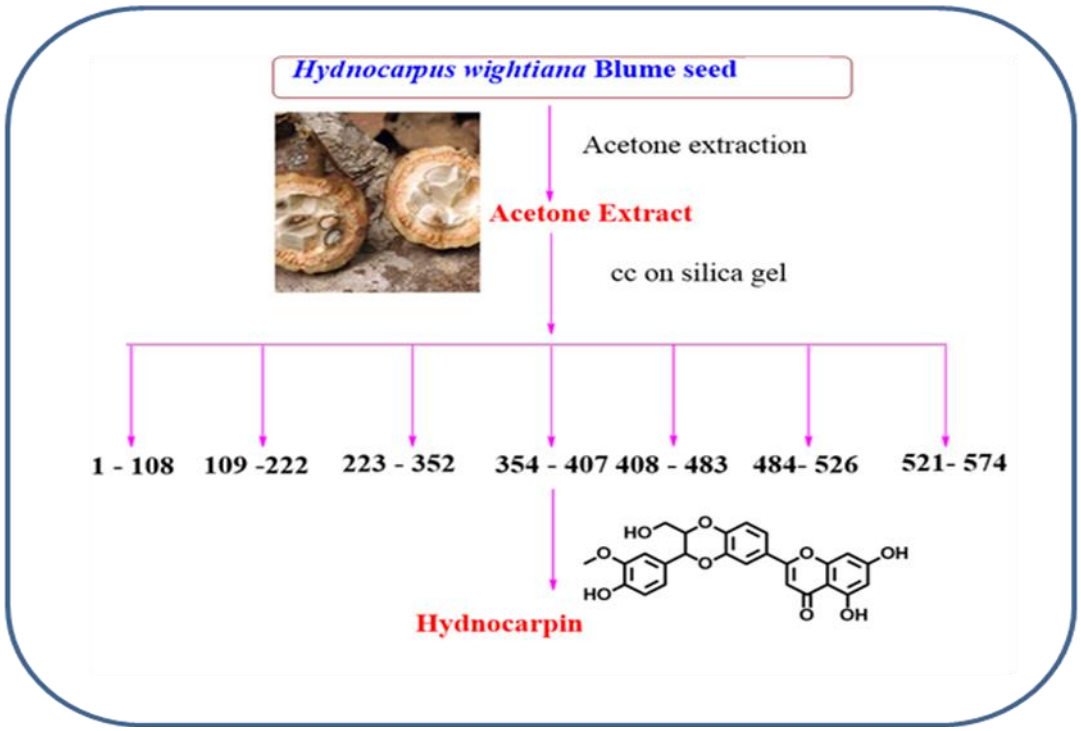

Figure 3.1. Isolation of compounds from acetone extracts of *Hydnocarpous Wightiana Blume* seeds.

3.3.2. Antioxidant action of acetone extract

Screening of acetone extract against a wide array of experimentally generated free radicals revealed the astonishing antioxidant property[26] of the extract. The DPPH[27] radical was considered to be a model of lipophilic radical, a chain reaction in lipophilic radicals was initiated by lipid autoxidation. The radical scavenging activity of acetone extract against experimentally generated DPPH ions is shown in **fig. 3.2A**, which showed excellent scavenging activity even at low concentrations. The scavenging activity increases in a concentration dependent manner. The IC_{50} value of acetone extract was found to be 262.7 ± 1.3µg/mL and for ascorbic acid it was 77.5 ± 1.5 µg/mL. FRAP assay directly measures total antioxidants or reductants in a sample. The antioxidant capacity of acetone extract based on the ability to reduce ferric ions was calculated as percent of inhibition as shown in **fig. 3.2B**. There is a gradual increase in antioxidant activity with an increase in concentration up to 500 µg/mL with an IC_{50} of 70 ± 1.8µg/mL, whereas the standard ascorbic acid showed relatively stable activity even from lower concentrations with an IC_{50} less than even 1µg/mL. Hydroxyl radical's attacks proteins, DNA, polyunsaturated fatty acid in membranes, and most biological molecule it contacts and is known to be capable of abstracting hydrogen atoms from membrane lipids and brings about peroxidic reaction of lipids. Acetone extract was not found to be a good scavenger of hydroxyl radical with a maximum inhibition of 40 % at

500µg/mL where as α-Tocopherol showed good scavenging effect with an IC_{50} at 64µg/mL (**fig. 3.2C**). The scavenging ability of acetone extract against superoxide ions generated in the PMS-NADH-NBT system was shown in **fig. 3.2D**. Acetone extract exhibited a dose dependent increase in scavenging activity with an IC_{50} at 299 ± 2.8µg/mL whereas the positive control α-Tocopherol generated IC_{50} at 61.5± 1.7µg/ mL. The radical scavenging activity of the acetone extract is promising and might be helpful in preventing or reducing the progress of various oxidative stress induced diseases including cancer and thereby beneficial for human health.

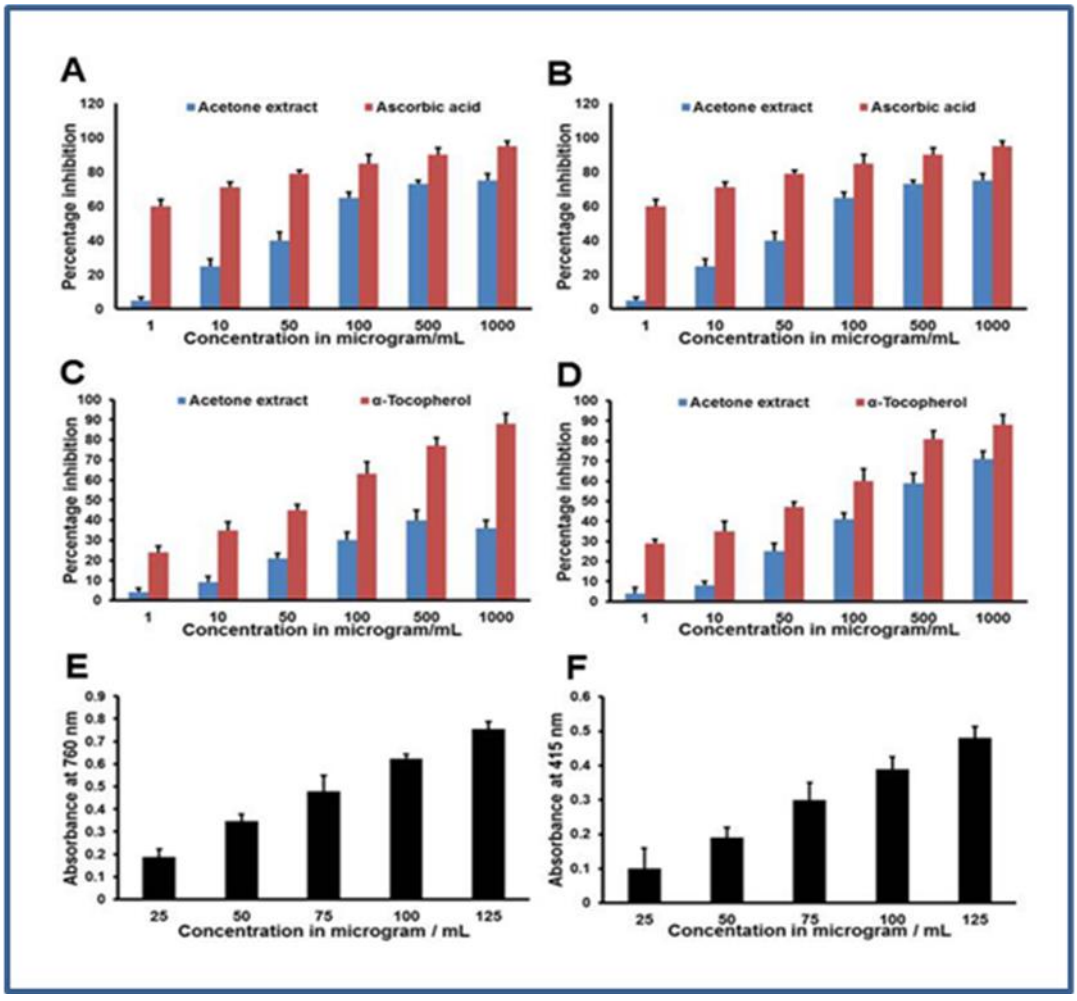

Figgure 3.2. Antioxidant activity of Acetone extract (A) DPPH radical scavenging assay using ascorbic acid as the standard, (B) FRAP assay using ascorbic acid as the standard, (C) Hydroxyl radical scavenging assay using alpha tocopherol as the standard and (D) Superoxide radical scavenging assay using alpha tocopherol as the standard. (E) Total phenolic content (absorbance value of Gallic acid at 760nm, expressed as Gallic acid equivalent in mg/g dry weight of sample) and (F) total flavonoid content (absorbance value of Quercetin at 415nm, expressed as quercetin equivalent in mg/g dry weight of sample.

3.3.3. Total phenolic and flavonoid content

The Estimation of total phenolic content revealed that the acetone extract contains 642± 27mg Gallic acid equivalents in 100g extract. Total flavonoid content was determined by plotting the quercetin calibration curve (20 to100 µg/mL) and expressed as milligrams of quercetin equivalents (mg QE/ 100gram of dry weight of sample). The study revealed that the acetone extract of *Hydnocarpus Wightiana Blume* seed contains 135 ± 9mg Quercetin equivalents in 100g acetone extract. The concentration and type of phenolic substances are mainly responsible for the biological activities of the extract and high phenolic contents often attributes to higher free radical scavenging properties.[28] Flavonoids are stable and effective scavengers of most oxidizing molecules, including singlet oxygen, and various free radicals[29] implicated in several diseases. The higher phenolic and flavonoid contents of acetone extract could be highly responsible for the observed superior free radical scavenging effects.

3.3.4. Synthetic modification of hydnocarpin

The flavonolignans hydnocarpin (**Hy**) was isolated from acetone extract, structure is mostly similar to silybin and it can be characterized as a small, highly functionalized molecule with alternating carbo and hetero-cycles. Preliminary screening for the cytotoxicity of **Hy** revealed moderate effects on cancer cells. The cytotoxic nature of **Hy** demanded us to investigate further structural modification in order to improve its bioavailability, water solubility and transformed **Hy** as an excellent anti-cancer agent. Octa-guanidine scaffold has been established as an excellent cell penetrating carrier which showed higher cellular uptake compared to **Arg-8-mer**, the well-known cell penetrating peptide.[13] It is having excellent selectivity towards lysosome and the transporter alone (**G8-PPI-FL**) is found to be non-toxic. The primary alcoholic group at C-23 position of **Hy** can be readily esterified and oxidized to a carboxylic acid. So we have conjugated the primary OH of **Hy** with acid terminal of molecular transporter Octa-guanidinium-poly-(propylene imine) hybrid dendron (**G8-Boc - PPI**) by ester coupling using carboxyl activating agent EDC in combination with DMAP (**scheme 3.2**). Finally, all the Boc groups of guanidine moieties were deprotected by treating with ethyl acetate saturated with HCl gas reagent. The **Hy** and final compound **Hy-G8** was characterized by HPLC, IR, NMR and HRMS spectroscopies. **Hydnocarpin (Hy):** ^{1}H-NMR (500 MHz, CD_3OD): δ1.19-1.55 (m, 22H), 2.49 (m, 20H), 2.52 (m, 16H), 3.08 (m, 16H), 3.36 (m, 8H), 3.52 (m, 2H), 3.56 (m, 6H), 3.68 (m, 4H). 3.74 (s, 3H,), 4.20 (d J=5Hz, 2H), 4.26 (m, 1H), 5.25 (d J=10Hz, 1H), 6.29 -7.57-(m, 9H). ^{13}C-NMR (125 MHz, DMSO D6)

δ181.7,164.2,162.8,161.3,157.3,147.6,147.1,147.0,143.6,126.9,123.6,120.5,119.8,117.5,115.3,114.7, 111.6,103.8,103.7, 98.9, 94.0, 77.9, 76.3, 60.0, 55.6; HR-MS (m/z):465.1183 (M+1+ peak). **Hypnocarpin Guanidium derivative (Hy-G8):** To the solution of hydnocarpin (15 mg, 0.3232 mmol) in dry DMF (3ml) Boc protected G8- PPI (92 mg, 0.03232 mmol, prepared using previous reported procedure from our group), catalytic amount of DMAP (base) and EDC (7.33 mg, 0.03879 mmol) were added. The mixture was stirred at room temperature for 24 hours. Completion of the reaction was monitored through TLC and the volatile components were removed under rotary evaporator and the Boc protected product formed was purified by column chromatography. Ethyl acetate (4ml) saturated with gaseous HCl was added to a solution Hy-Boc-G8 in ethyl acetate (1ml). The reaction mixture was stirred for 4hrs then the solution was concentrated and the residue was washed with ethyl acetate to remove less polar impurities. The residue was dried and purified using MPLC on supelclean LC-18 reverse-phase silica gel (MeOH /H_2O). The purified product was done HPLC and then dissolved in de-ionised water yielding Hy-G8. The compound was identified by spectroscopic techniques. IR (KBr, υmax, cm-1): 3473, 2922, 2817, 2579,2377,1747,1642, 1501, 1260, 1180, 1164; 1H NMR (500 MHz, CD3OD):7.5 – 6.17 (9H, m), 4.94 (2H, d, J= 5Hz), 3.83 (3H,s) (2H,m), 3.59 (3H,s), 2.62 – 1.26 (m) (100H,m).MALDI TOF MS Calculated 1720.2400 and found 1721.3258.

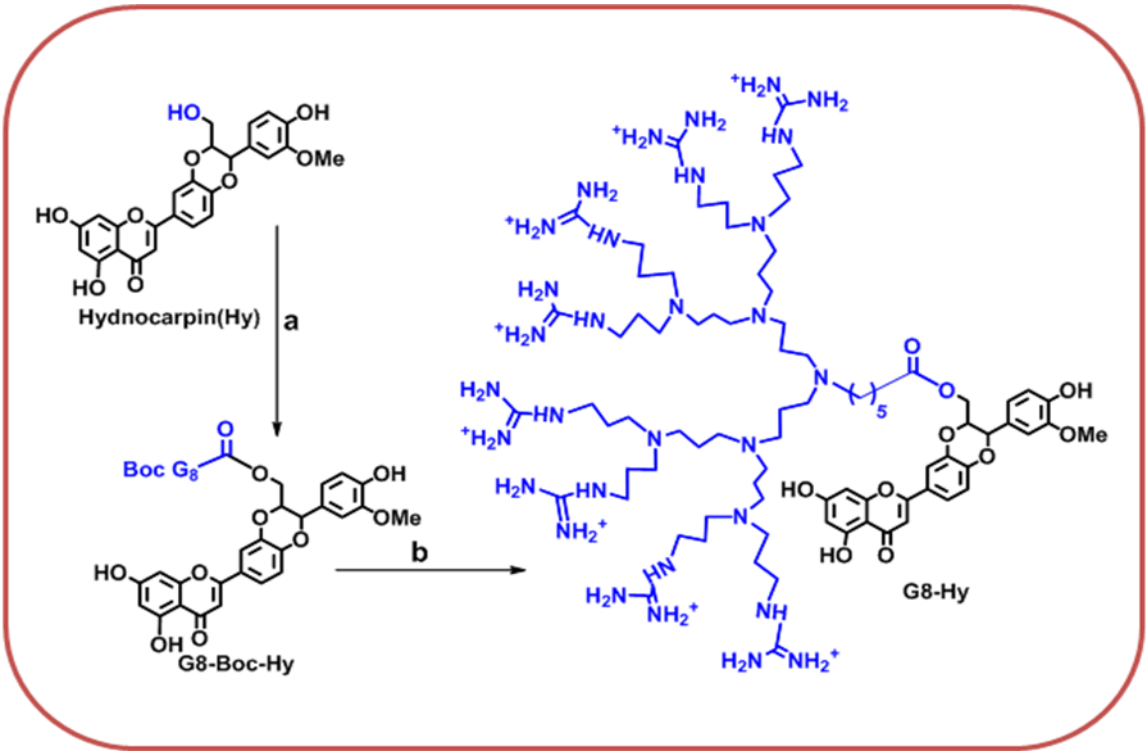

Scheme 3.2. Synthesis of Hy-**G8** derivative., Reagents and conditions: a) EDC, DMAP, dry DMF, N_2 atm 36 hrs, b) EtOAc saturated with HCl (g), EtOAc

3.3.5. Evaluation of cytotoxic potential

Evaluation of cytotoxicity is the major step for any lead compounds aimed with human therapeutic application. Cytotoxic potential was evaluated with **Hy**, **Hy-G8** and the carrier **G8** on melanoma (A375), lung adenocarcinoma (A549) and mouse fibroblast (3T3-L1) for 24 and 48 hrs from a wide dosage range of 2.5 to 80µM by MTT assay. **Hy-G8** executed superior cytotoxicity than **Hy** in all dosages and incubation time on A375 cells. **Hy** also executed significant cytotoxicity where as the carrier **G8** was found to be non-toxic (**fig. 3.3A** and **fig. 3.3B**). A375 cells were arrested by **Hy-G8** with an IC_{50} value of 22.7 ± 0.9 and 14.4 ± 0.7 at 24 and 48 hrs but **Hy** could generate an IC_{50} at relatively higher concentrations of 57.6 ± 1.3 and 41.5 ± 1.7 at 24 and 48 hrs respectively. A similar trend in cytotoxicity was observed with A549 cells, where **Hy** produced an IC_{50} of 72.7 ± 1.4 at 48 hrs but failed to generate IC_{50} at 24 hrs. A marked increase in cytotoxic potential was showed by **Hy-G8** (**fig. 3.3B, 3.3C and 3.3D**) with IC_{50}'s of 33.7 ± 0.9 and 24 ±1.2 at 24 and 48 hrs. The cytotoxic potential of **Hy** and **Hy-G8** increased in a dose-dependent manner in both the cancer cell lines. Absence of IC_{50} on normal fibroblast cell line by both **Hy** and **Hy-G8** highlights the cancer cell oriented cytotoxicity by the agents. The enhanced cytotoxic potential of **Hy-G8** in comparison with **Hy** evidenced on cancer cells was not observed on 3T3-LI (**fig. 3.3C, and fig. 3.3E, 3.3F**). Even though both **Hy** and **Hy-G8** produced a maximum cytotoxicity of 18 and 17 % on 3T3-L1 at 80µM at 48 hrs, lower dosages produced only negligible cytotoxicity, **G8** proved to be non-toxic towards non-cancer cells also. The increased cytotoxicity of **Hy-G8** than **Hy** on cancer cells was further tested with the quantification of lactate dehydrogenase (LDH) with 24 and 48 hrs of compound administration. **Hy-G8** exhibited a higher cytotoxicity on A375 (**fig. 3.3D**) and A549 (**fig. 3.3E**) cells with marginal cytotoxicity on 3T3-L1 cells (**fig. 3.3F**). The results obtained with LDH assay highly correlated with the cytotoxicity evaluation with MTT assay. The cytotoxicity of **Hy** and **Hy-G8** evaluated on lung adenocarcinoma, malignant melanoma and fibroblast-like mouse pre-adipocyte cell line deciphers a cancer cell oriented cytotoxicity profile. Even though **Hy** alone was found to be good cytotoxic agent, the **G8** coupled construct (**Hy-G8**) executes superior cytotoxicity on both the cancer cells, but a similar increase in cytotoxicity potential was not found on normal cells. Plasma membrane damage due to cytotoxic agents releases LDH into the cell culture media which could be quantified for determining the percentage of cytotoxicity caused by the

agent. Improved cytotoxicity of **Hy-G8**, which could be attributed to the enhanced water solubility of **Hy-G8** in contrast to **Hy** was confirmed with MTT and LDH assay.

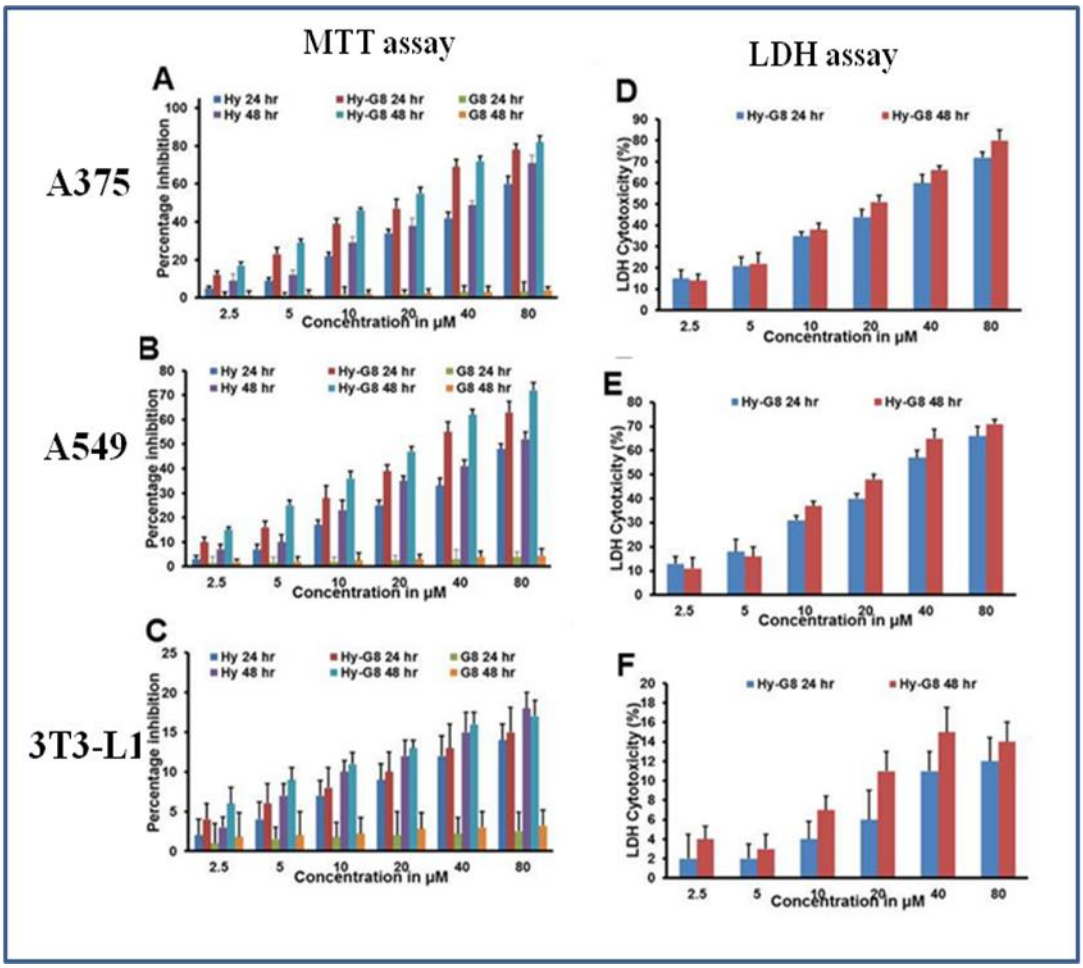

Figure 3.3. Assay for cytotoxicity in cancer cells and normal cells treated with **Hy**, **Hy-G8** and **G8** after 24 and 48 hrs of administration with MTT assay. (A) A375 cells, (B) A549 cells and (C) 3T3-L1cells. Assessment of cytotoxicity of **Hy-G8** by LDH assay on D) A375 (E) A549 cells and (F) 3T3-L1 cells.

3.3.6. Hy-G8 induced anticancer effects through apoptosis

To investigate the cell death mechanism induced by **Hy-G8** in cancer cells, various apoptotic assays were conducted on A375 and A549 cells after the administration of 20µM compound for 24 hrs. Morphological changes evaluated with phase contrast microscopy revealed a decrease in cell number, which was accompanied by salient morphological features of apoptosis, such as distorted shape, membrane blebbing, and the presence of apoptotic bodies compared to the control group on both A375 (**fig. 3.4A a**) and A549 (**fig. 3.4B a**) cells. In comparison with the respective controls, acridine orange- ethidium bromide staining displayed a change in colour from green to yellow/red, which is associated with other

apoptotic features such as the presence of apoptotic bodies, damaged cell membrane and nuclear condensation in **Hy-G8**-treated cells. Significant changes in fluorescence were observed for A375 (**fig. 3.4A b**) and A549 (**fig. 3.4B b**) cells. Cells undergoing apoptosis demonstrated nuclear condensation and DNA fragmentation, which was detected by Hoechst 33342 nuclear staining. The percentage of chromatin condensation after **Hy-G8** treatment was significantly higher in A375 (**fig. 3.4A c**) and A549 (**fig. 3.4B c**) cells as compared with the respective controls. The mechanism of cell death induced by **Hy-G8** was further confirmed with the TUNEL assay in which propidium iodide was used as counter stain. **Hy-G8** treated cells displayed green colour indicating TUNEL positivity, but control cells are largely TUNEL negative indicating the targeted apoptotic induction of compound on both A375 (**fig. 3.5A**) and A549 cells (**fig. 3.5B**). One of the mechanistic features of apoptotic cell death is the activation of caspases, a class of cysteine proteases and many anticancer drugs was reported to execute apoptosis through caspase dependent pathway.[30] Since caspases are the effective mediators of apoptosis, the expression of caspases 3, 8, 9 and 2 was estimated by using fluorimetry to thoroughly substantiate the cell death mechanisms induced by **Hy-G8**. Both A375 and A549 presented a significant ($P < 0.001$) increase in the expression of caspases 2, 3 and 8 (**fig. 3.5C**). Caspase 3 was the most over expressed one with 2.4 and 2.6 fold increases in A375 and A549 cells respectively in comparison with their controls. The expression pattern of caspase 9 was not that significant in comparison with other caspases in both the cells. Apoptosis is the most predominant mode of cell death, and several naturally occurring compounds have shown to induce apoptosis in cancer cell lines.[31] The presence of irregular bulges in the plasma membrane of the cell due to localized decoupling of the cytoskeleton from the plasma membrane is a hall mark of apoptosis. Although the budding phenomenon of apoptotic cells lasts for only a few minutes, the formation of apoptotic bodies remains visible for a few hours.[32] The enhanced cytotoxicity of the **Hy-G8** compared with **Hy** is found to be executed through caspase mediated apoptosis.

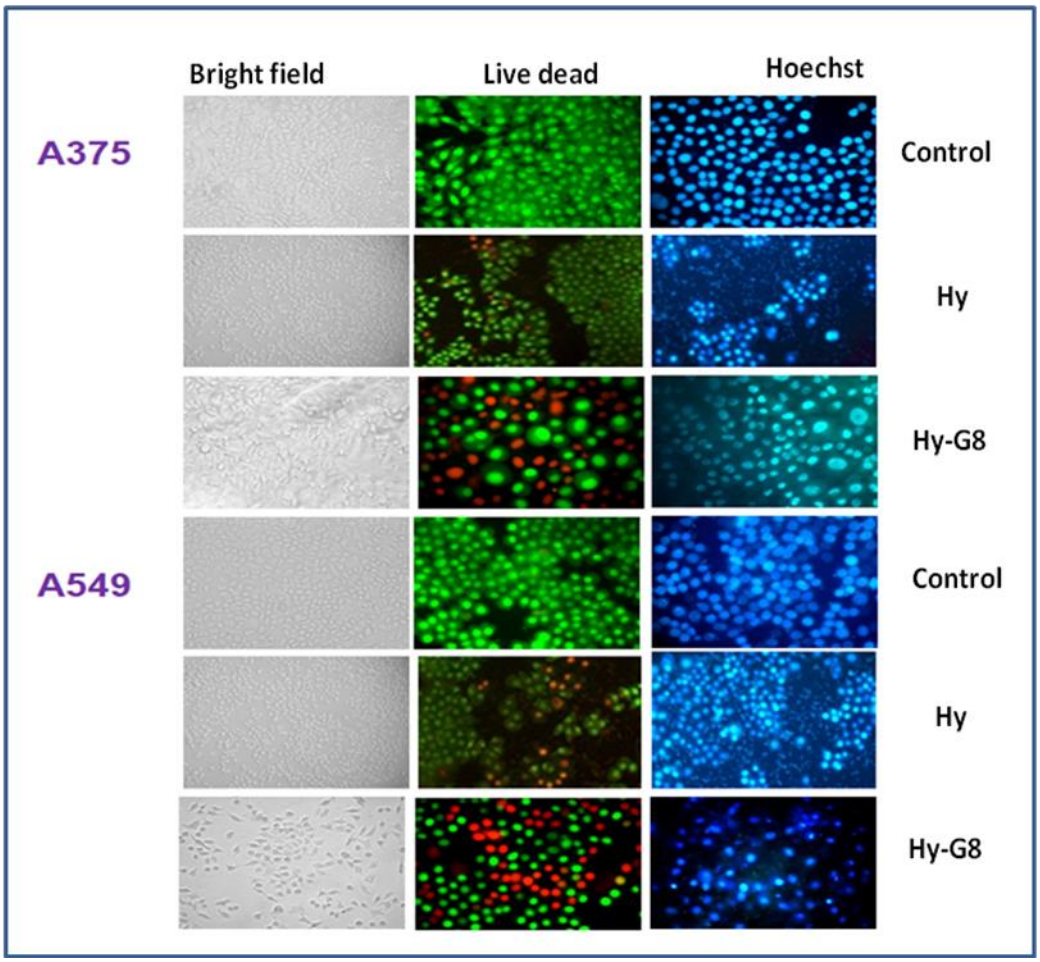

Figure 3.4. Morphological evaluation of apoptosis by the 24 hrs administration of **Hy-G8** (20µM) on (A) A375 and (B) A549. (a) Represents Phase contrast images, (b) Represents Acridine orange-ethidium bromide and (c) Represents Hoechst staining. Scale bar corresponds to 50µM.

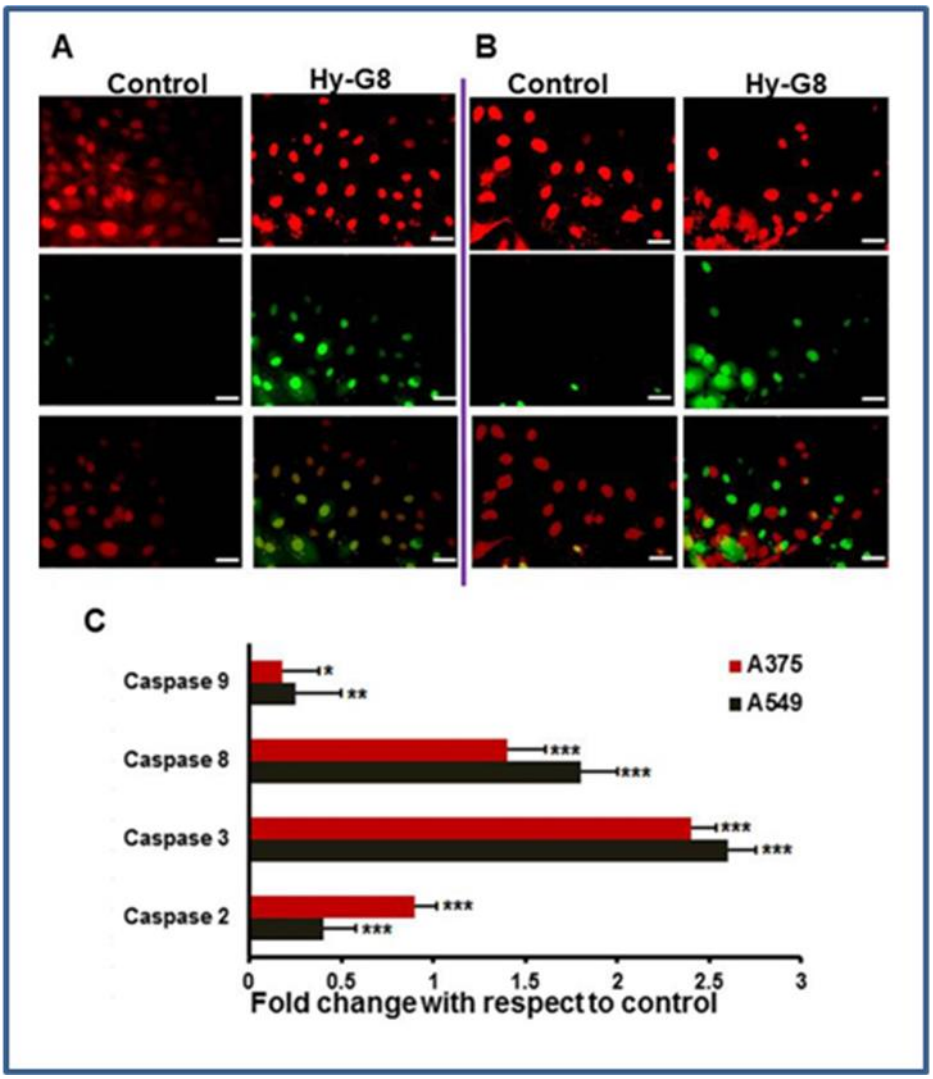

Figure 3.5. Morphological evaluation of apoptosis by TUNEL assay after 24 hrs administration of **Hy-G8** (20µM) on (A) A375 and (B) A549 cells. Left panel represents images with PI filter, middle panel represents FITC filter and right panel represents merged images. Scale bar corresponds to 50µM. (C) Caspase activity profiling after 24 hrs administration of **Hy-G8** (20µM) on A375 and A549 cells. Results are expressed as mean ±SD. Scale bar corresponds to 50µM.

3.3.7. Anti-metastatic potential

The wound healing assay is considered to be the standard to evaluate the cell migration, cell interactions and metastatic potential. It was clearly observed that **Hy-G8** could inhibit the migration of cells in a time dependent manner in both A375 (**fig. 3.6A**) and A549 cells (**fig. 3.6B**) whereas the untreated cells restore confluence within 24 hrs. The *in vitro* scratch assay is an easy and robust method to measure cell migration study. Compared to other methods, the *in vitro* scratch assay is particularly suitable for studies on the effects of cell-matrix and cell-cell interactions on cell migration, mimic cell migration during wound healing *in vivo*

and are compatible with imaging of live cells during migration to monitor intracellular events if desired.[33]

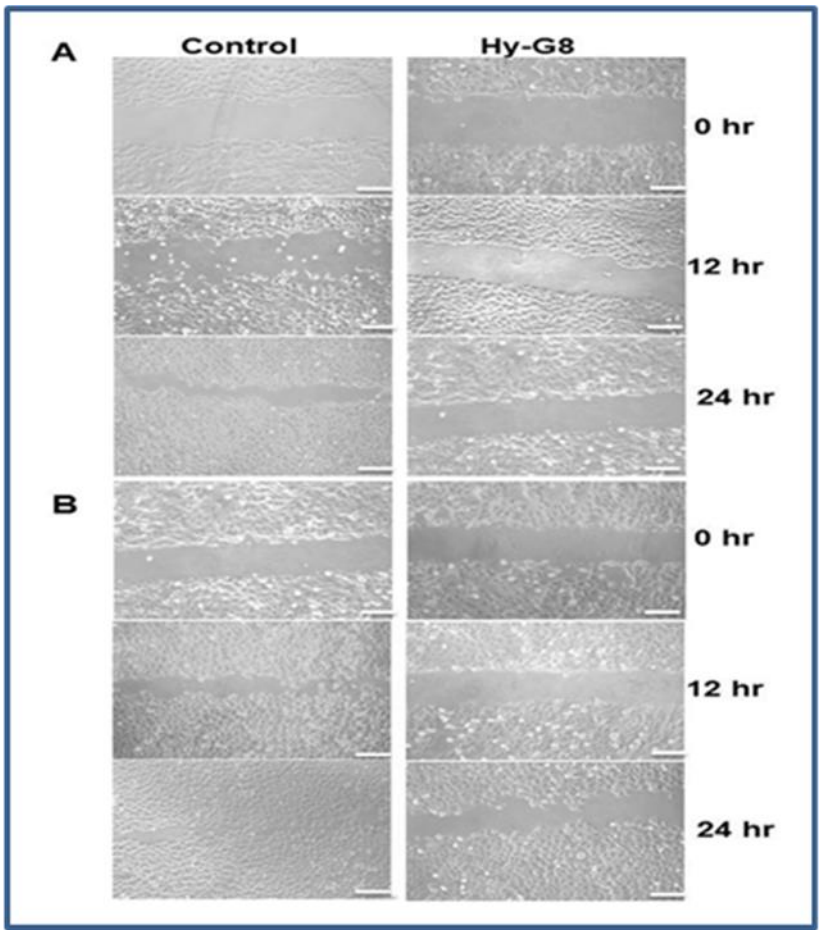

Figure 3.6. Representative wound healing images at 0, 12, and 24 hrs. Wounds were made with a pipette tip in confluent monolayers on (A) A375 and (B) A549 cells after administration of **Hy-G8** (20µM). Scale bar corresponds to 50µM.

3.4. Conclusions

Phytochemical investigations on the popularly used medicinal plant *Hydnocarpus Wightiana Blume* (seed) acetone extract revealed an excellent free radical scavenging property with high total phenolic and flavonoid content. The most abundant Hydnocarpin (**Hy**), which was isolated, purified and characterised from the extract demonstrated moderate cytotoxic potential on cancer cells. In an attempt to increase the anticancer potential of **Hy**, chemical conjugation with a highly efficient, non-toxic cell penetrating guanidinium rich poly-(propylene imine) dendron (**G_8**) was carried out via EDC coupling. The hybrid molecule (**Hy-G_8**) executed excellent cytotoxicity preferentially on lung adenocarcinoma and malignant

melanoma cells mediated through caspase dependent programmed cell death and also demonstrated anti-metastatic potential. Therefore, the superior anticancer potential of **Hy-G8** over hydnocarpin depicted in the present study enforces the need of detailed investigations into its molecular mechanistic mode of action both in vitro and in vivo animal models.

3.5. Materials and methods

All non-hydrolytic chemical reactions for the preparation of drug carrier constructs, unless otherwise indicated, were carried out in oven-dried glassware under an inert atmosphere of dry argon or nitrogen. Protected amino acids were purchased from Nova bio chem and Sigma Aldrich. Doxorubicin hydrochloride was obtained from Sigma Aldrich (St. Louis, MO, U.S.A.), Cathepsin B was acquired from Enzo life science. All the other chemicals and solvents were purchased from Sigma Aldrich, Merk, and Specrochem and were used without further purification. Analytical TLC was performed on a Merck 60 F254 silica gel plate (0.25mm thickness), and visualization was done with UV light (254nm and 365nm), or by spraying with a 5% solution of phosphomolybdic acid or ninhydrine solution followed by charring with a heat gun. Column chromatography was performed on Merck 60 silica gel (60-120 or 100-200 mesh). HPLC was performed by Shimadzu HPLC system (Kyoto, Japan) consisting of SCL-10Avp system controller, two LC-8A solvent delivery units, SPD-M20A UV-vis photo diode array (PDA) detector, equipped with Multi PDA- LC solution software on a 250mm x 4.6mm i.d, 5μM, YMC-Pack R&D ODS analytical column (9YMC Co., Ltd. Japan). NMR spectra were recorded on a Bruker AMX 500 (^{1}H-NMR at 500MHz; ^{13}C-NMR at 125MHz) spectrometers (Falladen, Switzerland). Tetra methyl silane was used as reference for ^{1}H-NMR, and the chemical shift were reported in ppm and the coupling constant in Hz. High resolution mass spectra were determined on a HR-EMI analysis of Thermo Scientific Exactive system (Berman, Germany). Liophilization was performed with lyophilizer Tenesis Wizard 2 (Germany). For biological studies 2-[4-(2-hydroxyethyl) piperazin-1-yl] ethanesulfonic acid (HEPES) was purchased from Himedia (Mumbai, India). 3-(4, 5-dimethylthiazol-2-yl)-2, 5-diphenyltetrazolium bromide (MTT), Dulbecco's modified eagle's medium (DMEM), trypsin-EDTA and dimethylsulfoxide (DMSO) for cell culture solution were purchased from Sigma Aldrich. Penicillin-Streptomycin, neutravidin, alexafluor 568-carboxylic acid succinimidyl ester, fetal bovine serum (FBS) and Mito Tracker red CMX Ros were purchased from Invitrogen (Merelbeke, Belgium). Annexin V-FITC apoptosis detection kit was purchased from BD Pharmingen (#556547, BD Biosciences, San Jose, CA) and TUNEL assay kit from Promega, USA.

Caspase assay was performed with ApoAlert™ Caspase Profiling kit (Clontech, CA, USA). Bisbenzimide H 33258 (Hoechst) was purchased from Calbiochem (San Diego, CA, USA) and Lyso Tracker Deep Red was purchased from Molecular probes Life technologies.

3.5.1. Preparation of extracts

The seeds of *Hydnocarpus Wightiana Blume* were thoroughly cleaned and dried in air oven maintained at 40°C for three days. It was then thoroughly powdered and weighed approximately 750g. The powdered material was first extracted using hexane in a mechanical stirrer (1.5L) three times at room temperature. Further it was extracted using chloroform (1.5L) three times and finally with acetone (1.5L) three times at room temperature. The total extracts were concentrated under reduced pressure using Buchii rotary evaporator. This yielded about 400g of the crude hexane extract, 25g of chloroform and 45g of acetone extract. Based on the observation in TLC, the hexane and chloroform extracts were selected for the isolation of compounds.

3.5.2. Antioxidant Activity

Earlier studies revealed that the hexane and chloroform extracts of *Hydnocarpus Wightiana Blume* does not have any appreciable free radical scavenging activity.[34] This encouraged us to examine the antioxidant activity of acetone extract against experimentally generated free radicals.

3.5.3. DPPH radical scavenging assay

The radical scavenging effects of the acetone extract on a 1, 1-diphenyl-2-picryl-hydrazil (DPPH) radical were estimated.[35] Various concentrations of samples and standards (3mL) were mixed with 1mL of 0.1mM of DPPH and the mixture were shaken vigorously and allowed to incubate at room temperature (25 ± 30°C) for 30min. The scavenging activity was quantified spectrophotometrically at 507nm against 95% ethanol as blank. Ascorbic acid was used as the standard and the percent DPPH scavenging effect was expressed as percent inhibition from the given formulae:

% inhibition of DPPH radical = $[A_0 – A_1/A_0] \times 100$

Where A_0 was the absorbance of the control and A_1 was the absorbance of the sample/standard.

3.5.4. FRAP (Ferric reducing antioxidant power) assay

This assay measures the total antioxidant capacity of the compound and the procedure was conducted according to Benzie and Strain[36] followed by modification. The working FRAP reagent was prepared by mixing 300mM acetate buffer (pH 3.6), 10mM 2, 4, 6-tripytidyl-s-triazine (TPTZ) solution and 20mM $FeCl_3.6H_2O$ in a 10:1:1 ratio prior to use and heated to 37°C in a water bath. Three milli litters (3mL) of FRAP reagent was added to 100µL of various concentrations of samples and standards. Absorbance was measured at 593nm at 0 min and again after 90min. Ascorbic acid was used as the standard and changes in the absorbance after 90min from initial reading were compared and percent inhibition was calculated as described.

3.5.5. Hydroxyl radical scavenging assay

Hydroxyl radical scavenging activity was measured comparing deoxy ribose and acetone extract for hydroxyl radical generated by the Fe^{3+} ascorbate-EDTA-H_2O_2 system (Fenton reaction).[37] The reaction mixture contained (1mL) 100µL 2-deoxy-2-ribose (28mM in 20mM phosphate buffer, pH 7.4), 500µl of different concentrations of samples and controls, 200µL 1.04mM $FeCl_3$, 100µL 1mM H_2O_2 and 100µL ascorbic acid, was incubated at 37°C for one hr. The barbituric acid (1%) and trichloro acetic acid (2.8%) were added and incubated at 100°C for 20min, after rapid cooling the absorbance was measured at 532nm. α-Tocopherol was used as the standard and the percentage inhibition was calculated.

3.5.6. Superoxide radical scavenging assay

The scavenging activity towards superoxide anion radicals was measured by the method of Liu et al.[38] Superoxide anions were generated in a non-enzymatic phenazine methosulfate nicotinamide adenine dinucleotide (PMS-NADH) system through the reaction of PMS, NADH and oxygen. It was assayed by the reduction of nitroblue tetrazolium (NBT). Superoxide anion was generated in 3mL of Tris-HCl buffer (100mM, pH 7.4) containing 0.75mL of NBT (300µM) solution, 0.75mL of NADH (936µM) solution and 0.3mL of various concentrations of samples and standards. The reaction was initiated by adding 0.75mL of PMS (120µM) to the mixture. After 5 min of incubation at room temperature (25±30°C), the absorbance at 560nm was measured. α-Tocopherol was used as the positive control and percent inhibition was calculated.

3.5.7. Total Phenolic Content (TPC)

Total phenolic content[39,40] (TPC) of the acetone extract was determined using the Folin-Ciocalteau reagent. Briefly, 0.5mL of freshly prepared Folin-Ciocalteu reagent in distilled water (1:2), was added to 1.0mL extracts of different concentrations (200-1000µg/mL) and mixed thoroughly and then neutralized with 1mL saturated sodium carbonate solution and made up to 10mL with distilled water. After 2hrs, the absorbance of the resulting solution was measured at 764nm using a spectrophotometer. The TPC was determined by plotting the Gallic acid calibration curve (20 to 100µg/mL) and expressed as Gallic acid equivalents (mg GAE / 100g dry weight of sample).

3.5.8. Total flavonoid content (TFC)

About 1mL of acetone extract (1mg/mL) was made up to 5 mL using distilled water and 0.3 mL of 5 % (w/v) NaNO2 was added to it and kept for 5 min. After 5 min. 0.3 mL of 10 % (w/v) $AlCl_3$ was added to form a flavonoid- aluminum complex. After 6min, 2 mL of 1M NaOH was added and the total volume was made up to 10mL using distilled water. The solution was mixed well again and the absorbance was measured against a reagent blank, at 415nm. Blank was prepared by adding all reagents except $AlCl_3$. Distilled water was added in place of $AlCl_3$ in the blank. The TFC was determined by plotting the quercetin calibration curve (20 to100µg/mL) and expressed as milligrams of quercetin equivalents (mg QE/ 100gram of dry weight of sample).[41]

3.5.9. Isolation of compounds and its chemical modification

Based on the observation in TLC, the hexane, and acetone extracts were used for the isolation of compounds. A fatty acid rich fraction was isolated from hexane extract. The acetone extracts which showed good anti-oxidant activity, total phenolic and good flavonoid content was selected for further in depth studies. Acetone extract was subjected to column chromatography using silica gel (100-200 mesh), the column was eluted with chloroform and increasing amount of methanol which yielded 574 different fractions. From 354-407 fractions, we have isolated our target compound hydnocarpin in good yield

3.5.10. *In vitro* cytotoxicity assays

The growth inhibition capacity of Hydnocarpin (**Hy**) and Hydnocarpin-G8 (**Hy-G8**) was evaluated in cancer cell lines using the 3-[4, 5-dimethylthiazol-2-yl]-2,5-diphenyltetrazolium (MTT) assay as previously reported.[42] This assay measures cell viability by assessing the cleavage of tetrazolium salt by mitochondrial dehydrogenase. The absorbance was measured at 570nm using a microplate spectrophotometer (BioTek Power Wave XS). The inhibitory rate on the cells was calculated using the following formulas:

Proliferation rate (PR) % = [Abs sample/Abs control] x 100;

Inhibitory rate (IR) % = 100 – PR.

MTT assays were performed on A375, A549 and 3T3-L1 with various concentrations of **Hy** and **Hy-G8** ranging from 2.5µg/mL to 80µM for 24 and 48hrs. Cytotoxicity of **Hy-G8** was further confirmed with LDH assay (Pierce LDH Cytotoxicity Assay Kit-88953, USA) as per protocol given in the kit using respective controls. Finally, the absorbance at 490nm and 680nm is measured using a plate-reading spectrophotometer to determine LDH activity.

$$\% \text{ Cytotoxicity} = \frac{\text{Compound treated LDH activity} - \text{Spontaneous LDH activity} \times 100}{\text{Maximum LDH activity} - \text{Spontaneous LDH activity}}$$

3.5.11. Apoptotic assays

Evaluation of the mode of cytotoxicity exhibited by the compounds was performed on cancer cells with various apoptotic assays after administration of 20µM Hy-G8 for 24hrs. Morphological evaluation for apoptotic changes were performed under phase contrast microscope (Olympus 1X51, Singapore) under suitable magnification. Observation of nucleus for any changes was done with Hoechst staining and the cells were observed under an inverted fluorescent microscope using a DAPI filter (Olympus 1X51). Acridine orange-ethidium bromide dual staining is the most commonly used method to detect apoptosis and is based on the differential uptake of two fluorescent DNA binding dyes by viable and nonviable cells, respectively. Assessment of apoptosis using the acridine orange-ethidium bromide dual staining procedure was performed as described earlier.[43] The cells were observed under an inverted fluorescent microscope, using a FITC filter (Olympus 1X51,

Singapore) to view the apoptotic or non-apoptotic cells. Furthermore, TUNEL assay (Dead EndTM fluorometric TUNEL system G3250, Promega, USA) was used to detect the incorporation of the fluorescein-12-dUTP in the fragmented DNA of apoptotic cells, using the terminal deoxynucleotidyl transferase recombinant (rTdT) enzyme as per the manufacturer's instruction using propidium iodide as counter stain.

3.5.12. Caspase assay

The effect of both initiator caspases (caspases 8, 9 and 2) and executioner caspases (caspase 3) was determined by using Apo Alert^{TM} Caspase Profiling kit (Clontech, CA, USA) as per the kit protocol. Cells were treated with 20µM **Hy-G8** for 24hrs and finally, samples were transferred to 96-well plates for fluorimetric reading (excitation: 380nm; emission: 460nm), and the OD obtained was recorded under a spectrofluorometer (FLx800, BioTek).

3.5.13. Wound healing assay

The scratch wound healing assay was performed to evaluate the anti-metastatic potential of **Hy- G8** on A375 and A549 cells, as described previously.[44,45] Briefly, cells were seeded into six-well plates at a density of 1.0×10^5/well until they reached 80% confluence. The scratching wounds were created in the monolayer of confluent cells with a pipette tip. The width of the wounds was assessed to be the same at the beginning of the experiments. The wells were rinsed with PBS three times to remove floating cells and debris. The culture plates were incubated at 37°C and in 5% CO_2. Wound healing was measured and recorded photographically over time using phase-contrast microscopy at 0, 24, and 48hrs.

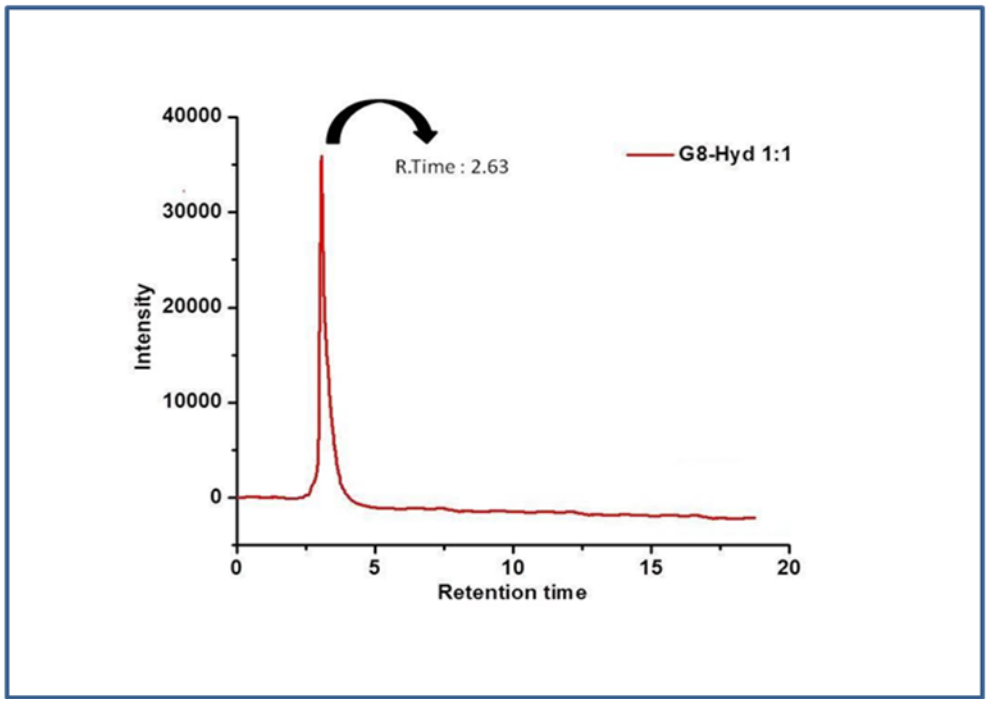

Figure 3.6. HPLC profile of **G8-Hy**.

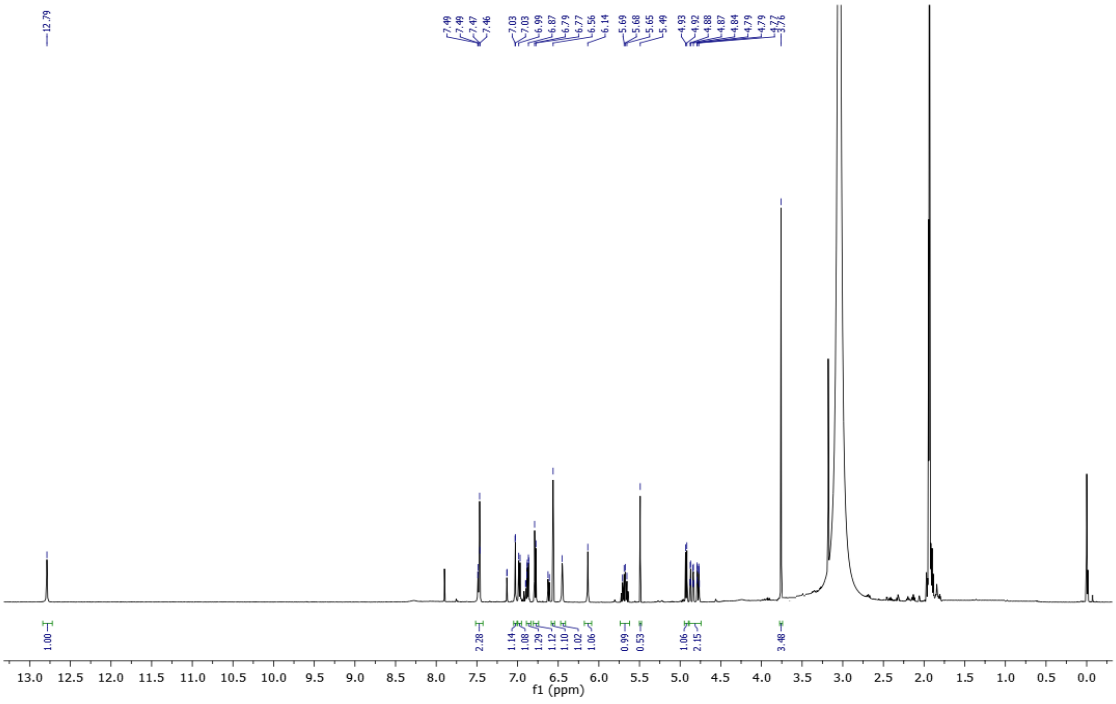

Figure 3.7. ^{1}H-NMR spectra of **Hy**

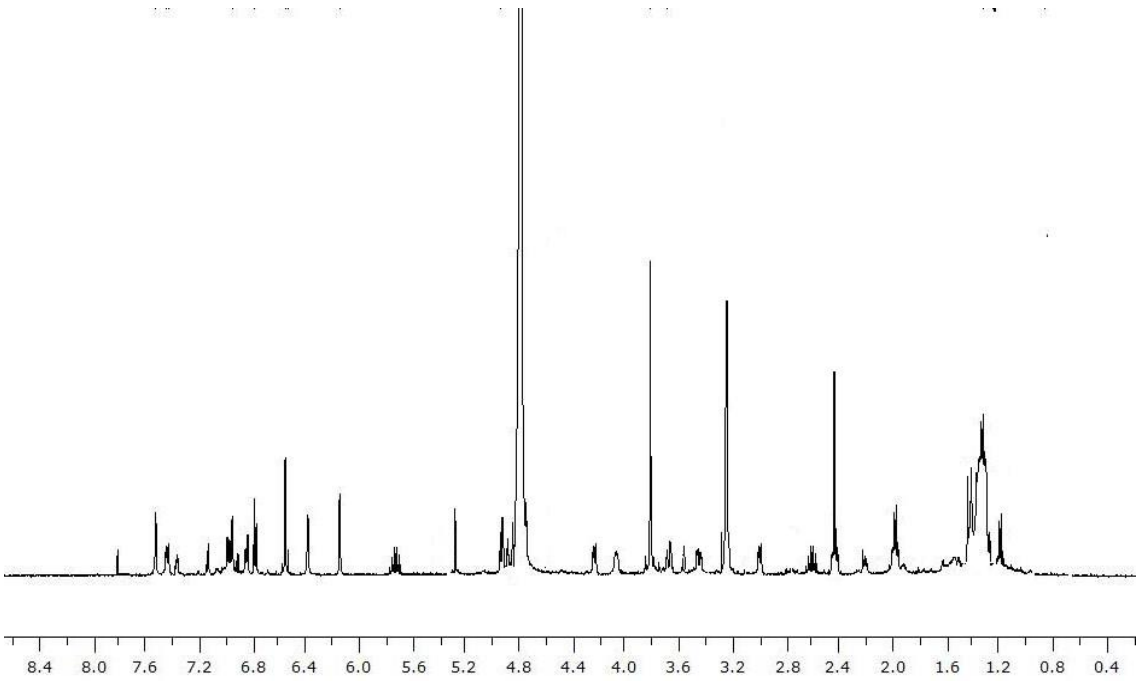

Figure 3.8. ^{1}H-NMR spectra of **G8-Hy**

3.6. References

[1]. Newman, D. J.; Cragg, G. M. *J. Nat. Prod,* **2012,** 75, 311.

[2]. Cragg, G. M.; Newman, D. J. *Ann. N. Y. Acad. Sci.* **2001,** 953, 3.

[3]. Brahmachari, G. World Scientific Publishing: Singapore, **2012,** 1.

[4]. Samuelsson, G. Drugs of Natural Origin: A Textbook of Pharmacognosy, 5th ed.; Swedish Pharmaceutical Press: Stockholm, **2004.**

[5]. Kinghorn, A. D. *J. Pharm. Pharmacol,* **2001,** 53, 135.

[6]. Newman, D. J.; Cragg, G. M.; Snader, K. M. *Nat. Prod. Rep*, **2000,** 17, 215.

[7]. Butler, M. S. J. *J. Nat. Prod,* **2004,** 67, 2141.

[8]. Johnson, T. CRC Ethnobotany Desk Reference; CRC Press: Boca Raton, FL, **1999.**

[9]. Farnsworth, N. R.; Akerele, R. O.; Bingel, A. S.; Soejarto, D. D.; Guo, Z. *Bull. World Health Organ,* **1985,** 63, 965.

[10]. Cragg, G. M.; Grothaus, P. G.; Newman, D. J. *Chem. Rev.* **2009,** 109, 3012.

[11]. Sneader, W. Drug Discovery: A History; John Wiley & Sons: Hoboken, NJ, **2005.**

[12]. Prakash, O.; Kumar, A.; Kumar, P.; Ajeet, A. *Am. J. Pharmacol. Sci*, **2013,** 1, 104.

[13]. DeCorte, B. L. *J. Med. Chem*, **2016,** 59, 9295.

[14]. Raman, B.V.; Krishna, N.V.; Rao, B.N.; Saradhi, M.P.; Rao, M.V.B. *Int. Res. J. Pharm,* **2012,** 3, 11.

[15]. Bhanot, A.; Sharma, R.; Noolvi, M. N. *Int. J. Phytomedicine,* **2011,** 3, 9.

[16]. Saha, A.; Mohapatra, S.; Kurkute, P.; Jana, B.; Sarkar, J.; Mondal, P.; Ghosh, S. *RSC Adv.,* **2015,** 5, 92596.

[17]. Sahoo, M.R.; Dhanabal, S.P.; Jadhav, A.N.; Reddy, V.; Muguli, G.; Babu, U.V.; Rangesh, P. *J. Ethnopharmacol,* **2014,** 154, 17.

[18]. Vimberg, V.; Kuzma, M.; Stodulkova, E.; Novak, P.; Bednarova, L.; Sulc, M.; Gazak, R. *J.Nat. Prod,* **2015,** 78, 2095.

[19]. Sharma, D.K.; Hall, I.H. *J. Nat. Prod*, **1991,** 54, 1298.

[20]. Vimberg, V.; Kuzma, M.; Stodulkova, E.; Novak, P.; Bednarova, L.; Sulc, M.; Gazak, R. *J.Nat. Prod,* **2015,** 78, 2095.

[21]. Sharma, D.K.; Hall, I.H. *J. Nat. Prod*, **1991,** 54, 1298.

[22]. Sahoo, M.R, Dhanabal, S.P.; Jadhav, A.N.; Reddy, V.; Muguli, G.; Babu, U.V.; Rangesh, P. *J. Ethnopharmacol,* **2014,** 154, 17.

[23]. Pan, L.; Chin, Y.W.; Chai, H.B.; Ninh, T.N.; Soejarto, D.D. *Bioorg. Med. Chem,* **2009,** 17, 2219.

[24]. Stanzl, E.G.; Trantow, B.M.; Vargas, J.R.; Wender, P.A. *Acc. Chem. Res.,* **2013,** 46, 2944.

[25]. Nair, J.B.; Mohapatra, S.; Ghosh, S.; Maiti, K.K. *Chem. Commun,* **2015**, 51, 2403.

[26]. Alam, M. N.; Bristi, N. J.; Rafiquzzaman, M.; *Saudi Pharm J,* **2013,** 21, 143.

[27]. Garcia, E. J.; Cadorin Oldoni, T. L.; de Alencar, S.; Reis, M. A.; Loguercio, A. D.; Miranda Grande, R. H. *Braz. Dent. J*, **2012,** 23, 22.

[28]. Meziti, A.; Meziti, H.; Boudiaf, K.; Mustapha, B. *World Acad. Sci. Eng. Technol*, **2012,** 64, 24.

[29]. Bravo, L.; Sources, D.; Significance, N. *Nutr. Rev*, **1998,** 56, 317.

[30]. Vaculova, A.; Kaminskyy, V.; Jalalvand, E.; Surova, O.; Zhivotovsky, B. *Mol. Cancer*, **2010,** 9, 87.

[31]. Dong, Y.; Kwan, C. Y.; Chen, Z. N.; Yang, M. M. *Res. Commun. Mol. Pathol. Pharmacol*, **1996,** 92, 140.

[32]. Barres, B. A. Hart, I. K. H. Coles, S.; Burne, J. F.; Voyvodic, J. T.; Richardson, W. D.; Raff, M. C. *Cell*, **1992,** 70, 31.

[33]. Liang, C.C.; Park, A. Y.; Guan, J.L. *Nat. Protoc*, **2007,** 2, 329.

[34]. Reddy, S. V.; Tiwari, A. K.; Kumar, U. S.; Rao, R. J.; Rao, J. M. *Phyther. Res*, **2005,** 19, 277; b) Nimse, S. B.; Pal, D. *R. Soc. Chem*, **2015,** 5, 27986.

[35]. Molyneux, P.; Songklanakarin. J. *Sci. Technol*, **2004,** 26, 211.

[36]. Benzie, I. F.; Strain, J. J. *Anal. Biochem*, **1996,** 239, 70.

[37]. Singh, R.; Singh, N.; Saini, B. S.; Rao, H. S. *Indian J. Pharmacol*, **2008,** 40, 147.

[38]. Liu, F.; Ooi, V. E. C.; Chang, S. T. *Life Sci*, **1997,** 60, 763.

[39]. Shaver, L. A.; Leung, S. H.; Puderbaugh, A.; Angel, S. *J. Chem. Educ*, **2011,** 88, 492.

[40]. Stankovi, M.; Kragujev. S. *J. Sci*, **2011,** 33, 63.

[41]. Sahu, R.; Saxena, J. *J. Pharmacogn. Phytochem*, **2013,** 2, 176.

[42]. Joseph, M. M.; Aravind, S. R.; Varghese, S.; Mini, S.; Sreelekha, T. T. *Biointerfaces*, **2013,** 104, 32.

[43]. Joseph, M. M.; Aravind, S. R.; George, S. K.; Raveendran Pillai, K.; Mini, S.; Sreelekha, T. T. *J. Biomed. Nanotechnol*, **2014,** 10, 3253.

[44]. Zhang, F.Y.; Hu, Y.; Que, Z.Y.; Wang, P.; Liu, Y.H.; Wang, Z.H.; Xue, Y.X. *Int. J. Mol. Sci*, **2015,** 16, 23823.

[45]. Shiozaki, A.; Bai, X.; Shen,T.; Moodley, G. S.; Takeshita, H.; Fung, S.Y.; Wang, Y.; Keshavjee, S.; Liu, M. *PLoS One*, **2012,** 7, 38049.

Chapter 4

Investigation of Multifunctional Targeted Nano-Carrier Delivery Vehicle for Stimuli-Responsive Co-Delivery of Doxorubicin and Resveratol in Breast Cancer cells

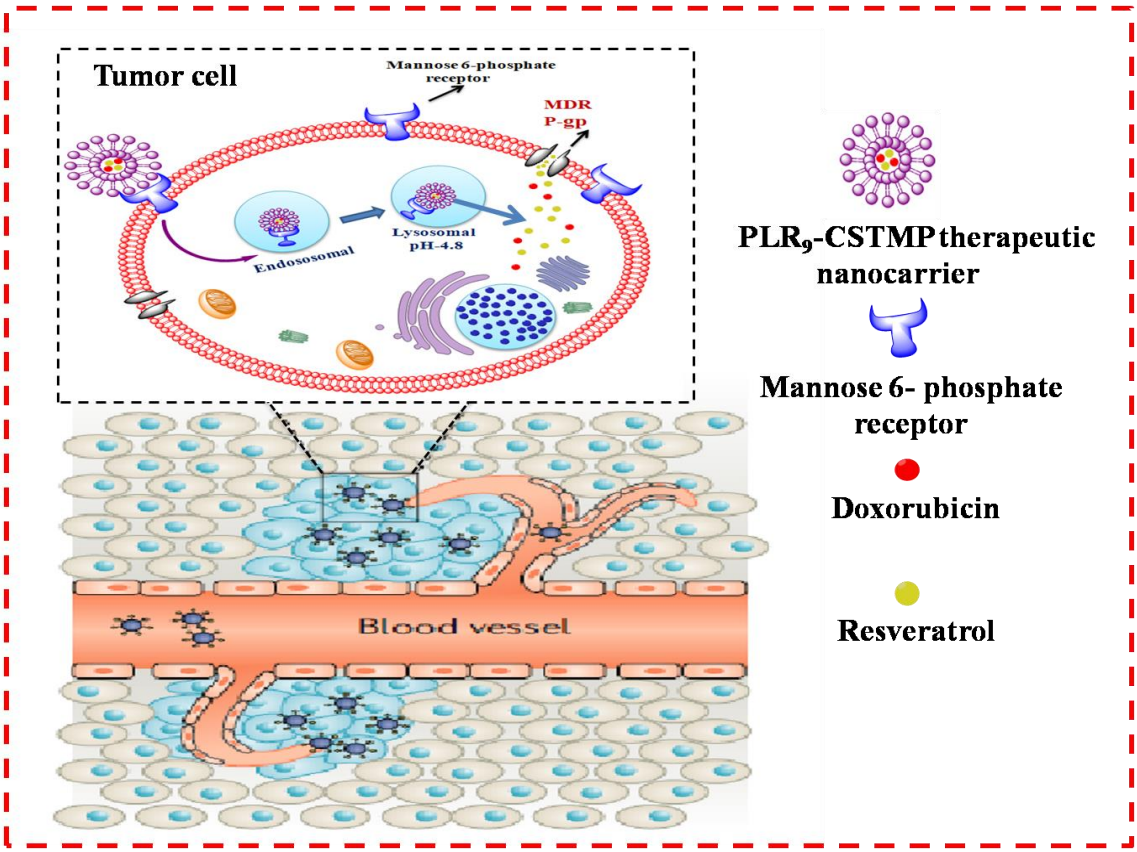

Abstract.4.1: Multifunctional targeted nano-carrier delivery vehicles functioned as stimuli-responsive co-delivery of doxorubicin and resveratol was exploited for an effective chemotherapy in breast cancer MCF7 cells. The nano-carrier consisted of poly-l-lactic acid-Arg 9-mer (**PL-R_9**) and chitosan-trimannose-6-phospharamidite (**CS-TMP**) which an effective binding motif to cell-surface cationic independent mannose-6- phosphate receptors (**CI-MPR**) via carbohydrate-endogenous lectin interactions. In a combination of doxorubicin (**Dox**) and resveratrol (**Res**) were co-loaded into **PLR$_9$-CSTMP** nano-carrier. Both **Dox** and **Res** were released in a synergistic fashion at lysosomal pH. In this contrast, **PLR$_9$-CSTMP-Dox/Res** combination showed higher cytotoxicity in compare to free **Dox**, free **Res**, free

Dox-Res combination in MCF7 cells. Furthermore, **Dox-Res** loaded nano-carrier significantly mitigates the **Dox** induced cytotoxicity towards normal cells.

4.2. Introduction

Breast cancer is the most front line cancer in women and one among the leading causes of cancer-related mortality worldwide. Extensive use of chemotherapeutic drugs generates resistance against the therapeutic agents. Hence, identifying alternative treatments is crucial to reduce the mortality rate related to breast cancer.[1] In addition, single drug chemotherapies are several constraints about systemic administration including a high dose of an individual drug is generally required, owing to the insufficient drug accessibility and accumulation to the tumor sites, which inevitably causes significant side-effects to normal tissues and increase multidrug resistance. Therefore, combination chemotherapy of multiple anticancer drugs has been extensively advanced since it could reduce multidrug resistance and side effects as a result of lower dosage. Therapeutic nanoparticle (NP) serves as an excellent carrier, such as liposomes, albumin NPs and polymeric micelles have been approved for cancer drug delivery with high therapeutic potential. Many other nano-carrier technology enabled therapeutic modalities are under clinical investigation, including chemotherapy, hyperthermia, radiation therapy, gene or RNA interference(RNAi) therapy and immunotherapy.[2-5] Current nano-carrier systems explore controlled, temporal, and spatial delivery that rationality, an effective development of such elegant systems, considerable challenges should be addressed, including the drug solubility, size, and molecular weight as well as the drug's type, as the successful co-delivery of hydrophobic and hydrophilic molecules is a far more formidable task than just delivering similarly soluble molecules. Owing to the passive targeting potency by the enhanced permeability and retention (EPR) effect, nano-carriers could preferentially deliver the loaded drugs into tumor tissues and improve anti-tumor efficacy.[6]

In recent years, the researchers evaluated carbohydrate-based liposomes, polymers and nanoparticles for their ability to deliver anticancer drugs into solid tumors. Carbohydrates play important roles in key recognition events with a variety of receptor proteins such as hormones, enzymes, toxins, lectins, antibodies, viruses, and bacteria.[7-10] Among these, endogenous lectin-type receptors are overexpressed in many tumors and can be used to selectively target and deliver drugs, or diagnostic probes to cancer cells by receptor-mediated endocytosis, providing better efficacy and lower toxicity in healthy tissues.[11,12] Mannose-6-phosphate/insulin-like growth factor-II (M6P/IGF-II) receptor of membrane lectin, the CI-MPR, is a multifunctional receptor, involved in the transport of cellular proteins from the cell

surface or trans-Golgi network to lysosomes.[13,14] There is also another type of receptor so-called cationic dependent mannose-6-phosphate receptors (CD-MPR) that also binds to mannose-6-phosphate-bearing proteins. Subsequently, it is not present on cell surface and only involved in the transport of some lysosomal enzymes from trans-Golgi network to lysosomes.[15] The CI-MPR has a role in the regulation of tumor growth and metastasis.[16,17] However, in adults CI-MPR has been reported to be induced in several human carcinoma cells such as breast cancer,[18] pancreatic cancer,[19] gastric cancer,[20] melanoma[21] and hepatocellular carcinoma.[22]

Dox is a one of the most commonly used therapeutic drug to date but accompanied with disadvantageous of toxicity to normal tissues such as cardiotoxicity and development of **Dox** resistance limit the clinical application of **Dox**. Naturally occurring compound Resveratrol is used as a nutraceutical and is known as phytoalexin, found in various plants, nuts, fruits and especially abundant in grapes and red wine. It has been extensively studied for its antioxidant, anti-aging and anti-inflammatory activities. In addition, as a therapeutic agent for many diseases it has been widely studied *in vivo* and *in vitro* modes which showed **Res** as potential anti-tumor activity against several malignancies.[23–27] Furthermore, **Res** can reduce cardiac toxicity and fibrosis that induced by **Dox**.[28,29] However, the metabolism of **Res** is extremely rapid and extensive, and its plasma half-life is only about 9 min in human.[30.]Moreover, the oral bioavailability of **Res** is nearly zero due to its poor water solubility and significant first-pass effect.[31,32] On the other side, the half-life of free **Dox** is about 30~40 h in human.[33,34] In these regard, only using mixture of free **Dox** and free **Res** without controlling their pharmacokinetic characteristic cannot overcome **Dox** side effects and enhance the anticancer effects of **Dox**.

In this chapter, a newly designed carbohydrate analogue of chitosan-trimannose-6-phospharamidite functionalized with poly-l-lactic acid-arg9-mer (**PL-R_9**) nano-carrier has been described and the synthesized nano-carrier was loaded with **Dox** and **Res** which showed significantly high drug content and multi-drug delivery properties towards breast cancer MCF7 cells. **PLR_9-CSTMP-Dox/Res** targeted nanoparticles were assessed primarily by MTT assays on MCF7 cells and its apoptotic cell death were evaluated by live-dead, Annexin V, and nuclear condensation assays. The combination chemotherapeutic approach was performed in order to overcome the drawbacks of single **Dox** delivery considering its systemic toxicity.

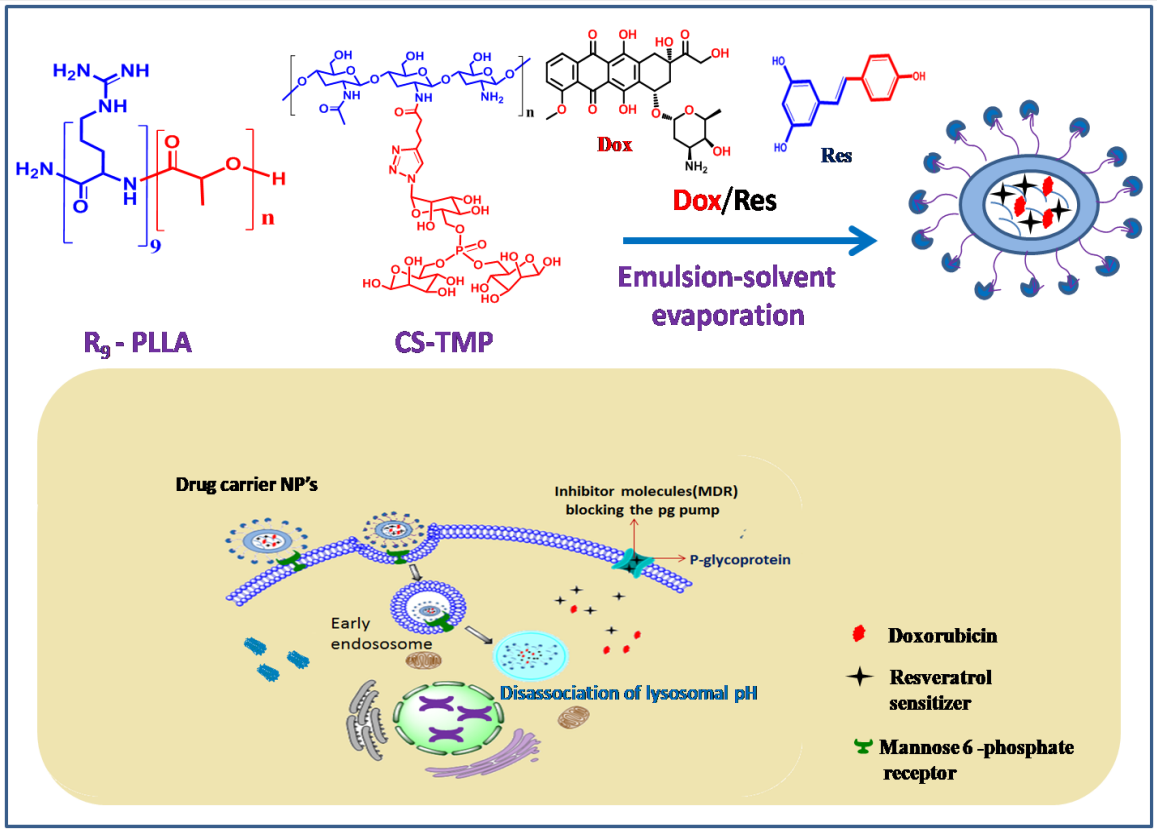

Scheme 4.1. Schematic representation of **PLR$_9$-CSTMP-Dox/Res** nanocarrier internalized by the receptor mediated endocytosis and drug release by pH stimuli

4.3. Results and discussion

4.3.1. Preparation and characterisation of the CS-TMP polymer

4.3.1.1. Preparation of CS-TMP polymer

Chitosan(50mg) was dissolved in 10mL of 1% acetic acid under vigorous stirring. Subsequently, 5-hexynoic acid (30mg), EDC.HCl (20mg) and catalytic amount of N-hydroxysuccinimide were added in the above reaction mixture at room temperature.[35]After 12hrs, solution mixture was washed with ethanol followed by acetone then centrifugation, the precipitation was re-suspended in water and fridge dried to obtain compound **10**.

To a solution of compound 10(20mg), sodium ascorbate (4mg) and $CuSO_4$. $5H_2O$ (3mg) were added in milli-Q water(5mL) then azido trimannose-6-phospharamidite(**8)** dissolved in methanol(5mL) was added. After, the mixture solution was stirred at room temperature for 2days and washed with acetone. Subsequently centrifugation, the precipitation was re-suspended in water, and then frozen dried to obtain compound as a powder of **CS-TMP**.

4.3.1.2. Characterisation of the CS-TMP polymer

FT-IR was recorded using a Fourier transform infrared (FT-IR) spectrometer (Bruker AlphaT FT-IR spectrometer) with a KBr film for measurement. **ATMP** conjugation to **CS-HN** polymer was confirmed by FT-IR the important characteristic 2120.98cm^{-1} peak of **ATMP** disappear (shown in circle on comparison spectrum) and **CS-TMP** showed the characteristic absorption peaks of the polymer backbone at 3416 cm^{-1} (O-H, stretching), 1644cm^{-1}(C=O, amide stretching) and 1625cm^{-1}(C=C, alkenyl stretching) stretching bonds and is compared with ATMP (As shown in **fig 4.1).**

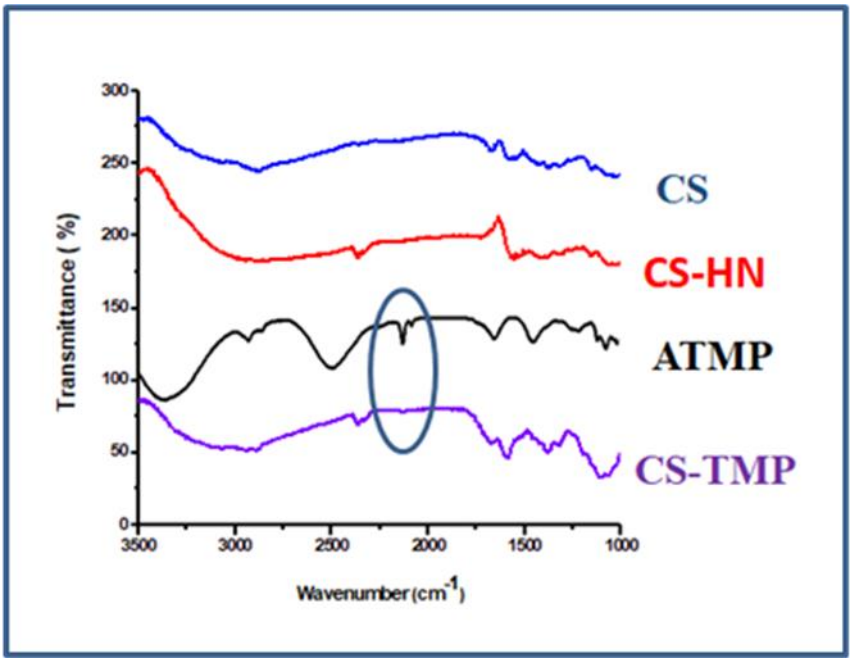

Figure 4.1. FT-IR spectra of chitosan, **CS-HN** polymer, **ATMP** and a polymer of **CS-TMP**.

4.3.2. Preparation and characterisation of the PL- R_9 polymer

4.3.2.1. Preparation of PL- R_9 polymer

PL– R_9 was synthesized by according to a modified literature procedure. To a solution of poly-l-lactic acid (40mg, 0.24mmol), EDC.HCl (8mg, 0.04mmol) and N-hydroxysuccinimide (catalytic amount) were dissolved in DMF (5mL) then nonamer of arginine (20mg, 0.02mmol) dissolved in milli-Q water (3mL) was added. The reaction solution was stirred at room temperature for 3 days after then the reaction mixture was washed with acetone (3x10mL) to remove of unreacted **PLLA**s. The obtained precipitate was collected by centrifugation and dried under vacuum overnight to yield the white crystalline solid of **PL–R_9 (13).**

4.3.2.2. Characterisation of the PL- R_9 polymer

Fig 4.2 shows the spectra of the FT-IR of the **PLLA**, **Arg_9** and **PLLA-Arg_9**. Compared with the FT-IR spectrum of **PLLA** and **Arg_9** there were absorption peaks in the spectrum of **PL-R_9** appearing around 3420cm^{-1}, 2993cm^{-1}, 2907cm^{-1}, 2845cm^{-1}, 2367cm^{-1},2361cm^{-1},2100cm^{-1}, 1753cm^{-1},1457cm^{-1}, 1360cm^{-1}, 1206cm^{-1}, 1133cm^{-1}, 1047cm^{-1}. Among the new appear peaks were at C=O, shifted amide stretching 1753cm^{-1} and C-H deformation stretching at 1457cm^{-1} and 1360cm^{-1}.

Fig. 4.2B shows the ^{1}H-NMR spectra of **PLLA**, **Arg_9** and **PLLA-Arg_9** polymers. The signals at 4.22 ppm and 1.55 ppm can be assigned to the **PLLA** protons. Compared with **PLLA** and **Arg_9**, a new signal at 3.21 ppm in the **PLLA-Arg_9** polymer can be assigned to the methylene protons, proving the existence of the **Arg_9**.

Fig. 4.3 shows the MALDI-TOF-MS spectra of **Arg_9** peptide molecular ion (M+1) peak appear at 1424.038.

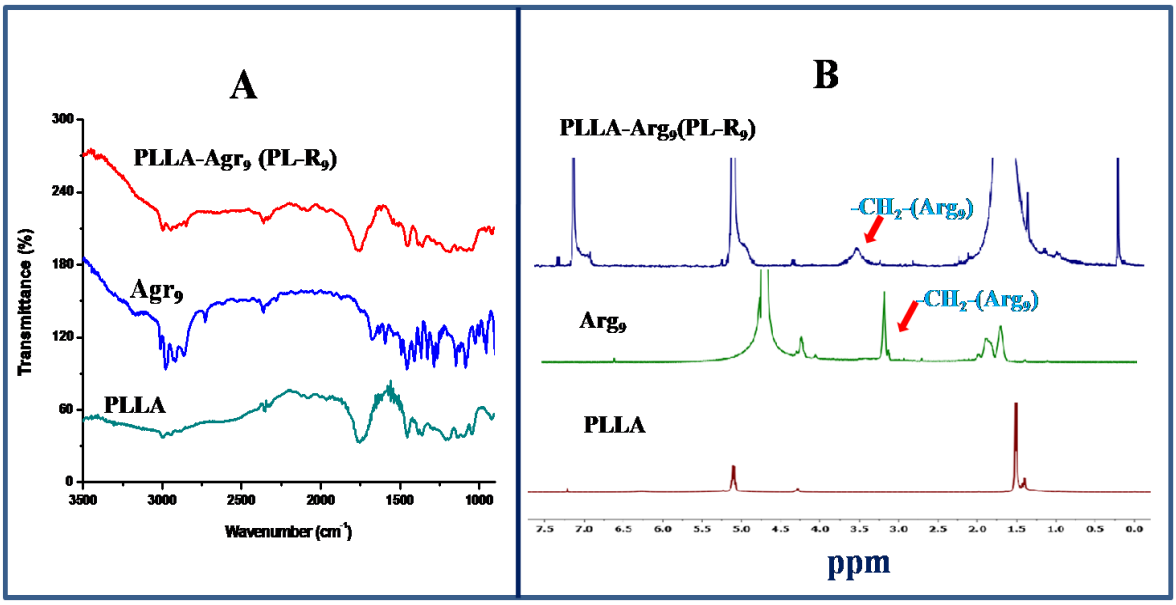

Figure 4.2. A) IR spectra of **PLLA, Arg_9** and **PLLA-Arg_9**; B) ^{1}H-NMR spectra of **PLLA, Arg_9** and **PLLA-Arg_9**.

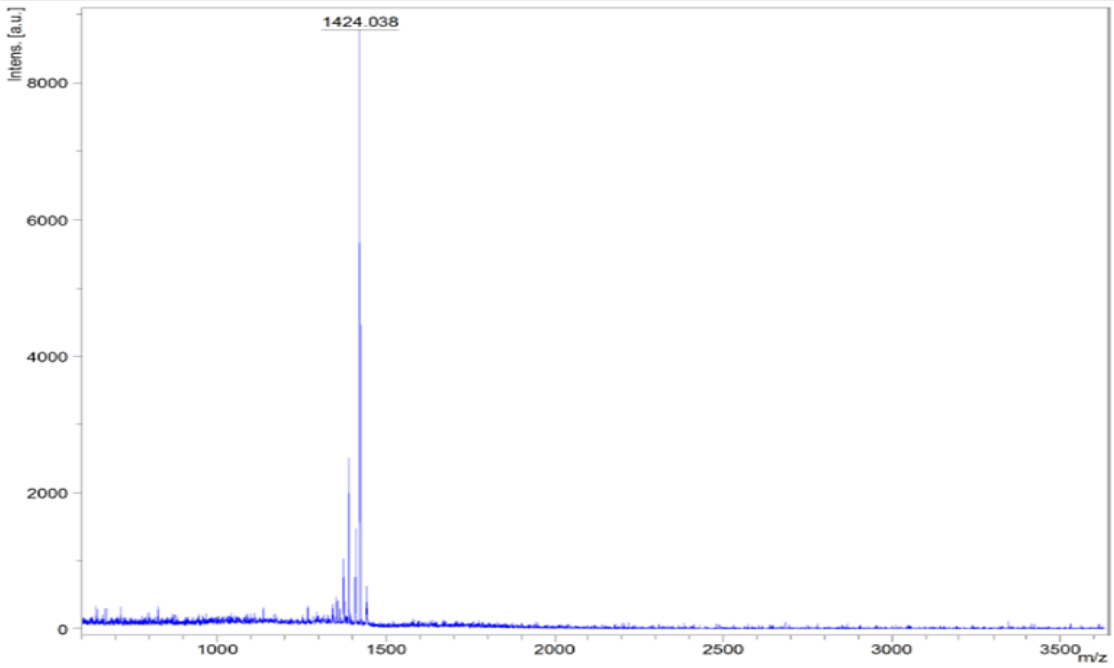

Figure 4.3. MADI-TOF-MS spectra of **Arg9-mer** molecular ion (M+1) peak

4.3.3. Preparation of Dox/Res-loaded PLR_9-CSTMP nanoparticles (NPs)

Dox/Res-loaded **PLR_9-CSTMP NPs** was prepared by using emulsion-solvent evaporation method.[36] Briefly, 10 mg **PLR_9** and 5 mg **PLR_9-CSTMP** were dissolved in dichloromethane (3 mL), 8 mg **Res** was dissolved in ethanol (0.5 mL), and 3 mg **Dox·HCl** was dissolved in distilled water (6 mL). The above solution was mixed and emulsified by using ultrasound for 3 min at 0 °C. After that, 0.3% PVA (10 mL) was added into the mixture solution and further emulsified by using ultrasound for 3 min at 0 °C. Finally, the mixture solution was stirred at room temperature for 4 hrs to remove dichloromethane. After centrifugation, the precipitation was re-suspended in water, and then frozen-dried to obtain **Dox/Res**-loaded **PLR_9-CSTMP** NPs powder.

4.3.4. Drug loading efficiency and release rate of PLR_9-CSTMP NPs

To determine the amount of **Dox** or **Res** encapsulated by a **PLR_9-CSTMP NPs**, the encapsulation efficiencies (EE) of **PLR_9-CSTMP** nanoparticles that contain **Res** and/or **Dox** were measured. The drug contents of the **PLR_9-CSTMP NPs** were analysed with a fluorescence spectrometer. As presented in **Table 4.1**, single-**PLR_9-CSTMP NPs** exhibited efficient encapsulating ability for either **Dox** or **Res**, with EE reaching levels of 86.4% ± 1.2% and 91.3% ± 2.6%, respectively. For **PLR_9-CSTMP NPs** with both **Dox** and **Res**, the EE was 52% ± 3.7% for **Dox** and 56% ± 3.3% for **Res**. These results indicated that **Dox** and **Res** could be loaded together into a **PLR_9-CSTMP NPs,** there by achieving an EE greater

than 50%. Thus, the **PLR$_9$-CSTMP NPs** is a feasible method for the co-delivery of both agents to tumor cells in one package.

For further the evaluate of **Dox** and/or **Res** could be released by the **PLR$_9$-CSTMP NPs**, the standard drug release rate (RR) was measured for each agent at 37 °C in PBS (pH 7.4, 6.5 and 5.0). The cumulative release curves of **Res** and **Dox** from the **PLR$_9$-CSTMP NPs** are presented in **fig 4.2.** Relatively faster release of **Dox** and **Res** was observed from the **PLR$_9$-CSTMP NPs** in the first 24 hrs (**Dox**, 81.4% ±2.6%; **Res**, 78.6% ± 2.3%). At 48 hrs, the cumulative release reached 86.4% ± 1.2% for **Dox**, and 91.3% ± 2.6% for Res.

Drug	Dox- PLR$_9$-CSTMP NPs	Res- PLR$_9$-CSTMP NPs	Combine- PLR$_9$-CSTMP NPs
Dox	86.4% ± 1.2%	NA	21.5% ± 3.2%
Res	NA	91.3% ± 2.6%	54.8% ± 4.0%

Table 1. Encapsulation efficiency of various **PLR$_9$-CSTMP** nanoparticles for **Dox** or **Res**

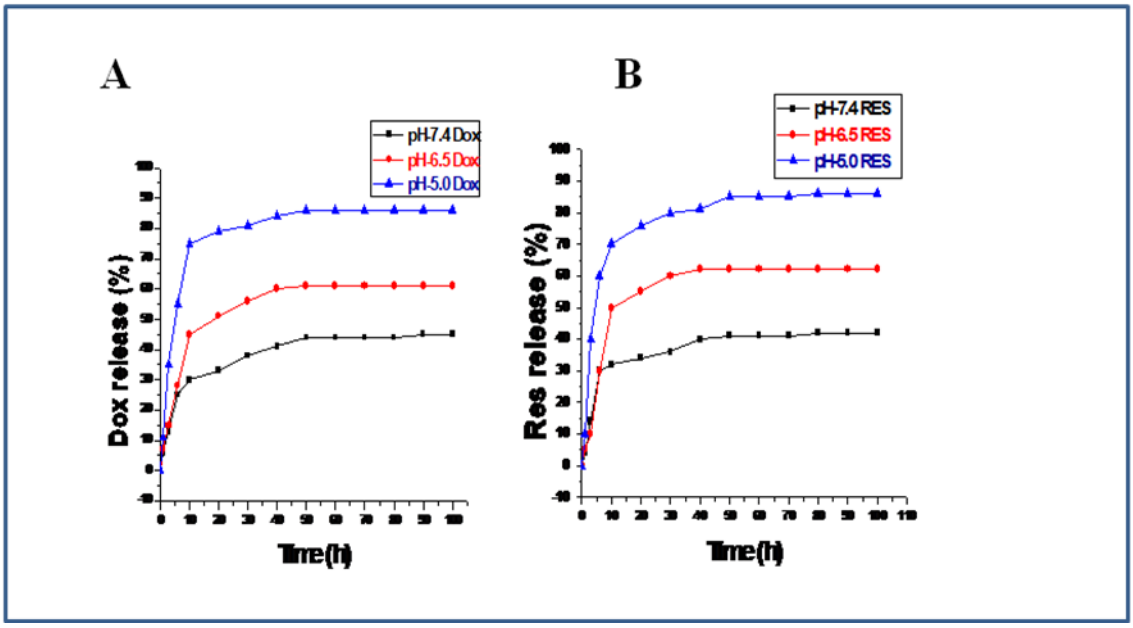

Figure 4.4. Panels A and B are *in vitro* **Dox** and **Res** release curve from **Dox/Res**-loaded **PLR$_9$-CSTMP** nanoparticles in different PBS (pH 5.0, pH6.5 and pH 7.4) at 37 °C. Data are mean ± SD. n = 3.

4.3.5. Cytotoxic effect of the Dox/Res-loaded PLR_9-CSTMP NPs

In vitro cytotoxic effect of the **Dox/Res**-loaded **PLR_9-CSTMP NPs** was evaluated by 24 and 48 hrs MTT assay using human breast cancer cells MCF-7 (Mannose-6-phosphate receptor positive), human colon cancer cells HCT-116 (Mannose-6-phosphate receptor negative) and WI-38 (Normal lung fibroblast) cell line. Since the **Dox/Res**-loaded **PLR_9-CSTMP NPs** is having **Res/Dox** combination in 10:3 ratio, a wide range of concentrations of **Res/Dox** combinations like 100/30, 75/22.5, 50/15, 20/6, 10/3 and 5/1.5 µg/mL is tested for the **PLR_9-CSTMP NPs** as well as for the mix of these two drugs. Bare **PLR_9-CSTMP NPs**, **Dox** and **Res** alone were also tested using the effective concentration of each as in the **PLR_9-CSTMP NPs**. Maximum cell death was observed for both the **PLR_9-CSTMP NPs** and the mix of **Res/Dox** combination at 100/30 in all the three cell lines and a concentration of 20/6 was selected for further studies which was found to be non-toxic to the normal cell (WI-38). The **PLR_9-CSTMP NPs** was found to exhibit enhanced cytotoxic effects towards MCF-7 cells in 48 hrs MTT assay when compared to 24 hrs. At 48 hrs the construct was able to provide more cytotoxic effects than **Res/Dox** mix and this effect may be due to the fact that being low molecular weight drugs, **Res** and **Dox** can diffuse in to the cells and can provide immediate effect, where as in the case of **PLR_9-CSTMP NPs**, receptor mediated endocytosis and slow and continuous release of the drug from the construct may be happening. Moreover, the **PLR_9-CSTMP NPs** was found to be more cytotoxic towards mannose-6-phosphate receptor positive cells than the receptor negative (HCT-116) or normal cell (WI-38) (As showing **fig.4.5**).

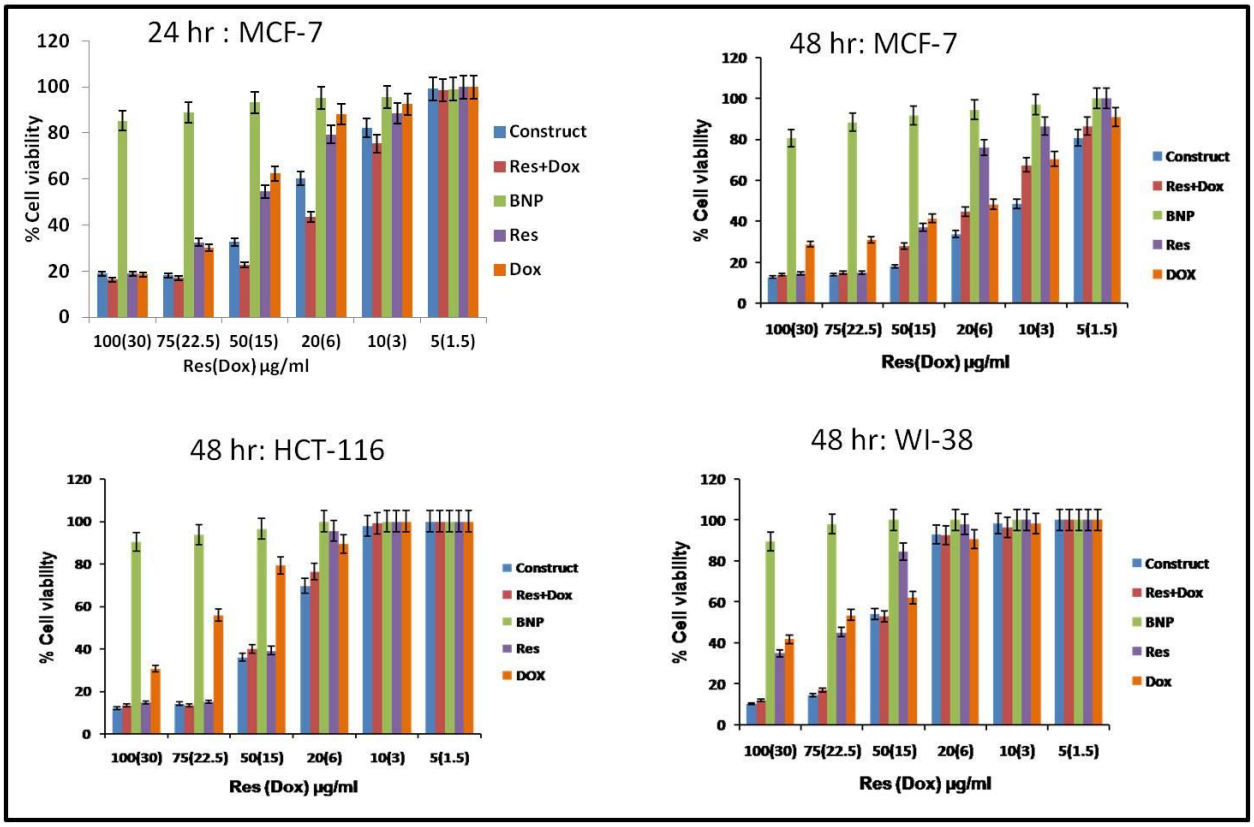

Figure 4.5. Evaluation of the cytotoxic effect by MTT assay with **PLR_9-CSTMP NPs** at different time intervals in MCF-7, HCT-116 and WI-38 cell lines.

4.3.6. Nuclear co-localization of Dox

In order to evaluate the nuclear co-localization of the **Dox** in the **PLR_9-CSTMP NPs**, MCF-7 cells were incubated with the **PLR_9-CSTMP NPs** and after 6 hrs the cells were treated with Hoechst 33342 nuclear staining dye and observed using fluorescent microscope, the red fluorescence from nuclear region indicated the nuclear co-localisation of **Dox** in the **PLR_9-CSTMP NPs**, and the merged images of Hoechst and **Dox** fluorescence undoubtedly confirms the same (As shown **fig.4.6**)

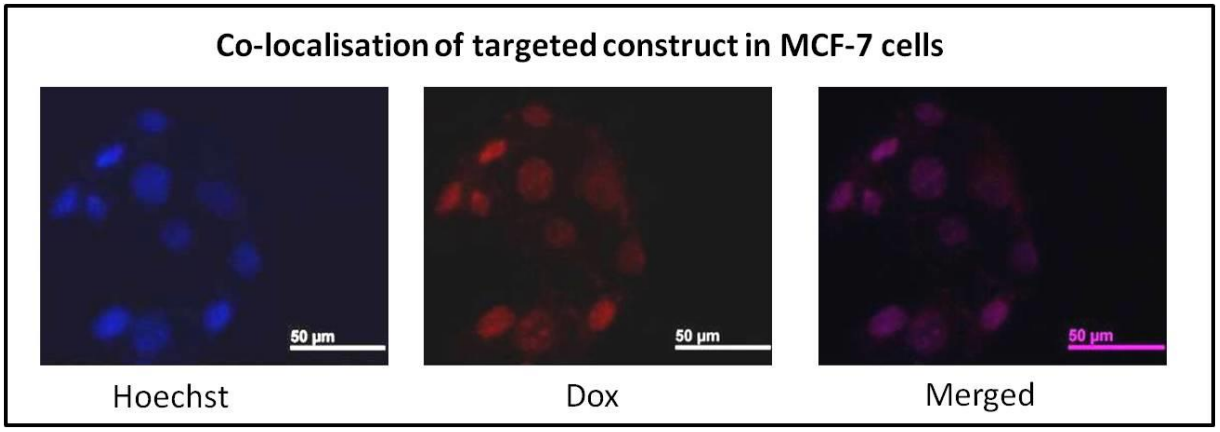

Figure 4.6. Nuclear co-localisation of **Dox** from the **PLR_9-CSTMP NPs**.

4.3.7. Effect of targeted construct on Apoptosis

To evaluate the apoptotic effects induced by the **PLR_9-CSTMP NPs**, different apoptotic assays were performed on MCF-7 cell line using the concentration, **Res/Dox** 20/6µg/mL for 48 hrs. For a comparison, drug alone (simple mix of **Res** and **Dox** in the same concentration) treated group was also included in the study. Phase contrast microscopic images of the non-treated control cells, drug alone treated cells and **PLR_9-CSTMP NPs** treated cells were analysed for the morphological changes associated with apoptosis, which deciphered a decreased cell number, membrane blebbing and formation apoptotic bodies in the drug alone and **PLR_9-CSTMP NPs** treated groups when compared to the control (**fig.4.7a**). The apoptotic event was more pronounced by the **PLR_9-CSTMP NPs** treated group at 48 hrs than the drug alone as shown **fig 4.7.** Live dead assay using acridine orange- ethidium bromide staining showed the presence of more number of apoptotic cells (yellow/red) in the treated groups with a maximum death rate upon treatment of **PLR_9-CSTMP NPs** (**fig.4.7b**). APOP staining was performed to confirm the apoptotic cells in the treated groups compared to the untreated control cells. Deeply stained pink coloured cells indicated the apoptotic cells in each panel, with the maximum effect in the construct treated group (**fig.4.7c**).

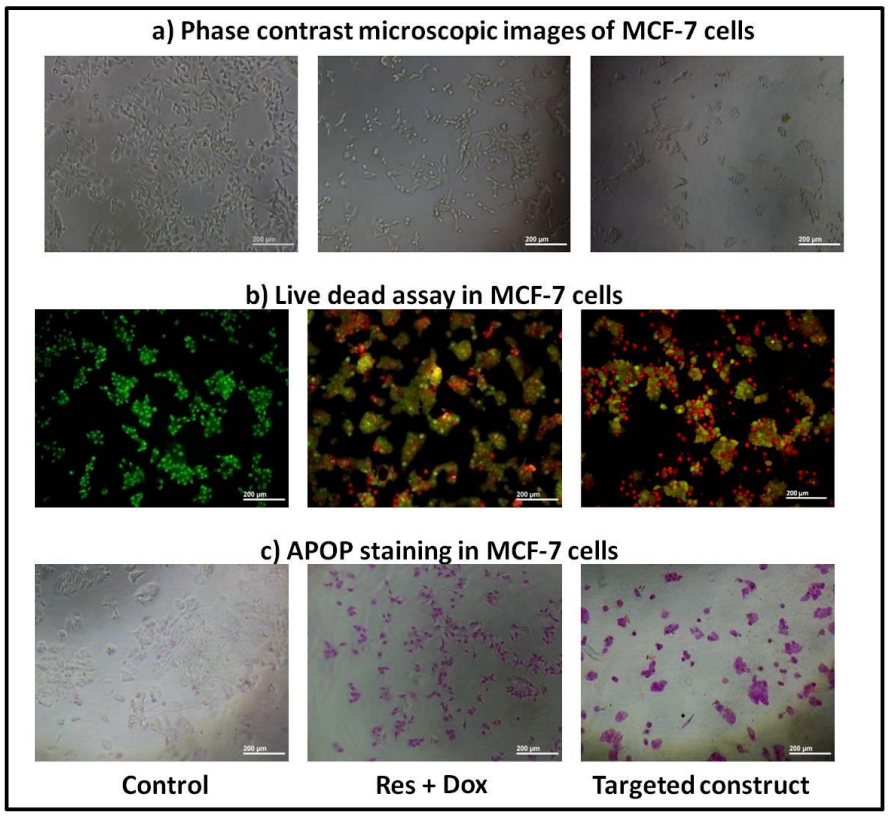

Figure 4.7. Apoptotic effects induced by the construct on MCF-7 cells. a) Phase contrast microscopic images of untreated control cells and cells treated with **Res/Dox** 20/6

µg/mL & **PLR_9-CSTMP NPs** (targeted construct) with same drug concentration for 48 hrs. b) Live dead assay by acridine orange-ethidium bromide dual staining. c) Bright field microscopic images of cells stained with APOP stain.

4.3.8. Hoechst nuclear staining and Caspase-3 flourometric assesses

Hoechst 33342 nuclear staining was performed to evaluate the chromatin condensation which also leads to the same pattern of results as in the previous experiments (**fig.4.8a**) with the maximum chromatin condensation in the **Res/Dox - 20/6 µg/mL** &**PLR_9-CSTMP NPs** treated group. In order to study the changes occurred to the nuclear DNA in the cells of the upon treatment of the drug loaded nanoparticle, DNA was isolated from the treated as well as the control cells and analysed using surface enhanced Raman scattering (SERS) technique where the signature peaks associated with DNA and related biomolecules were identified. When compared with the SERS spectrum of the control DNA, certain signature peaks of DNA *viz.,* 666 cm^{-1} - Guanine and Thymine peak and 826 cm^{-1} DNA O-P-O stretching peak were completely absent in the SERS spectrum derived from the DNA of the cells treated with drug loaded nano-construct as well as drug alone. The strong peaks from the control DNA *viz.*, 1173 cm^{-1}corresponding to Cytosine and Guanine, 1288 cm^{-1}corresponding to phosphate back bone of nucleic acid were found to be less intense in the case of both treatments, indicating DNA damage. Raman peak at 1493 cm^{-1} in the control DNA was found to be shifted to right in both the treatment groups, showing more intense peaks for ring breathing of DNA bases. Adenine and Guanine (1575cm^{-1}) which may be due to the disruption of normal DNA conformation (**fig.4.8b**). Further the effect of construct on the expression of Caspase 3 was evaluated using Caspase fluorometric assay kit in MCF-7 cells, which indicated a 9.03 and 1.32fold increase in the expression in the targeted construct treated group when compared to the control and drug alone treated groups respectively (**fig.4.8b**).[37]

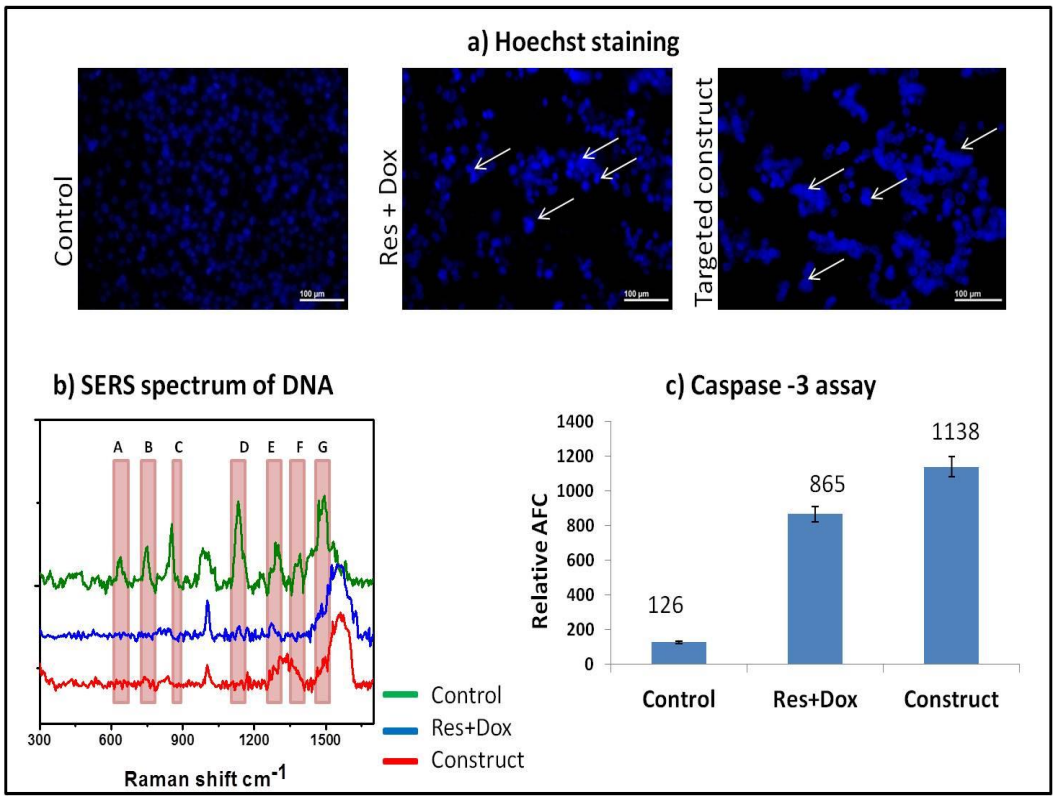

Figure 4.8. a) Hoechst nuclear staining for chromosome condensation. b) SERS fingerprinting of isolated DNA from the **Res/Dox -PLR$_9$-CSTMP NPs** treated and untreated cells (A, B, C, D, E, F, G showing Raman shift at., A-666 cm^{-1}, B-748 cm^{-1}, C-826cm^{-1}, D-1173cm^{-1}, E-1288 cm^{-1}, F-1373 cm^{-1}, G-1493 cm^{-1}). c) Caspase-3 fluorometric assay performed with untreated control MCF-7 cells and **Res/Dox -PLR$_9$-CSTMP NPs** treated cells for 48 hrs.

4.3.9. Apoptosis induction by PLR$_9$-CSTMP NPs in MCF-7 cells determined using Annexin V staining

To confirm the early apoptosis in the construct treated cells, the cells were treated with the construct as well as drug alone for 24 hrs followed by Annexin V staining. It was found around 42% of the cells were in apoptotic stage even at 24 hrs upon the treatment with the **PLR$_9$-CSTMP NPs**, which validated the programmed cell death mediated orchestration in the mode of cytotoxicity(f**ig 4.9**).

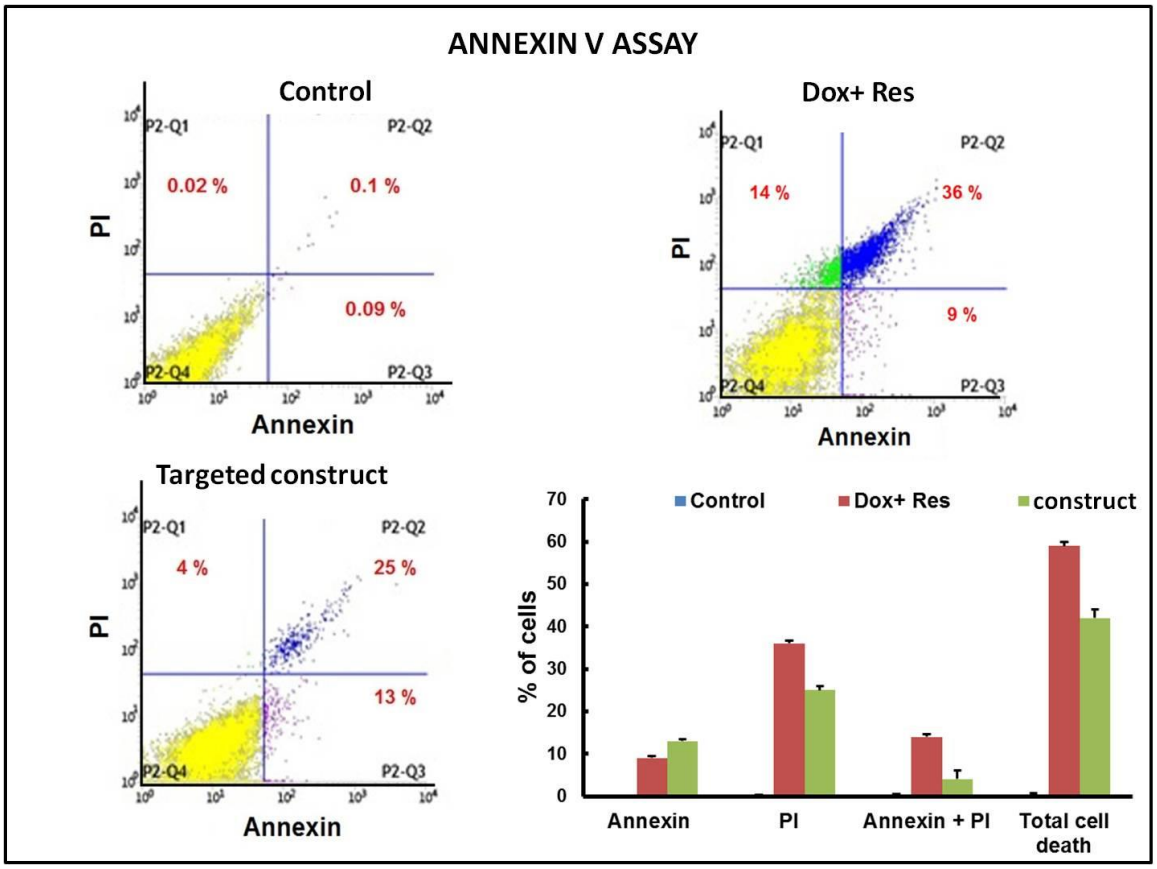

Figure 4.9. Annexin V assay with the untreated control cells, **Dox/Res** alone treated cells and targeted construct treated cells for 24 hrs. Graphical representation of the number of cells in each treatment undergoing early apoptosis is also provided.

4.4. Conclusion

In conclusion, an analogue of mannose-6-phosphate (M6P) was synthesized to target CI-MPR and successfully demonstrated the M6P-functionalized **PLR_9-CSTMP NP's** for efficient CI-MPR targeting towards breast cancer MCF7 cells. The targeting nanoparticles co-loaded with **Dox** and **Res** showed efficient pH responsive cargo release kinetics. The nano-carrier system developed for the combination chemotherapy resembled a proof-of-concept in the applications of nanomedicine in oncology which has dominant features like: 1) prolong half-life of **Dox** and **Res**, 2) mitigation of **Dox** resistance in the target cells, and 3) reduce the toxicity of **Dox** in healthy tissues. For further, **Dox/Res**-loaded **PLR_9-CSTMP NP's** exhibited greater cytotoxicity than free **Dox** and free **Res** on MCF-7 cells. The cytotoxicity of a mixture of free **Dox** and free **Res** was higher than free **Dox** and free **Res**.

Such multifunctional nano-carrier targeting-platforms may open up a new avenue for cancer treatment, possibly leading to clinical applications.

4.5. Experimental section

4.5.1. Materials and methods

Doxorubicin hydrochloride, MTT reagent, JC1 Dye, BrDU Kit, D-(+)-Mannose, Chitosan(~60kDa), Poly-L-Lactic acid (~32kDa), Lipase from *Candida rugosa* were obtained from Sigma-Aldrich (St. Louis, MO). Fmoc protected amino acid *i.c.* Fmoc- Arg (pbf)- OH was acquired from Nova biochem. All the other common reagents and solvents were purchased from Sigma-Aldrich, Merk, and Spectrochem, was used without further purification. High performance liquid chromatography (HPLC) was accomplished by Shimadzu HPLC system consisting of SCL-10Avp system controller, two LC-8A solvent delivery units, SPD-M20A UV-VIS photo diode array (PDA) detector, equipped with Multi PDA-LC solution (software) on a 250 mm x 4.6 mm i.d, 5μM, YMC-Pack R&D Octa-decane silane (ODS) analytical column (9YMC Co., Ltd. Japan). NMR spectra were recorded on a Bruker AMX 300 (^{1}H-NMR at 500MHz, ^{13}C-NMR at 125MHz) spectrometer. Tetra methyl silane was used as reference for ^{1}H-NMR, and the chemical shift were reported in ppm and the coupling constant in Hz. High resolution mass spectra were determined on a HR-EMI analysis of Thermo Scientific Exactive system, and MALDI-TOF mass spectra on a Shimadzu Biotech, AXIMA-CFR PLUS system. Lyophilization was performed with lyophilizer, Scan Vacfreez drier model: cool safe 110-4 PRO system (-110^{0}C).

4.5.2. Synthesis of azido tri mannose- 6-phospharamidite (ATPM)

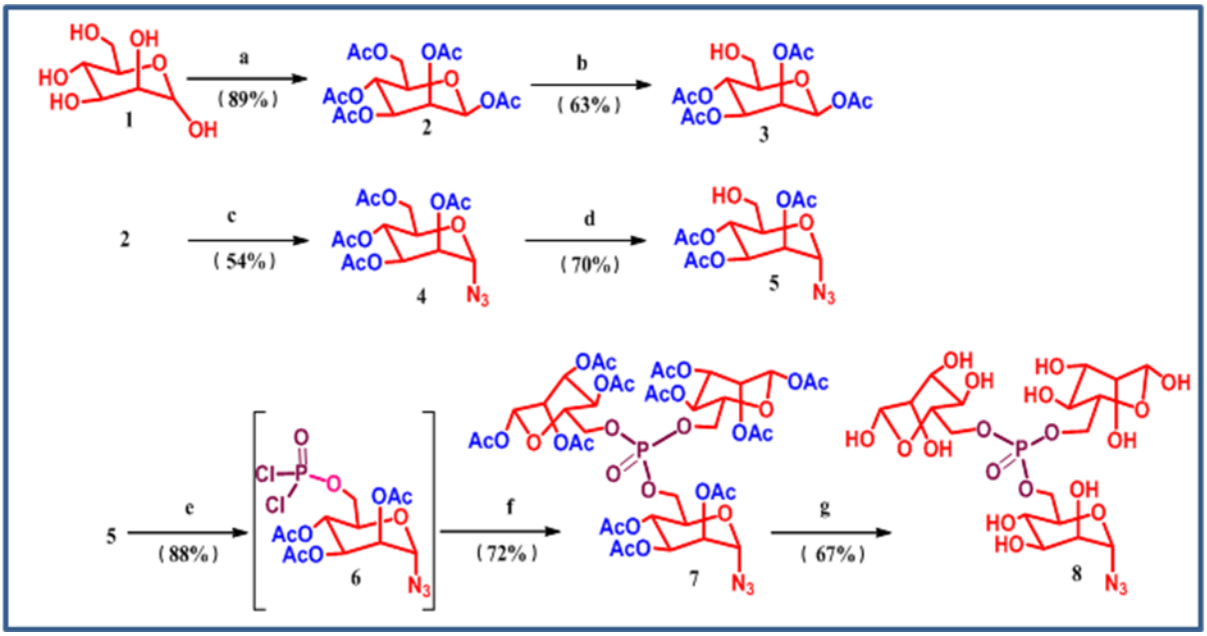

Scheme 4.2. Synthesis of azido tri mannose- 6-phospharamidite., Reagents and conditions:(a) Ac_2O, Conc.H_2SO_4 (four drops) ; (b)*Candida rugosa* lipase, 25mM KH_2PO_4,pH 4, 1,4-dioxane(20%); (c)(i) 33% HBr/AcOH (25^{o}C); (ii) $TMSN_3$, TBAF,CH_2Cl_2; (d) *Candida rugosa* lipase, 25mM, KH_2PO_4 pH-4, 1,4-dioxane(20%);(e) $POCl_3$, NMI,CH_2Cl_2; (f) **3**, NMI,CH_2Cl_2; (g) dry MeOH,1M NaOMe/MeOH, Dowex-50Wx8 (H+) ion-exchange resin.

4.5.2.1. 1,2,3,4,6-Penta-*O*-acetyl-D-mannopyranose (2)

This compound was synthesized according to a modified literature procedure. D-(+)-Mannose **1**(10g,55.5mmol) was added in acetic anhydride (25mL) and the solution was cooled at 0 °C, followed by dropwise addition of concentration sulfuric acid (4 drops)in reaction mixture. After stirring 30 min at 0^{o}C and an additional 4 hrs at r.t., then reaction mixture was poured onto ice/water (100mL) and the organic phase was extracted with EtOAc (120 mL). The organic extract was washed with water (1 × 100 mL), sat aq. $NaHCO_3$ (4 × 60 mL), brine (60 mL), dried (Na_2SO_4) and concentrated under reduced pressure. The crude product was subjected to column chromatography (EtOAc:Hexane, 4:6v/v) to afford the acetylated sugar as a mixture of a nomers (9:1, β:α) as a colorless oil (19.4 g, 89%).^{1}H-NMR (500 MHz, $CDCl_3$):δ 6.10 (d, $^3J_{1,2}$ = 1.5 Hz, 1H, H_1), 5.37-5.36 (m, 2H, H_3, H_2); 5.28-5.27 (m, 1H, H_4), 4.31 (dd, $^2J_{6a,6b}$ = 10.0 Hz, $^3J_{6b,5}$ = 5.0 Hz, 1H, H_{6b}), 4.13 (dd, $^2J_{6a,6b}$ = 10.0 Hz, $^3J_{6a,5}$ = 2.5Hz, 1H, H_{6a}), 4.07-4.05 (m, 1H, H_5), 2.19-2.02 (5 x s, 15H, $COCH_3$);^{13}C-NMR (500 MHz,$CDCl_3$)δ 170.68, 170.01, 169.56, 168.08, 90.61,70.62, 68.75, 68.34, 65.55, 62.11, 20.77, 20.72, 20.66, 20.65. HR-ESI-MS (m/z) for $C_{16}H_{22}O_{11}$ $[M + Na]^+$= 413.2103 ; found, 413.1015.

4.5.2.2. 1,2,3,4-Tetra-*O*-acetyl-β-D-mannopyranose (3)

Compound **3** was synthesized according to a literature procedure.[38] A mixture of **2**(500 mg, 0.107 mmol), *Candida rugosa* lipase (250 mg), and 25mM phosphate buffer pH-4 which contain 20% of 1,4-dioxane (50 mL) was stirred (300 rpm) at 30°C during 48 hrs. The suspension was filtered through Celite, the enzyme washed with 1,4-dioxane and EtOAc, and the residue extracted with EtOAc. The combined organic layers were washed with aqueous $NaHCO_3$ and dried over Na_2SO_4 after the evaporation of the solvent, the resulting crude product was purified by columnchromatography (hexanes/AcOEt 5:5) to give 1,2,3,4-tetra-*O*-acetyl-β-D-mannopyranose**3** as a colorless oil (281mg,63%).^{1}H-NMR (500 MHz, $CDCl_3$):δ 6.09 (d, $^3J_{1,2}$ = 2.0 Hz, 1H, H_1), 5.41 (dd,$^3J_{3,4}$ = 3.5 Hz, $^3J_{3,2}$ = 2.0 Hz,1H, H_3); 5.33 (t, $^3J_{4,3}$ = 10.0 Hz, 1H, H_4), 5.28-5.27 (m, 1H, H_2), 3.87-3.84 (m, 1H, H_5),3.73 (dd, $^2J_{6a,6b}$= 10.5 Hz, $^3J_{6b,5}$= 2.0 Hz, 1H, H_{6b}), 3.64 (dd, $^2J_{6a,6b}$= 6.5 Hz, $^3J_{6a,5}$= 4.5Hz, 1H, H_{6a}), 2.17-2.02 (4 x s, 12H, COCH_3);^{13}C-NMR (500 MHz,$CDCl_3$)170.48, 170.08, 169.88, 168.38, 90.65, 72.85, 68.58, 68.38, 65.77, 61.07, 20.70, 20.68, 20.66, 20.63.HR-ESI-MS (m/z) for $C_{14}H_{20}O_{10}$ [M + Na]$^+$= 371.3026 ; found, 371.0937.

4.5.2.3. 2,3,4,6-Tetra-O-acetyl-α-D-mannopyranosylazide (4)

Compound **4** was synthesized according to a modified literature procedure. To a solution containing 1,2,3,4,6-Penta-O-acetyl-D-mannopyranose **2**(3g, 7.69mmol) was added HBr in AcOH (9 mL) at 0 °C. The mixture was allowed to stir overnight before removing the solvent *in vacuo*. The resulting mixture was dissolved in 1 M TBAF in THF (3.03mL, 10.76mmol) followed by the addition of $TMSN_3$ (1.43mL, 10.76mmol). After 6 hrs, the mixture was diluted with CH_2Cl_2 and washed successively with water, sat.aq.$NaHCO_3$ and brine. The organic portion was collected, dried over Na_2SO_4 and concentrated. The crude product was purified by column chromatography(EtOAc/Hex 4:6) to obtain compound **4** as a white solid(1.54g, 54%).^{1}H-NMR (500 MHz, $CDCl_3$):δ 5.38(dd, $^3J_{2,3}$ = 2.0 $^3J_{2,1}$ = 1.0 Hz, 1H, H_2), 5.21 (t,$^3J_{4,3}$ = 20.5Hz, 1H, H_4); 4.99 (dd, $^3J_{3,4}$ = 6.5Hz,$^3J_{3,2}$ = 3.5 Hz, 1H, H_3), 4.67 (d,$^3J_{1,2}$ = 2.0 Hz, 1H, H_1), 4.23 (dd, $^2J_{6a,6b}$ = 6.5 Hz,$^3J_{6a,5}$ = 6Hz,1H, H_{6a}),4.15(dd, $^2J_{6a,6b}$= 9.5 Hz, $^3J_{6b,5}$= 2.5 Hz, 1H, H_{6b}), 3.64 (m, 1H, H_5), 2.14-1.92 (4 x s, 12H, COCH_3);^{13}C-NMR (500 MHz,$CDCl_3$)δ 170.67, 169.99, 16958, 85.10,70.94,69.23, 65.32, 62.29, 20.73, 20.72, 20.69, 20.67.HR-ESI-MS (m/z) for $C_{14}H_{19}N_3O_9$ [M + Na]$^+$= 396.1026; found, 396.0937.

4.5.2.4. 2,3,4,-Tri-O-acetyl-α-D-mannopyranosylazide (5)

Compound **5** was synthesized according to modified literature procedure. To a solution of 2,3,4,6-Tetra-O-acetyl-α-D-mannopyranosylazide**4** (200 mg, 0.27mmol) and *Candida rugosa*

lipase (100mg) in 25 mM phosphate buffer pH-4 which contain 20% of 1,4-dioxane (50 mL) was stirred (300 rpm) at 30°C during 48 hrs. The suspension was filtered through Celite, the enzyme washed with 1,4-dioxane and EtOAc, and the residue extracted with EtOAc. The combined organic layers were washed with aqueous $NaHCO_3$ and dried over Na_2SO_4 then after the evaporation of the solvent, the resulting crude product was purified by columnchromatography (hexanes/AcOEt 5:5) to give 2,3,4-tri-*O*-acetyl-α-D-mannopyranose azide **3** as a white solid (281mg, 63%).^{1}H-NMR (500 MHz, $CDCl_3$): δ 5.39 (dd, $^3J_{2,3}$ = 2.5Hz,$^3J_{2,1}$ = 1.0 Hz, 1H, H_2), 5.19 (t,$^3J_{4,3}$ = 10.0Hz, 1H, H_4), 5.03 (dd, $^3J_{3,4}$ = 3.5Hz,$^3J_{3,2}$ = 3.0 Hz, 1H, H_3), 4.70 (d,$^3J_{1,2}$ = 0.5 Hz, 1H, H_1), 3.73 (dd,$^2J_{6a,6b}$ = 11.0 Hz,$^3J_{6a,5}$ = 2.0 Hz, 1H, H_{6a}),3.64 (dd, $^2J_{6b,6a}$= 8.0 Hz, $^3J_{6b,5}$= 4.5 Hz, 1H, H_{6b}), 3.55 (m, 1H, H_5), 2.13-1.93 (3 x s, 9H, COCH_3);^{13}C-NMR (500 MHz,$CDCl_3$): 170.33, 170.18, 170.07, 85.12, 70.89, 69.33, 65.48, 61.32, 20.71, 20.67, 20.55. IR ν_{max}(neat) cm^{-1}: 3426.99m, 2120.98s (N_3), 1644.38s, 1372.21s, 1258.71s. HR-ESI-MS (m/z) for $C_{12}H_{17}N_3O_8$[M + Na]$^+$= 354.1026 ; found, 354.2787.

4.5.2.5. Synthesis of compound (7)

This compound was synthesized according to a modified literature procedure. A solution of phosphorus oxychloride (14µL, 0.15mmol) and 2,3,4,-Tri-O-acetyl-α-D-mannopyranosylazide **5** (100mg, 0.30mmol) in dry CH_2Cl_2 was cooled at 0°C, followed by the slow addition of N-methyl imidazole(30µL,0.36mmol). After one hour the reaction mixture was allowed to warm up to room temperature and stirred overnight. The reaction was monitored by ^{31}P-NMR, and when the analysis showed the completed disappearance of the starting material, then the imidazole salt was filtered off, and the filtrate was concentrated under reduced pressure to given the sticky oil **6**(120 mg, 88%), which was used for the next step without further purification.

To a solution of Compound **6** (80mg, 0.18mmol), 1,2,3,4-Tetra-O-acetyl-β-D-mannopyranose **3** (125mg, 0.35mmol) and N-methyl imidazole (37µL, 0.45mmol) were dissolved in CH_2Cl_2 (4 mL) at room temperature. After 12hrs completion of the reaction (monitored by ^{31}P-NMR) then the reaction mixture was diluted with CH_2Cl_2 and filtered through Celite. The organic phase was dried over anhydrous Na_2SO_4 and then concentrated under reduced pressure. The crude residue was then purified by column chromatography (CH_2Cl_2/MeOH 95: 5) to given a light yellow sticky oil**7**(138 mg, 72%).^{1}H-NMR (500 MHz, CD_3OD) δ 6.00 (d, *J*= 1.5 Hz, 2H), 5.38 (t, *J* = 2.0 Hz, 1H), 5.23 (dd, *J* = 1.5 Hz, 2H), 5.14 (dd, *J* = 6.5 Hz, 2H), 4.96 (d,*J* = 1.0 Hz, 1H), 4.55 (dd, *J* = 6.0 Hz, 1H), 4.53 (dd,*J* = 10.5 Hz,

1H), 4.39 (dd, *J* = 10.0 Hz, 2H), 4.30-4.26 (m, 3H),3.97-3.87 (m, 4H), 3.81-3.76 (m, 2H), 2.18-2.02 (11 x s, 33H, COCH3);^{13}C-NMR (500 MHz,CD_3OD) δ 171.30, 170.73, 170.54, 170.36, 170.16, 168.78, 90.88, 84.64, 76.34, 73.45, 72.77, 71.37, 69.91, 68.43, 64.16, 64.07, 63.00, 62.90, 48.24, 48.07, 47.90, 47.73, 47.56, 47.39, 47.22, 19.49, 19.44, 19.41, 19.38, 19.32. ^{31}P-NMR (500 MHz, CD_3OD): δ 1.58; HR-ESI-MS (m/z): for $C_{40}H_{54}N_3O_{29}P[M + 1]^+$ 1071.8332, found, 1072.2581.

4.5.2.6. Synthesis of azido trimannose6-phospharamidite (8).

This compound was synthesized according to a modified literature procedure. Into a solution of **7** (80mg, 0.18mmol) in dry MeOH (3 mL) was added 1M NaOMe in MeOH, (2 mL) at 0°C, under nitrogen atmosphere.[39] The resulting mixture was allowed to stir at room temperature for one hour. The reaction mixture was neutralized by addition of Dowex-50Wx8 (H+ form) until pH-6.0 and filtered off the resin. The filtrate was concentrated and dried under vacuum to give the light yellow sticky oil **8** (44mg, 96%).^{1}H-NMR (500 MHz, CD_3OD) δ 3.98 (d, 1H),3,94 (d, *J* = 2.0 Hz, 1H), 3.91 (d, *J* = 2.0 Hz, 1H), 3.88- (d, *J* = 3.0 Hz, 3H), 3.94(m, 9H), 3.66-3.64 (m, 2H), 3.61-3.57 (m, 2H), 3.49-3.41 (m, 2H) ^{13}C-NMR (500 MHz,CD_3OD) δ 94.44, 87.17, 79.28, 73.73, 72.53, 72.00, 71.58, 70.88, 67.32, 66.73, 61.54, 61.44, 48.14, 47.98, 47.80, 47.63, 47.46, 47.29, 47.12.IR ν_{max}(neat) cm^{-1}: 3358.80m, 2925.23m, 2489.20s, 2123.75s(N_3), 1650.62s, 1454.08s, 1209.94s, 1113.95s, 1068.81s, 1008.58s, 971.29s. ^{31}P-NMR (500 MHz, CD_3OD)δ 1.18; HR-ESI-MS (m/z): for $C_{18}H_{33}O_{18}P$ $[M +1]^+$609.4297, found, 609.1418.

4.5.3. Synthesis of chitosan conjugated trimannose phospharamidite (TMP)

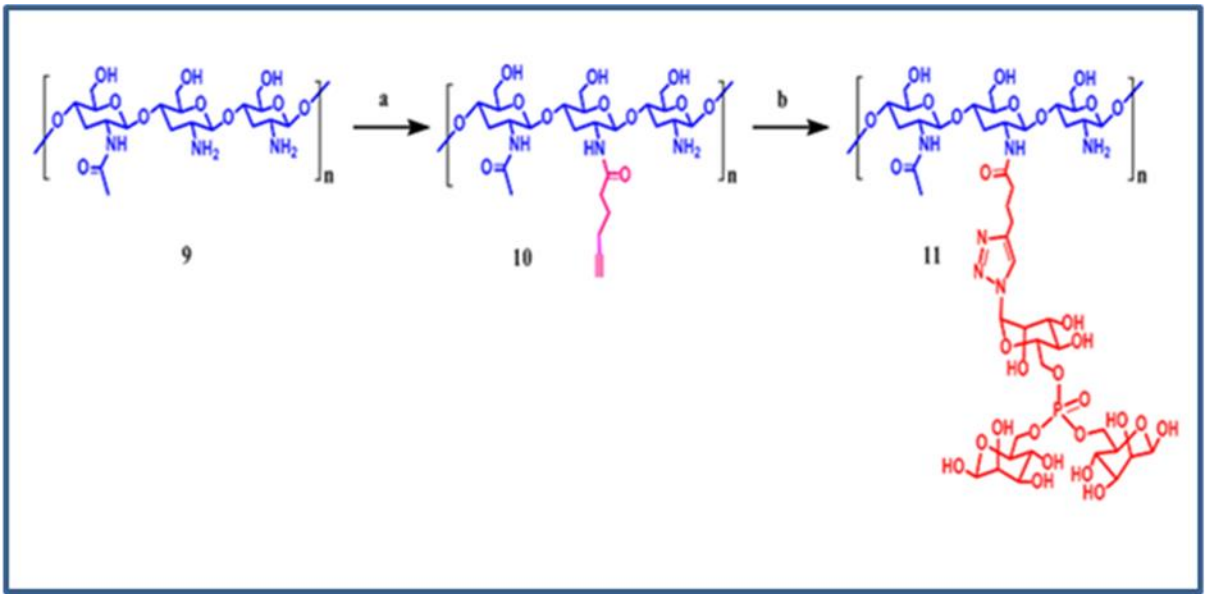

Scheme 4.3. Synthesis of chitosan conjugated trimannose phospharamidite., Reagents and conditions**:** (a) 5-Hexynoic acid, EDC.HCl, NHS, 1%$AcOH_{(aq)}$,RT.,(b) CuSO4. $5H_2O$, Ascorbic acid, MeOH: H2O (1:1), 50°C.

4.5.3.1. Synthesis of CS-HN (10)

Chitosan (50mg) was dissolved in 10mL of 1% acetic acid under vigorous stirring. Subsequently, 5-hexynoic acid (30mg), EDC.HCl (20mg) and catalytic amount of N-hydroxysuccinimide were added in the above reaction mixture at room temperature. After 12hrs, solution mixture was washed with ethanol followed by acetone then centrifugation, the precipitation was resuspended in water and frozen- dried to obtain compound **10 (**24mg).IR ν_{max}(neat) cm^{-1}: 3426.99m, 2120.98s (N_3), 1644.38s, 1372.21s, 1258.71s.

4.5.3.2. Synthesis of CSHN-TMP (11)

To a solution of compound 10(20mg), sodium ascorbate(4mg) and $CuSO_4$. $5H_2O$ (3mg) were added in milli-Q water (5mL) then azido trimannose6-phospharamidite **8** dissolved in methanol (5mL) was added. After, the mixture solution was stirred at room temperature for 2days and washed with acetone. Subsequently centrifugation, the precipitation was re-suspended in water, and then frozen- dried to obtain compound as a powder **11**(14mg). IR ν_{max}(neat) cm^{-1}: 3426.99m, 2120.98s, 1644.38s, 1613.54s 1372.21s, 1258.71s.

4.5.4. Synthesis of poly- l-lactic acid linked nonamer of arginine(PL–R_9)

4.5.4.1. Synthesis of nonamer of arginine (R_9)

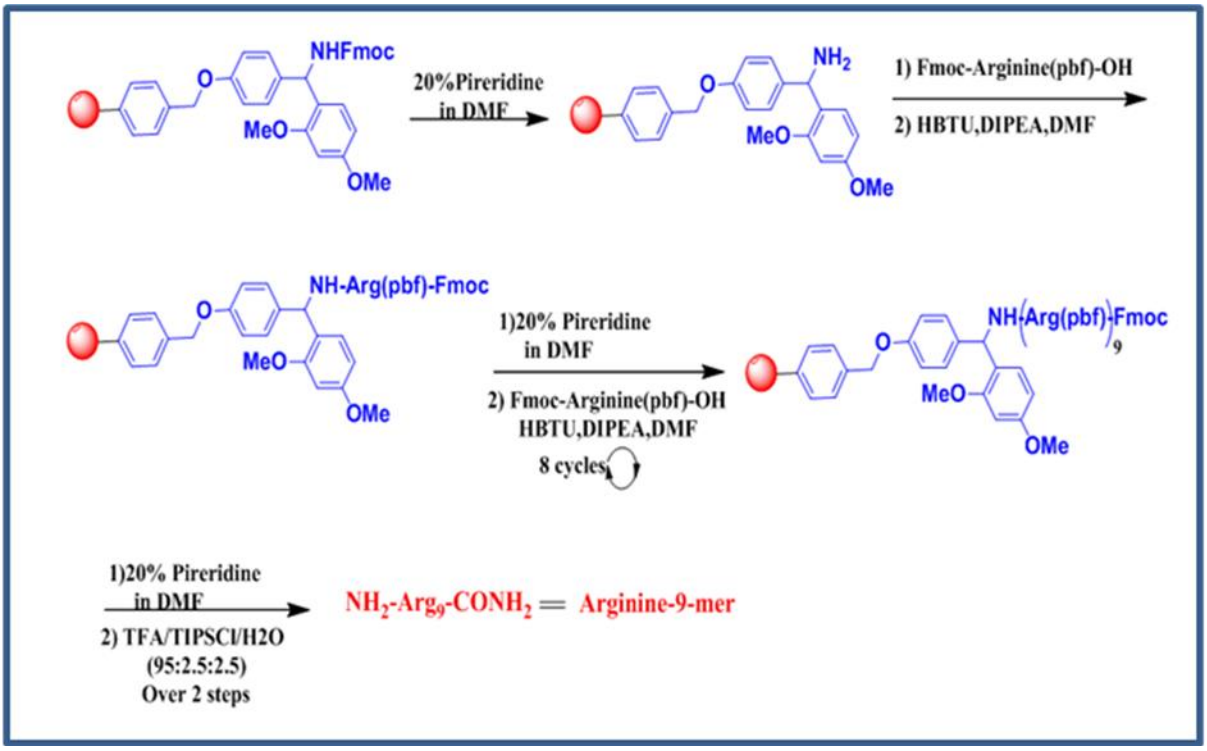

Scheme 4.4. Synthesis of nonamer of arginine (**R_9**)., Reagents and conditions:a)Rink amide resin(0.71meq/g, 100–200 mesh),20% Piperidine in DMF, dry DCM, RT., b)Fmoc-Arg-(pbf)-OH, HBTU, DIPEA, DMF., c) 20% Piperidine in DMF,TFA/TIPSCl/H_2O.

Arginine -9mer Peptide was synthesized to a manual fashion, in a 0.14 mmol scale on Rink amide resin (0.71meq/g, 100–200 mesh) employing a standard Fmoc solid-phase peptide synthesis (SPPS) method. Nonamer of arginine (**R_9**) for peptide coupling, to a DMF (10 mL) of Fmoc-protected arginine amino acid (276mg, 0.42mmol) and N,N,N′,N′-tetramethyl-O-(1H-benzotriazol-1-yl)uranium hexafluorophosphate (HBTU, 162mg, 0.43mmol) was added N,N-diisopropylethylamine (DIPEA, 200µL, 1.5mmol), and the mixture was stirred for 10mins for activation. The mixture was then added into peptidyl resin, and the reaction syringe was shaken for 6 hrs at 25 °C. For Fmoc deprotection, after the coupling solution was drained off, the peptidyl resin was washed with DMF (3 times) and 20% piperidine in DMF (v/v) was added to the peptidyl resin. After shaking for 1h, the reaction solution was drained off. This reaction was repeated eight cycles, and the resulting peptidyl resin was washed with DMF (3 times), CH_2Cl_2 (2 times) and Hexane (1 time) then dried and stored until needed. The dried resin was swollen in CH_2Cl_2 for 1 hr, filtered to remove excess solvent, and placed in a round-bottom flask. Cleavage from the support and removal of acid labile protecting

groups were afforded by the treatment with 10 mL of a 95% trifluoroacetic acid/2.5% water/2.5% triisopropylsilane (TIPS) solution. The resin was removed by filtration, and the filtrate of viscous solution was concentrated under reduced pressure. Cold diethyl ether (10 mL) was added to facilitate precipitation of the crude peptide. The crude peptide was dissolved in 50%/50% acetonitrile/ H_2O (0.1% TFA) solution and purified through RP-HPLC and the isolated product was lyophilized to afford a white solid **12**. ^{1}H-NMR (500 MHz, D_2O): δ 4.221 (t, *J*= 5.0 Hz, 10H), 3.104-3.039 (m, 20H), 1.754-1.56 (m, 40H); IR ν_{max}(neat) cm^{-1}: 3169m, 3010m, 2913m, 2725s, 2361s(C=N), 1679s, 1595s,1445s, 1400s, 1267s, 1155s, 1065s, 1013s, 945s; MALDI-TOF-MS (m/z): for $C_{60}H_{120}N_{40}O_{11}[M+1]^+$ = 1423.917, found 1424.038.

4.5.4.2. Synthesis of PL- R_9

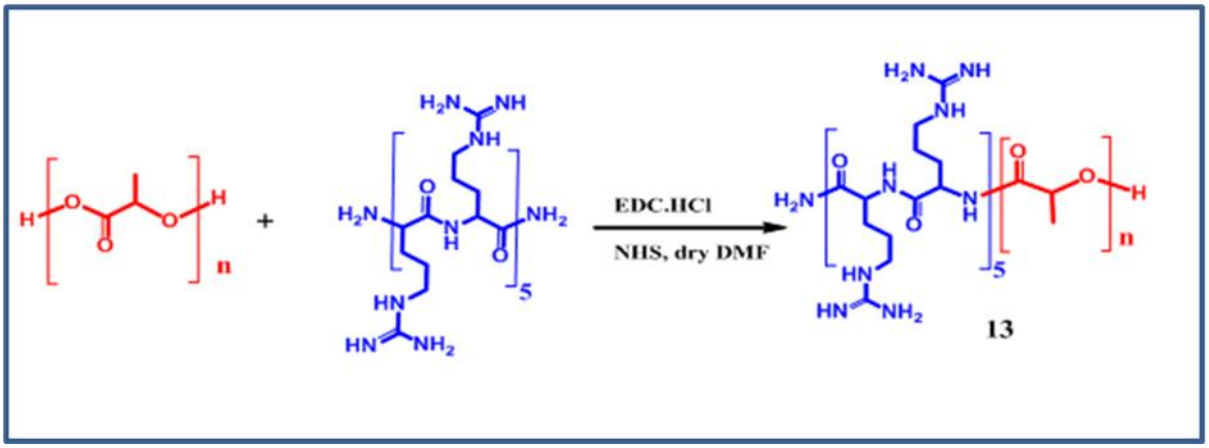

Scheme 4.5. Synthesis of **PL-R$_9$**., Reagents and conditions: Poly L-lactic acid, arginine- 9mer, EDC.HCl, NHS, dry DMF.

PL– R$_9$ was synthesized by according to a modified literature procedure. To a solution of poly l-lactic acid (40mg, 0.24mmol), EDC.HCl (8mg, 0.04mmol) and N-hydroxysuccinimide (catalytic amount) were dissolved in DMF (5mL) then nonamer of arginine (20mg, 0.02mmol) dissolved in milli-Q water (3mL) was added. The reaction solution was stirred at room temperature for 3days after then the reaction mixture was washed with acetone (3x10mL) to removed of unreacted **PLLAs**. The obtained precipitate was collected by centrifugation and dried under vacuum overnight to yield the white crystalline solid of **PLLA –R$_9$ 13**(42mg).^{1}H-NMR (500 MHz, $CDCl_3$) δ 5.11-4.93 (m), 3.48-3.45 (m), 1.51-1.50 (m). IR ν_{max}(neat) cm^{-1}: 3420b, 2993m, 2907m, 2845m, 2367s,2361s,2100s, 1753s,1457s, 1360s, 1206s, 1133s, 1047s.

4.5.5. Synthesis of Resveratrol

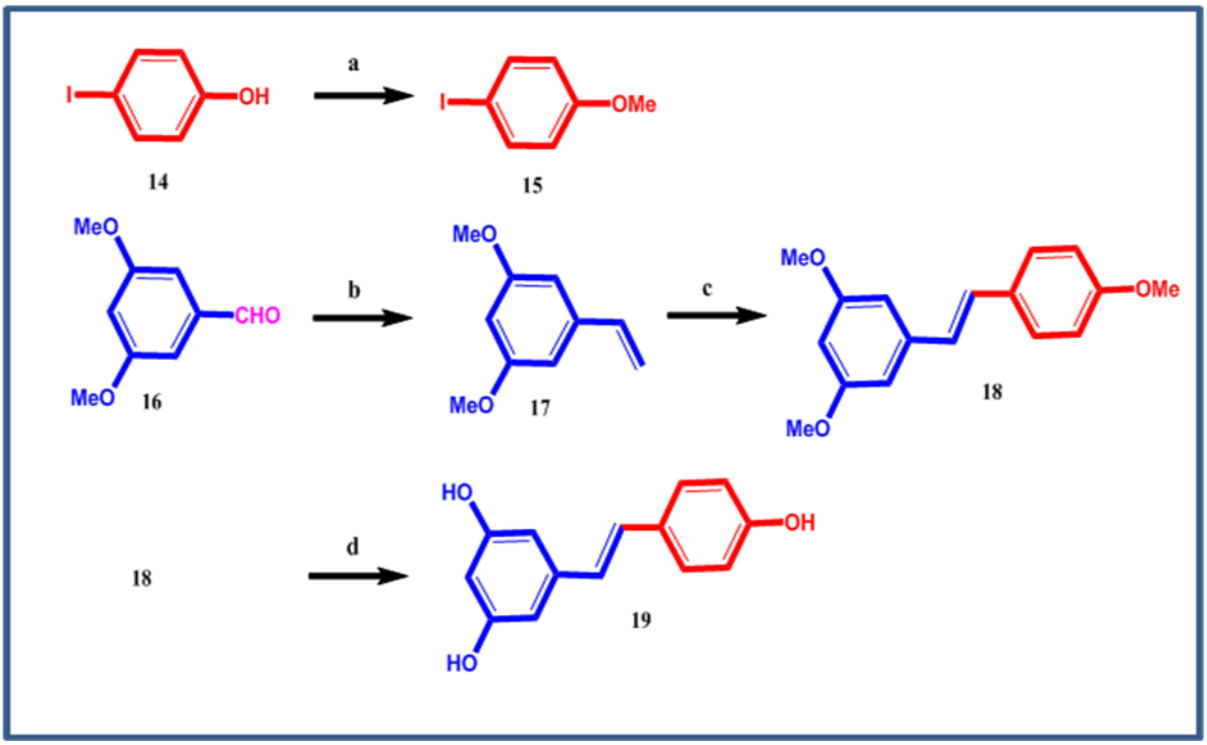

Scheme 4.6. Synthesis of resveratrol., Reagents and conditions: (a) 4- Iodophenol, Iodomethane, Sodium hydride, dry DMF, reflux; (b) Methyltriphenylphosphonium bromide, K_2CO_3, THF, reflux; (c) $Pd(OAc)_2$, PPh_3, DIPEA, toluene, reflux; (d) BBr_3, dry CH_2Cl_2, 0°C.

4.5.5.1. Synthesis of 4-Iodoanisole (15)

Sodium hydride (60% dispersion in mineral oil, 200mg, 1.82mmol) was added slowly at 0°C to a solution of **14 (**200mg, 0.91mmol)and iodomethane (60 µL, 1.10mmol**)** in DMF then the solution was stirred at 0°C for 30min. Subsequently, the reaction was allowed to reflux for overnight. The resulting heterogenous mixture was cooled to 0°C, quenched by slow addition of aqueous sat.NH_4Cl (30mL) and extracted with ethyl acetate (3 x 50mL). The combined organic fractions were washed with brine (60mL), dried over $MgSO_4$, and concentrated under vacuum to given the crude product was purified by columnchromatography (hexanes/AcOEt 9: 1) to give white solid **15**(185mg, 87%).^{1}H-NMR (500 MHz, $CDCl_3$): δ 7.56 (dd, *J*= 2.0 Hz, 2H), 6.69 (dd, *J* = 2.5 Hz, 2H); ^{13}C-NMR (500 MHz,$CDCl_3$)δ 162.09, 139.93, 118.08, 84.74, 58.13;HR-ESI-MS (m/z): for C_7H_7IO $[M+1]^+$: 233.9503; found: 233.9507.

4.5.5.2. Synthesis of 3,5-Dimethoxystyrene (17)

A solution of 3,5-dimethoxybenzaldehyde **16 (**200mg, 1.20mmol) and methyl triphenylphosphine bromide (643mg, 1.80mmol) in THF(10mL), followed by the addition of

K_2CO_3 (498mg, 3.60mmol). The reaction mixture was stirred under N_2 stream and reflux. After 16 hrs, the mixture was diluted with EtOAc and washed successively with water and brine. The organic portion was collected, dried over Na_2SO_4 and concentrated. The crude product was purified by columnchromatography (EtOAc/Hex 1:20) to obtain compound **17** as a colorless oil product(177.91mg, 72%).^{1}H-NMR (500 MHz, $CDCl_3$): δ 6.58-6.52 (m, *J*=11Hz, 1H), 6.48 (d, *J* = 2.0 Hz, 2H), 6.30 (t, *J*=2.5Hz, 1H), 5.66 (dd, *J* = 17.0 Hz, 1H), 5.17 (dd, *J* = 7.5 Hz, 1H), 3.70(s, 1H); ^{13}C-NMR (500 MHz, CDCl3) δ 159.88, 138.59, 135.83, 113.26, 103.28, 99.04, 54.25; HR-ESI-MS (m/z): for $C_{10}H_{12}O_2[M+1]^+$: 165.0909; found: 165.3143.

4.5.5.3. Synthesis of (E)- 3',4, 5'-trimethoxy-stilbene (18)

To a solution contain 3, 5-dimethoxystyrene **17**(600mg, 3.65mmol), 4-iodoanisole **15**(1.2g, 7.30mmol), $Pd(OAc)_2$ (50mg, 0.183mmol), PPh_3(95mg, 0.36mmol) and DIPEA (1.3mL, 7.30mmol)in toluene (25mL). The reaction mixture was stirred under N_2 atmosphere and reflux, after 16hrs the mixture was diluted with ethylacetate and washed with water and brine. The organic portion was collected, dried over Na_2SO_4 and concentrated. The crude product was subjected to columnchromatography (EtOAc /Hexane 5:95) to obtained compound **18** as a colorless oil product(415mg, 42%).^{1}H-NMR (500 MHz, $CDCl_3$)δ 7.36(d, *J*= 8.5Hz, 2H,$H_{2'}$, $H_{6'}$), 6.96(d, *J*= 16.5Hz, 1H, H_β), 6.82 (d, *J*= 16.5Hz, 1H, *Hα*), 6.81 (dd, *J*=2.0 Hz, 2H, $H_{3'}$, $H_{5'}$), 6.56 (d, *J* = 2.0 Hz, 2H, H_2,H_6), 6.29 (t, *J* = 3.5 Hz, 1H, H_4);^{13}C-NMR (500 MHz, $CDCl_3$) δ 160.94, 159, 149.45, 133.66, 129.37, 113.51, 113.02, 106.63, 99.81, 55.38; HR-ESI-MS (m/z): for $C_{16}H_{16}O_3[M+1]^+$:257.1099; found: 257.3103.

4.5.5.4. Synthesis of (E)- 3',4, 5'-trihydroxy-stilbene(resveratrol) (19)[40]

Into a solution of **18** (100mg, 0.39mmol) in dry CH_2Cl_2 (10mL) was added BBr_3 (2mL) at 0°C. The resulting mixture was allowed to stir for 5 hrs and left at room temperature over 1hr. The mixture was poured onto ice, and the organic layer was separated and the aqueous layer extracted with CH_2Cl_2. The combined organic layer was washed with saturated NaCl, dried over anhydrous Na_2SO_4 and evaporated under reduced pressure to dryness. The crude was subjected to column chromatography to afford as an off-white powder (50mg, 56%).^{1}H-NMR (500 MHz, $CDCl_3$): δ 7.269(d, *J*=8.5Hz, 2H, $H_{2'}$, $H_{6'}$), 6.87 (d, *J*=15Hz, 1H, H_β), 6.71(d, *J*=15Hz, 1H, *Hα*), 6.67(d, *J*=8.5Hz, 1H, *H3', H5'*), 6.34(d, *J*=2.0Hz, 2H, H_2, H_6), 6.06 (t, *J*=2.5Hz, 1H, H_4).^{13}C-NMR (500 MHz,CDCl3) δ158.25, 156.98, 139.91, 129.04, 128.00, 127.39, 125.60, 115.10, 104.39, 101.27; HR-ESI-MS (m/z): for $C_{14}H_{12}O_3[M+1]^+$:230.0786; found: 230.0858.

4.5.6. Cell line studies

All the cell lines used in this study were obtained from American Type Culture Collection (ATCC, USA). The cells were maintained in DMEM media supplemented with 10% fetal bovine serum and antibiotics (100U mL-1 penicillin/100 µg mL^{-1} streptomycin mixture) in a 5 % CO_2 incubator at 37°C.

4.5.6.1. *In vitro* cytotoxicity assay

MCF-7, HCT-116 and WI-38 cells were seeded on 96 well plate in DMEM (10%FBS) at a density of $5x10^3$ cells/well and after 24 hrs, cells were treated with various concentrations **PLR_9-CSTMP NPs** so that the final effective concentration of **Res/Dox** will be, 5(1.5), 10(3), 20(6), 50(15) and 100(30) µg/mL, bare nanoparticle (without loading **Res** and **Dox**), **Res** alone (5, 10, 20, 50 and100 µg/mL) **Dox** alone (1.5, 3, 6, 15 and 30 µg/mL) and the combination of these two were also included in the study. After 24 and 48 hrs of treatment cytotoxicity was analyzed by MTT [3-(4,5-dimethylthiazol-2-yl)-2,5-diphenyltetrazolium].[41]

4.5.6.2. Co-localisation studies

Nuclear co-localization of **Dox** from the construct was confirmed by treating the MCF-7 cells for 6hrs with the selected concentration of the **PLR_9-CSTMP NPs**. Nucleus was counter stained with Hoechst stain and observed under DAPI filter as well as FITC filter (Nikon, Japan) and the images were merged using ImageJ software.

4.5.6.3. Apoptotic Assays

Morphological changes were analyzed using phase contrast microscope (Nikon-TS100 Inverted microscope) and for all further studies a concentration of 20/6µg/mL was used. MCF-7 cells were treated with the **PLR_9-CSTMP NPs** at 20/6µg/mL **Res/Dox** concentration for 48 hrs and Ethidium bromide acridine orange dual staining was performed. For this, 100µg/mL of both the stains in were mixed in 1:1 ratio, and 100 µL of this working solution was added to the cells. After few minutes cells were washed twice with PBS and observed under fluorescent microscope.[42] APOP staining for apoptotic cells in control and treated cells were performed with 1: 2 diluted APOP stain solution (Biocolor Life Science) for 2 minutes and washed twice with PBS and observed under microscope. Similarly, nuclear condensation effects by the treatment with **PLR_9-CSTMP NPs** as well **Res/Dox** mix was also performed by staining the treated cells with Hoechst 33342 stain (10 µg/mL) and by observing under

DAPI filter (Nikon, Japan).[43] SERS finger printing of isolated DNA from the control as well as the **PLR_9-CSTMP NPs** treated cells were carried out by mixing the DNA with gold nanoparticle at 1:9 ratio and SERS spectrum was collected using Raman spectroscope (Witek, Germany). For this, DNA was isolated using Geneaid DNA isolation kit as per the described protocol. Caspase -3 expression in the **PLR_9-CSTMP NPs** and drug alone treated cells were analyzed using Caspase-3 flourometric assay kit (Biovision, USA). Briefly the cells were treated with the respective **PLR_9-CSTMP NPs** for 48 hrs and the cell were lysed and incubated with 1mM DEVD-AFC substrate and incubated at 37^{o}C for 1-2 hrs. Samples were read in flourometer with 400 nm excitation filter and 505-nm emission filter (FLx800, BioTek).

4.5.6.4. Annexin -V assay

Evaluation of apoptosis by FITC-Annexin-Vstaining (BD Pharmingen no. 556547, BD Biosciences, San Jose, CA) was also performed by flow cytometry, using kit-specified instructions. Briefly, after the treatment with compounds, cells were washed twice with cold PBS and then re-suspended the cells in 1x binding buffer at a concentration of 1x 10 ^{6} cells / mL and 1x 10^5 cells (100µL) were transferred to a 5mL tubes and 5µL of Annexin V FITC and 5µL of Propidium iodide (PI) were added to each tube. Gently vortex the cells and incubated for 15 minutes at room temperature (25ºC) in the dark. Four hundred microliter (400µL) of 1x binding buffer was added to each tube. FITC-conjugated Annexin V, which binds to phosphatidylserine, was detected using a FACSJazz flow cytometer (BD Biosciences, San Jose, CA), and the data were analyzed with the FACSDIVA software.

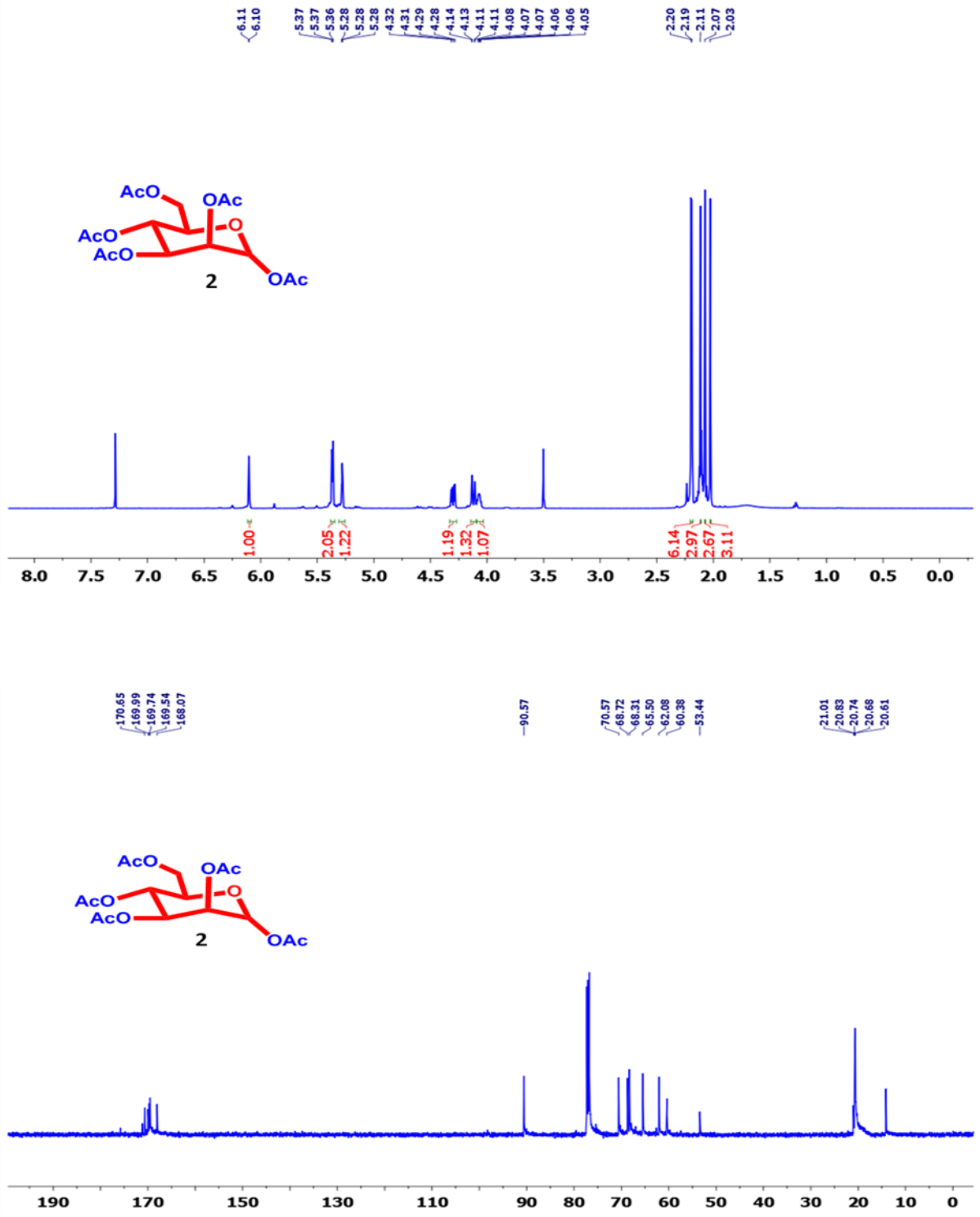

Figure 4.10 .^{1}H and ^{13}C-NMR spectra for compound **2**

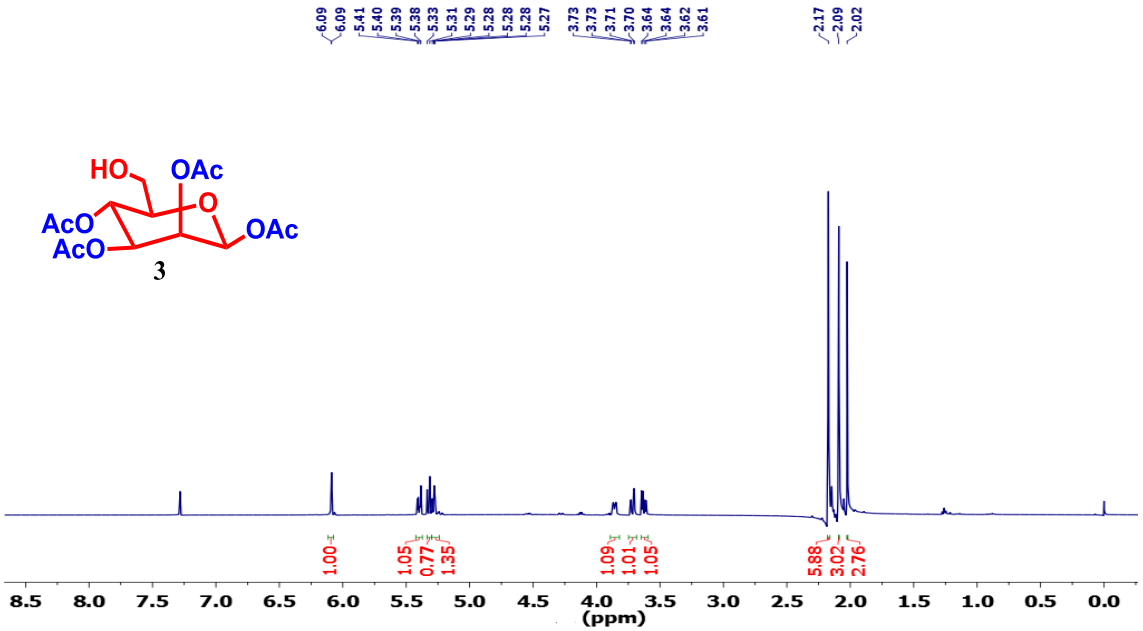

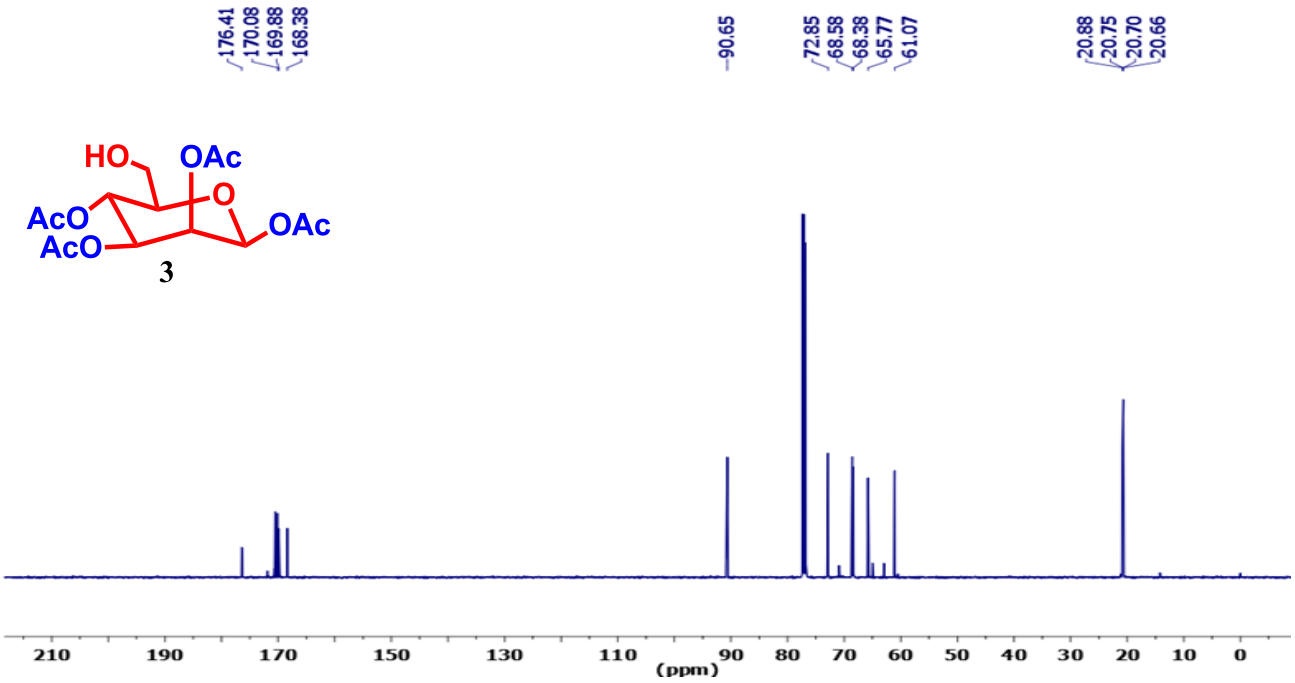

Figure 4.11. ^{1}H and ^{13}C-NMR spectra for compound **3**

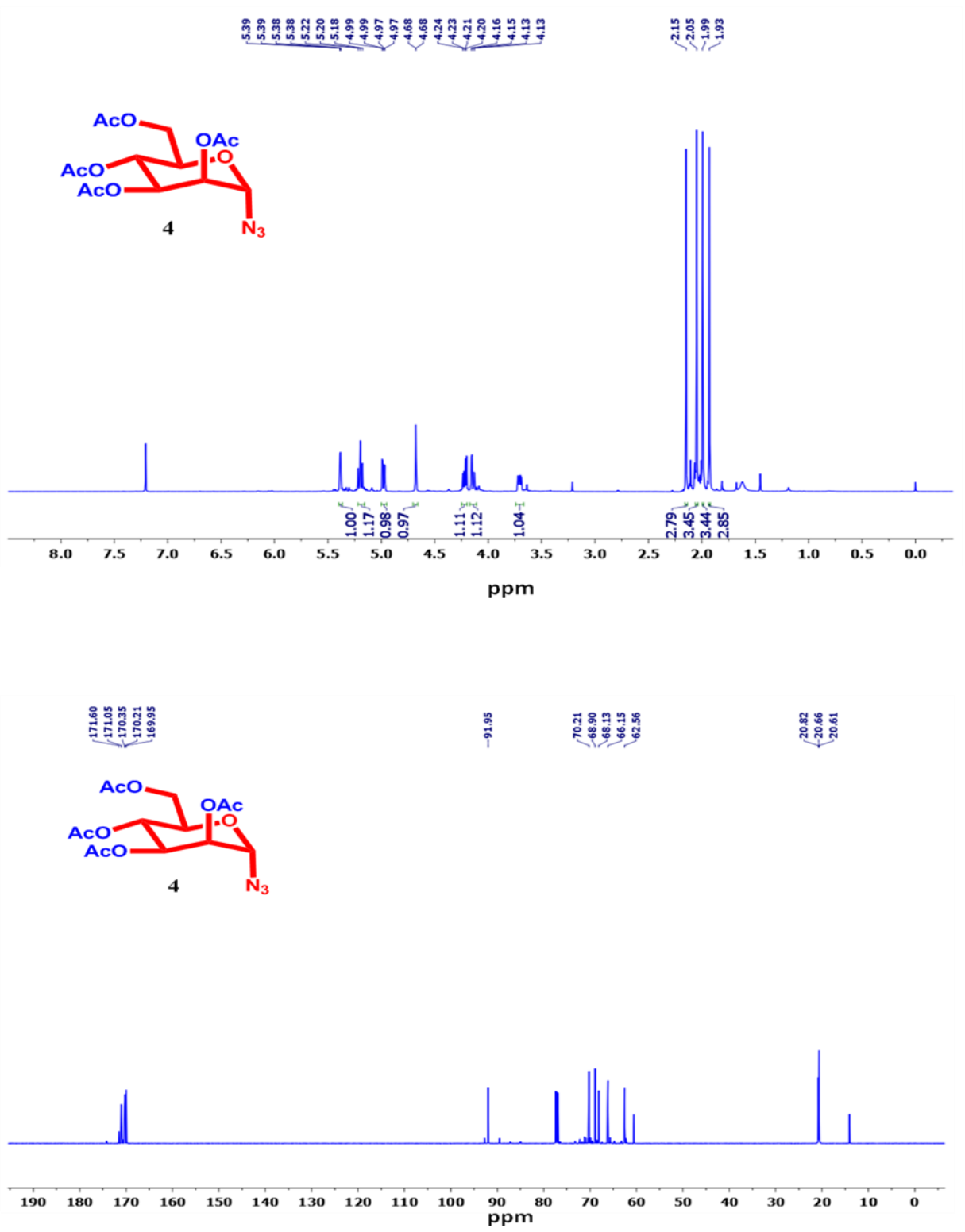

Figure 4.12. ^{1}H and ^{13}C-NMR spectra for compound **4**

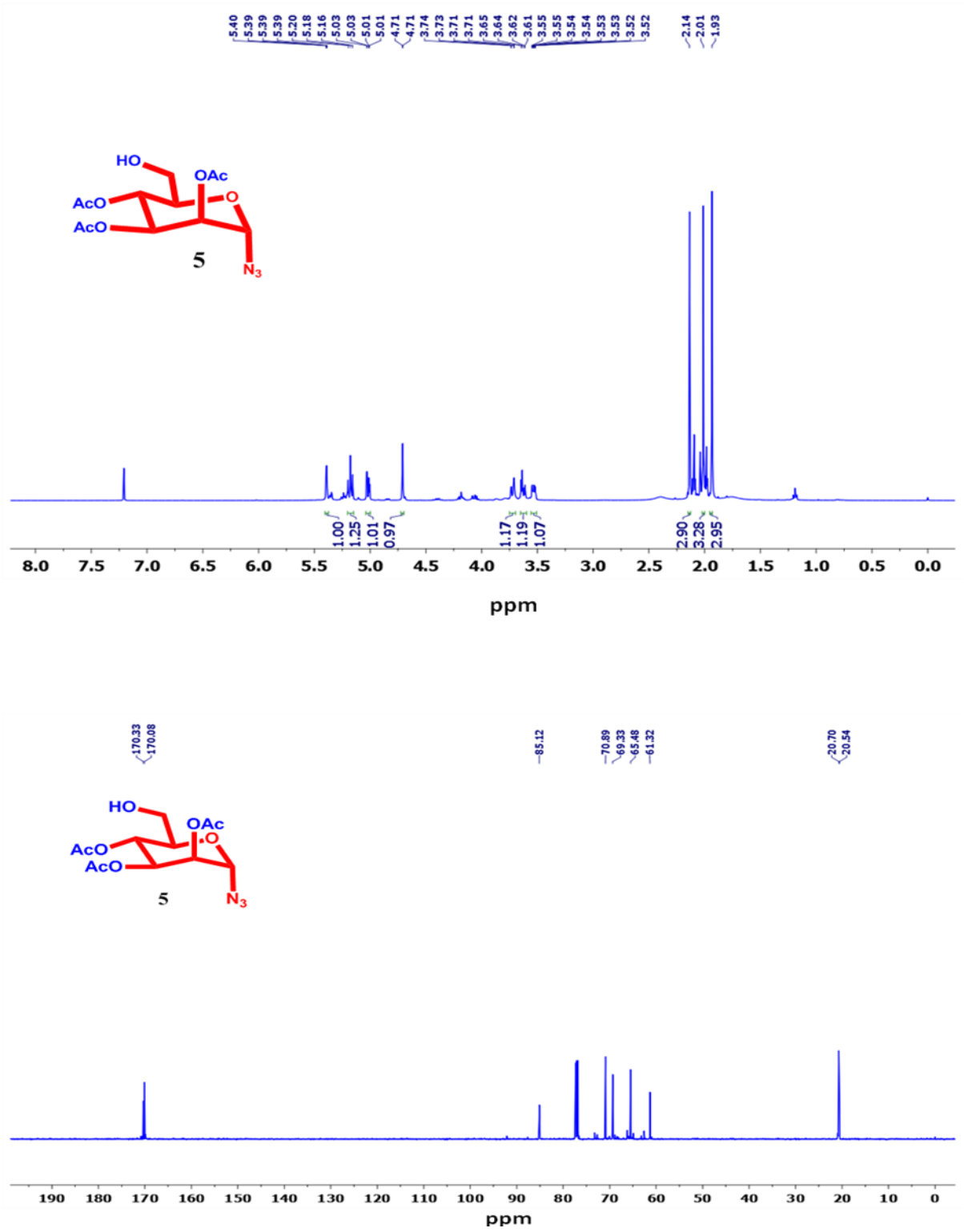

Figure 4.13. ^{1}H and ^{13}C-NMR spectra for compound **5**

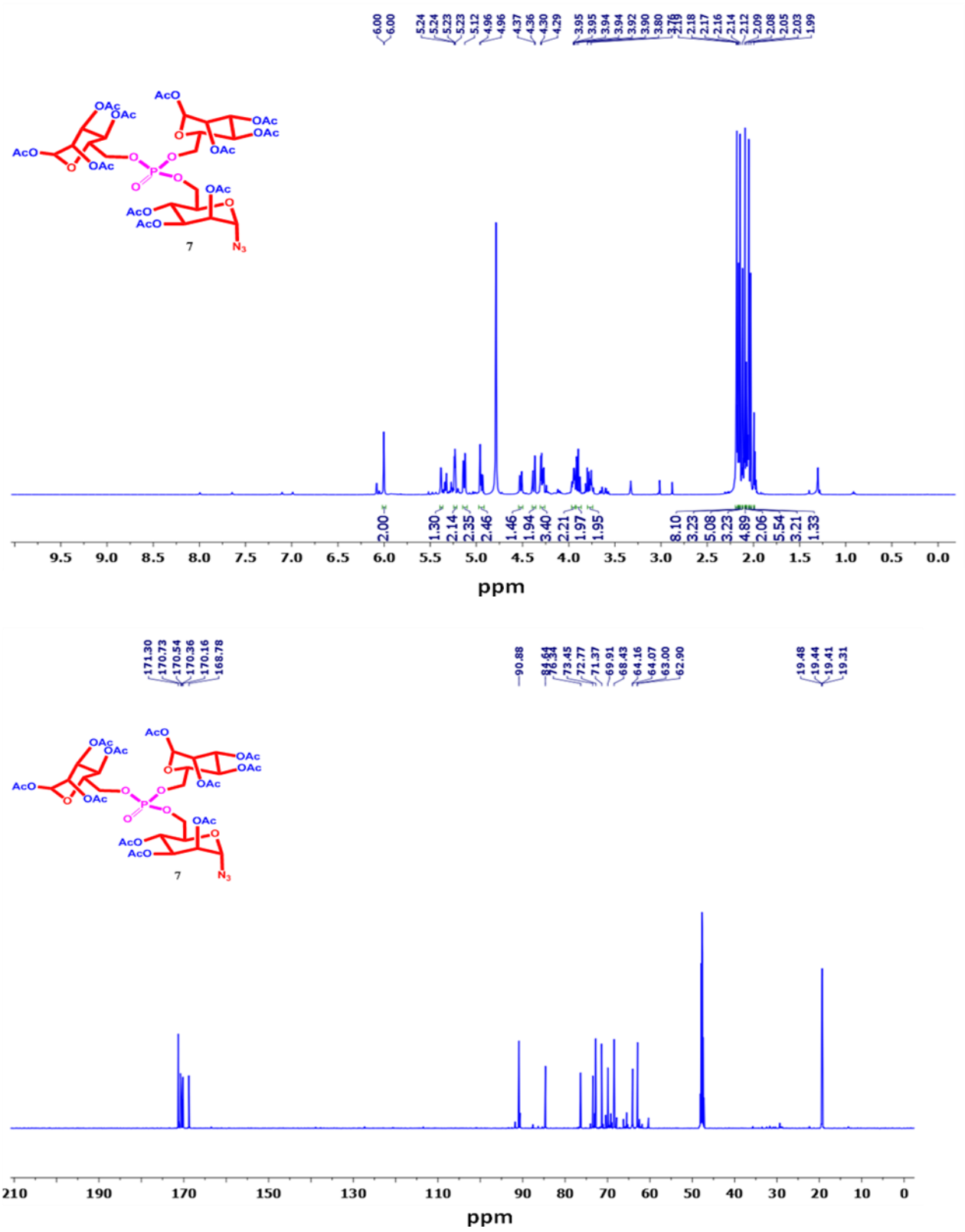

Figure 4.14. ^{1}H and ^{13}C-NMR spectra for compound **7**

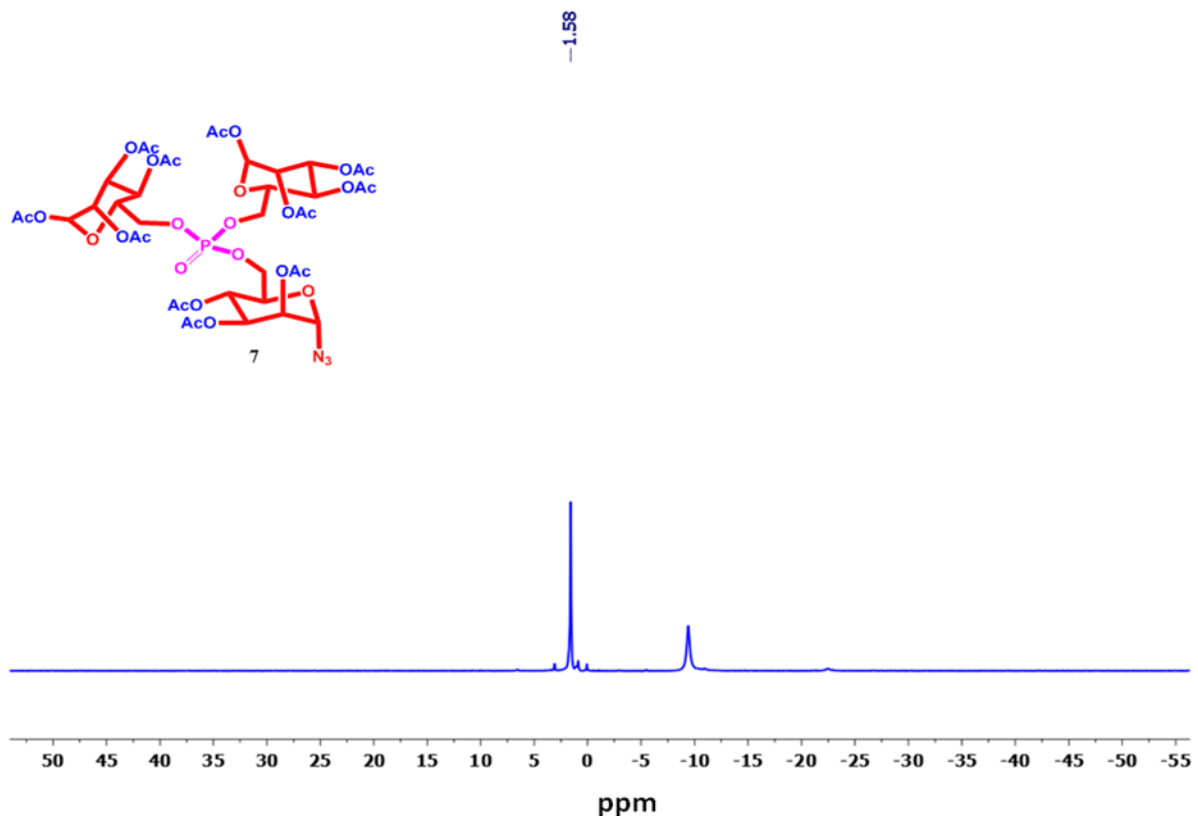

Figure 4.15. ^{31}P -NMR spectra for compound **7**

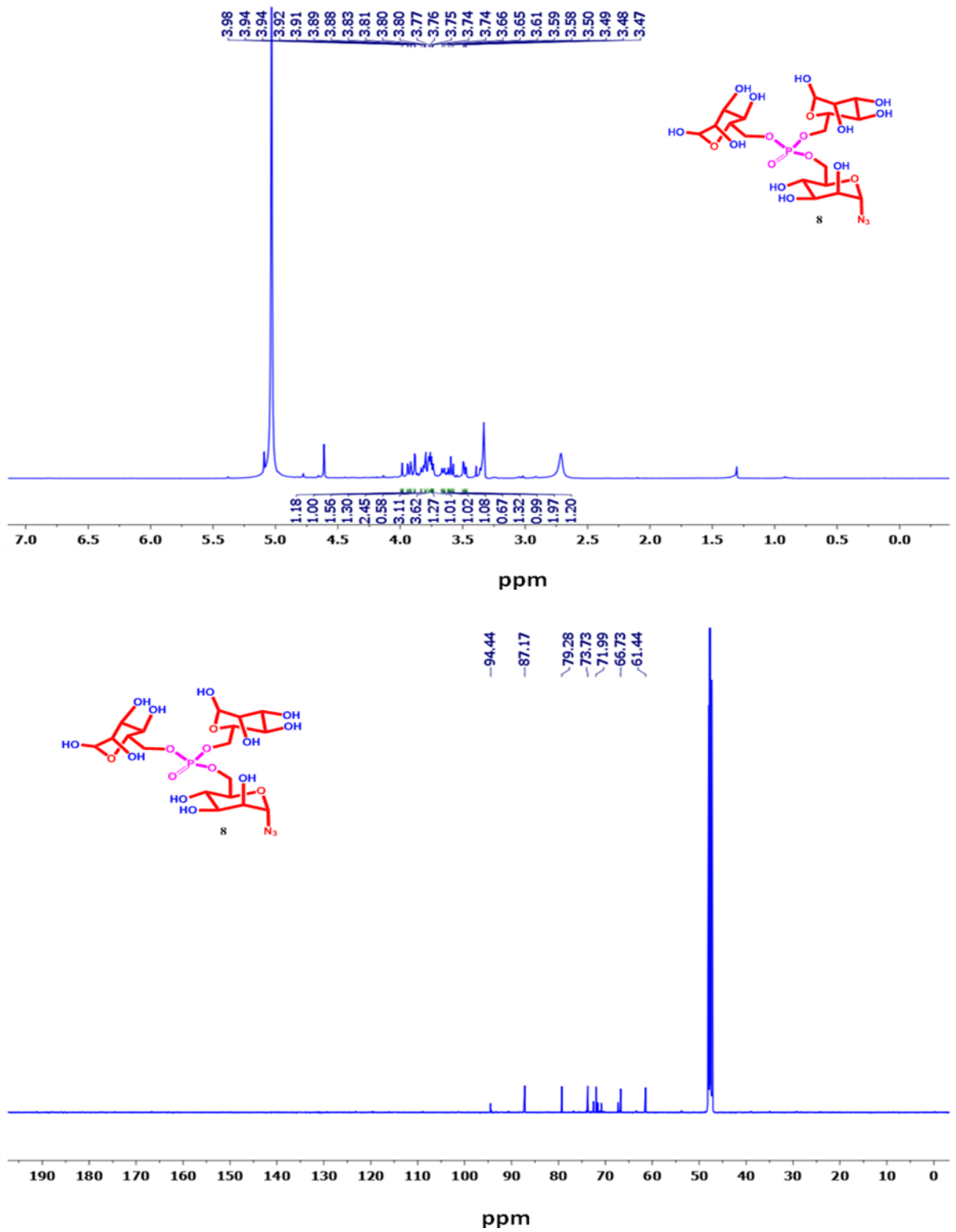

Figure 4.16. ^{1}H and ^{13}C-NMR spectra for compound **8**

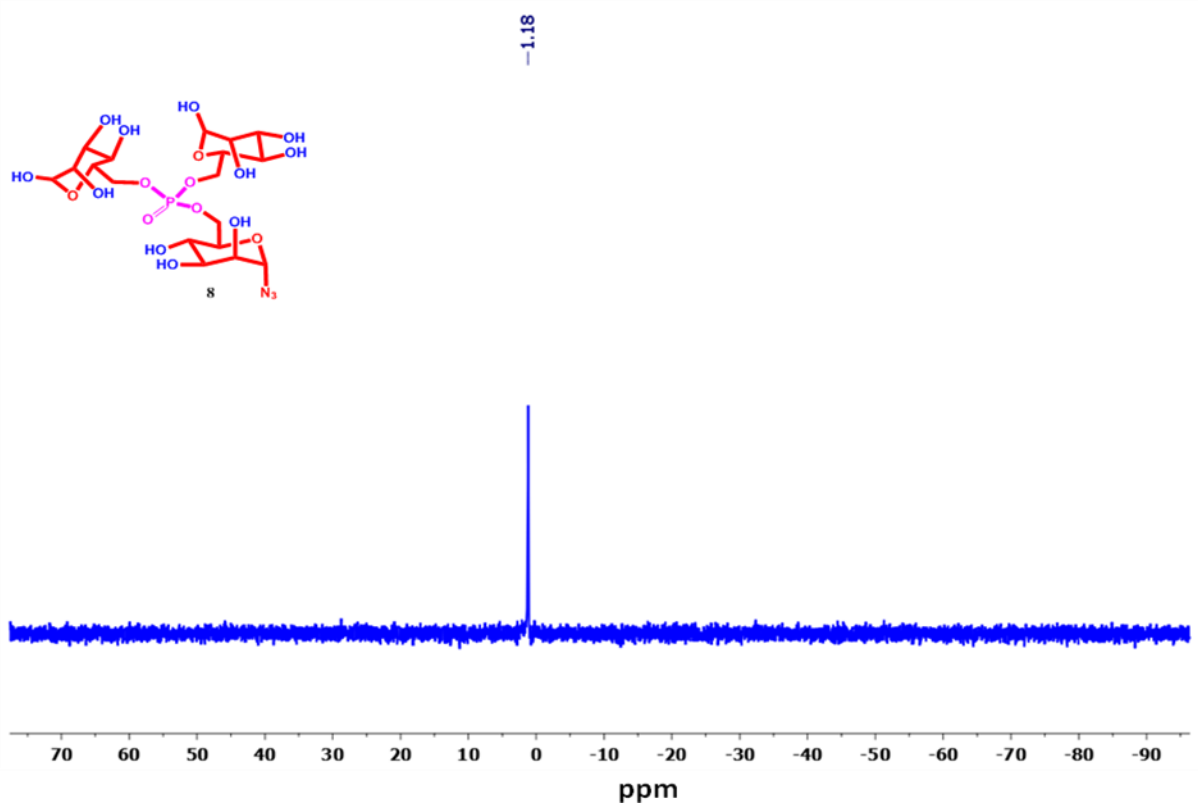

Figure 4.17. ^{31}P-NMR spectra for compound **8**

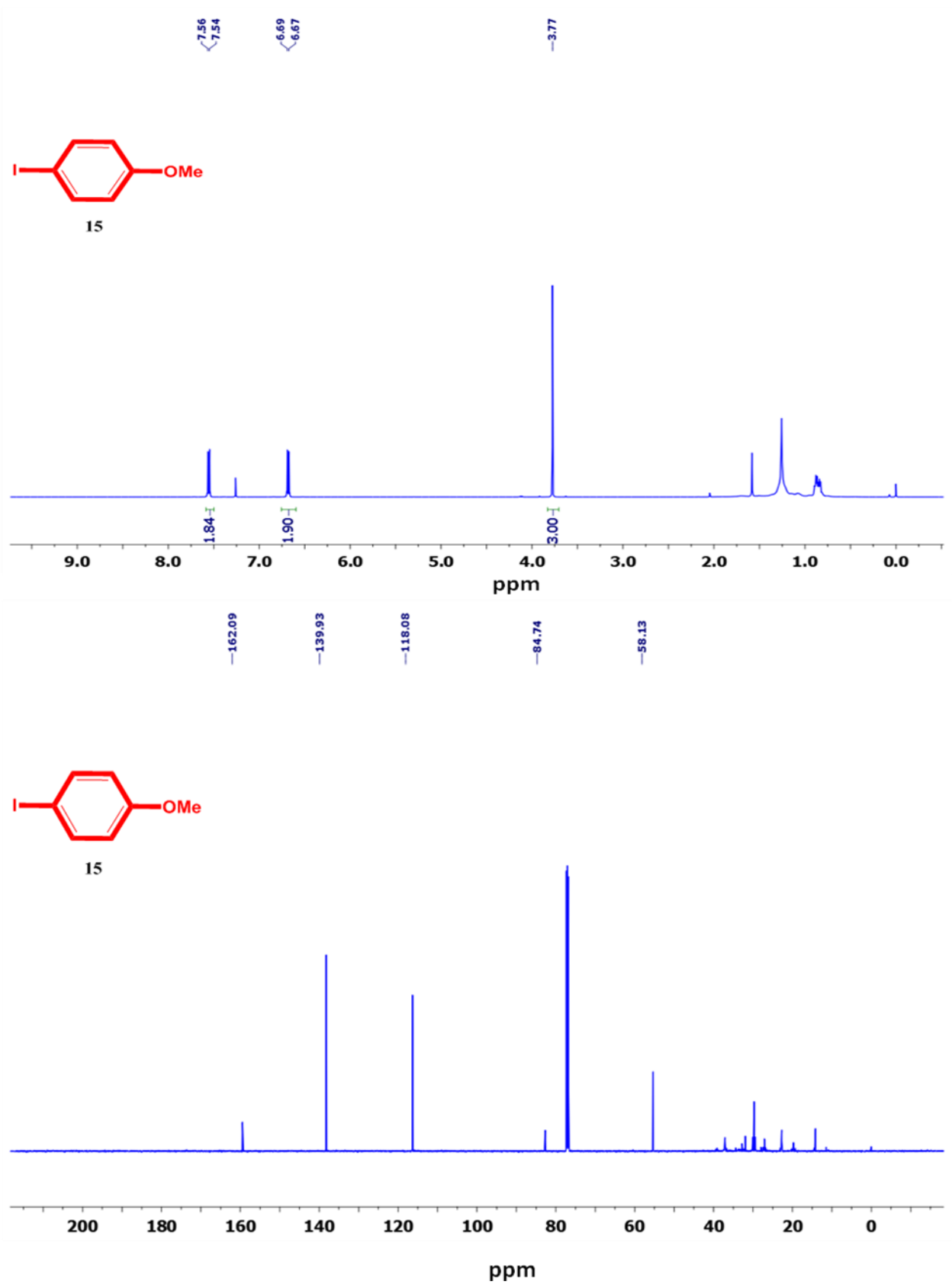

Figure 4.18. ^{1}H and ^{13}C-NMR spectra for compound **15**

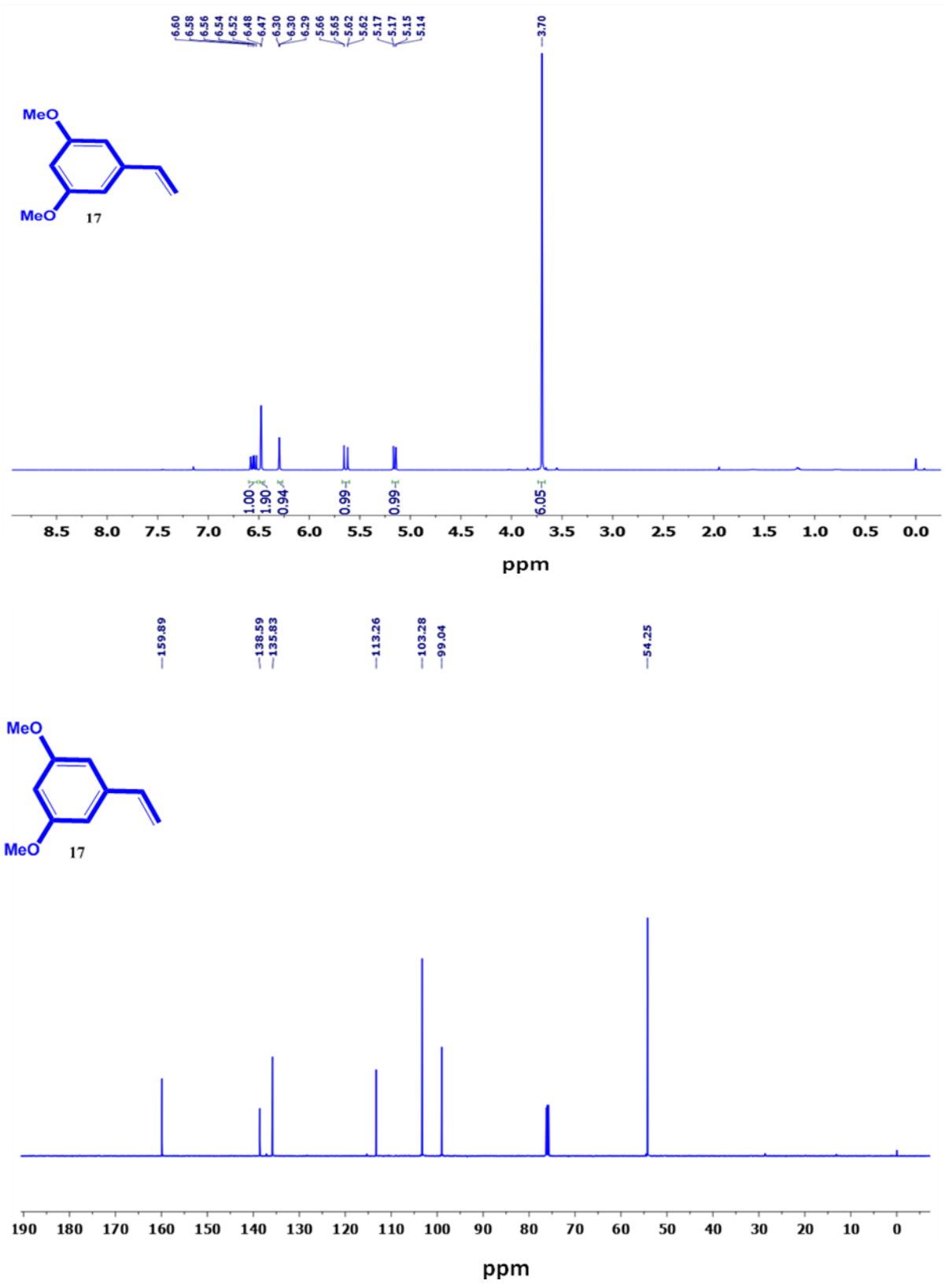

Figure 4.19. ^{1}H and ^{13}C-NMR spectra for compound **17**

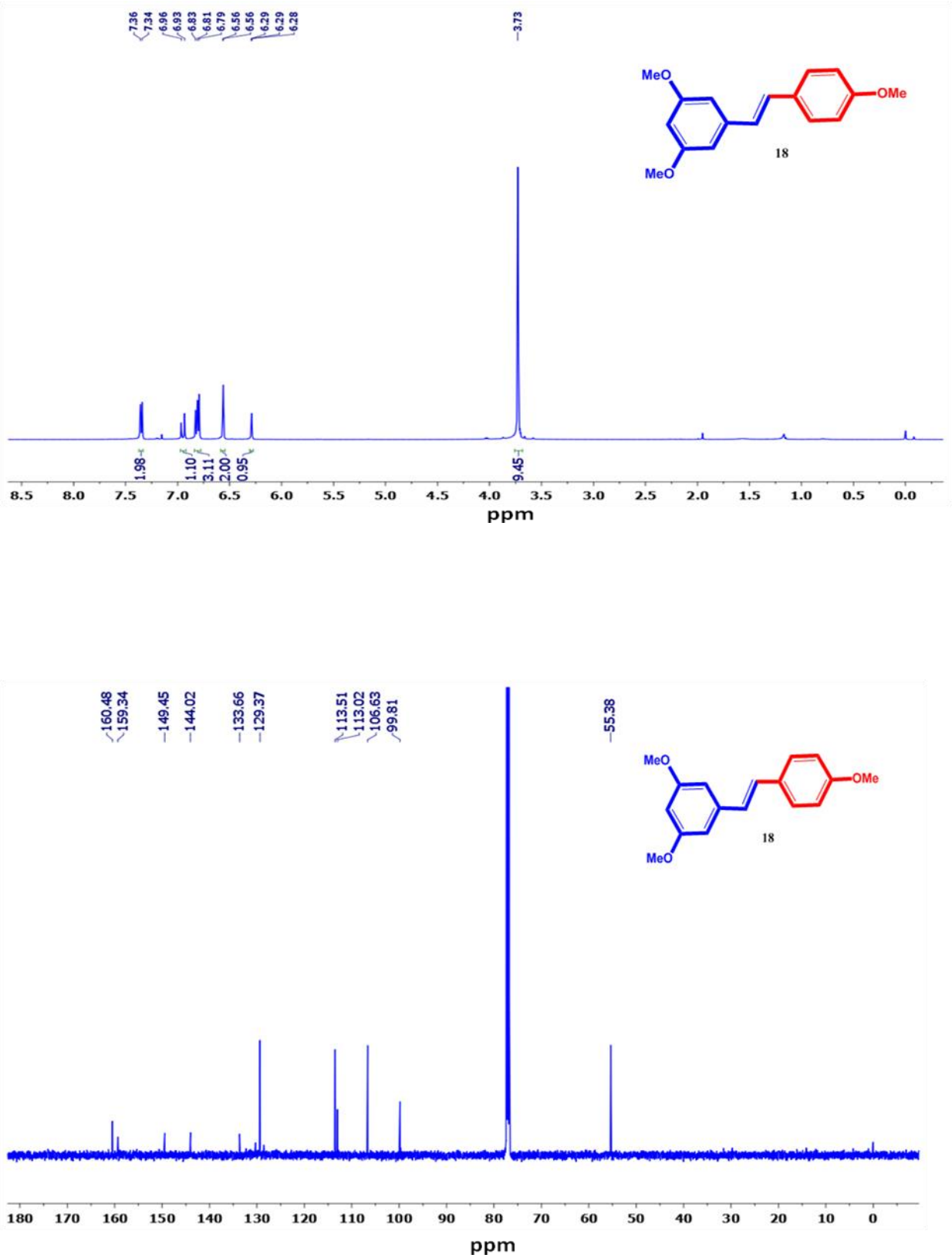

Figure 4.20. ^{1}H and ^{13}C-NMR spectra for compound **18**

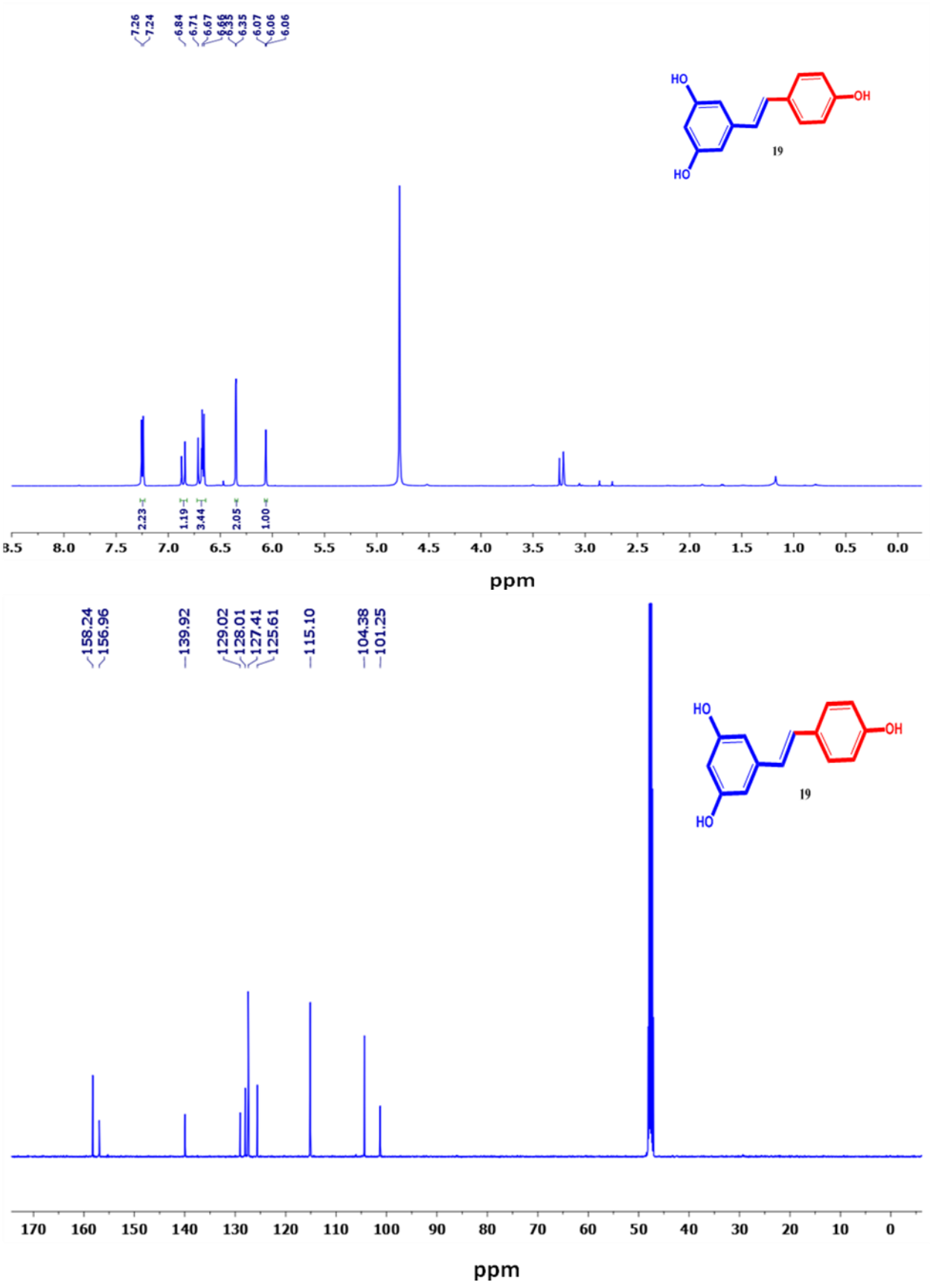

Figure 4.21. ^{1}H and ^{13}C-NMR spectra for compound **19**

4.6. References

[1]. Venkatadri,R.;Muni, T.;Iyer,A.K.V.;Yakisich,J.S.;Azad,N. *Cell Death Dis,***2016,** 7

[2]. Matsumura, Y.; Maeda, H. *Cancer Res,***1986,** 46, 6387.

[3]. Gerlowski, L. E.; Jain, R. K. *Microvasc. Res,***1986,** 31, 288.

[4]. Bertrand, N.; Wu, J.; Xu, X.; Kamaly, N.; Farokhzad, O. C. *Adv. Drug Deliv. Rev,***2014,** 66, 2.

[5]. Maeda, H.Adv. *Drug Deliv. Rev,***2015,** 91, 3.

[6]. Zhang, Y.;, Yang, C.; Wang, W.; Liu, J.; Liu, Q.; Huang, F.; Chu, L.; Gao, H.; Li, C.;Kong, D.; Liu,Q.; Liu, J.*Sci Rep,* **2016,** 6, 21225.

[7]. Varki, A. *Glycobiology,***1993,** 3, 97.

[8]. Dwek, R. A. *Chem. Rev,***1996,** 96, 683.

[9]. Davis, B. G.; Robinson, M. A. *Curr. Opin. Drug DiscovDevel,***2002,** 5, 279.

[10]. Zhang, H.; Ma, Y.; Sun, X. L. *Med. Res. Rev,***2010,** 30, 270.

[11]. Ahire, J. H.; Behray, M.; Webster, C. A.; Wang, Q.; Sherwood, V.; Saengkrit, N.; Ruktanonchai, U.; Woramongkolchai, N.; Chao, Y. *Adv.Healthcare Mater,***2015,** 4, 1877.

[12]. Dalle Vedove, E.; Costabile, G.; Merkel, O.M.*Adv Healthc Mater,***2018,** 7, 1701398.

[13]. Ghosh, P.; Dahms, N.M.; Kornfeld, S.*Nat Rev Mol Cell Biol,***2003,** 4, 202.

[14]. Hassan, A.B. *Am J Pathol,* **2003,** 162, 3.

[15]. Dahms, N.M.; Olson, L.J.; Kim, J.J. *Glycobiology,***2008,** 18, 664.

[16]. De Leon, D.D.; Issa, N.; Nainani, S.; Asmerom,Y. *Horm Metab Res,***1999,** 31,142.

[17]. Wise, T.L.; Pravtcheva, D.D. *Cancer Res,***2006,**66, 1327.

[18]. Berthe, M.L.; Esslimani, S.M.; Roger, P.; Gleizes, M.; Lemamy, G.J.; Brouillet, J.P.; Rochefort. H. *Eur J Cancer,***2003,**39, 635.

[19]. Ishiwata, T.; Bergmann, U.; Kornmann, M.; Lopez, M.; Beger, H.G.; Korc, M. *Pancreas,***1997,**15, 367.

[20]. Pavelic, K.; Kolak, T.; Kapitanovic, S.; Radosevic, S.; Spaventi, S.; Kruslin, B.; Pavelic, J. *Pathol,***2003,** 201, 430.

[21]. Laube, F. *Anticancer Res,***2009,** 29, 1383.

[22]. Cariani, E.; Lasserre, C.; Seurin, D.; Hamelin, B.; Kemeny, F.; Franco, D.; Czech, M.P.; Ullrich, A.; Brechot ,C. *Cancer Res,***1988,** 48, 6844.

[23]. Guerrero, R. F.; Garcia-Parrilla, M. C.; Puertas, B.; Cantos-Villar, E. *Natural productcommunications,***2009,** 4, 658.

[24]. Chan, M. M. *Biochemical pharmacology,***2002,** 63, 99.

[25]. Brisdelli, F.; D'Andrea, G.; Bozzi, A. *Current drug metabolism,***2009,**10, 530.

[26]. Abdel-Wahab, B. A.; Abdel-Wahab, M. M. *Behavioural brain research,***2016,** 305, 65.

[27]. Kaminski, B. M.; Steinhilber, D.; Stein, J. M.; Ulrich, S. *Curr Pharm Biotechnol,***2012,**13, 137.

[28]. Arafa, M. H.; Mohammad, N. S.; Atteia, H. H.; Abd-Elaziz, H. R. *J Physiol Biochem,***2014,** 70, 701.

[29]. Dolinsky, V.W.; Jones, K.E.; Sidhu, R.S.; Haykowsky, M.; Czubryt, M.P.; Gordon, T.; Dyck, J.R.*J Physiol,***2012,**590, 2783–2799.

[30]. Walle, T.; Hsieh, F.; DeLegge, M. H.; Oatis, J. E. Jr.; Walle, U. K. *Drug Metab Dispos,***2004**, 32, 1377.

[31]. Aleksandra, K. G.; Nikhil, R. M.; Stacie, M. B.; Sarah, D. E.; Zofia, Mazersk.; Howard, P. H.; Peter, A. C.; Anna, R.P.*Chem Res Toxicol,***2014,** 27, 536.

[32]. Speth, P. A.;Van Hoesel, Q. G.; Haanen, C. *Clin Pharmacokinet,* **1988,** 15, 15.

[33]. Megalizzi, V.; Le Mercier, M.; Decaestecker, C. *Med Res Rev,***2012,** 32, 410.

[34]. Wihlm, J.; Limacher, J.M.; Leveque, D.; Duclos, B.; Dufour, P.; Bergerat, J.P.; Methlin, G.*Bulletin du cancer,***1997,**84, 603.

[35]. Ramya, A.N.; Joseph, M.M.; Maniganda, S.; Karunakaran, V.; Sreelekha, T .T .; Maiti K.K. *Small.***2017,** 31, 1700819.

[36]. Pawar, V.; Borse, V.; Thakkar, R.; Srivastava, R.*Curr Drug Deliv,***2018,** 15, 716.

[37]. Movasaghi, Z.; Rehman, S.; Rehman, I.U. *Applied Spectroscopy Reviews,***2007,** 42, 493.

[38]. Rodriguez-Perez, T.; Lavandera, I.; Fernandez, S.; Y. Sanghvi, S.; Ferrero, M.; Gotor, V. *Eur. J. Org. Chem,* **2007,** 2769.

[39]. Elharar, Y.; Podilapu, A.R.; Guan, Z.; Kulkarni,S.S.; Eichler, J.*Bioconjug Chem,***2017,** 28, 2461.

[40]. Guiso,M.; Marra, C.; Farina, A. *Tetrahedron Lett,***2002,** 43, 597.

[41]. Joseph, M. M.; Aravind, S. R.; Varghese, S.; Mini, S.; Sreelekha, T. T.*Biointerfaces,***2013,**104, 32.

[42]. Joseph, M. M.; Aravind, S. R.; George, S. K.; RaveendranPillai, K.; Mini, S.; Sreelekha, T. T. *J. Biomed. Nanotechnol,***2014,** 10, 3253.

[43]. Narayanan, N.; Nair, L. V.; Karunakaran, V.; Joseph, M. M.; Nair,J. B.;Ramya, A. N.; Jayasree, R. S.;K. K. Maiti.*Nanoscale,***2016,** 8,11392.

List of Publications

[1].**Maniganda, S**.; Sankar, V.; Nair, J. B.; Raghu, K. G.; Maiti, K. K. A Lysosome-Targeted Drug Delivery System Based on Sorbitol Backbone towards Efficient Cancer Therapy. ***Org. Biomol. Chem.*** **2014,** *12*, 6564–6569.

[2]. Mathai, B. M.; Joseph, M. M.; **Maniganda, S**.; Nair, J. B.; J.S, A.; Karunakaran, V.; Radhakrishnan, K.V; Maiti, K.K. Guanidinium Rich Dendron- Appended Hydnocarpin Executes Superior Anti-Neoplastic Effects Through Caspase Mediated Apoptosis. ***RSC Adv.*** **2016**, *6*, 52772–52780.

[3]. Adukkadan N. Ramya; Joseph, M.M.; **Maniganda, *S.*;**Varsha, K.; Sreelekha, T.T. Maiti, K. K. Emergence of gold-mesoporous silica hybrid nanotheranostics: Dox-encoded, folate targeted chemotherapy with modulation of SERS fingerprinting for apoptosis toward tumor eradication, ***Small,*** **2017**, 13, 31.

[4]. **Maniganda, S.**;Vishnupriya,M.;Maiti, K. K. Investigation of Multifunctional Targeted Nano-carrier for Stimuli-responsive Co-delivery of Doxorubicin and Resveratol in Breast Cancer cells,2019, Manuscript in preparation.

[5]. **Nair, J. B.,** S. Mohapatra., Joseph, M.M., Maniganda S., S. Ghosh . Sers guided targeted paclitaxel delivery towards glioblastoma via octa-guanidinium sorbitol scaffold. ACS Med. Chem. Lett. Under revision.

List of Posters & Conferences

[1]. Presented poster in The 27th International Carbohydrate Symposium (ICS-27), the bi-annual symposium of the International Carbohydrate Organization (ICO), an associate organization of IUPAC, was held at the Indian Institute of Science, Bangalore, India, 12–17 January 2014.A lysosome-targeted drug delivery system based on sorbitol backbone towards efficient cancer therapy; Poster presentation : Maniganda S., Vandhana S., Ragu, K.G and Kaustabh Kumar Maiti.

[2]. Presented poster in The Ramanbhai Foundation 7th International Symposium on Current Trends in Pharmaceutical Sciences ”Advances in New Drug Discovery & Development”; Organized by Zydus Research Centre, Ahmedabad, India (Feb, 2- 4th, 2015); An Efficient Approach on Guanidium Appended Molecular Transporter For Targeted Delivery of Doxorubicin Towards Malignant Cells: A Future Prospect in Cancer Therapy; Poster presentation : Jyothi B Nair, SanthiManiganda, VarshaKarunakaran, Kaustabh Kumar Maiti.

[3]. Prsented poster in Transending frontiers in organic chemistry(October,2014) An Effiecient Approach on Guanidium Appended Molecular Transporter For Targeted Delivery of Doxorubicin Towards Malignant Cells, Poster presentation: Jyothi B Nair, Santhi Maniganda, Vandana Sanker, Kaustabh Kumar Maiti.